The single Cooper pair transistor: a macroscopic quantum system

P. Joyez

THESE DE DOCTORAT DE L'UNIVERSITE PARIS 6

spécialité:

Physique des solides

présentée par

Philippe JOYEZ

pour obtenir le grade de DOCTEUR de l'UNIVERSITE PARIS 6

Sujet de la thèse :

LE TRANSISTOR A UNE PAIRE DE COOPER : UN SYSTEME QUANTIQUE MACROSCOPIQUE

Soutenue le 6 mars 1995

devant le jury composé de MM.:

A. Benoit
J. Bok
M. Devoret
L. Geerligs
D. Haviland
S. Reynaud

à Anaïs, Charlie et Jules

à Cécile

à mes parents

REMERCIEMENTS

J'ai certainement eu beaucoup de chance de pouvoir préparer ma thèse dans le groupe de Quantronique. Pendant plus de trois ans, Michel Devoret, Daniel Esteve et Cristián Urbina m'ont apporté tout ce dont un chercheur débutant peut rêver : dévouement, compétence, rigueur, créativité, avec en plus une formidable atmosphère de travail dans la bonne humeur.

Je suis très reconnaissant envers Pief Orfila qui, par un soutien technique exceptionnel et par ses conseils astucieux, a rendu possible ce travail. Je lui sais gré aussi de m'avoir initié à l'usinage au tour, à la soudure sous argon, etc.

Toute ma sympathie va aussi à Philippe Lafarge qui m'a précédé d'un an dans le laboratoire. Il m'a patiemment montré les techniques de fabrication des échantillons et de prise de données, et il a participé au premières expériences présentées ici.

J'ai eu le plaisir de retravailler avec Denis Vion (un camarade du lycée) qui nous a rejoint il y a un an et demi. Le travail sur l'hystérèse des petites jonctions Josephson qui est présenté ici est aussi le sien. Je le remercie également pour son expertise de *Mathematica* qui m'a souvent été précieuse.

Je remercie également Vincent Bouchiat, Andrew Cleland, Antoine Filipe, Sophie Guéron, Thorsten Holst, Gert Ingold, Hugues Pothier et Jan van Ruitenbek pour leurs apports scientifiques et les discussions enrichissantes que nous avons pu avoir à tous sujets.

Lors de leurs visites à Saclay, j'ai apprécié les discussions avec Hermann Grabert et John Martinis. Je sais aussi gré à John Martinis de nous avoir tenu au courant de ses expériences.

Je remercie Emmanuel Turlot et la société Balzers qui ont réalisé les dépôts de nitrure de silicium sur les substrats utilisés dans nos expériences avec « environnement électromagnétique contrôlé ».

Je remercie toutes les personnes du Service de Physique de l'Etat Condensé et du Département de Recherche sur l'Etat Condensé, les Atomes et les Molécules qui, à des titres divers, ont contribué à faciliter mon travail par leurs conseils ou leur aide. Je remercie également Daniel Beysens, Pierre Bergé et toutes les personnes qui ont œuvré pour mon embauche à l'expiration de mon Contrat de Formation par la Recherche, me permettant ainsi de terminer ce travail dans des conditions idéales.

Pendant ces trois années j'ai eu la chance de participer à plusieurs conférences ou écoles de physique en France et à l'étranger. J'ai pu y exposer mes travaux, mais surtout y découvrir des personnes et des sujets passionnants. Je remercie vivement tous ceux qui m'ont offert ces

opportunités, particulièrement Eric Akkermans, Christian Glattli, Gilles Montambaux, Jean-Louis Pichard, Marc Sanquer et Tito Williams.

Le manuscrit de cette thèse a bénéficié au cours de son élaboration des multiples conseils de Michel Devoret. Il aussi profité de la lecture attentive et des remarques de Daniel Esteve, Cristián Urbina, Denis Vion et de Sophie Guéron qui a également corrigé mon anglais quelquefois défaillant. Je leur en suis très reconnaissant.

Enfin, je remercie Alain Benoit, Julien Bok, Michel Devoret, Bart Geerligs, David Haviland et Serge Reynaud d'avoir accepté de faire partie du jury.

CONTENTS

I. INTRODUCTION

Although the microscopic behavior of electrons in conductors is strongly affected by quantum mechanical effects, the macroscopic behavior of usual electronic circuits is classical : voltages and currents obey Kirchhoff rules, and their evolution is determined by the current-voltage relations of the various elements. The search for electronic circuits exhibiting quantum properties in their macroscopic behavior arose when Caldeira and Leggett realised that electronic circuits were the best candidates to test for a possible limit of validity of quantum mechanics at the macroscopic level [1]. They explained quantitatively how dissipation, which is unavoidable in a macroscopic system, usually prevents the observation of a quantum behavior. Nevertheless, they showed that for a Josephson junction placed in a superconducting ring, dissipation can be made small enough to observe quantum tunneling of the flux threading the ring. Quantum tunneling out of a metastable flux state has indeed been observed in these systems [2]. Furthermore, observation of quantum tunneling in a slightly different system where the Josephson junction is biased with a current source, was found to be in good agreement with the predictions, once the effect of residual dissipation is taken into account [3]. The next step in this new field of macroscopic quantum mechanics then clearly appeared to be the realisation of a coherent superposition of two quantum states which differ at the macroscopic level. This extreme quantum situation is called macroscopic quantum coherence. Despite numerous attempts, it could not be achieved in the above Josephson systems because a static coherent superposition of two flux states is much more fragile with respect to residual dissipation than quantum tunneling of flux [4].

In this work I will describe experiments done on a new “quantum” electronic component : the superconducting single electron transistor. The device consists of two nanoscale series-connected superconducting tunnel junctions (see Fig. 1). A tunnel junction consists of two metallic electrodes separated by a thin insulating layer (typically 1 nm thick). Since the electrode between the two junctions is isolated from the rest of the circuit, we call it the “island”. The principle of this device is based on a tunable coherent superposition of two island states whose charges differ by $2e$, a difference which affects the macroscopic behavior of the device. The advantage of dealing with charge variables instead of flux variables is due to a very fundamental asymmetry : the typical dissipation felt by a charge variable is smaller than that felt by a flux variable in a ratio of the order of $Z_0/R_K = 2\alpha \ll 1$, where $Z_0 = 1/\varepsilon_0 c \approx 377\ \Omega$ is the impedance of the vacuum, $R_K = h/e^2 \approx 25.8\ \mathrm{k}\Omega$ is the resistance quantum and $\alpha = e^2/4\pi\varepsilon_0\hbar c \approx 1/137$ is the fine structure constant (see Refs. 4 & 5 in the case of flux and charge, respectively).

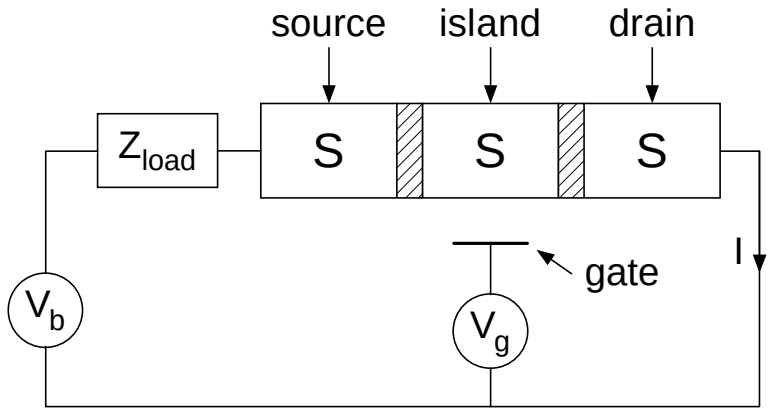

Fig. 1. *Schematic representation of a superconducting single electron transistor and its bias circuit. The transistor itself consists of three superconducting electrodes (rectangles marked S) separated by tunnel barriers (represented by the hatched rectangles) and a gate capacitor. The middle electrode is called the island, while the other elements are named by analogy with a field effect transistor (FET). The biasing circuit is represented by an ideal voltage source V_b in series with a load impedance Z_{load}. The gate voltage source V_g is supposed ideal.*

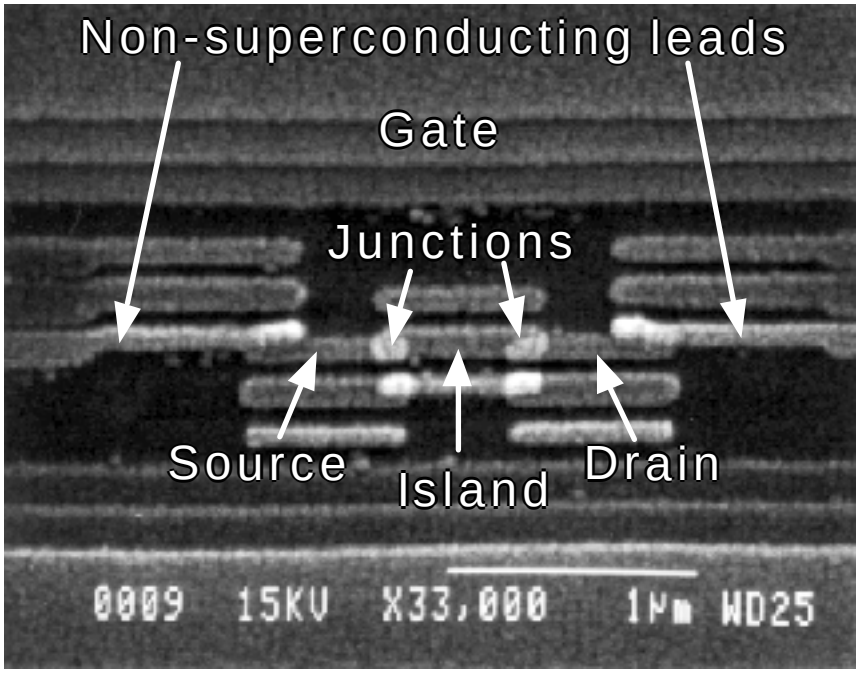

Fig. 2. *Scanning electron micrograph of a sample. The sample fabrication will be described in Chap. V. The junctions are formed at the overlap of two aluminum films. The insulating tunnel barrier is made by oxidizing the first aluminum layer prior to the deposition of the second layer. The non-superconducting copper leads participate in the impedance Z_{load} of the electromagnetic environment of the transistor. They provide a relaxation mechanism for unpaired electrons. This relaxation is essential for the observation of macroscopic quantum coherence.*

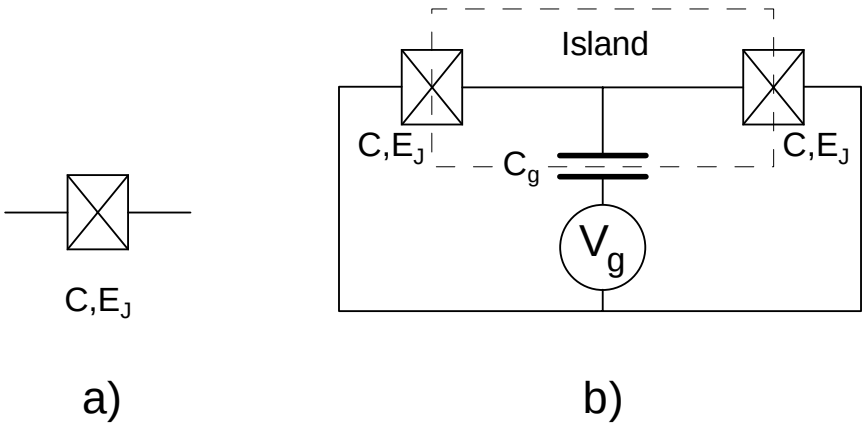

Fig. 3. ***a)*** *Symbolic representation of a small area superconducting tunnel junction. The relevant macroscopic parameters which characterise the junction are its capacitance C and its Josephson coupling energy* E_J. ***b)*** *Schematic electrical diagram of the superconducting single electron transistor at zero bias voltage and without environmental impedance. The tunnel junctions (supposed identical) are connected in series thereby defining an isolated island (enclosed by dashes).*

A gate electrode capacitively coupled to the island controls the mixing of charge states in the island : it arbitrates the competition between the electrostatic charging energy of the island which tends to impose the charge of the island, and the Josephson coupling energy which tends to mix charge states in the superconducting electrodes and particularly in the island. The maximum supercurrent which can flow through the device depends on the relative weights of the quantum superposition of charge states in the island. Hence, the measurement of the maximum supercurrent of the transistor constitutes an observation of macroscopic quantum coherence in the island.
In the following we describe more precisely how the gate voltage controls the macroscopic quantum superposition and we explain the possible difficulties associated with the observation of the macroscopic quantum coherence.

A convenient scale for the electrostatic energy cost of charging the island is the electrostatic energy $E_C = e^2/2C_\Sigma$ of one extra electron on the island, where C_Σ is the total capacitance of the island. The capacitance C_Σ is dominated by the capacitances of the two junctions. Nowadays junctions made using electron-beam lithography (see Fig. 2) commonly have areas of the order of 100 nm×100 nm resulting in capacitances in the fF (10^{-15} F) range. This yields a charging energy E_C of the order of 1 K.k_B. For thermal fluctuations not to spoil the operation of a transistor made with such junctions, one must lower the temperature much below 1 K. Such temperatures (10-100 mK) are routinely achieved in a ^{3}He-^{4}He dilution refrigerator.
A second fundamental energy scale in the transistor results from an interplay between superconductivity and tunneling. This effect is named after Josephson who discovered it in

1962 [6]. We will first describe the behaviour of a single superconducting tunnel junction (Fig. 3a). It will serve as a basis to the understanding of the transistor. Charge carriers in the superconducting electrodes of the junction are Cooper pairs. The states of a single junction can be indexed by the number k of Cooper pairs having crossed the tunnel barrier. At zero voltage across the junction, all these states are degenerate in electrostatic energy (Fig. 4a). Classically, a current flowing through the device would result from a succession of transitions between k-states. Josephson showed that quantum tunneling between the electrodes of the junctions induces an elastic coupling between the k-states whose matrix element is $-E_J/2$ where E_J is known as the Josephson coupling energy, a quantity which depends on the transparency of the tunnel barrier. This coupling is symbolised by arrows in Fig. 4a. The situation is identical to the one found in the tight binding description of a one-dimensional crystal with one atom per unit cell : the electrostatic energy plays the role of the energy of the orbitals, while the Josephson energy is equivalent to the hopping energy. We can apply the Bloch theorem as in the crystal. Therefore, a good quantum number will be the phase δ across the junction which is the conjugate quantity of k. The eigenstates of the system are characterised by a well-defined value of δ, which in the k-states picture corresponds to a coherent superposition of an infinite number of states : the number of Cooper pairs having crossed the junction is completely undetermined quantum mechanically. The eigenenergies of the system form a band parametrised by δ, with energy $E(\delta) = -E_J \cos\delta$ (Fig. 4b). The existence of such a band enables a supercurrent flow (that is a current with no voltage drop) through the junction. The theoretical maximum supercurrent (hereafter called the critical current) the junction can transmit is proportional to the width of the band.

The transistor can be described in terms very similar to those we used here for the single junction. The states of the transistor can be indexed by the combination of the number k of Cooper pairs having crossed the device and the number p of excess Cooper pairs on the island (Fig. 5a). At zero bias voltage on the transistor the energies of the states of the system are degenerate with respect to k. If one starts in the ground state of the island, there is a minimal electrostatic energy cost $U = 4E_C\left|1-(Q_g \bmod 2e)\right|$ associated to the entrance or exit of a Cooper pair in the island, where $Q_g = C_g V_g$ is what we call the gate charge. This electrostatic energy can be tuned between 0 and $4E_C$ by varying the gate voltage V_g, with a periodicity corresponding to adding one Cooper pair on each plate of the capacitor C_g. The behaviour of the system is thus $2e$-periodic in Q_g. If we suppose that $E_J \lesssim E_C$, in a first approach we can consider only the two states of lowest electrostatic energy in a given Q_g-period. These two states differ by one Cooper pair in the island. The classical succession of electrostatic energy levels of the system corresponding to a current flow at zero bias voltage, as a function of k, is shown in Fig. 5b. The Josephson couplings are still symbolised by arrows, and the junctions are assumed to have the same Josephson coupling energy E_J. The system is again analogous to a one-dimensional crystal but now with two atoms per unit cell. Thus, in our simplified

description of the transistor which neglects the influence of the bias circuit (we have supposed $V_b = 0$, $Z_{load} = 0$), we can still apply the Bloch theorem. The phase δ across the source and drain which is the conjugate quantity of k (see Fig. 5c) is a good quantum number. The eigenstates of the system now form two bands parametrised by δ (Fig. 5b). The width of the bands depends on the relative strength of U and E_J. Hence, the transistor is a (maybe unique) example of a device whose quantum band structure can be modulated by simply changing the gate voltage : as U is changed from 0 to $4E_C$ by varying the gate voltage, the width of the bands varies between E_J (half that of a single junction) and $E_J^2/2E_C$. As long as the system stays in the lowest band, the physics of the transistor is that of a single Josephson junction with a gate-voltage tunable effective Josephson coupling. This modulation of the effective Josephson coupling translates into a modulation of the maximum supercurrent (see Fig. 6 & 7). This justifies the name of "transistor" given to the device : it can be considered a superconducting field effect transistor.

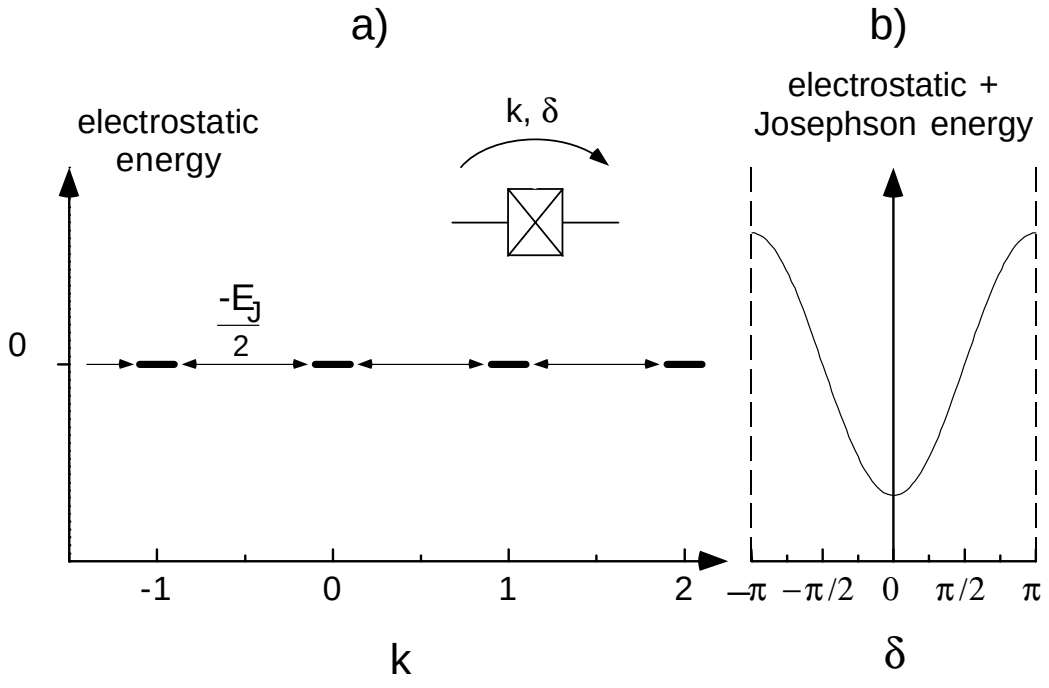

Fig. 4. ***a)*** *Electrostatic energy states of a single Josephson junction indexed by the number k of Cooper pairs having crossed the tunnel barrier. The states are coupled by the Josephson coupling energy as symbolised by the arrows joining adjacent states. The description is analogous to that of a 1-D crystal with one atom per unit cell in the tight-binding model.* ***b)*** *Translational invariance of a) can be used to diagonalize the system in the δ representation where δ is the phase difference across the junction. The variable δ is canonically conjugated with the variable k.*

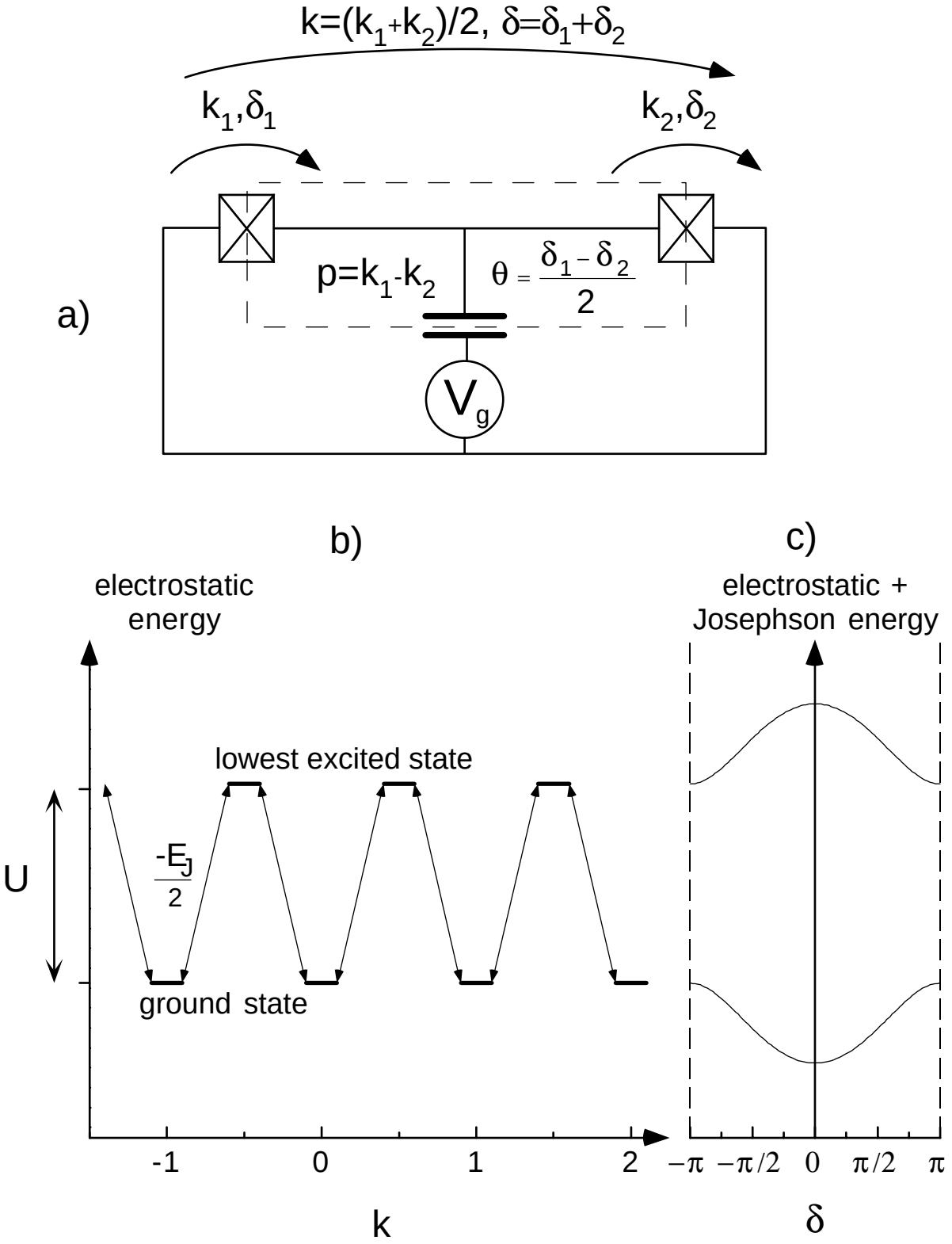
k=(k1+k2)/2, δ=δ1+δ2
k1,δ1
k2,δ2
a)
p=k1-k2
θ = (δ1 − δ2)/2
Vg
b)
c)
electrostatic energy
electrostatic + Josephson energy
lowest excited state
U
-EJ/2
ground state
-1
0
1
2
k
−π
−π/2
0
π/2
π
δ

Fig. 5. *(previous page)* ***a)*** *Variables which can be used to describe the state of the system. The state of each junction can be specified in terms of k_i (i = 1,2) the number of Cooper pairs having crossed each junction or δ_i the phase across the junctions. From these four variables we define four other variables which are more convenient for describing the state of the whole transistor. These variables are canonically conjugate two by two: (i) k, the number of Cooper pairs having crossed the whole transistor and δ the total phase difference across the transistor, and (ii) p, the number of excess Cooper pairs in the island and θ the phase of the superconducting condensate in the island.* ***b)*** *Electrostatic energy states of transistor, for the two lowest electrostatic energy states of the island as a function of the number k of Cooper pairs having crossed both junctions. The ground state and the first excited state differ by one Cooper pair in the island ($\Delta p = \pm 1$). The Josephson coupling energy (supposed the same for both junctions) is symbolised by the arrows joining adjacent states. The description is analogous to that of a 1-D crystal with two atoms per unit cell.* ***c)*** *As in Fig. 4, translational invariance of b) can be used to diagonalize the system in the δ . We have now two bands. The amplitude of the bands depends on the relative magnitude of E_J and U which itself can be adjusted by varying the gate voltage. The switching property of the transistor is based on this modulation of the band structure by the gate voltage.*

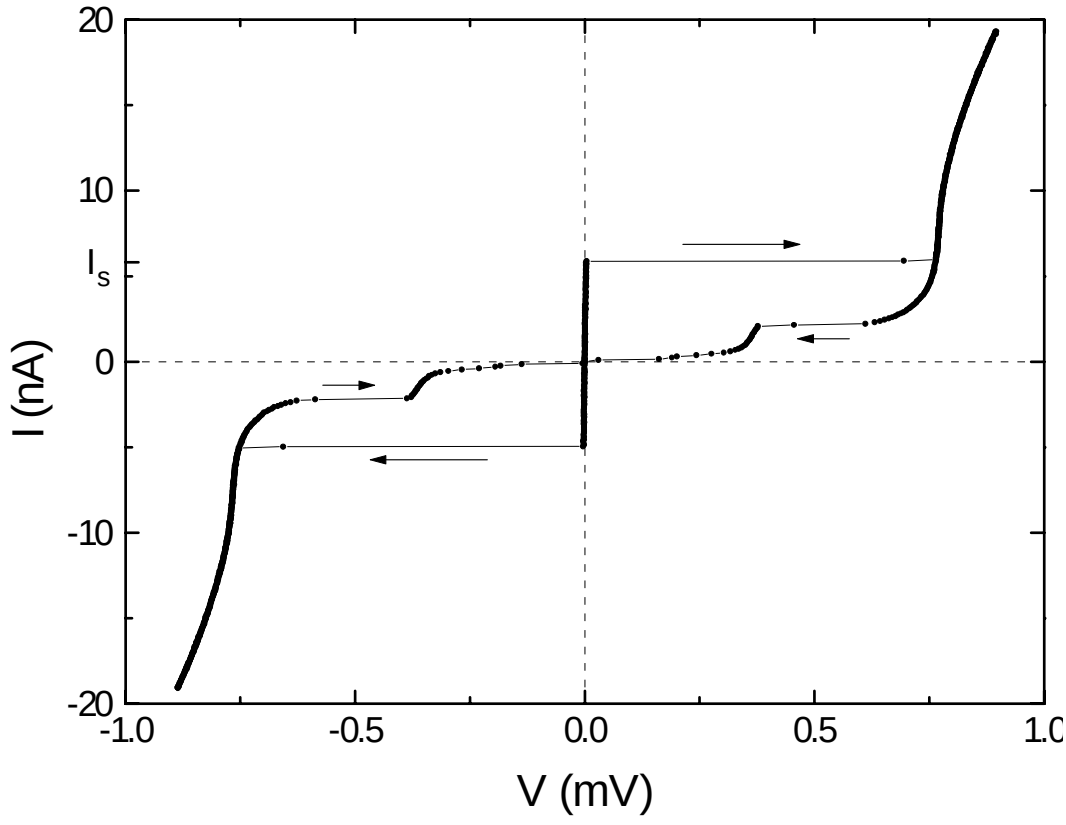

Fig. 6. *Experimental current-voltage characteristic of one of our samples (# 13) biased by a nearly ideal current source. Data points on the zero-voltage axis correspond to the superconducting state of the transistor. When the driving current is increased above the switching current I_s , the voltage across the transistor suddenly increases. The value of the switching current is modulated by the gate voltage (see Fig. 7).*

As we explained in the beginning of this introduction, the quantum character of the transistor lies in the variable p indexing the number of Cooper pairs in the island and its conjugate variable, the phase θ of the superconducting condensate in the island (Fig. 5a). These variables obey an Heisenberg uncertainty relation of the type $\delta\theta.\delta p \gtrsim 1$ [7]. When U is tuned to its maximum by adjusting the gate voltage, the electrostatic energy cost of changing p is significant and this nearly suppresses quantum fluctuations of p. Of course, at the same time, θ is completely undetermined quantum-mechanically. In this situation the bands of the transistor are narrow, and the maximum supercurrent is weak. On the contrary, when $U = 0$, p fluctuates between the two values corresponding to the lowest electrostatic energy level : $\delta p = 1$ and $\delta\theta$ is reduced. In this situation, the state of the transistor has no classical description : it is in a coherent superposition of states. The width of the bands are now maximum and the critical current of the transistor is also maximum. Thus, from the point of view of p and θ, the gate voltage controls the “squeezing” of the fluctuations of p. The larger the squeezing, the smaller the critical current of the device.

The behaviour of the transistor is shown in Fig. 7 where we plot the variations of the maximal experimental supercurrent (hereafter called the switching current) of one of the samples we have fabricated, as a function of the gate charge. This switching current is compared with the maximum supercurrent given by the theory (see Fig. 7). Our results shown in Fig. 7 constitute the first observation of the modulation predicted by Likharev who first discussed the set-up of the transistor nearly a decade ago [8]. During a long time experiments could not confirm these predictions [9,10,11]. There were indeed reasons to suspect that some fundamental problems could prevent the observation of these predictions. One can think of two types of problems :

i) The first type of problems concerns the possibility of defects in the superconducting order. In the description of the transistor we have presented, we have made a crucial assumption which was not correctly justified : we implicitly invoked the BCS theory of superconductivity [12] to assume that the electrons in the island were all paired (and therefore, in even number) at low temperature. The BCS theory of superconductivity is known to be rigorous in the thermodynamic limit of a large system. In small islands such as that of the transistor, one cannot predict what will be the influence of disorder, impurities, boundaries etc. on the states of the superconducting system : there might be available states of any parity at any energy in the island. Furthermore, even if one follows the BCS theory literally (*i.e.* assuming the validity of the thermodynamic limit in a finite non-ideal system), there are excited states of the superconductor in which the electrons are not all paired, *i.e.* with an odd electron number in the island. Considering these excited states, Matveev *et al.* [13] showed that when the charging energy E_C is greater than the gap of the superconductor in the island, the state of maximum quantum superposition in the island of the transistor is metastable and may well be unobservable in practice. Finally, even if we suppose that the lowest energy states of the island are really those of even parity, is it possible practically to place and keep the system in

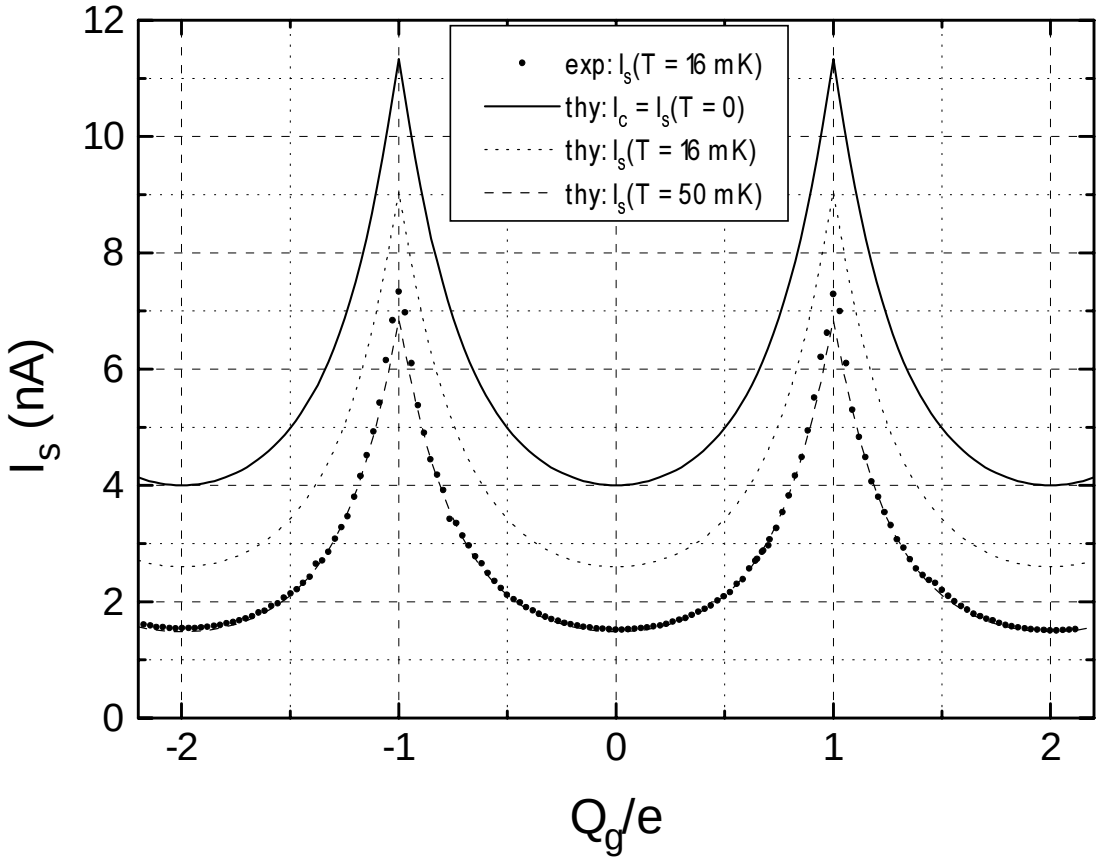

Fig. 7. *Low temperature switching current (dots) and the critical current of a transistor (top curve, no fitting parameters), as a function of the gate charge $Q_g = C_g V_g$ for sample #13. The critical current which is the theoretical maximal supercurrent would correspond to the switching current at T=0. The data we have obtained in our experiments are the first to reproduce faithfully the variations of the critical current. Moreover, for this particular sample, the difference between the experimental data and the maximum achievable supercurrent is unprecedentedly small for an unshunted small junction system. This close agreement was obtained by implementing a specially designed electromagnetic environment for the transistor. The remaining difference is explained by a hot-electron effect : the experimental data is in good agreement with a calculation of the switching current where the temperature of the electromagnetic environment is taken to be 50 mK (dashes). The heating of electrons in this sample results of Joule effect in a resistance in series with the transistor. See Chap. V & VI for further details.*

these states? In other words, won't external perturbations unavoidably disturb the system in a real experiment?

ii) The second type of problem is related to the electromagnetic environment of the transistor. The effect of the dissipation on the macroscopic quantum coherence of charge states is analysed in Ref. 5, where it is shown to be hardly observable for usual circuits. However, the description of the transistor we have made appeals to the notion of Josephson coupling. This notion is known to be perfectly valid for a large-area superconducting tunnel junction where the capacitance is such that $E_C \ll E_J$: the capacitance of the junction shunts the

electromagnetic environment of the junction which is then irrelevant (the impedance of the environment can be taken equal to zero). On the contrary, for small junctions, one cannot *a priori* disregard the role of the environment and the theory of Josephson coupling must be reexamined. Another important issue is the way the experimentally measured quantity is related to the prediction concerning the critical current of the transistor : The critical current only sets an upper limit for the intensity of the supercurrent flowing through the transistor. In systems of large junctions it is known that the environment has an influence on the experimental critical current : when dissipation is increased, one observes a transition from the regime of macroscopic quantum tunneling of the phase to the classical regime of thermal activation over a barrier [3]. How does the environment influence the effective maximum supercurrent in a small-junction system? What is the “best” environment to perform the experiment if one wishes the largest possible supercurrent?
In this work, we address all these problems both theoretically and experimentally, and we bring answers to most of the above questions.
Finally, in this work we will also show that the transistor is more than just a switch for the supercurrent (*i.e.* at $V = 0$) : its quantum character yields a rich behaviour at finite voltage as well. For example, we will demonstrate the existence of a hierarchy of “resonant Cooper pair tunneling” processes which has been predicted [14,15] and whose first order has recently been observed by Haviland *et al.* [16]. We will also show evidences for Zener tunneling between the two lowest bands of the transistor. These quantum effects must be separated from the more classical Shapiro steps which we have also observed, both with external irradiation, and without (self-induced Shapiro steps).

Organisation of this work

In Chap. II we describe the quantum mechanics of a tunnel junction in an electromagnetic environment treated as a perturbation. For a superconducting tunnel junction we find that the electromagnetic environment renormalizes the Ambegaokar-Baratoff [17] value of the Josephson coupling energy.

In Chap. III we develop a model of the transistor based on the Josephson Hamiltonian. We first justify the use of the Josephson Hamiltonian by a microscopic analysis of charge transfer in the transistor. Then, using a phase representation of the Hamiltonian of the transistor, and keeping only a finite number of charge states of the island, we show that it behaves as a tunable Josephson junction. We derive the gate-voltage dependence of the critical current using a simple two-band model which we extend and compare to a three-band model. We then describe rapidly the principle of the “poisoning” of the supercurrent by quasiparticles. Finally further extend our theoretical description of the transistor by presenting an analytic calculation

of the "resonant Cooper pair tunneling" current which is responsible for the gate voltage dependent resonances appearing in the current-voltage characteristic of the transistor.

In Chap. IV we introduce the notion of the generalised current-voltage characteristic of a Josephson junction to explain the relationship between the critical current and the experimentally measured switching current of small-area Josephson junctions. Our main result is the understanding of the crucial role of the dissipation on the magnitude of the switching current of small unshunted junctions.

Our experimental techniques are described in Chap. V. We focus in particular on the fabrication of the samples and on the experimental set-up.

In Chap. VI we present our experimental results. We first give an overview of the current-voltage characteristic of the transistor. We then discuss the following effects concerning the switching current :

- Effect of the dissipation on the magnitude of the supercurrent,
- Effect of charge noise on the switching current histograms,
- Poisoning of the supercurrent by quasiparticles.

These effects can be quantitatively accounted for by the theory developed in Chap. II, III and IV. We finally describe effects observed in the current-voltage characteristic at finite voltage :

- Resonant Cooper pair tunneling,
- AC Josephson effect under irradiation and self-induced AC Josephson effect,
- Zener tunneling between bands of the transistor.

Our results on the first effect agree semi-quantitatively with theory. We give a qualitative explanation of the last two effects.

In the conclusion, we summarize the results obtained, we draw the scope of this work and we point out possible future directions.

The thesis includes two appendices :
Appendix A consists of a reprint of a paper on the poisoning of the supercurrent (Phys. Rev. Lett., **72**, 2458 (1994)).
Appendix B presents a table of parameters and miscellaneous information on the samples involved in the experiments.

References

[1] A. O. Caldeira and A. J. Leggett, Ann. Phys. (N.Y.) **149**, 374 (1983).

[2] see *e. g.* D. B. Schwartz, B. Sen, C. N. Archie, and J. E. Lukens, Phys. Rev. Lett. **55**, 1547 (1985) and reference therein.

[3] M. H. Devoret, D. Esteve, C. Urbina, J. Martinis, A. Cleland and J. Clarke in *Quantum Tunneling in Condensed Media* edited by Yu. Kagan and A. J. Leggett (Elsevier, Amsterdam, 1992), Chap. 6.

[4] H. Grabert in SQUID'85, proceedings of the Third International Conference on Superconducting Quantum Devices, edited by H. D. Hahlbohm and H. Lübbig (de Gruyter, New York, 1985)

[5] F. Neumann, G.-L. Ingold, and H. Grabert, Phys. Rev. **B 50**, 12811 (1994) and P. Lafarge, Ph.D. Thesis, Université Paris 6 (1993).

[6] B. D. Josephson, Phys. Lett., **1**, 251 (1962)

[7] W. J. Elion, M. Matters, U. Geigenmüller, and J. E. Mooij, Nature **373**, 594 (1994).

[8] see D. V. Averin and K. K. Likharev, in *Mesoscopic Phenomena in Solids*, ed. by B. Al'tshuler, P. Lee, and R. Webb (Elsevier, Amsterdam, 1991), Chap. 6, sec. 3.1.2

[9] T. A. Fulton, P. L. Gammel, D. J. Bishop and L. N. Dunkleberger, Phys. Rev. Lett. **63**, 1307 (1989).

[10] L. J. Geerligs, V. F. Anderegg, J. Romijn, and J. E. Mooij, Phys. Rev. Lett. **65**, 377 (1990).

[11] M. T. Tuominen, J. M. Hergenrother, T. S. Tighe and M. Tinkham, Phys. Rev. Lett. **69**, 1997 (1992).

[12] J. Bardeen, L. N. Cooper and J. R. Schrieffer, Phys. Rev. **108**, 1175 (1957).

[13] K. A. Matveev, M. Gisselfält, L. I. Glazman, M. Jonson and R. I. Shekhter, Phys. Rev. Lett. **70**, 2940, 1993.

[14] P. A. Bobbert and A. A. Odintsov, unpublished (1991).

[15] A. Maassen van den Brink, A. A. Odintsov, P. A. Bobbert, and G. Schön, Z. Phys. **B 85**, 459 (1991).

[16] D. B. Haviland, Y. Harada, P. Delsing, C. D. Chen, and T. Claeson, Phys. Rev. Lett. **73**, 1541 (1994)

[17] V. Ambegaokar and A. Baratoff, Phys. Rev. Lett. **10**, 486 (1963).

II. QUANTUM MECHANICS OF A TUNNEL JUNCTION IN AN ELECTROMAGNETIC ENVIRONMENT

A. Quantum description of circuits

1. Electrons in metals

The problem of electrons in a metal is an *N*-body problem which cannot be solved exactly. Fortunately, we do not need to know the exact structure of the electronic states of the metal to model its macroscopic dynamics. All we need to know are the excitations of the system above the ground state. The typical energies we will consider are the energy of thermal fluctuations $k_B T$, potential energies eV associated with voltage drops V, electrostatic energies E_C… All these energies will be much less than the Fermi energy E_F which in metals is of the order of the electron-volt. For such low energies, the excitations are well separated into two kinds (see Fig. 1) :

i) Long wavelength collective excitations of electromagnetic nature such as surface charge, and the associated currents. These excitations propagate at the speed of light.

ii) Short wavelength collective excitations inside the metal with $k \approx k_F$ which are of kinetic nature. They are the electronic part of what electrical engineers call heat. These kinetic excitations can be described by the Fermi-liquid theory developed by Landau [1]. He showed that in the vicinity of the Fermi surface these kinetic excitations can be put in correspondence with those of a system of free fermionic particles hence their name : “quasiparticles”. Because of the screening of charge in a metal, these quasiparticles have no electrostatic charge in the usual sense. There is no long range electric field which is associated with a quasiparticle, and this is consistent with the fact that quasiparticles behave like free fermions. The quasiparticles propagate at the Fermi velocity $v_F = \hbar k_F / m^*$ where m^* is the effective mass of the quasiparticles. This velocity is typically 10^6 ms^{-1}.

In most circumstances the long wavelength excitations can be ignored and one can treat currents by assigning a charge $-e$ to electron-like quasiparticles. In this work we must go beyond this simple scheme.

The separation of excitations described here breaks down when one dimension of the metallic circuit becomes comparable to the screening length, which is of the order of the inter-atomic distance, or at high energies. We will stay away from these limits in this discussion.

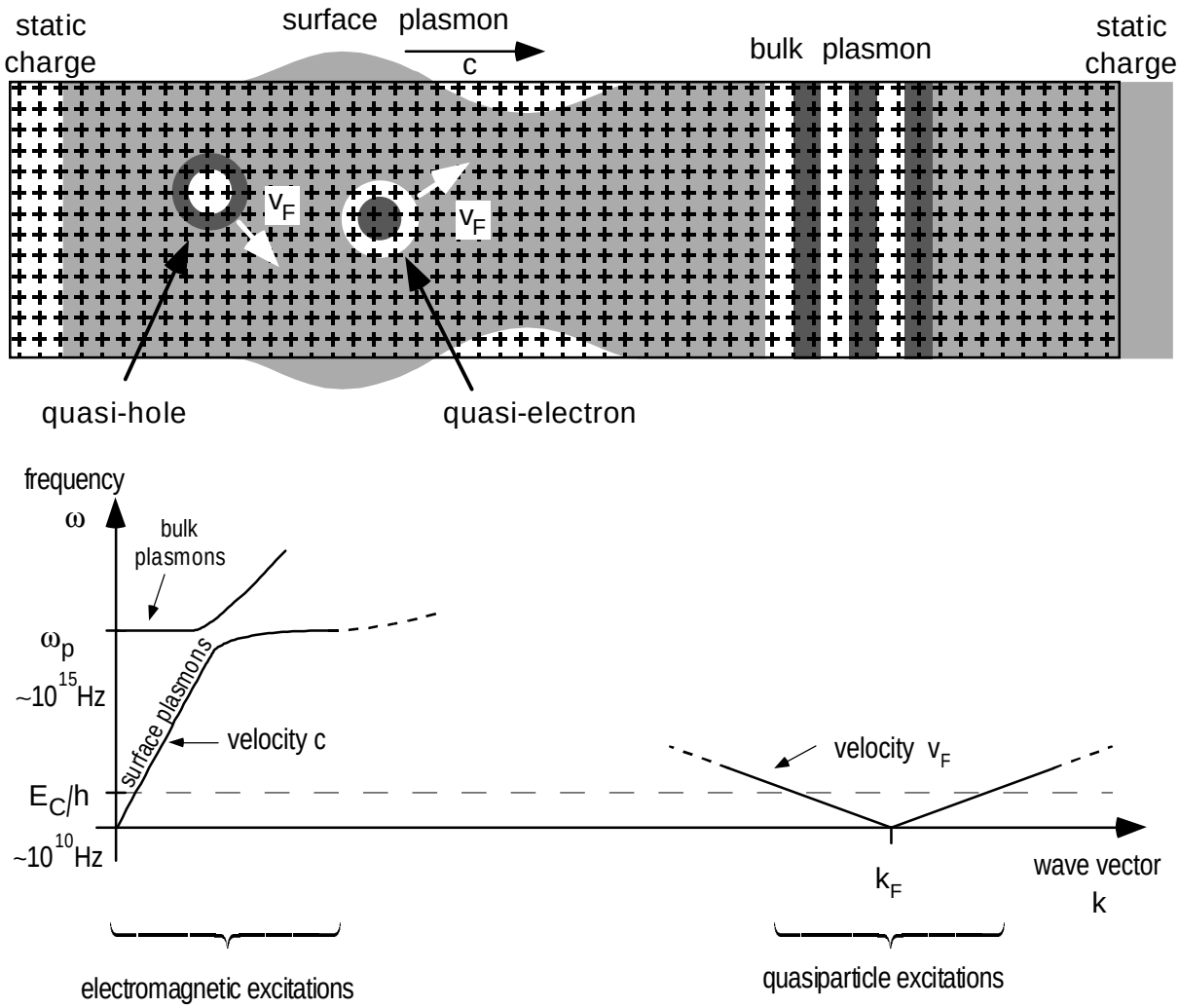

Fig. 1. *Schematic representation of the excitations of a metallic wire (top panel), and their frequencies as a function of the wave vector of the excitation (bottom panel). The lattice of ions is represented by the network of + symbols and the electronic fluid by the grey shade. The variations of the density of the electronic fluid are represented by the darkness of the grey shade. Short wave-vector excitations are separated into two types. The first type which we call "surface plasmons" corresponds to the usual currents and charges in the wire; they propagate at the velocity of light. The static charge is a degenerate $k = 0$ surface plasmon. The second type consists of bulk plasmons which are much higher in energy : they are not relevant for the energies we consider. Excitations with wave vectors of the order of k_F are Landau's quasiparticles of the Fermi liquid theory. They are microscopic uncharged excitations of the metal which propagate at the Fermi velocity.*

2. Quantum state of a metallic electrode and of an electrical circuit

The above considerations lead us to describe an excitation state of a metallic electrode by a ket $|em\rangle|qp\rangle$ in the Hilbert space $\mathcal{E}_{metal} = \mathcal{E}_{em} \otimes \mathcal{E}_{qp}$, where $\mathcal{E}_{em}$ is the Hilbert space for all the electromagnetic degrees of freedom, and $\mathcal{E}_{qp}$ the space of quasiparticle states which is usually the only one considered in the theory of electric transport.

In the case of an electrical circuit, the total Hilbert space is also a tensorial product $\mathcal{E}_{circuit} = \mathcal{E}_{em}^{circ} \otimes \mathcal{E}_{qp}^{circ}$. In this case, $\mathcal{E}_{qp}^{circ} = \mathcal{E}_{qp}^{1} \otimes \ldots \otimes \mathcal{E}_{qp}^{N}$ is itself the tensorial product of the quasiparticle Hilbert spaces for the various elements of the circuit. On the contrary, $\mathcal{E}_{em}^{circ}$ cannot generally be divided in the same way because different parts of the circuit can interact via electromagnetic fields. It will rather be separated into spaces corresponding to the different modes of the fields.

3. Quantum mechanics of electromagnetic degrees of freedom in a circuit

In this section we explain how to form a Hamiltonian operator in the space $\mathcal{E}_{em}^{circ}$. We suppose that the circuit is a network of non-dissipative discrete dipoles. This is not a restriction since any linear element, dissipative or not, (*e.g.* a resistor, a transmission line) can be modelled by a network of infinitesimal discrete elements (see Ref. 2 and Sec. B.1.a).

Let us first describe the circuit using the classical Hamiltonian formalism. Currents (i) and voltages (v) are not adapted for this formalism. In a given branch of the circuit, we rather define

$$Q(t) = \int_{-\infty}^{t} i(t')\mathrm{d}t',$$

the charge having flown through the branch and the generalized flux

$$\Phi(t) = \int_{-\infty}^{t} v(t')\mathrm{d}t'.$$

We then write the electromagnetic energy $E(Q,\Phi)$ in the branch as a function of Q and/or Φ (*e.g.* $E = Q^2/2C$ or $E = \Phi^2/2L$ for a capacitor or an inductor, respectively). Then we sum up the energies of the $\mathcal{N}$ branches of the circuit

$$E_{tot} = \sum_{i=1}^{\mathcal{N}} E_i\left(Q_i, \Phi_i\right).$$

This is not yet a classical Hamiltonian because the variables Q_i, Φ_i are not independent. To obtain a Hamiltonian, we further need to eliminate some variables by making use of the Kirchhoff's relations obeyed by the Q's and Φ's. These relations include constants which correspond to initial conditions of the variables. The number of such independent relations will determine the final number of variables in the Hamiltonian. The elimination procedure is not unique. Depending on the elimination procedure, we will obtain different Hamiltonians $H(\{Q_k\}, \{\Phi_k\})$ depending on different sets of variables. These Hamiltonians are related to one another by a canonical transformation. For a given choice of the Hamiltonian H, among the $2\mathcal{R}$ remaining variables, the variables Q_k and Φ_k pertaining to a particular branch are canonically conjugate variables :

$$\dot{\Phi}_k = \frac{\partial H}{\partial Q_k} \qquad \dot{Q}_k = -\frac{\partial H}{\partial \Phi_k} \qquad k \in \{1,\ldots,\mathcal{R}\}.$$

The above Hamilton equations reproduce the standard electrical equations of the circuit for the usual orientation convention of dipoles

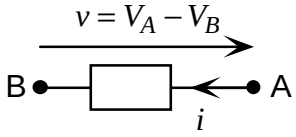

With this convention, flux is a position-like quantity and charge is momentum-like.
At this point, the quantization procedure is straightforward. Variables become operators

$$Q_i \rightarrow \hat{Q}_i$$
$$\Phi_i \rightarrow \hat{\Phi}_i$$

and canonical conjugate operators obey the commutation relation

$$\left[\hat{\Phi}_i, \hat{Q}_i\right] = i\hbar.$$

Since from now on we will be dealing only with the operators $\hat{\Phi}_i, \hat{Q}_i$ we will drop the circumflex mark on these operators. It is sometimes more convenient to use the equivalent dimensionless operators obtained by introducing the fundamental constants e and $e/\hbar$:

$$k = Q/e \qquad \varphi = e\Phi/\hbar,$$

which are the operators corresponding to the number of transferred electrons and the phase across the element. It is very important to stress here that the spectrum of k (and Q) is *a priori* continuous. This is because the electrons form a fluid in the conductors and it is possible to displace this fluid by an arbitrarily small amount.

B. Tunneling of electrons

We now come to the description of an essential ingredient of our experiments : the tunnel junction. As already explained, a tunnel junction consists of two metallic electrodes separated by a thin insulating layer. In such a junction, what tunnels through the barrier are real charged electrons, not quasiparticles. The reason for this is that the charge of the tunneling electrons cannot be screened inside of the insulator. A tunnel process can be seen as follows : a quasielectron incident on the barrier undresses itself of its positive screening cloud as it penetrates the barrier, and dresses up again in the other electrode. Since a charge -e is transferred in the process, tunneling couples quasiparticle and electromagnetic degrees of freedom. It is essential that the Hamiltonian used to describe the junction and its

electromagnetic environment correctly treats this coupling in order to reach a consistent description of our circuits.

1. Description of the junction + environment system

We consider here a single junction in an arbitrary linear electromagnetic environment. This environment can contain other junctions which we will treat here as capacitors (this corresponds to neglecting the possibility of simultaneous tunneling events [3]). Let us first define the general form of the electromagnetic environment of the junction.

a) GENERAL ELECTROMAGNETIC ENVIRONMENT FOR A TUNNEL JUNCTION

In great generality we can assume that the junction is biased by several ideal voltage and/or current sources through a linear circuit (Fig. 2 a). Using Thévenin's theorem (Fig. 2 b), this junction environment can be reduced to an ideal voltage source V_s in series with an impedance $Z_s(\omega)$. We then separate the junction's capacitive and tunnel functions because the junction's capacitance participates in the electromagnetic environment : the junction is decomposed as the parallel combination of a “pure tunnel element” and a capacitor of capacitance C. The circuit is equivalent (Fig. 2 c) to a pure tunnel element in series with an effective impedance

$$Z(\omega) = \frac{Z_s(\omega)}{1 + j\omega C Z_s(\omega)}$$

and a voltage source

$$V = \frac{C_s V_s}{C_s + C}$$

where

$$C_s = \left(\lim_{\omega \to 0} j\omega Z_s(\omega) \right)^{-1}$$

is the series capacitance of $Z_s(\omega)$ which is possibly infinite (so-called low impedance environment case in Refs. 4,5,6).

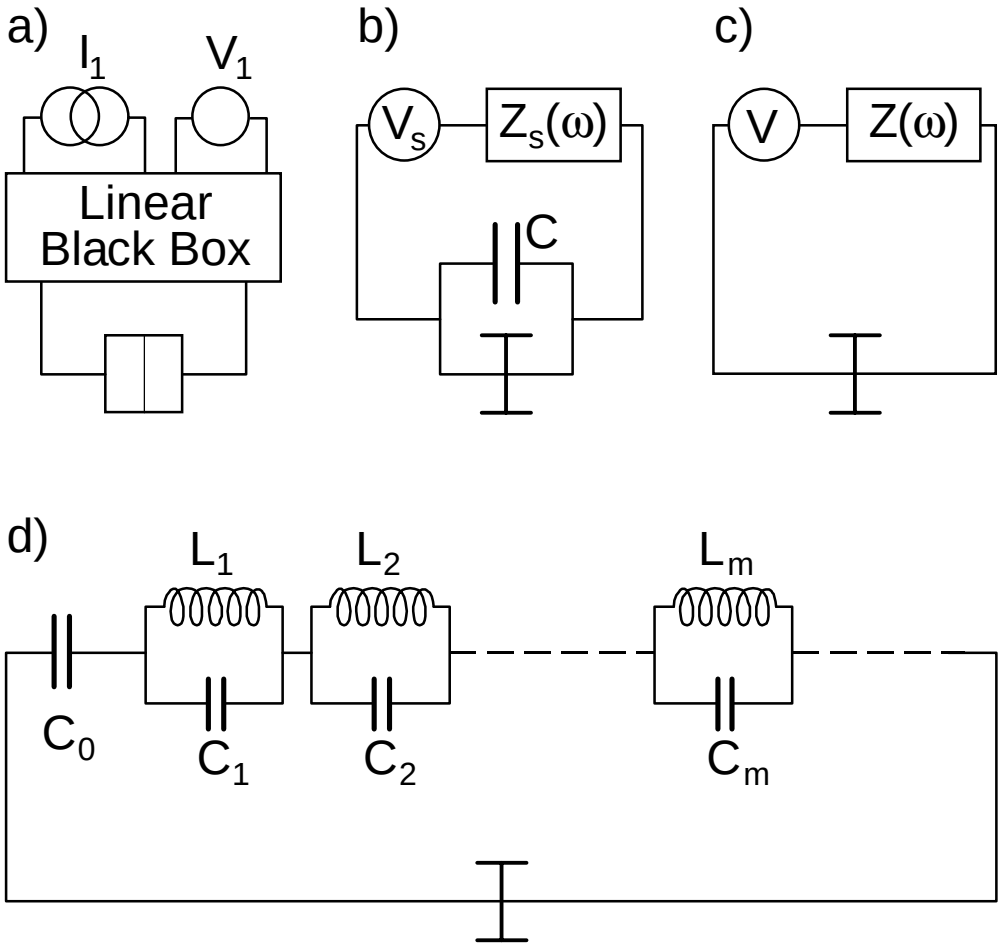

Fig. 2. ***a)*** *A tunnel junction in an arbitrary linear environment, biased by multiple current and/or voltage sources.* ***b)*** *From Thévenin's theorem the environment is equivalent to a voltage source V_s in series with an impedance Z_s. The junction is formally split into the parallel combination of a capacitor C and a "pure tunnel element" represented by the double T symbol.* ***c)*** *The electromagnetic environment of the pure tunnel element is equivalent to an impedance Z (equal to the capacitance of the junction in parallel with Z_s) in series with a renormalized voltage source V.* ***d)*** *Finally, the impedance seen by the pure tunnel element is decomposed into an infinite number of LC oscillators, and the voltage source is treated as a precharging of the capacitor C_0.*

Finally, we use the fact that an arbitrary impedance can be decomposed as an infinite set of LC oscillators evenly distributed in frequency [2] (Fig. 2 d). The parameters of the oscillators are given by the capacitances C_m (m = 0,1,…,∞) and inductances L_m (m = 1,2…,∞) formally defined by the relations

$$Z(\omega) = \lim_{\eta\to 0^+}\lim_{\varepsilon\to 0}\left\{\frac{C_0^{-1}}{j\omega} + \sum_{m=1}^{\infty}\left[\frac{\frac{1}{2}C_m^{-1}}{j(\omega-\omega_m)+\eta} + \frac{\frac{1}{2}C_m^{-1}}{j(\omega+\omega_m)+\eta}\right]\right\}$$

$$\omega_m = m\varepsilon = \frac{1}{\sqrt{L_m C_m}}$$

The real part of the impedance then appears as the spectral density of the set of oscillators :

$$\mathrm{Re}\, Z(\omega) = \frac{\pi}{2} \lim_{\varepsilon \to 0} \left(\sum_{m=1}^{\infty} Z_m \omega_m \delta(\omega - \omega_m) \right) \tag{1}$$

where $Z_m = \sqrt{L_m / C_m}$ is the mode impedance.

In this decomposition of the impedance, the series capacitance C_0 of $Z(\omega)$[1]

$$C_0 = \left(\lim_{\omega \to 0} j\omega Z(\omega) \right)^{-1} = C_s + C,$$

corresponding to the zero-frequency mode is singled out and it will play a particular role hereafter.

The voltage source V is easily incorporated in this description of the environment of the junction. It is modelled by an infinitely large capacitor $\mathcal{C}$ with an infinitely large charge $\mathcal{Q}$ such that $V = \mathcal{Q}/\mathcal{C}$. This capacitor $\mathcal{C}$ is connected in series with C_0 so it is equivalent to having only C_0 (which is possibly infinite too) charged up to

$$Q_0 = C_0 V + Q^*, \tag{2}$$

where Q^* is an initial condition constant.

2. Description of tunneling

We now turn to the description of tunneling through the pure tunnel element that we have introduced in the previous section. We introduce the flux Φ_T and the charge Q_T of the tunnel element :

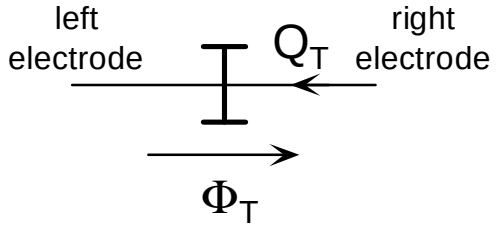

Electrons tunneling through the barrier will be handled in a perturbative approach. The idea is that if the two sides of the junction were far away, the appropriate Hamiltonian for the quasiparticle part of the system would simply be the sum of the Hamiltonians H_{qp}^L and H_{qp}^R describing the excitation states of the left and right electrode respectively

$$H_{qp}^{tot} = H_{qp}^L + H_{qp}^R$$

$$H_{qp}^L = \sum_{\ell,\sigma} \varepsilon_\ell a_{\ell\sigma}^\dagger a_{\ell\sigma} \qquad\qquad H_{qp}^R = \sum_{r,\sigma'} \varepsilon_r b_{r\sigma'}^\dagger b_{r\sigma'}$$

[1] This capacitance is often noted C_Σ in the literature. We prefer to use here C_0 for coherence of notation.

The operators $a^{\dagger}_{\ell\sigma}$ and $a_{\ell\sigma}$ ($b^{\dagger}_{r\sigma'}$ and $b_{r\sigma'}$) are the creation and annihilation operators for quasiparticles of spin σ in the eigenstate ℓ (spin σ' and eigenstate r) of the unperturbed Hamiltonian H_L (H_R, respectively).

When electrons are allowed to tunnel between the two electrodes, we simply add a coupling operator of the form [4]

$$\mathcal{H}_T = \sum_{\ell,r,\sigma} \mathrm{e}^{i\varphi_T} T_{\ell r} a_{\ell\sigma} b^{\dagger}_{r\sigma} + h.c.$$

where ℓ and r are used to index states to the left and right side of the barrier, σ is the spin index, and φ_T is the phase across the tunnel element. This coupling operator is called the "tunneling Hamiltonian"[2]. This Hamiltonian couples states of the system differing by one electron transferred through the barrier. For example, acting on a given state of the system, the $a_{\ell\sigma} b^{\dagger}_{r\sigma}$ term destroys a quasiparticle on the left side and creates a new one on the right side. We suppose that the factor $T_{\ell r}$ which measures the strength of the coupling is independent of spin (no magnetic impurities in the barrier). The $\mathrm{e}^{i\varphi_T}$ factor is an operator that shifts Q_T by e, implementing the transfer of the charge $-e$ of the electron. From the commutation relation between the tunnel element's electromagnetic operators Q_T and φ_T we have

$$\mathrm{e}^{-i\varphi_T} Q_T \mathrm{e}^{i\varphi_T} = Q_T + e\,.$$

We see here how the tunneling Hamiltonian couples electromagnetic and quasiparticles degrees of freedom.

In principle the $T_{\ell r}$ can be calculated from the knowledge of the wavefunctions on both sides of the junctions and of the barrier geometry. In practice, we cannot and we do not want to reach such a microscopic description of our systems. We rather try to describe our systems using a few macroscopic phenomenological parameters. We will see that such a macroscopic description is possible for our tunnel junctions : all we need to know is a single phenomenological parameter which is proportional to the second moment of the $T_{\ell r}$ distribution versus energy. Thus, contrarily to what one would think at first glance, our predictive power is not reduced to zero by this lack of microscopic knowledge.

a) DOMAIN OF VALIDITY, APPROXIMATIONS

The description of tunneling adopted here is based on the hypothesis that the states in the left and right electrode are not affected by the coupling term. This is evidently a limit of very weak

---

[2] This denomination can be misleading because, as we explained in sec. A.3, a Hamiltonian can only be written for the total system (junction + environment). By analogy with the classical description given in sec. A.3, we would rather call the coupling operator a (non-diagonal) energy operator. The coupling operator really becomes "a Hamiltonian" (*i.e.* part of the total Hamiltonian) after the elimination of superfluous variables in the total energy of the system has been performed.

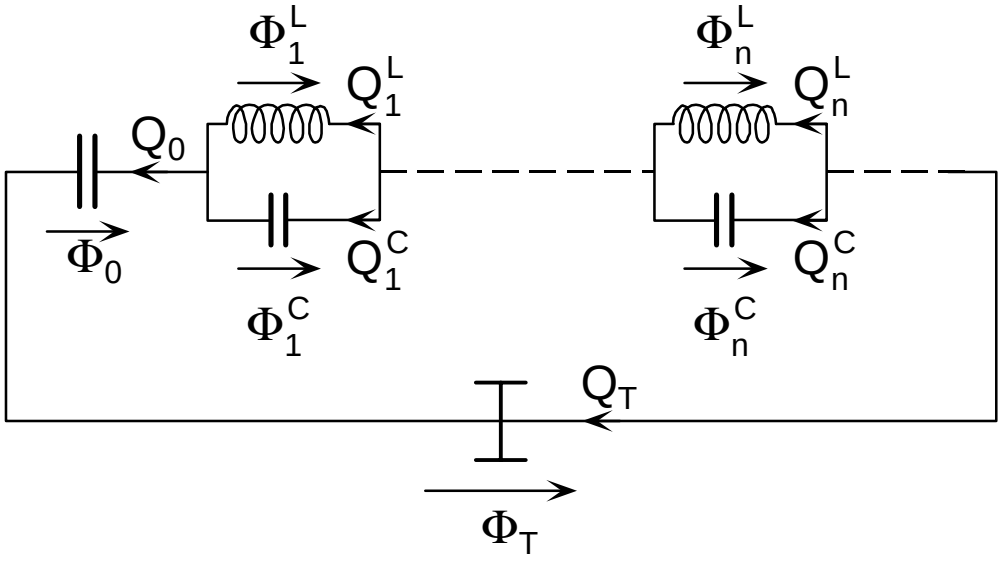

Fig. 3. *Convention of orientation used for the charges and fluxes.*

coupling. This weak coupling hypothesis allows the use of the Fermi golden rule to evaluate transitions induced by $\mathcal{H}_T$. This approach is well suited for our junctions but it would not be applicable to barriers of even moderate transparency.

3. Hamiltonians for the electromagnetic environment + tunnel junction system

Following the prescriptions we gave in §A.3 we write the total energy operator of the junction + environment system as a function of the fluxes and charges of all the branches

$$E = \frac{Q_0^2}{2C_0} + \sum_{m=1}^{\infty} \frac{\left(Q_m^C\right)^2}{2C_m} + \frac{\left(\Phi_m^L\right)^2}{2L_m} + \mathcal{H}_T + H_{qp}^{tot}$$

where the Q^C's refer to charges of the capacitor branches and Φ^L's to fluxes of the inductor branches of the oscillators. We will transform this energy into an Hamiltonian H for the system by eliminating superfluous variables.

a) KIRCHHOFF'S LAWS

For the orientations specified by Fig. 3, Kirchhoff's laws yield

$$
\begin{aligned}
Q_T(t) &= -Q_m^C(t) - Q_m^L(t) \qquad (\forall m) \\
Q_T(t) &= -Q_0(t) + Q_0(0) \\
\Phi_m^C(t) &= \Phi_m^L(t) \qquad (\forall m) \\
\Phi_T(t) &= \Phi_0(t) + \sum_{m=1}^{\infty} \Phi_m^L(t) + Constant
\end{aligned}
\tag{3}
$$

where Φ_T and Q_T refer to the tunnel element and Φ_0 and Q_0 refer to the source C_0. We have supposed that at $t = 0$, when the source is connected, the oscillators were not excited. The initial value $Q_0(0)$ of the charge Q_0 of the source capacitor is fixed by Eq. (2).

b) First form of the Hamiltonian

By using the third and fourth Kirchhoff equation we can write the Hamiltonian of the system as

$$H = H_{em} + H_T + H_{qp}$$

where

$$
\begin{aligned}
H_{em} &= \frac{Q_0^2}{2C_0} + \sum_{m=1}^{\infty} \frac{\left(Q_m^C\right)^2}{2C_m} + \frac{\left(\Phi_m^C\right)^2}{2L_m} \\
H_T &= \sum_{\ell,r,\sigma} \mathrm{e}^{i\varphi} T_{\ell r} a_{\ell\sigma} b_{r\sigma}^{\dagger} + h.c.
\end{aligned}
$$

Note that according to the fourth Kirchhoff equation, the phase $\varphi_T = e\Phi_T/\hbar$ in the tunneling Hamiltonian has been replaced by the operator

$$\varphi = \sum_{n=0}^{\infty} \varphi_n$$

where the $\varphi_n = e\Phi_n^C/\hbar$ are the phases across the capacitors, conjugate to the charges Q_n^C. We see that with this choice, only the quantities pertaining to the capacitors are left, those relative to the inductors and the tunnel element have been eliminated. The Hamiltonian H_{em} is that of harmonic oscillators, plus a quadratic term in Q_0. With this writing of the Hamiltonian, an eigenstate of the environment is specified by giving the occupation numbers N_m of the oscillators and Q_0. An eigenvector of the environment will be noted

$$|\psi_{env}\rangle = |Q_0\rangle |N_1, N_2, \ldots, N_m, \ldots\rangle$$

It is sometimes practical to use the bosonic creation and annihilation operators $c_n^{\dagger}$ and c_n of the harmonic oscillators. They are given by

$$
\begin{aligned}
\frac{1}{\sqrt{2}}\left(c_n + c_n^{\dagger}\right) &= \frac{1}{\sqrt{2r_n}}\,\varphi_n \\
\frac{i}{\sqrt{2}}\left(c_n^{\dagger} - c_n\right) &= \sqrt{2r_n}\; k_n
\end{aligned}
\tag{4a}
$$

where

$$r_n = \frac{\pi Z_n}{R_K}, \qquad Z_n = \sqrt{\frac{L_n}{C_n}} \tag{4b}$$

and where $R_K = h/e^2$ is the quantum of resistance. Using these operators, the Hamiltonian of the environment can be written

$$H_{em} = \frac{Q_0^2}{2C_0} + \sum_{n=1}^{\infty} h_n$$

where

$$h_n = \hbar\omega_n\left(N_n + \tfrac{1}{2}\right), \qquad N_n = c_n^\dagger c_n\,, \qquad \omega_n = 1/\sqrt{L_n C_n}\,. \tag{4c}$$

c) Other choice of variables for the Hamiltonian

To illustrate the fact that the expression of the Hamiltonian is not unique, let us indicate another simple and interesting choice of variables. Elimination is now performed using the first and second lines of the Kirchhoff laws (3). We obtain

$$H = H_{em} + H_T + H_{qp}$$

where

$$H_{em} = \frac{\left(Q_0(0) - Q_T\right)^2}{2C_0} + \sum_{m=1}^{\infty} \frac{\left(Q_T - Q_m^L\right)^2}{2C_m} + \frac{\left(\Phi_m^L\right)^2}{2L_m}$$

$$H_T = \sum_{\ell,r,\sigma} \mathrm{e}^{i\varphi_T} T_{\ell r} a_{\ell\sigma} b_{r\sigma}^\dagger + h.c.$$

Here, along with the operators Q_T and φ_T of the tunnel element, only the quantities pertaining to the inductors are left. The Hamiltonian H_{em} is that of harmonic oscillators shifted by Q_T, plus a quadratic term in Q_T-$Q_0(0)$. An eigenstate of the environment would still be given by a ket of the same form as in the previous section

$$|\psi_{env}\rangle = |Q_T\rangle|N_1, N_2, \ldots, N_m, \ldots\rangle$$

but the charge factor now has a different meaning.

If the squares are expanded in the latter Hamiltonian H_{em}, one obtains after factorisation of linear and quadratic terms in Q_T

$$H_{em} = \frac{Q_0(0)^2}{2C_0} + \sum_{m=1}^{\infty}\left[\frac{\left(Q_m^L\right)^2}{2C_m} + \frac{\left(\Phi_m^L\right)^2}{2L_m}\right] - Q_T\left[\frac{Q_0(0)}{C_0} + \sum_{m=1}^{\infty}\frac{Q_m^L}{C_m}\right] + Q_T^2\sum_{m=0}^{\infty}\frac{1}{2C_m}$$

Besides the constant $Q_0(0)^2/2C_0$, we recognise the Hamiltonian of the oscillators, a term of the form $-Q_T\mathcal{U}$ (where $\mathcal{U}$ is a voltage) and an effective charging energy. The voltage $\mathcal{U}$ can be decomposed as $\mathcal{U} = V_0 + U$, the sum of the static voltage $V_0 = Q_0(0)/C_0$ and the fluctuating total voltage across the oscillators $U = \sum_{n=1}^{\infty} Q_n^L/2C_n$. The effective charging energy itself can be re-interpreted as the bare charging energy of the junction, owing to the relation :

$$\sum_{m=0}^{\infty}\frac{1}{C_m} = \frac{1}{C_0} + \sum_{m=1}^{\infty}\frac{1}{C_m} = \frac{1}{C_0} + \frac{2}{\pi}\int_0^{\infty} d\omega\, \mathrm{Re}\, Z(\omega) = \frac{1}{C}$$

where C is the capacitance of the sole junction. Thus, dropping the constant, we rewrite

$$H_{em} = \sum_{n=1}^{\infty} h_n - Q_T\mathcal{U} + \frac{{Q_T}^2}{2C}.$$

In this formulation, the coupling of the oscillators to the quasiparticles is due to two terms of the total Hamiltonian : H_T and $Q_T U$.

4. Tunneling rate, tunnel resistance of a junction

To illustrate the above considerations, we will now derive the tunneling rate of electrons through a junction in an arbitrary linear electromagnetic environment. As previously, if the circuit contains other tunnel junctions, we treat them as capacitors. Thus, our calculation will fail to describe tunnel events occurring simultaneously on several junctions[3]. The tunneling rate is then used to compute the *I-V* characteristic of a normal-metal junction.

a) Calculation of the tunneling rate

We will use here the second form of the Hamiltonian given in Sec. 3.c above, where we keep the variables φ_T and Q_T of the tunnel element as independent degrees of freedom. A state of the total system writes

$$\begin{aligned}|\Psi\rangle &= |em\rangle\,|qp_L\rangle\,|qp_R\rangle \\ &= |Q_T\rangle\,|N_1, N_2, \ldots, N_m, \ldots\rangle\,|\ldots, n_p^L, \ldots\rangle\,|\ldots, n_q^R, \ldots\rangle\end{aligned}$$

where $n^{L,R} \in \{0,1\}$ are the occupation numbers of the quasiparticle states in the left and right electrode.

The rate of electron transfer through the junction is given by Fermi's golden rule

---

[3] These events involve higher orders of the tunneling Hamiltonians and they can be neglected for our purpose.

$$\Gamma_{i\to f} = \frac{2\pi}{\hbar}\left|\langle f|H_T|i\rangle\right|^2 \delta\left(E_f - E_i\right)$$

where $|i\rangle$ and $|f\rangle$ are the initial and final state of the system and where $E_{i,f}$ are the total energies (electromagnetic plus quasiparticle) of the initial and final states. Using the decomposition of the states $|i\rangle$,$|f\rangle$ into electromagnetic and quasiparticle degrees of freedom we write

$$\langle f|H_T|i\rangle = \langle f_{em}|e^{i\varphi_T}|i_{em}\rangle\langle f_{qp}|T|i_{qp}\rangle + \langle f_{em}|e^{-i\varphi_T}|i_{em}\rangle\langle f_{qp}|T^\dagger|i_{qp}\rangle$$

where the operator

$$T = \sum_{\ell,r,\sigma} T_{\ell r} a_{\ell\sigma} b^\dagger_{r\sigma}$$

acts only on the quasiparticle space.

Let us now compute the rate for an electron going from the left electrode to the right electrode. The $T^\dagger$ term does not contribute since it transfers in the wrong direction. The total rate is obtained by summing over all the possible initial and final states

$$\vec{\Gamma} = \frac{2\pi}{\hbar}\sum_{i,f}\left|\langle f_{em}|e^{i\varphi_T}|i_{em}\rangle\right|^2 \times \left|\langle f_{qp}|T|i_{qp}\rangle\right|^2 \delta\left(E_i^{em} + E_i^{qp} - E_f^{em} - E_f^{qp}\right)$$

As already mentioned, $e^{i\varphi_T}$ shifts Q_T by e, thus Q_{Tf} must equal $Q_{Ti}+e$ for the rate not to vanish. At zero temperature the oscillators are in their ground state. In the case of experiments with nanojunctions the usual electromagnetic environments are such that the dominant $\langle f_{em}|e^{i\varphi_T}|i_{em}\rangle$ term is the one where all the oscillators remain in the ground state[4]. In this simple case we can calculate

$$\Delta E^{em} = E_f^{em} - E_i^{em} = -\frac{e\left(C_0 V + Q^* - Q_i\right)}{C_0} + \frac{e^2}{2C_0}$$

which simply reduces to $\Delta E^{em} = -eV$ when $C_0 = \infty$.

The factor involving T can be rewritten using the Fermi functions $f_{L,R}$ giving the occupancy of the energy levels as a function of the temperature

$$\left|\langle f_{qp}|T|i_{qp}\rangle\right|^2 = \sum_{\ell,r,\sigma}|T_{\ell r}|^2 f_L(\varepsilon_\ell)\left(1 - f_R(\varepsilon_r)\right)$$

thus,

---

[4] The case of arbitrary impedance and temperature can also be treated exactly. See for instance Ref. 5. The result is that the tunneling rate can be expressed as

$$\vec{\Gamma} = \frac{1}{e^2 R_T}\iint f_R(\varepsilon)\left(1 - f_L(\varepsilon')\right)P(\varepsilon - \varepsilon' - \Delta E^{em})\,d\varepsilon d\varepsilon'$$

where $P(E)$ is the probability of transfering the energy E to the electromagnetic environment. The function $P(E)$ can be calculated from the impedance and the temperature.

$$\vec{\Gamma} = \frac{2\pi}{\hbar} \sum_{\ell,r,\sigma} |T_{\ell r}|^2 f_L(\varepsilon_\ell)\big(1 - f_R(\varepsilon_r)\big)\delta(\varepsilon_\ell - \varepsilon_r - \Delta E^{em})$$

This summation will be dominated by a small fraction of $T_{\ell r}$ terms, those corresponding to pairs of quasiparticle states on both sides which have a strong overlap under the barrier. To go further we replace the distribution $|T_{\ell r}|^2$ by its average value $|T|^2$ which we suppose independent of energy[5] and we integrate over the energy levels:

$$\begin{aligned}
\vec{\Gamma} &= \frac{2\pi}{\hbar}|T|^2 g \iint \rho_L(\varepsilon)\rho_R(\varepsilon') f_L(\varepsilon)\big(1 - f_R(\varepsilon')\big)\delta(\varepsilon - \varepsilon' - \Delta E^{em})\mathrm{d}\varepsilon\mathrm{d}\varepsilon' \\
&= \frac{2\pi}{\hbar}|T|^2 g \int \rho_L\big(\varepsilon + \Delta E^{em}\big)\rho_R(\varepsilon) f_L\big(\varepsilon + \Delta E^{em}\big)\big(1 - f_R(\varepsilon)\big)\mathrm{d}\varepsilon \\
&= \frac{2\pi}{\hbar}|T|^2 g \rho_L^0 \rho_R^0 \int f\big(\varepsilon + \Delta E^{em}\big)\big(1 - f(\varepsilon)\big)\mathrm{d}\varepsilon \\
&= \frac{1}{e^2 R_T} \int f\big(\varepsilon + \Delta E^{em}\big)\big(1 - f(\varepsilon)\big)\mathrm{d}\varepsilon
\end{aligned}$$

where the ρ are the quasiparticle density of states on each side, *not including spin degeneracy* and $g = 2$ is a factor accounting for the spin 1/2 of the electrons. To write the third expression we have replaced the densities of states by the densities ρ^0 at the Fermi level. In the last expression we have introduced the so-called tunnel resistance of the junction

$$R_T = \frac{R_K}{4\pi^2 |T|^2 g \rho_L^0 \rho_R^0} \tag{5}$$

where $R_K = h/e^2$ is the quantum of resistance. The name of "tunnel resistance" is justified below.

b) VOLTAGE BIASED JUNCTION, TUNNEL RESISTANCE.

When the environment impedance has no series capacitor ($C_0 = \infty$) a current can flow through the junction in response to the applied voltage V:

$$I = (-e)\big(\overleftarrow{\Gamma} - \vec{\Gamma}\big) = \frac{1}{eR_T} \int \big(f(\varepsilon - eV) - f(\varepsilon)\big)\mathrm{d}\varepsilon$$

The remaining integral involving Fermi functions on the right hand side gives eV, independently of the temperature. Thus we recover an "ohmic" law

$$I = \frac{V}{R_T}$$

for the normal tunnel junction, hence the name of "tunnel resistance" given to R_T. One should be cautious, however, that charge transport in a tunnel junction is different from that in a resistor, yielding in particular a different noise spectrum [8]. Also, it should be remembered

---

[5] This replacement corresponds to making the assumption of instantaneous tunneling [7].

that R_T was defined from averaged quantities. Thus, in sufficiently small systems, deviations from the ohmic law can appear, revealing microscopic details of the barrier. Our junctions however are very well described by this ohmic law.
As announced previously, we do not need to bother about the specific matrix elements of the tunnel Hamiltonian : we have obtained a single, easy to measure, macroscopic phenomenological parameter which correctly describes the junction for our purposes. This will remain valid even when the junction becomes superconducting, as we shall see later.

c) LINK WITH THE LANDAUER FORMULA

The latter result can be related to the similar one given by the Landauer formula, using the somewhat different language of scattering. This formula expresses the conductance of the junction in terms of transmission probability of incident wave packets [9]

$$G_T = \frac{e^2}{h} g \sum_{n=1}^{\mathcal{N}} \mathcal{T}_n$$

where $\mathcal{N}$ is the number of incident channels on the junction and $\mathcal{T}_n$ is the transmission of the n^{th} channel. Defining $\mathcal{T} = \Sigma \mathcal{T}_n / \mathcal{N}$, the average transmission per channel, and identifying $G_T = 1/R_T$, we obtain

$$\mathcal{N}\mathcal{T} = 4\pi^2 |T|^2 \rho_L^0 \rho_R^0$$

which links the average transmission coefficient to the average matrix element of T.

C. Josephson coupling

1. Tunnel coupling between two superconducting electrodes

When the two electrodes of a tunnel junction are in their superconducting ground state, the electrons form Cooper pairs, and there are no quasiparticles. This situation prevails at very low temperature and at voltages lower than $2\Delta/e$ where Δ is the superconducting gap (we assume that the electrodes are made from the same metal. The general case would not be much more complicated). The tunneling Hamiltonian which in the normal state coupled states of the system at the first order in perturbation theory, can now only couple states at higher orders since creation of quasiparticle is not energetically allowed. We want to evaluate the coupling induced by the tunneling Hamiltonian between two generic states $|A\rangle$ and $|B\rangle$ of the junction + environment system, limiting ourselves to the second order in H_T. We thus have to evaluate the sum over all intermediate states $|i\rangle$

$$W_{AB} = \sum_{i \neq A,B} \langle B|H_T|i\rangle \frac{1}{E_0 - E_i} \langle i|H_T|A\rangle \tag{6}$$

where $E_0 = (E_A + E_B)/2$. This expression [10] is valid as long as W_{AB} remains much smaller than the minimum value of the energy difference $(E_0 - E_i)$. In other words E_A and E_B must always be somewhat smaller than the smallest E_i which is twice the superconducting gap. Hence, this calculation of the coupling will only be valid in a sub-space of states of low energy. In the following, we will denote by P a projector onto this subspace. The projector can be formally written

$$P = \frac{1}{2i\pi} \oint_{\mathcal{C}} \frac{\mathrm{d}z}{z - H_0},$$

where $\mathcal{C}$ is a contour in the complex plane which encloses the part of the real axis on which lie the energies of the states we project onto, and H_0 is the Hamiltonian of the system without the perturbation (*i. e.* without the tunneling Hamiltonian).

In the remaining part of the chapter we will use the representation of the Hamiltonian of the junction in its electromagnetic environment which was introduced in Sec. B.3.b., where we use only the degrees of freedom of the capacitors. Similarly to what was done in the normal case, we write the tunnel Hamiltonian as $H_T = T e^{i\varphi} + T^\dagger e^{-i\varphi}$, where

$$\varphi = \sum_{n=0}^{\infty} \varphi_n$$
$$T = \sum_{\ell,r,\sigma} T_{\ell r} a_{\ell\sigma} b^\dagger_{r\sigma}$$

the φ_n being the phases of the capacitors of the environment.

Then for a given intermediate state $|i\rangle$ in the sum (6), we have:

$$\langle B|H_T|i\rangle \frac{1}{E_0 - E_i} \langle i|H_T|A\rangle =$$
$$\frac{1}{E_0 - E_i} \Big\{ \langle B|e^{i\varphi} T|i\rangle\langle i|e^{i\varphi} T|A\rangle + \langle B|e^{-i\varphi} T^\dagger|i\rangle\langle i|e^{-i\varphi} T^\dagger|A\rangle +$$
$$\langle B|e^{i\varphi} T|i\rangle\langle i|e^{-i\varphi} T^\dagger|A\rangle + \langle B|e^{-i\varphi} T^\dagger|i\rangle\langle i|e^{i\varphi} T|A\rangle \Big\}$$

The last two terms vanish unless $|A\rangle = |B\rangle$ in which case they give a contribution to the correction in energy of $|A\rangle$ due to the perturbation H_T. On the contrary the first two terms can only contribute when $|A\rangle \neq |B\rangle$ and they are responsible for the coupling. Each of these two terms transfers a charge of $2e$ through the junction, but not in the same direction ; they are complex-conjugated. We then write the energy denominator as a time integral :

$$\frac{1}{E_0 - E_i} = -\int_0^{+\infty} \exp\left[-\frac{(E_i - E_0)t}{\hbar} \right] \frac{\mathrm{d}t}{\hbar}.$$

which permits to rewrite W_{AB} as

$$W_{AB} = \langle B|H_J|A\rangle$$

where

$$H_J = -\int_0^{+\infty} \frac{\mathrm{d}t}{\hbar} \mathrm{e}^{\frac{Ht}{2\hbar}} \mathrm{e}^{i\varphi} T \mathrm{e}^{\frac{-Ht}{\hbar}} \mathrm{e}^{i\varphi} T \mathrm{e}^{\frac{Ht}{2\hbar}} + h.c. \tag{7a}$$

is called the Josephson Hamiltonian. As already mentioned, this expression of H_J is meaningful only in a subspace of low energy states. This writing has the great advantage that it can be factored into the contributions of the charge, oscillators and quasiparticles degrees of freedom. To perform this factorisation we decompose the states of the system into charge ($|Q_0\rangle$), oscillator ($|\Psi\rangle$) and quasiparticle ($|\Xi\rangle$) part, and the Hamiltonian H_0 into the corresponding parts :

$$H_0 = H^Q + H^\Psi + H^\Xi$$

$$H^Q = \frac{Q_0^2}{2C_0}$$

$$H^\Psi = \sum_{m=1}^{\infty} \frac{\left(Q_m^C\right)^2}{2C_m} + \frac{\left(\Phi_m^C\right)^2}{2L_m}$$

$$H^\Xi = H_{qp}^L + H_{qp}^R$$

The integrand of (7a) becomes a tensorial product

$$\left[\mathrm{e}^{\frac{H^Q t}{2\hbar}} \mathrm{e}^{i\varphi_0} \mathrm{e}^{\frac{-H^Q t}{\hbar}} \mathrm{e}^{i\varphi_0} \mathrm{e}^{\frac{H^Q t}{2\hbar}}\right] \otimes \left[\mathrm{e}^{\frac{H^\Psi t}{2\hbar}} \mathrm{e}^{i\tilde{\varphi}} \mathrm{e}^{\frac{-H^\Psi t}{\hbar}} \mathrm{e}^{i\tilde{\varphi}} \mathrm{e}^{\frac{H^\Psi t}{2\hbar}}\right] \otimes \left[\mathrm{e}^{\frac{H^\Xi t}{2\hbar}} T \mathrm{e}^{\frac{-H^\Xi t}{\hbar}} T \mathrm{e}^{\frac{H^\Xi t}{2\hbar}}\right] \tag{7b}$$

We have also decomposed the operator φ into $\varphi_0+\tilde{\varphi}$ which act on the zero-frequency and finite-frequency modes ($\tilde{\varphi} = \sum_{n=1}^{\infty} \varphi_n$) of the environment, respectively.

2. Josephson's calculation

We will first recover Josephson's results [11]. This calculation of the Josephson coupling corresponds to the case where the environmental degrees of freedom (including charge) can be neglected and when only the quasiparticles need to be considered. Furthermore, since we couple states with no quasiparticles, there is no energy in the final and initial states. Thus we can drop the $\exp(Ht/2\hbar)$ terms, and only one matrix element needs to be calculated :

$$H_J = -\mathrm{e}^{2i\varphi} |0\rangle\langle 0| \int_0^{+\infty} \frac{\mathrm{d}t}{\hbar} \langle 0|T \mathrm{e}^{\frac{-Ht}{\hbar}} T|0\rangle + h.c. \tag{8}$$

where $|0\rangle$ denotes the vacuum state for the quasiparticles. The vacuum state for the quasiparticles is also referred to as the BCS ground state. Inserting the closure relation, the integrand can be written

$$\sum_{\Xi_i} \langle 0|T|\Xi_i\rangle e^{\frac{-E_i t}{\hbar}} \langle \Xi_i|T|0\rangle. \tag{9}$$

Let us first compute the matrix elements

$$\langle 0|T|\Xi_i\rangle\langle \Xi_i|T|0\rangle$$

These matrix elements correspond schematically to the process described in Fig. 4. In the intermediate step we necessarily have created two excitations of the superconductors, one on each side. These excited states are obtained by applying the Bogoliubov fermionic quasiparticle operators on the vacuum of quasiparticles $|0\rangle$ [12]. We will note $\mathcal{L} = (\ell, \bar{\ell})$ (respectively, $\mathcal{R} = (r, \bar{r})$) a pair of time-reversed electronic states in the left (resp. right) electrode of the junction. In this notation, the index ℓ (r) of the electronic state incorporates

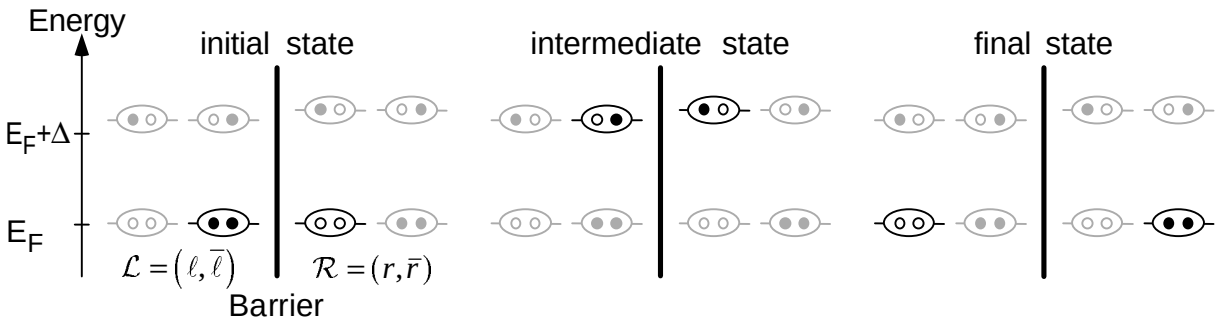

Fig. 4. *Schematic representation of the second order tunnel process responsible for the Josephson coupling in a superconducting tunnel junction. This coupling between ground states of the system results from the elastic transfer of two electrons across the junction. This transfer can be decomposed into two steps, corresponding to the sequential transfer of two electrons between two pairs of time reversed states* $\mathcal{L} = (\ell, \bar{\ell})$ *and* $\mathcal{R} = (r, \bar{r})$*, with the overline indicating the time-reversed state. In the diagram, ovals represent pairs of time-reversed quasi-electron states. In the ovals, a full (open) dot symbolises an occupied (empty) quasi-electron state. This representation corresponds to the projection of the BCS state on a state of given total number of electrons in the system. The four possible states of the two pairs involved in the process are drawn, their energy being indicated by their position on the vertical axis. The actual state of a pair is indicated by the use of black colour, while the other accessible states are dimmed. In this picture, the name of "Cooper pair" can only be given to a full or empty oval, while the half-occupied ovals are called "quasiparticle excitations" or broken Cooper pairs. In the first step of the transfer, a full pair breaks on the left side. One electron of the pair crosses the barrier and fills an empty electronic state on the right side : this breaks the empty pair on the right side. The resulting intermediate state has two quasiparticle excitations of opposite spin, one on each side. In the second step, the second electron crosses the barrier and recombines with its companion electron on the right side. Both pairs return to the ground state upon completion of this second transfer.*

both the indexing of the electronic trajectory and the electron spin and the overline indicates time-reversal symmetry. The Bogoliubov quasiparticle creation and annihilation operators on the left (resp., right) side for a quasiparticle in state p with energy ε_p are noted $\alpha_p^\dagger$ and α_p (respectively, $\beta_p^\dagger$ and β_p). These operators are related to the ordinary quasiparticle operators through the transformation

$$\begin{aligned} \alpha_\ell^\dagger &= u_{\mathcal{L}} a_\ell^\dagger - v_{\mathcal{L}} a_{\bar{\ell}} & \beta_r^\dagger &= u_{\mathcal{R}} b_r^\dagger - v_{\mathcal{R}} b_{\bar{r}} \\ \alpha_{\bar{\ell}}^\dagger &= u_{\mathcal{L}} a_{\bar{\ell}}^\dagger + v_{\mathcal{L}} a_\ell & \beta_{\bar{r}}^\dagger &= u_{\mathcal{R}} b_{\bar{r}}^\dagger + v_{\mathcal{R}} b_r \end{aligned} \tag{10}$$

involving the BCS u and v coherence factors.

In the first step of the process, under the action of the term of H_T containing $b_r^\dagger a_\ell$ on $|0\rangle$, an electron of the left side tunnels through the barrier. The intermediate state expressed in terms of Bogoliubov operators is $\alpha_{\bar{\ell}}^\dagger \beta_r^\dagger |0\rangle$ with an energy $\varepsilon_{\mathcal{L}}+\varepsilon_{\mathcal{R}}$. The projection of the state created by $b_r^\dagger a_\ell$ on this intermediate state yields $v_{\mathcal{L}}^* u_{\mathcal{R}}^*$ (we used anticommutation properties of the fermionic operators a and b).

In the second step, the electron $\bar{\ell}$ on the left crosses the barrier under the action of the $T_{\bar{\ell},\bar{r}} b_{\bar{r}}^\dagger a_{\bar{\ell}}$ term of H_T and recombines with the previous one to give the final state ($|0\rangle$). The action of $b_{\bar{r}}^\dagger a_{\bar{\ell}}$ on the intermediate state yields $v_{\mathcal{R}} u_{\mathcal{L}} |0\rangle$ (here again anticommutation rules were used). Finally we project onto $|0\rangle$, and collecting all the factors, this process gives:

$$T_{\ell,r} T_{\bar{\ell},\bar{r}} u_{\mathcal{L}} v_{\mathcal{L}}^* u_{\mathcal{R}}^* v_{\mathcal{R}} = \frac{|T_{\ell,r}|^2 \Delta^2}{4\varepsilon_{\mathcal{L}} \varepsilon_{\mathcal{R}}}.$$

To obtain the last expression we have made use of the relation

$$u_p v_p^* = (u_p v_p^*)^* = \frac{\Delta}{2\varepsilon_p}$$

and of the time-reversal symmetry of H_T.

We can now sum all the contributions to (9) coming from the different intermediate quasiparticle states, including spin index, with their proper energy-time exponential

$$\sum_{\ell,r,\sigma} \frac{|T_{\ell,r}|^2 \Delta^2}{4\varepsilon_{\mathcal{L}} \varepsilon_{\mathcal{R}}} \mathrm{e}^{-(\varepsilon_{\mathcal{L}} + \varepsilon_{\mathcal{R}})t/\hbar} \tag{11}$$

To go further, we replace the $|T_{\ell,r}|^2$ by their average value $|T|^2$ as in the case of the normal metal junction. Summation over all states is replaced by integration over energy with the BCS density of excited states

$$\rho(\varepsilon) = 2\rho_0 \frac{\varepsilon}{\sqrt{\varepsilon^2 - \Delta^2}}.$$

Here ρ_0 is, as previously, the normal-metal density of states at the Fermi level, *not including spin degeneracy*, and the factor of 2 is counting for the two branches of excitations. We can rewrite (11) as:

$$\Delta^2 g\rho_0^2|T|^2 \iint\limits_{\Delta\le\varepsilon_{\mathcal{L}},\varepsilon_{\mathcal{R}}\le\infty} \frac{d\varepsilon_{\mathcal{L}}d\varepsilon_{\mathcal{R}}\,\exp\left[-(\varepsilon_{\mathcal{L}}+\varepsilon_{\mathcal{R}})t/\hbar\right]}{\sqrt{\varepsilon_{\mathcal{L}}^2-\Delta^2}\sqrt{\varepsilon_{\mathcal{R}}^2-\Delta^2}},$$

where $g=2$ is the spin degeneracy of the intermediate state. The double integral factors itself and each factor yields $K_0(\Delta t/\hbar)$, where K_0 is the modified Bessel function of the second kind. We finally get for the integrand of (8):

$$\Delta^2 g\rho_0^2|T|^2 K_0^2(\Delta t/\hbar) \tag{12}$$

Thus, the Josephson Hamiltonian writes in this case

$$H_J = -e^{2i\varphi}|0\rangle\langle 0|\Delta g\rho_0^2|T|^2\int_0^{+\infty}\frac{\Delta dt}{\hbar}K_0^2(\Delta t/\hbar)+h.c.$$

The remaining integral yields $\pi^2/4$. This result is usually written (forgetting the projector on the vacuum of quasiparticles)

$$H_J = -\frac{E_J}{2}e^{2i\varphi}+h.c.=-E_J\cos 2\varphi$$

thereby defining the Josephson coupling energy E_J

$$E_J=\frac{\pi^2}{2}\Delta g\rho_0^2|T|^2. \tag{13}$$

a) AMBEGAOKAR-BARATOFF RELATION

By making use of (5), we obtain an important relation linking E_J and R_T, the tunnel resistance of the junction defined in the normal-state :

$$E_J=\frac{h\Delta}{8e^2R_T}. \tag{14a}$$

This result is often expressed in a different way, using the current $I_0=2eE_J/\hbar$ which, we will see, is the critical current of the junction. The latter equation is then equivalent to

$$I_0=\frac{\pi}{2}\frac{\Delta}{eR_T} \tag{14b}$$

which is known as the Ambegaokar-Baratoff relation [13].

3. Effect of an electromagnetic environment on the Josephson coupling

a) CHARGE CONTRIBUTION

We now evaluate the charge factor of the integrand (7b).

$$e^{\frac{Q_0^2 t}{4C_0\hbar}} e^{i\varphi_0} e^{\frac{-Q_0^2 t}{2C_0\hbar}} e^{i\varphi_0} e^{\frac{Q_0^2 t}{4C_0\hbar}}$$

Inserting $e^{i\varphi_0}e^{-i\varphi_0}$ and $e^{-i\varphi_0}e^{i\varphi_0}$ on the left and on the right, respectively, and using the fact that $e^{i\varphi_0}$ translates Q_0 by e, we can rewrite this as

$$e^{i\varphi_0} \exp\left\{\frac{t}{2C_0\hbar}\left[\frac{1}{2}(Q_0+e)^2 - Q_0^2 + \frac{1}{2}(Q_0-e)^2\right]\right\} e^{i\varphi_0}$$

Working out the algebra the operator Q_0 vanishes, yielding the simple result

$$e^{2i\varphi_0} e^{\frac{E_C t}{\hbar}}$$

where $E_C = e^2/2C_0$ is the charging energy of a single electron on the capacitance C_0. This charging energy is non zero only when $Z(\omega)$ has a finite series capacitance. This latter case corresponds to a circuit having an isolated island connected to the junction, E_C being the charging energy of a single electron on this island.

The latter result could have been obtained more simply by noting that the electrostatic contribution to the energy denominators of (6) gives, whatever the states considered, the constant

$$E_0^Q - E_i^Q = \frac{e^2}{2C_0} = E_C.$$

b) MODIFICATION OF THE COUPLING IN PRESENCE OF AN ISLAND

The result of the last paragraph, along with (12) can be used to evaluate the Josephson Hamiltonian (7) in the absence of oscillators in the environment. The presence of an island simply amounts to a renormalization of E_J :

$$E_J = E_J^0 F\left(\frac{E_C}{\Delta}\right) \tag{15}$$

where the notation E_J^0 is used for the Ambegaokar-Baratoff value of the Josephson coupling energy (14a) and where the function F is defined by

$$F(x) = \frac{4}{\pi^2}\int_0^{+\infty} dy\, e^{xy} K_0^2(y). \tag{16}$$

This Laplace transform of K_0^2 can be expressed in terms of special functions :

$$F(x) = \frac{2x}{\pi^2}\, {}_3F_2\left(1,1,1;\tfrac{3}{2},\tfrac{3}{2};\tfrac{x^2}{4}\right) + \frac{2}{\pi}K\left(\tfrac{x^2}{4}\right)$$

where ${}_3F_2$ is the generalised hypergeometric function and K is the complete elliptic integral of the first kind.

A numerical evaluation of F is plotted in Fig. 5. We see that it diverges for $x = 2$. In this region however, the hypotheses for the calculation of the coupling are not satisfied any longer : the energy of the intermediate states is not far enough from the energy of the initial and final states. Thus, quite paradoxically, in presence of charging effects the Josephson coupling energy is **enhanced** as compared to the Ambegaokar-Baratoff value. This is because in this case the electrostatic energy of the intermediate step is lowered due to the concavity of the electrostatic potential, and it reduces the energy denominator of (6).

We can evaluate the actual correction to the Josephson coupling brought by the charging in our experiments. In the experiments we have conducted we had $E_C \lesssim 1\,\mathrm{K}$ and Δ was the gap of aluminum which is about 2 K. The argument of F thus remained under 0.5. The corresponding enhancement of E_J is then of the order of 10-15%.

The result we obtain here extends a calculation previously published by Matveev *et al.* [14].

c) ELECTROMAGNETIC CONTRIBUTION

We now decompose the oscillator factor in (7b) into a product of factors corresponding to each oscillator :

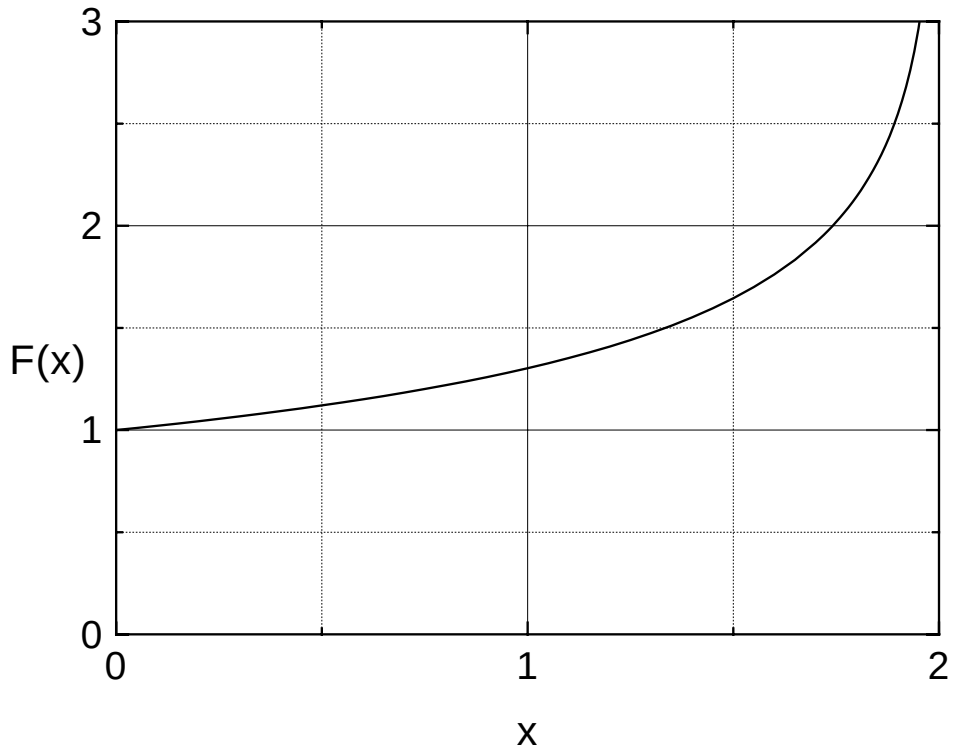

Fig. 5. *function giving the renormalized Josephson coupling in presence of a charging energy term.*

$$\mathrm{e}^{\frac{H^{\Psi}t}{2\hbar}}\mathrm{e}^{i\tilde{\varphi}}\mathrm{e}^{\frac{-H^{\Psi}t}{\hbar}}\mathrm{e}^{i\tilde{\varphi}}\mathrm{e}^{\frac{H^{\Psi}t}{2\hbar}} = \prod_n \mathrm{e}^{\frac{h_n t}{2\hbar}}\mathrm{e}^{i\varphi_n}\mathrm{e}^{\frac{-h_n t}{\hbar}}\mathrm{e}^{i\varphi_n}\mathrm{e}^{\frac{h_n t}{2\hbar}} \tag{17}$$

where we have used the notations h_n and φ_n for the Hamiltonian and the phase of the n^{th} oscillator as defined by (4). Using the commutation rules of the bosonic creation and annihilation operators $c_n^{\dagger}$ and c_n of the harmonic oscillators, each factor in (17) can be transformed to

$$\mathrm{e}^{\frac{h_n t}{2\hbar}}\mathrm{e}^{i\varphi_n}\mathrm{e}^{\frac{-h_n t}{\hbar}}\mathrm{e}^{i\varphi_n}\mathrm{e}^{\frac{h_n t}{2\hbar}} = \mathrm{e}^{2i\varphi_n \mathrm{ch}\frac{\omega_n t}{2}}\mathrm{e}^{r_n \mathrm{sh}\omega_n t} \tag{18}$$

This expression cannot by used directly in the Josephson Hamiltonian because it would always diverge as $t \to +\infty$. This divergence is an artefact of the calculation because we have allowed states with an arbitrary number of photons, which is in contradiction with the hypothesis of coupling only states of low energy. To satisfy this hypothesis, we must impose that all the oscillators of frequency higher than a cut-off frequency $\omega_c \ll \Delta/\hbar$ are in their ground state in both the final and initial states. For these oscillators, the factors we must compute in (17) reduce to

$$\begin{aligned}\left\langle 0_n \left| \mathrm{e}^{\frac{h_n t}{2\hbar}}\mathrm{e}^{i\varphi_n}\mathrm{e}^{\frac{-h_n t}{\hbar}}\mathrm{e}^{i\varphi_n}\mathrm{e}^{\frac{h_n t}{2\hbar}} \right| 0_n \right\rangle &= \left\langle 0_n \left| \mathrm{e}^{i\varphi_n}\mathrm{e}^{\frac{-h_n t}{\hbar}}\mathrm{e}^{i\varphi_n} \right| 0_n \right\rangle \\ &= \left\langle 0_n \left| \mathrm{e}^{2i\varphi_n} \right| 0_n \right\rangle \mathrm{e}^{r_n\left(1-\mathrm{e}^{-\omega_n t}\right)}\end{aligned} \tag{19}$$

where $|0_n\rangle$ is the vacuum of photons for the n^{th} oscillator. For the oscillators of low frequency ($\omega < \omega_c$), Eq. (18) can be linearized in $\omega_n t$ for the calculation of the Josephson Hamiltonian because $K_0^2(\Delta t/\hbar)$ then decreases on a much shorter time scale. This amounts to stopping the integration over time at a few $\hbar/\Delta$ to remove the divergence caused by an arbitrarily high number of photons in these low frequency modes. At this point one notices that the same linear terms are obtained by linearizing (19), so that this high frequency term incidentally also gives the correct answer for the low frequency oscillators. Another way to see this result is to say that it simply corresponds to neglecting the small energy E_0 in the denominator of (6), which is a good approximation as long as $E_0 \ll 2\Delta$. Taking advantage of these remarks, (17) can be written

$$P\prod_n \mathrm{e}^{2i\varphi_n}\mathrm{e}^{r_n\left(1-\mathrm{e}^{-\omega_n t}\right)} P \approx P\mathrm{e}^{2i\tilde{\varphi}} P \exp\left[\sum_n r_n\left(1-\mathrm{e}^{-\omega_n t}\right)\right]$$

Going to the continuous limit, the discrete sum on modes is replaced by an integral over frequency (see Eq. (1)) :

$$\sum_n r_n\left(1-\mathrm{e}^{-\omega_n t}\right) \to G(t) = 2\int_0^{\infty} \mathrm{d}\omega \frac{\left(1-\mathrm{e}^{-\omega t}\right)}{\omega}\frac{\mathrm{Re}\, Z(\omega)}{R_K} \tag{20}$$

and (17) writes

$$P\mathrm{e}^{2i\tilde{\varphi}}P\mathrm{e}^{G(t)}.$$

The function $G(t)$ we have found here is closely related to the phase-phase correlation function $J(t)$ introduced in Refs. 4 & 5 in the context of the Coulomb blockade of tunneling. More precisely, we have $G(t)= -J(-it)$.

d) MODIFICATION OF THE JOSEPHSON HAMILTONIAN BY THE ENVIRONMENT

Collecting results obtained in a) and c) one can write the restriction of the Josephson Hamiltonian to the subspace of low-energy states in the form:

$$PH_JP = -E_J\ P\cos 2\varphi P$$

where P is the projector onto this subspace and where E_J is a renormalized Josephson coupling energy :

$$E_J = E_J^0\,\frac{4}{\pi^2}\int_0^{+\infty}\frac{\Delta \mathrm{d}t}{\hbar}\exp\left[E_C t/\hbar + G(t)\right]K_0^2(\Delta t/\hbar) \qquad (21)$$

where $G(t)$ is defined by (20) and E_J^0 is the Ambegaokar-Baratoff value of the coupling (14).

e) SINGLE-OSCILLATOR ENVIRONMENT

In this paragraph we apply the result we have just obtained to the case where the environment consists of a single oscillator. In this case the function $G(t)$ simply writes

$$G(t) = \frac{\pi Z}{R_K}\left(1-\mathrm{e}^{-\omega t}\right)$$

where $Z=(L/C)^{1/2}$ and $\omega=(LC)^{-1/2}$. The Josephson coupling is given by (21) which now writes

$$E_J = E_J^0\,\frac{4}{\pi^2}\int_0^{+\infty}\frac{\Delta \mathrm{d}t}{\hbar}\exp\left[\frac{\pi Z}{R_K}\left(1-\mathrm{e}^{-\omega t}\right)\right]K_0^2(\Delta t/\hbar)\,.$$

Since K_0^2 acts as a window of width $\hbar/\Delta$ in the integral, this expression admits simple limits in the cases where $\hbar\omega \ll \Delta$ or $\hbar\omega \gg \Delta$:

$$\frac{E_J}{E_J^0} = \begin{cases} F\left(\pi Z/R_K\right) & \text{if } \hbar\omega \gg \Delta \\ 1 & \text{if } \hbar\omega \ll \Delta \end{cases}$$

The function F that appears here is that which gives the renormalization of the Josephson coupling by a charging energy (16). Reciprocally, here, the effect of the environmental impedance can be interpreted as a renormalization of the charging energy of the circuit.

f) APPLICATION TO THE SINGLE ELECTRON TRANSISTOR

To illustrate further the calculation we have made, we now apply it to the case of a superconducting single electron transistor connected in series with a resistor (Fig. 6a). This is a

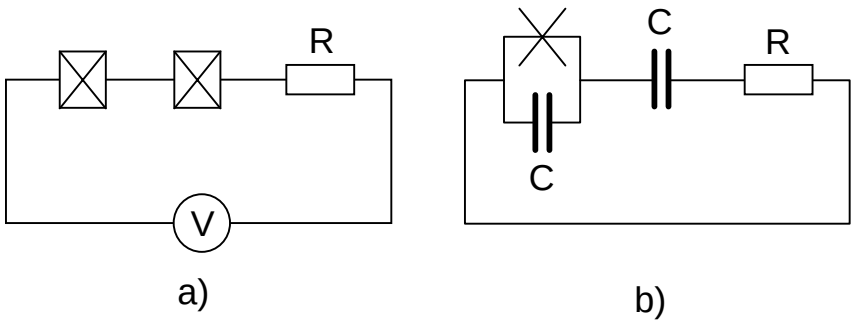

Fig. 6. *a) Realistic description of the electromagnetic environment of the superconducting single electron transistor in some of our experiments. b) Schematic representation of the impedance seen by a pure tunnel element (symbolised by the cross) of the transistor. The symbol C designates the capacitance of the junctions and R is the resistance of the normal-metal leads of the transistor.*

realistic description of the configuration we had in several of our experiments (see Chap. V&VI). The electromagnetic environment seen by each junction of the transistor is well described in a lumped element model. A pure tunnel element of the transistor sees the capacitance of its junction in parallel with the series combination of the capacitance of the other junction and the resistance (Fig. 6b).

The impedance $Z(\omega)$ seen by the pure tunnel element is then

$$Z(\omega) = \frac{R - i\left(R^2 C\omega + 2/C\omega\right)}{4 + (RC\omega)^2}. \tag{22}$$

The real part of this impedance is

$$\mathrm{Re}\, Z(\omega) = \frac{R}{4 + (RC\omega)^2}$$

and the series capacitance, which is the capacitance of the island, is given by

$$C_0 = \left(\lim_{\omega \to 0} i\omega Z(\omega)\right)^{-1} = 2C.$$

For the impedance (22) the function $G(t)$ can be expressed in terms of the special functions cosine-integral and sine-integral

$$G(t) = \frac{R}{2R_K}\left[\gamma + \mathrm{Log}\frac{t}{\tau} - \mathrm{ci}\frac{t}{\tau}\cos\frac{t}{\tau} + \left(\frac{\pi}{2} - \mathrm{si}\frac{t}{\tau}\right)\sin\frac{t}{\tau}\right]$$

where $\gamma = 0.577216\ldots$ is Euler's constant and where

$$\tau = \frac{\pi}{2}\frac{R}{R_K}\frac{\hbar}{E_C},$$

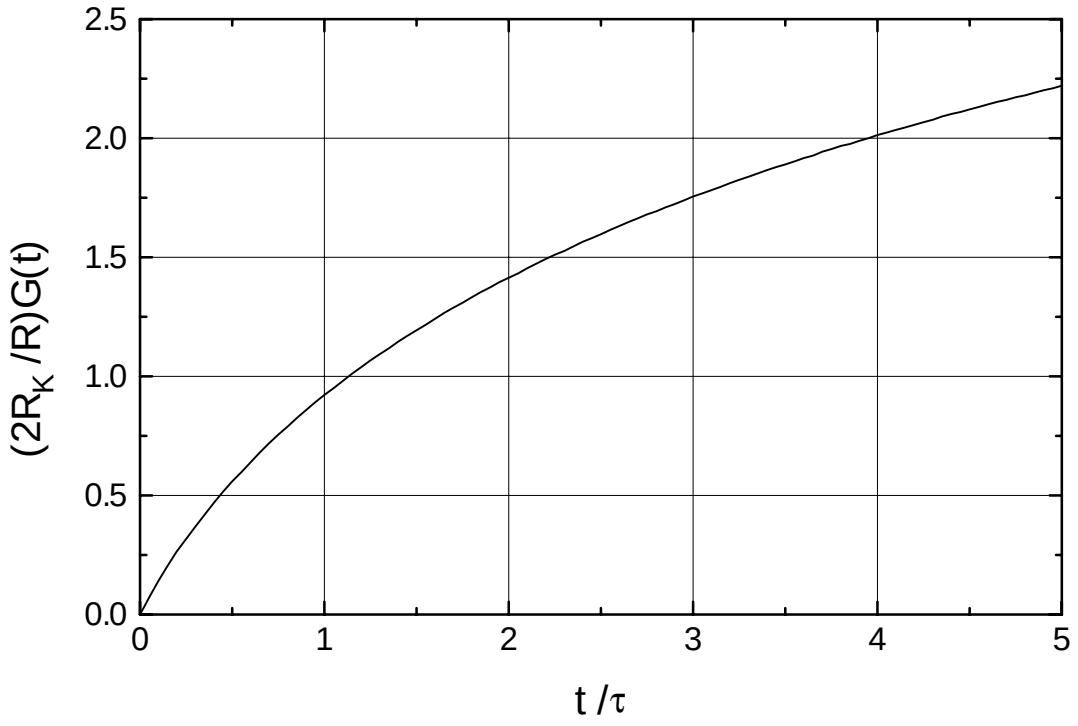

Fig. 7. *Plot of the function G(t) for the impedance seen by a tunnel element in the superconducting single electron transistor.*

E_C being defined as $e^2/2C_0$, the charging energy of an electron on the island of the transistor. A plot of the function $G(t)$ is given in Fig. 7. The renormalized Josephson energy can then be calculated numerically for any value of R/R_K and E_C/Δ (see Fig. 8). The value of E_J/E_J^0 for R=0 is determined by the plain charging effect renormalization $F(E_C/\Delta)$ (see Sec. 3.a & b, Eq. (15)). The saturation of the renormalized coupling observed at large values of R is also easily explained : for $\Delta R \gg R_K E_C$ we can make a short-time expansion of $G(t)$ in (21). For this purpose we can go back to the definition (20) and linearize the exponential

$$G(t) = 2\int_0^\infty \mathrm{d}\omega \frac{\left(1-\mathrm{e}^{-\omega t}\right)}{\omega} \frac{\mathrm{Re}\, Z(\omega)}{R_K}$$
$$\approx \frac{2t}{R_K}\int_0^\infty \mathrm{Re}\, Z(\omega)\mathrm{d}\omega = \frac{2t}{R_K}\frac{\pi}{4C} = \frac{tE_C}{\hbar}.$$

Thus, for large resistances ($\Delta R \gg R_K E_C$) we obtain a Josephson coupling

$$E_J = E_J^0\, F\left(2E_C/\Delta\right)$$

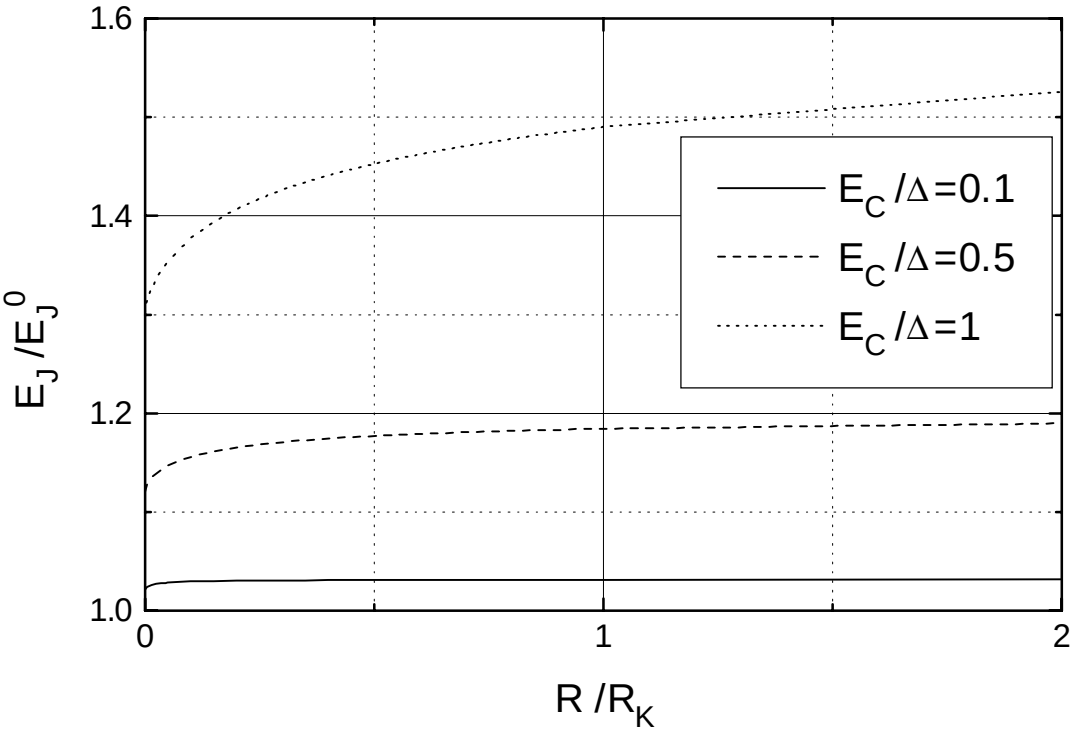

Fig. 8. *Renormalization of the Josephson coupling energy (with respect to the Ambegoakar-Barratoff value E_J^0) as a function of the resistance in series with the transistor, for different values of the charging energy. The value at R = 0 is given by the function $F(E_C/\Delta)$ previously defined (Eq. (16)) while the asymptotic value is $F(2E_C/\Delta)$.*

similar to the zero-resistance value but with a doubled effective charging energy. The short-time expansion of $G(t)$ corresponds to the limit where the capacitance of the second junction of the transistor does not have time to change its charge during the virtual state of the Josephson tunneling process, due to the *RC* delay. The relevant charging energy is then that of a single junction, $e^2/2C$. This limit where only the capacitance of the junction counts is reminiscent of the "local rules" obtained in the context of Coulomb blockade for a normal-state junction [15]. Note that the high-resistance asymptotic value is not defined if $E_C > \Delta$ since F diverges for arguments greater than 2.

For most of the samples we fabricated, we had $E_C \leq \Delta/2$ and R/R_K in the 10^{-4}. In one experiment however, we had increased this resistance to $R/R_K \approx 1.5\%$. Combining this value with the measured ratio $E_C/\Delta = 0.29$, this gives a renormalization of E_J of about 8.5%.

Conclusion

In this chapter we have calculated the Josephson Hamiltonian for low-energy states of the junction + environment system in presence of an arbitrary environment impedance $Z(\omega)$. The

essential result of this chapter is that the form of the Josephson Hamiltonian originally computed by Josephson when $Z(\omega) = 0$ is preserved, with simply a renormalization of the Josephson coupling energy given by Eq. (21). For states of the environment of higher energy or for high charging energy, the perturbative approach we have used here fails. In these cases, it seems that the structure itself of the Josephson Hamiltonian is modified.

References for Chap. II

[1] see *e.g.* D. Pines and P. Nozières, *The theory of Quantum Liquids*, (Addison-Wesley, Menlo Park, 1966).

[2] A. O. Caldeira and A. J. Leggett, Ann. Phys. (N.Y.) **149**, 374 (1983).

[3] D. V. Averin and Yu. V. Nazarov, in *Single Charge Tunneling*, edited by H. Grabert and M. H. Devoret (Plenum, New York, 1992), Chap. 6.

[4] M. H. Devoret, D. Esteve, H. Grabert, G.-L Ingold, H. Pothier, and C. Urbina, Phys. Rev. Lett. **64**, 1824 (1990).

[5] G.-L. Ingold and Yu. V. Nazarov, in *Single Charge Tunneling*, edited by H. Grabert and M. H. Devoret (Plenum, New York, 1992), Chap. 2.

[6] H. Pothier, Ph.D. Thesis, Université Paris 6 (1991), unpublished.

[7] M. Büttiker and R. Landauer, Phys. Rev. Lett. **49**, 1739 (1982)

[8] M. J. M. de Jong and C. W. J. Beenakker in *Coulomb and Interference Effects in Small Electronic Structures*, proceedings of the XXIXth Rencontres de Moriond workshop, edited by D. C. Glattli and M. Sanquer, (Editions Frontières, Gif-sur-Yvette, France, 1994)

[9] C. W. J. Beenakker and H. van Houten, Solid State Phys. **44**, 1 (1991)

[10] C. Cohen-Tannoudji, J. Dupont-Roc and G. Grynberg, *Atom-photon interactions. Basic processes and applications*, (Wiley, New York, 1992).

[11] B. D. Josephson, Phys. Lett., **1**, 251 (1962)

[12] M. Tinkham, *Introduction to Superconductivity* (McGraw-Hill, New York, 1975).

[13] V. Ambegaokar and A. Baratoff, Phys. Rev. Lett. **10**, 486 (1963).

[14] K. A. Matveev, M. Gisselfält, L. I. Glazman, M. Jonson and R. I. Shekhter, Phys. Rev. Lett. **70**, 2940, 1993.

[15] U. Geigenmüller and G. Schön, Europhys. Lett. **10**, 765 (1989).

III. THEORY OF THE SUPERCONDUCTING SINGLE ELECTRON TRANSISTOR

In this theoretical treatment of the transistor we will limit ourselves to temperatures $T \ll \Delta/k_B$ at which thermally excited quasiparticles in the superconductor can be neglected and to bias voltages such that $V \ll 2\Delta/e$. In this voltage range, the electrical sources cannot provide the energy necessary to break Cooper pairs in a single pair tunneling process. Thus, the main charge transport process through the transistor will be the transfer of Cooper pairs. In Sec. A we describe charge transfer from the point of view of the single electron tunneling Hamiltonian to justify the use of the individual Josephson Hamiltonians of the junctions in the rest of the chapter. In Sec. B, we show that at zero voltage, the whole transistor can be treated as an effective Josephson junction with a gate voltage dependent effective Josephson energy. In Sec. C we discuss the possibility of the presence of one quasiparticle in the circuit and its consequences. Finally, in Sec. D, we analyse the behaviour of the system at finite but low voltage.

A. Microscopic description of charge transport in the transistor

For the whole transistor, the single electron tunneling Hamiltonian can be written (see Sec. II.B)

$$\begin{aligned}\mathcal{H}_T &= \mathcal{H}_{T1} + \mathcal{H}_{T2}\\ \mathcal{H}_{T1} &= \sum_{s,i,\sigma} \mathrm{e}^{i\varphi_1} T_{1si} a_{s\sigma} b^\dagger_{i\sigma} + h.c.\\ \mathcal{H}_{T2} &= \sum_{i,d,\sigma} \mathrm{e}^{i\varphi_2} T_{2id} b_{i\sigma} c^\dagger_{d\sigma} + h.c.\end{aligned}$$

where the operators a, b, c and $a^\dagger$, $b^\dagger$, $c^\dagger$ are the annihilation and creation operators for the quasielectrons and quasiholes in the source, the island and the drain of the transistor, respectively, and $T_{1,2}$, $\varphi_{1,2}$ are the tunnel coupling matrices and the phases of each junction of the transistor. Starting from the single electron tunneling Hamiltonian, we can try to evaluate the effective Josephson coupling of the transistor in the same way as we did for the single junction (see Sec. II.C). To stay at the lowest order in perturbation theory, we will consider only processes in which no more than two Cooper pairs are broken at the same time. For the quasiparticle part of the tunneling Hamiltonian, these processes can be separated into two types which both decompose in four steps (see Fig. 1) :

Type A. The first step consists in breaking a Cooper pair on the left side and transferring an electron to the island. In the second step, the quasiparticle in the island is transferred to the right electrode. At this point the island is neutral, and the system has two quasiparticles in it.

The third and fourth step repeat the first and second to achieve the transfer of a whole pair. In this type of processes it is also possible to swap the first and second and/or the third and fourth steps (using an occupied pair in the island).

Type B. The first step is the same as previously. The second step now consists of transferring the second electron of the broken pair in the island and to recombine the quasiparticles into the ground state. In this intermediate step, there are no quasiparticles in the system but the island is charged. The third and fourth steps are analogous to the first and second but involve the second junction. In this second type of process, the first two and last two transfers can be swapped. The only effect of this swapping is to change the electrostatic energy in the intermediate state.

Even though type A processes seems favoured because their second intermediate state is highly degenerate, their total amplitude is drastically reduced because they require transferring exactly the same quasiparticle state through both junctions. In our disordered islands, it is extremely unlikely that a single state has a significant coupling to both source and drain electrodes. In the following we will neglect this possibility and focus on type B pair transfer. The situation could be quite different in a clean system like a 2-dimensional electron gas (assuming it could be made superconducting, though).

In the type of transfer we retain here, we can regroup electronic transfers two by two and speak in terms of two Josephson tunneling of Cooper pairs instead of four electron tunnel events. Taking advantage of this remark, in the next section we will obtain the effective coupling of the transistor by diagonalization of a Hamiltonian where only Josephson transfers are considered.

Fig. 1. *(next page) Two generic types of fourth-order processes in the tunneling Hamiltonians to transfer a Cooper across the transistor. Electronic states including spin index are indexed by a letter and time-reversed states are indicated by an overline. The convention used to represent the states of the superconductors is the same than that of Fig. 4 of Chap. II, except that only the actual state of pairs is drawn, instead of the four accessible states. Only the quasiparticle energy is taken into account, not the charging energy of the states. Type A processes where the same quasiparticles must tunnel through the two barriers are very unlikely in our experiments.*

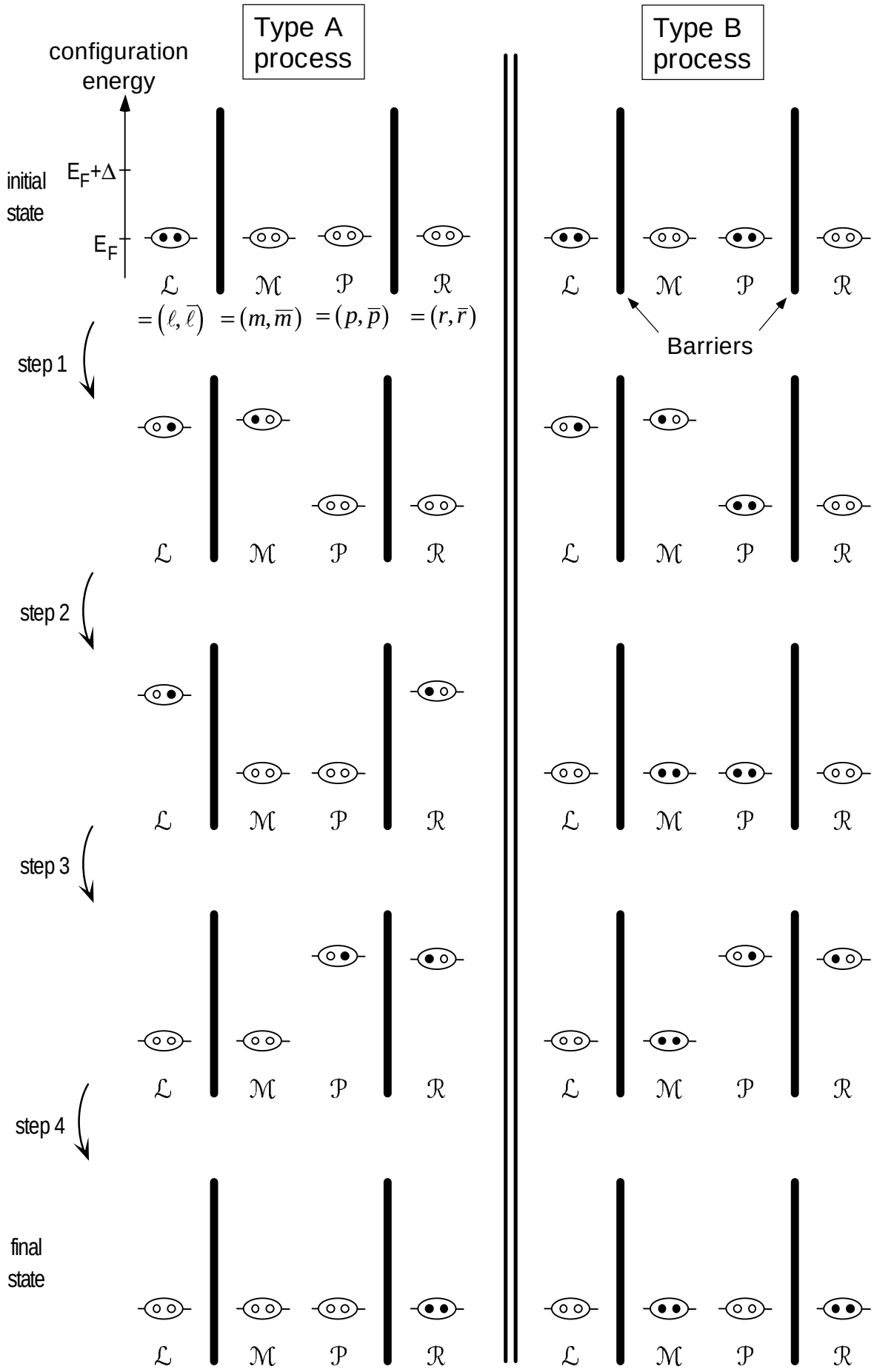
Type A process
Type B process
configuration energy
initial state
$E_F+\Delta$
E_F
$\mathcal{L}$ $\mathcal{M}$ $\mathcal{P}$ $\mathcal{R}$
$=(\ell,\bar{\ell})$ $=(m,\bar{m})$ $=(p,\bar{p})$ $=(r,\bar{r})$
Barriers
step 1
step 2
step 3
step 4
final state

B. Phase representation of the transistor ; effective Josephson coupling

In this section we make the hypothesis that the environment of the transistor is such that we can use the renormalized Josephson Hamiltonian introduced in Sec. II.C. We will here only consider internal degrees of freedom of the transistor.

1. Good quantum variables for the transistor

It is easy to convince oneself that the transistor has two internal degrees of freedom (for a general discussion of this problem see Ref. 1). For example we can choose to index the state of the transistor by the numbers k_1 and k_2 of Cooper pairs having crossed the left and right junction, respectively. However we anticipate that like in a single Josephson junction neither of these will be a good quantum number. The electrostatic energy rather favours states with a given $n = 2(k_1\text{-}k_2)$ measuring the excess number of electrons on the island.

Since the junctions are superconducting, another possibly good choice of variables could be the phases differences[1] δ_1 and δ_2 of the junctions, which are conjugate variables of k_1 and k_2, respectively. Again, these are not good quantum numbers because the phase $\theta = (\delta_1 - \delta_2)/2$ (θ is the conjugate of n) of the superconducting wave function in the island will have large quantum fluctuations since n tends to be fixed. A better suited variable is $\delta = \delta_1 + \delta_2$. The conjugate variable of δ is $k = (k_1 + k_2)/2$, measuring the number of Cooper pairs having flown through the transistor.

Given this set of variables, with the phases defined using the superconducting flux quantum $h/2e$, we have the commutation relations

$$[\delta_1, k_1] = [\delta_2, k_2] = [\theta, n/2] = [\delta, k] = i$$
$$[n, k] = [\delta, n] = [\theta, k] = [\delta, \theta] = 0$$

---

[1] In the following the phases operators are noted by the Greek letter δ and are defined by reference to the "superconducting" flux quantum $\Phi_0 = h/2e$ as opposed to the phases φ we have used in Chap. II which were defined with respect to the flux quantum h/e. The notation we use here follows the usual convention in the context of Josephson junctions. The dimensionless number of charge operator k is also taken relative to the charge $2e$ of Cooper pairs. This double change of units preserves the commutation relation $[\delta, k] = i$. With this new definition of the phase, the Josephson Hamiltonian writes $H_J = -E_J \cos\delta$ instead of $-E_J \cos 2\varphi$.

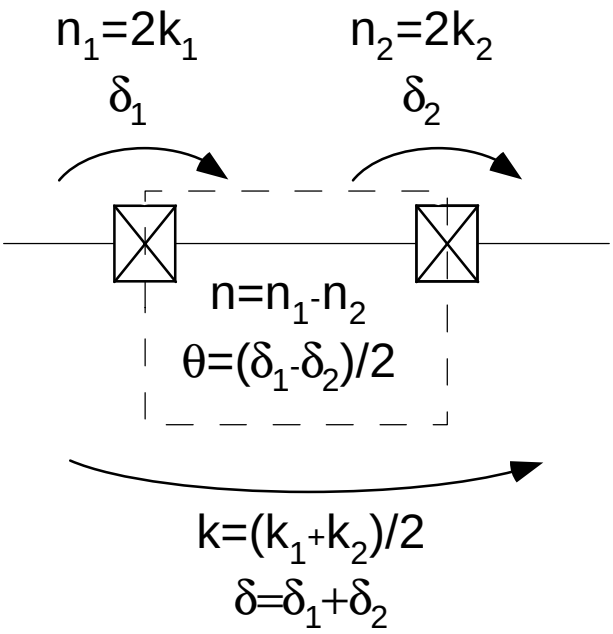

Fig. 2. *Pairs of conjugate variables in the transistor. The sysmbols k's refer to Cooper pair numbers, n's to electron numbers, Greek letters to phases defined using* $\Phi_0 = h/2e$*, the superconducting flux quantum. The variables we choose to describe the transistor are* n*, the excess electron number in the island and* δ*, the total phase difference across the transistor.*

Following the above considerations, we introduce the basis of states $|n,\delta\rangle$ of the transistor indexed by the values of n and δ that we anticipate to be the good quantum numbers in the problem. It will sometimes be useful to use an alternate basis indexed by the values of n and k. These sets of states are Fourier transformed pairs:

$$|n,\delta\rangle = \frac{1}{\sqrt{2\pi}} \sum_k e^{i\delta k} |n,k\rangle$$

$$|n,k\rangle = \frac{1}{\sqrt{2\pi}} \int_I d\delta e^{-i\delta k} |n,\delta\rangle$$

where I is a 2π-long interval.

2. Form of the Hamiltonian

From the previous sections, the Hamiltonian of the transistor itself can be written as:

$$H = H_{el} + H_{J1} + H_{J2} + H_{qp}.$$

The first term $H_{el} = E_C(n-n_g)^2$ is the electrostatic Hamiltonian of the circuit in which $E_C = e^2/(2C_\Sigma)$ denotes the electrostatic energy of a single electron on the island, while $n_g = C_g V_g/e$ is the charge (in units of e) on the gate capacitor induced by the gate voltage V_g, which is our control "knob" over the transistor (C_Σ and C_g denote the total capacitance of the island and the gate capacitance, respectively). In writing H_{el} we have assumed that the gate capacitance is negligible compared with the junctions capacitances. The second and third terms

are the Josephson coupling Hamiltonians of the two junctions. These terms can be written (see Sec. II.C) :

$$H_{J1} = -E_{J1}\cos\delta_1$$
$$H_{J2} = -E_{J2}\cos\delta_2.$$

Here $E_{J1,2}$ are the Josephson coupling energies of junction 1 and 2, respectively. We will first suppose that $E_{J1} = E_{J2} = E_J$ since our junctions are fabricated to be nominally identical (the general case is treated in Sec. 4). By making use of the relations between δ_1, δ_2, θ and δ, the Josephson Hamiltonians can be rewritten as

$$H_{J1} = -E_J\cos(\theta + \delta/2),$$
$$H_{J2} = -E_J\cos(\theta - \delta/2),$$
$$H_{J1} + H_{J2} = -2E_J\cos\frac{\delta}{2}\cos\theta$$

The last term of the Hamiltonian accounts for the internal degrees of freedom of the superconductors:

$$H_{qp} = \sum_j \varepsilon_j \gamma_j^\dagger \gamma_j .$$

In this expression $\gamma_j^\dagger$ and γ_j are the Bogoliubov quasiparticle creation and annihilation operators and ε_j, the energy of the quasiparticle. In the present section (B), we will assume that all the electrons in the superconductors are paired (i.e. there are no quasiparticles). In that case, at $T = 0$, H_{qp} can be dropped. Of course, only even-n states can be considered with this hypothesis of perfect parity. We further assume for simplicity, that the island, when neutral, has an even number of electron (if this were not the case, this would only induce a unit shift on the variable n_g).

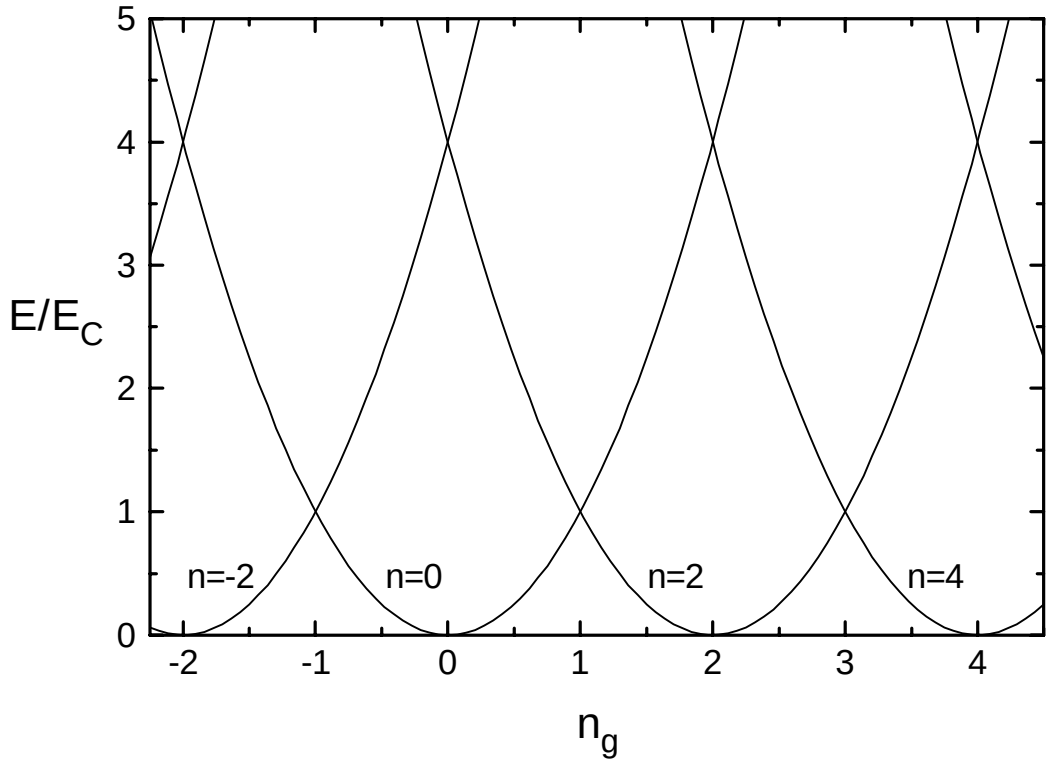

Fig. 3. *Electrostatic energy levels of even-n states for the transistor, versus the dimensionless gate charge. The energy diagram is periodic in the gate charge. As a first approximation, one can describe the transistor by retaining only the two lowest electrostatic states at any given gate charge.*

3. Two-band model of the transistor

At $T = 0$ we are only interested in the lowest energy bands. Also, since in practice we have $E_J \leq E_C$, we can compute these bands by neglecting n-states whose electrostatic energies are above a few E_C. As the Josephson Hamiltonians couple states whose n differ only by two electrons, the simplest possible approach to compute the ground band is to retain only the two states $|n,\delta\rangle$ of lowest electrostatic energy and to make a linear superposition out of them. To do so we will divide the n_g domain into intervals of the form $2q \leq n_g < 2(q+1)$, where the two lowest n-states are $n = 2q$ and $n = 2(q+1)$ (see Fig. 3). We diagonalize the Hamiltonian in the subspace spanned by these two lowest states. There is however a problem at the boundaries of these intervals where the lowest electrostatic energy state becomes coupled to two degenerate states and one of them is not taken into account in the diagonalization. These degeneracies can be treated correctly in the restricted space spanned by the three lowest electrostatic energy states of each interval, but this necessitates the diagonalization of a 3×3 matrix, resulting in complicated expressions. This treatment is made in Sec. 4. The two-level approach is

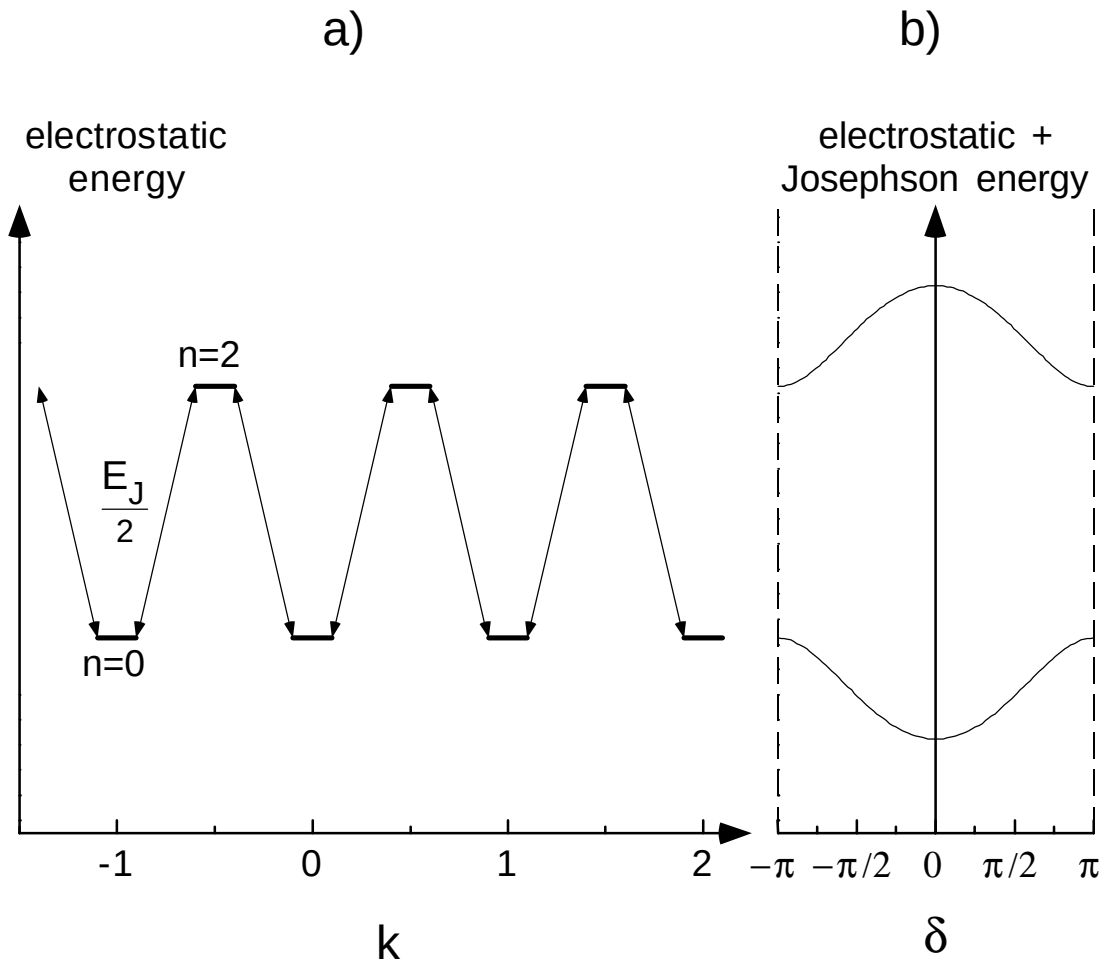

Fig. 4. *Analogy of the two-state model of the transistor with a 1-D crystal with two atoms per lattice period. The Josephson coupling (thin lines in the left panel) is equivalent to the exchange energy. The Bloch theorem ensures that* δ*, the conjugate variable of k, is a good quantum number. The eigenstates of the system form bands parametrized by* δ.

nevertheless useful as a first approximation to the essential features of the device and their qualitative discussion.

a) ANALOGY WITH A 1-D CRYSTAL

This restriction of keeping only two states in solving the problem brings us to a simpler, well-known problem : a 1-D crystal in the tight binding model as already mentioned in Chap. I (see Fig. 4). We are faced with a problem which is equivalent to finding electronic states in a 1-D crystal with two atoms per unit cell. Here *n* labels the atoms in the unit cell and the variable δ plays the role of the wave vector. The electrostatic and Josephson energies are equivalent to the energies of the orbitals and hopping energy, respectively.

b) DIAGONALIZATION OF THE HAMILTONIAN

In the domain where $0 \le n_g < 2$ the even-n states of lowest electrostatic energy are $|0,\delta\rangle$ and $|2,\delta\rangle$. In this basis, the matrix of the Hamiltonian writes:

$$H = \begin{bmatrix} E_C(-n_g)^2 & -E_J \cos\dfrac{\delta}{2} \\ -E_J \cos\dfrac{\delta}{2} & E_C(2-n_g)^2 \end{bmatrix}$$

The system can be treated as a fictitious spin 1/2 in a magnetic field. Let us define the energies

$$M = E_C\left(n_g^2 - 2n_g + 2\right)$$
$$D = 2E_C\left(1 - n_g\right)$$
$$J = E_J \cos\frac{\delta}{2}$$

where M and D are the mean and half difference of the electrostatic energies of the states $|0,\delta\rangle \equiv |\uparrow\rangle$ and $|+2,\delta\rangle \equiv |\downarrow\rangle$, and J the coupling energy. We can rewrite the Hamiltonian as

$$H = M - \vec{h}.\vec{\sigma}$$

with

$$\vec{h} = (J,0,D)$$
$$\vec{\sigma} = \left(\sigma_x, \sigma_y, \sigma_z\right)$$

where σ_x, σ_y and σ_z are the Pauli matrices. Introducing the angle 2α between $\vec{h}$ and $\hat{z}$, the unit vector in the z direction, the eigenstates and eigenenergies are given by

$$\left|\psi_0\right\rangle = \cos\alpha\left|\uparrow\right\rangle + \sin\alpha\left|\downarrow\right\rangle \qquad \mathcal{E}_0 = M - \sqrt{D^2 + J^2}$$
$$\left|\psi_1\right\rangle = \sin\alpha\left|\uparrow\right\rangle - \cos\alpha\left|\downarrow\right\rangle \qquad \mathcal{E}_1 = M + \sqrt{D^2 + J^2}$$

For any given value of n_g, and by analogy with the Bloch states in a crystal, we will call these eigenenergies, energy bands for the variable δ (see Fig. 4). The position, shape and amplitude of the bands depend on the value of n_g (see Fig. 5). The treatment we have applied is valid only in the domain where $0 \le n_g \le 2$ but, since the electrostatic energy diagram is periodic in n_g, the eigenenergies of the total Hamiltonian must be periodic with n_g, with period 2, each interval of the form $2q \le n_g \le 2(q+1)$ corresponding to a different set of two lowest electrostatic energy states. To extend the solution we have found, we simply duplicate it to cover the whole range of n_g values. The bands are also 2π-periodic functions of δ (they involve δ only through $\cos^2\delta/2$).

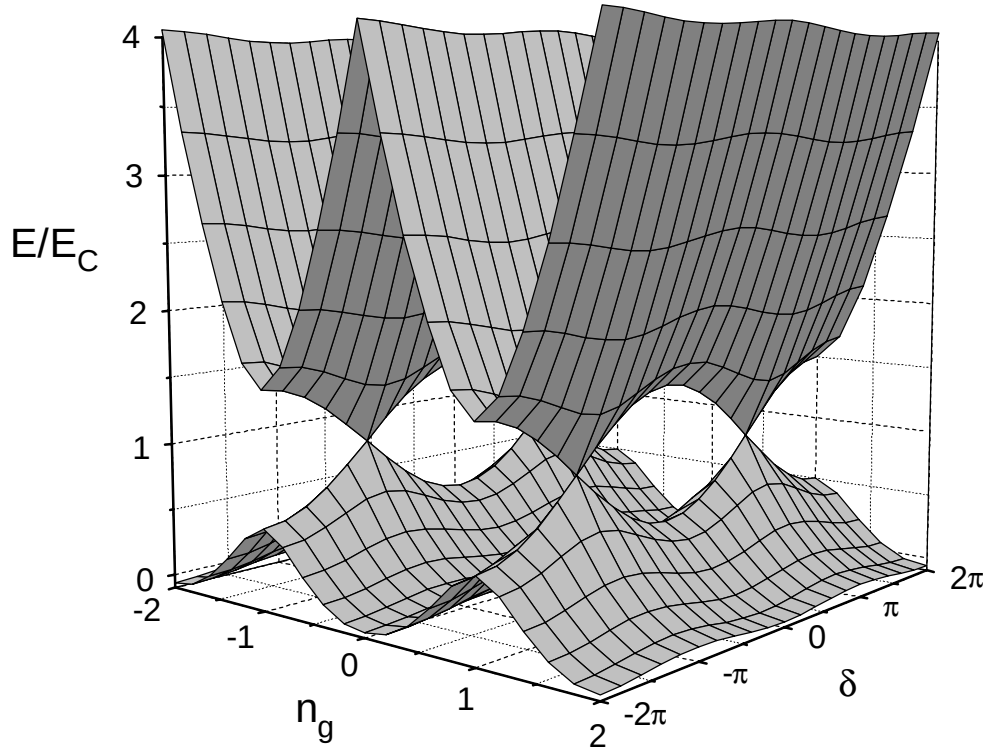

Fig. 5. *3D plot of the energy bands as functions of* δ *and* n_g *calculated for* $E_C = 2E_J$*. Note that the bands touch at points where* n_g *is an odd integer and* $\delta = \pi$ *mod* 2π*. This degeneracy is non-generic : it is lifted if the two Josephson energies of the junctions are not rigorously equal as usually happens in the experiments. The band separation is then* $|E_{J1} - E_{J2}|$ *(see Sec. 4).*

c) EFFECTIVE JOSEPHSON COUPLING

The energy-phase relation in the ground band ($\mathcal{E}_0(\delta,n_g)$) is the equivalent for the transistor of the $-E_J\cos\delta$ relation for the single Josephson junction. Its functional dependence even has very similar properties. For example, its extrema sit at $\delta = 0$ and $\delta = \pi$. To carry this analogy further we introduce the notation:

$$\mathcal{E}_0(\delta, n_g) = E_0(n_g) f_0(n_g, \delta)$$

where

$$E_0(n_g) = \frac{1}{2}\left(\sqrt{D^2 + E_J^2} - |D|\right)$$

is the effective Josephson coupling energy of the transistor and the function f_0 is such that

$$f_0(n_g, \pi) - f_0(n_g, 0) = 2$$

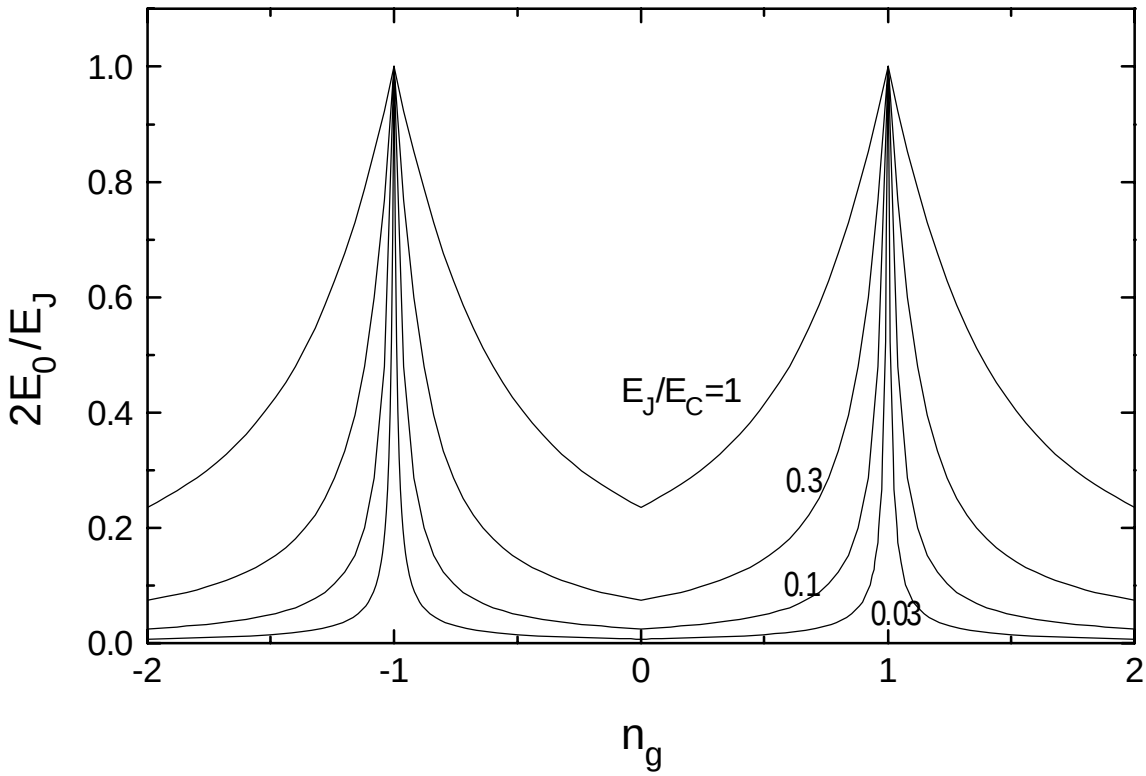

Fig. 6. *Ratio of the effective Josephson energy of the transistor to the single-junction Josephson energy as a function of the gate charge, for the two-charge-states-model. The cusp occurring at even integer values of n_g is an artefact of the model which neglects the degeneracy of charge states that exists at these gate charges. The essential features of the transistor are well captured however : the effective Josephson energy presents sharp peaks of height $E_J/2$ centred around odd integer values of n_g. The width of these peaks is of the order of E_J/E_C.*

which is equivalent to the cosine of the single junction. The strength of the effective Josephson coupling for different values of E_C at a given E_J is plotted in Fig. 6.

As far as interband transitions are neglected, the transistor behaves essentially as a single Josephson junction. The band $E_0(\delta)$ can then be considered as a potential for the phase δ. For the typical electromagnetic environment of a transistor one can furthermore show that the phase behaves as a classical variable [2]. The superconducting state of the transistor corresponds to a static solution for δ.

4. Three-band model

As announced previously, we can improve the two-band model of the transistor by going to a three-band model. This will complicate the calculations, but the equation of the bands remains analytic. To be complete, we will furthermore consider here the general case where the two junctions have different Josephson coupling energies.

In the domain where $-1 \le n_g \le 1$ the even-n states of lowest electrostatic energy are $n = 0, \pm 2$, with the $n = \pm 2$ being degenerate at $n_g = 0$. This degeneracy was neglected in the two-band model, but it can be treated correctly in the restricted space generated by the three lowest states, $|-2, \delta\rangle$, $|0, \delta\rangle$ and $|2, \delta\rangle$. In this basis, the matrix of the Hamiltonian writes:

$$H = \begin{bmatrix} E_C(-2-n_g)^2 & -\frac{1}{2}\left(E_{J1}e^{-i\delta/2} + E_{J2}e^{+i\delta/2}\right) & 0 \\ -\frac{1}{2}\left(E_{J1}e^{+i\delta/2} + E_{J2}e^{-i\delta/2}\right) & E_C(-n_g)^2 & -\frac{1}{2}\left(E_{J1}e^{-i\delta/2} + E_{J2}e^{+i\delta/2}\right) \\ 0 & -\frac{1}{2}\left(E_{J1}e^{+i\delta/2} + E_{J2}e^{-i\delta/2}\right) & E_C(2-n_g)^2 \end{bmatrix},$$

and the secular equation takes the form of a polynomial of third degree in E:

$$\left(E - E_C n_g^2\right)\left(E - E_C\left(n_g - 2\right)^2\right)\left(E - E_C\left(n_g + 2\right)^2\right) - a\left(2E - E_C\left(8 + 2n_g^2\right)\right) = 0,$$

where

$$a = \frac{1}{4}\left(E_{J1}^2 + E_{J2}^2 + 2E_{J1}E_{J2}\cos\delta\right).$$

This equation is exactly solvable. Introducing intermediate quantities:

$$\lambda = \frac{2}{3}a + \frac{16}{3}E_C^2\left(\frac{1}{3} + n_g^2\right); \quad \mu = \frac{8}{3}aE_C + \frac{128}{3}E_C^3\left(\frac{1}{9} - n_g^2\right) \quad \text{and} \quad \theta = \text{Arccos}\,\frac{-\mu}{2\lambda^{3/2}},$$

the three roots are given by:

$$\mathcal{E}_m\left(\delta, n_g\right) = \left(\frac{8}{3} + n_g^2\right)E_C + \sqrt{4\lambda}\cos\left(\frac{\theta + 2\pi(m+1)}{3}\right) \qquad \text{with } m = 0,1,2\,.$$

Exactly as in the two-band model, these eigenenergies form bands parametrized by δ, whose positions, shapes and amplitudes depend on the value of n_g (see Fig. 7). The treatment we have applied is valid only in the domain where $-1 \le n_g \le 1$ but, since the electrostatic energy diagram is periodic in n_g, the eigenenergies must be periodic with n_g, with period 2, each interval of the form $2q\text{-}1 \le n_g \le 2q\text{+}1$ corresponding to a different set of three lowest electrostatic energy states. To extend the solution we have found, we simply duplicate it to cover the entire range of n_g values. The bands are still 2π-periodic functions of δ (they involve δ only through $\cos\delta$).

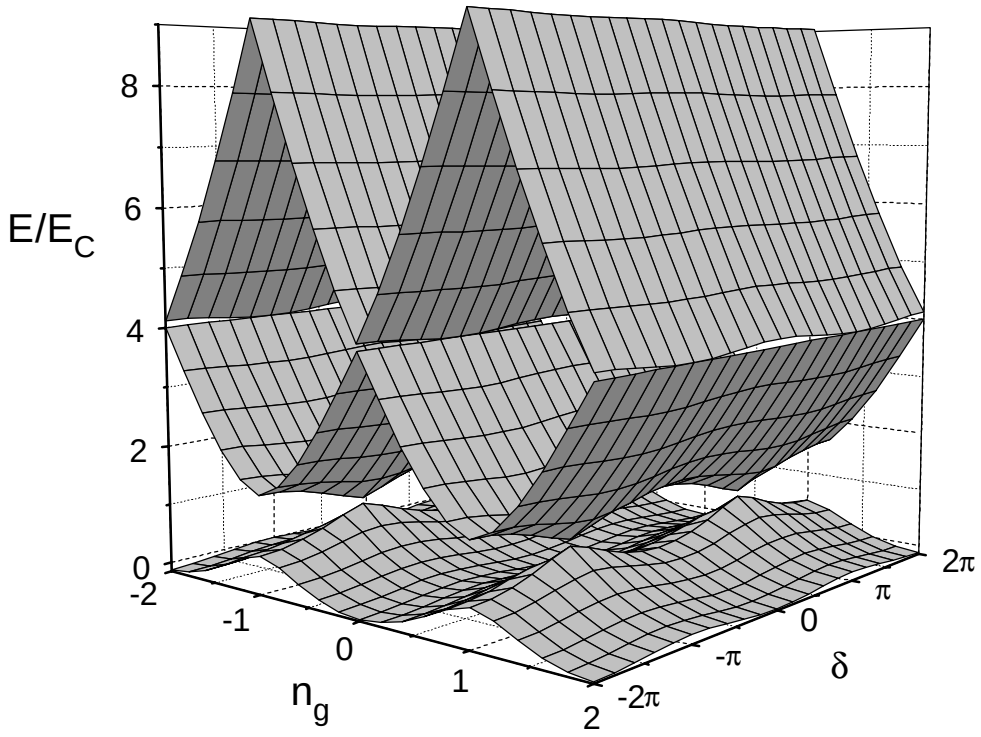

Fig. 7. *3D plot of the bands of the transistor calculated with the three band model, for an average Josephson coupling energy of the two junctions $E_J = E_C/2$ and a relative difference between the two Josephson energies $\Delta E_J/E_J = 20\%$.*

EFFECTIVE JOSEPHSON COUPLING

As in the two-band model, the energy-phase relation in the ground band ($m = 0$) is equivalent to the $-E_J\cos\delta$ relation of the single Josephson junction. We keep the notation:

$$\mathcal{E}_0(\delta, n_g) = E_0(n_g) f_0(n_g, \delta) \quad \text{with} \quad f_0(n_g, \pi) - f_0(n_g, 0) = 2.$$

where f_0 plays the role of the $\cos\delta$ in the single Josephson junction and $E_0(n_g)$ represents the effective Josephson coupling energy of the transistor. The strength of the effective Josephson coupling for different values of E_C/E_J, in the case of identical junctions ($E_J = E_{J1} = E_{J2}$) is plotted in Fig. 8 along with the predictions of the two band model, for comparison. The present model predicts an effective Josephson coupling about twice as large as the two-band model at $n_g = 0$. This discrepancy is due to the fact that the two-band model neglects one of the two available excited charge state in the vicinity of $n_g = 0$.

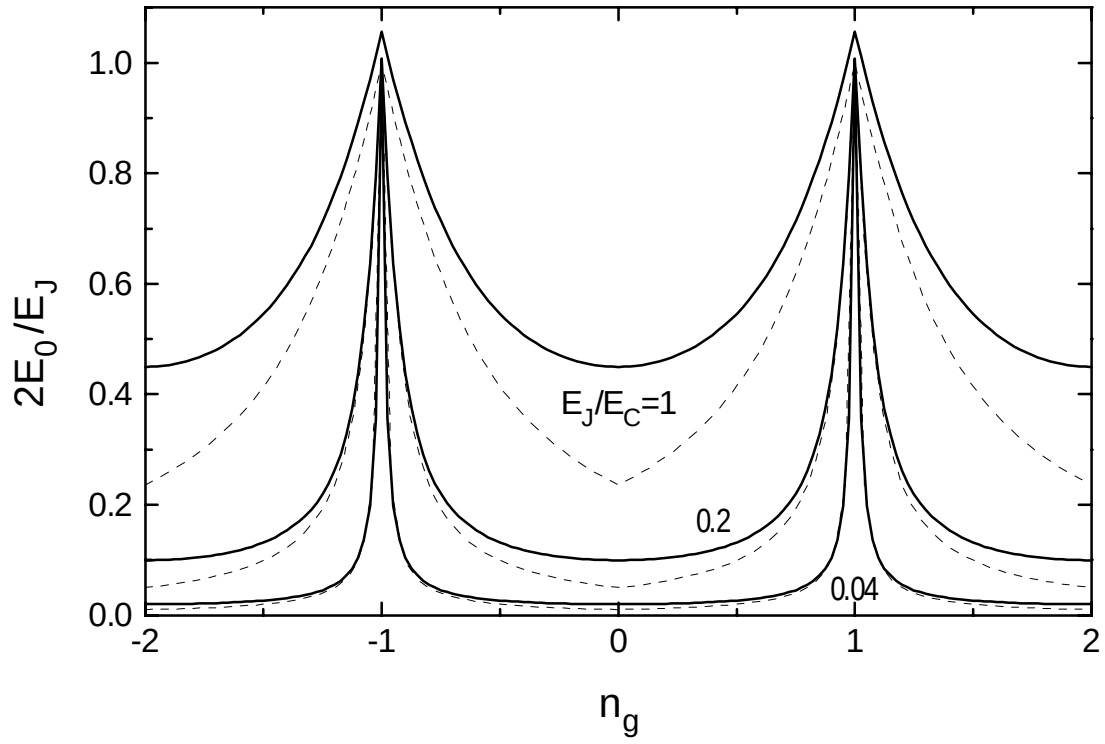

Fig. 8. *Ratio of the effective Josephson coupling of the transistor to the single junction Josephson coupling, as a function of the gate voltage. Full heavy lines are the results of the calculation for the three band model for identical junctions, for various E_J/E_C. The light dashed lines are the results obtained by the two band model which does not treat the degeneracy occurring at even integer values of n_g. We see that the simple two-band model underestimates by a factor of ≈2 the effective Josephson coupling at even integer values of n_g, while its predictions on the amplitude and the width of the peaks are essentially correct.*

5. Critical current of the transistor

When a current I is driven through the transistor, one must add an extra term $-2\pi\delta I/\Phi_0$ to the Hamiltonian H_{el} introduced in Sec. 2 [3]; this amounts to tilting the potential in which the phase evolves. The critical current I_C of the transistor is the maximum theoretical supercurrent that can flow through the transistor. It corresponds to the critical tilting of the band for which local minima of the potential disappear, thus removing the possibility of static solutions for δ. The critical current is given by the relation:

$$I_C(n_g) = \frac{2\pi}{\Phi_0} \operatorname*{Max}_{\delta}\left\{\frac{\partial \mathcal{E}_0}{\partial \delta}(\delta, n_g)\right\} = \frac{2\pi}{\Phi_0} E_0(n_g) \operatorname*{Max}_{\delta}\left\{\frac{\partial f_0}{\partial \delta}(\delta, n_g)\right\}$$

To simplify the notations, we introduce a function $\varepsilon(n_g)$ such that

$$I_C(n_g) = \frac{2\pi}{\Phi_0}\left(1+\varepsilon(n_g)\right)E_0(n_g)$$

The last equation links the effective Josephson coupling and the critical current of the transistor. This equation is similar to the single junction equation, for which we have $\varepsilon \equiv 0$. For the two-band model we also find $\varepsilon(n_g) \equiv 0$. This happens because the maximum of the derivative of f_0 is exactly 1 independent of the value of n_g, just as for the cosine in the case of the single junction. This exact relation between the effective Josephson energy and the critical current of the transistor breaks down when more charge states are taken into account in the diagonalization of the Hamiltonian ($\mathrm{Max}\{\partial f_0/\partial\delta\} \neq 1$ in this case ; it is not even analytic for the three-band model). However for any reasonable set of parameters for which the approach we have used here is valid ($E_{J1}, E_{J2} \lesssim E_C$), we find numerically that $\varepsilon(n_g) \ll 1$. Thus the equation linking the critical current and the Josephson coupling energy of the single Josephson junction

$$I_C = \frac{2\pi}{\Phi_0} E_J$$

remains “numerically true” to a high degree of accuracy for the transistor at any gate charge, with the definition of the effective Josephson coupling energy that we have adopted.

6. Relation with the superconducting “electron box”

In the absence of current, the superconducting SET can be considered as a superconducting single electron box [1,4] (the two junctions of the transistor in parallel are equivalent to the single junction of the box. See Fig. 9). The absence of current corresponds to setting $\delta = 0$ in all the results previously obtained.

In the box experiment, one measures the charge of the ground state of the island. In the vicinity of $n_g = 1$, we keep only the two states $n = 0$ and $n = 2$, as in the two-band model. The ground state of the box is then $|\Psi_0\rangle = \cos\alpha|0\rangle + \sin\alpha|2\rangle$ where $\cos 2\alpha = D/\sqrt{D^2 + E_J^2}$ (we use here the

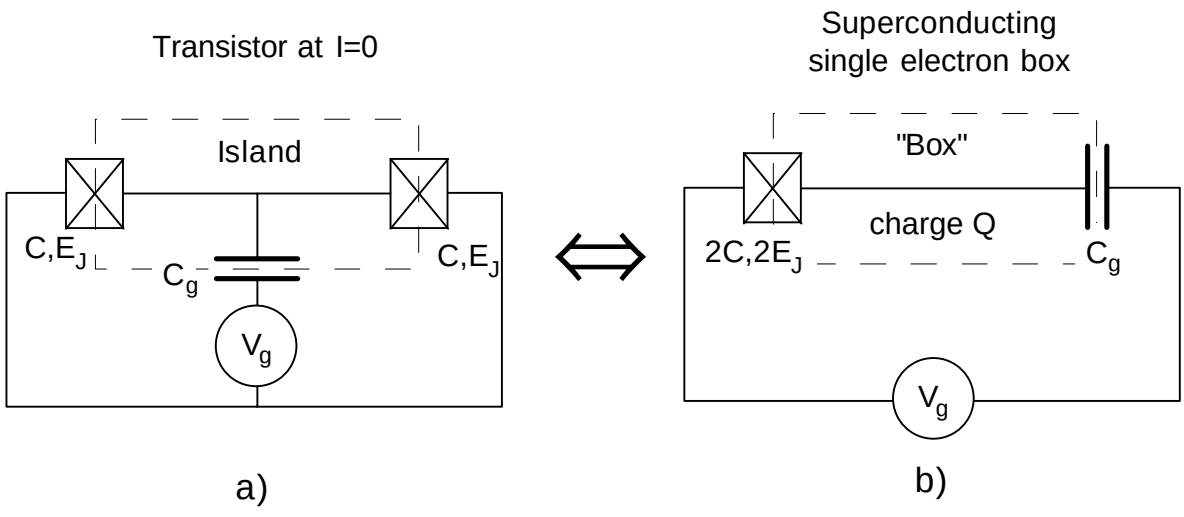

Fig. 9. *At zero current, the transistor is equivalent to the superconducting single electron box.*

notation $D = 2E_C(1-n_g)$ already used in Sec. 3.b.). The charge is given by

$$\langle Q\rangle/e = 2\left|\langle 2|\Psi_0\rangle\right|^2 = 2\sin^2\alpha$$
$$= 1 - \frac{D}{\sqrt{D^2 + E_J^2}}$$

With the same notations, the critical current of the transistor is given by (we use here the two-band model which is sufficient since $n_g \approx 1$)

$$\frac{\Phi_0}{2\pi} I_C(n_g) = E_0(n_g) = \frac{1}{2}\left(\sqrt{D^2 + E_J^2} - |D|\right)$$

The two quantities are obviously related. Indeed, one can compare the fluctuations of the charge in the island $\langle Q^2\rangle - \langle Q\rangle^2 = E_J^2/(E_J^2 + D^2)$ with the critical current I_C of the transistor as a function of the gate charge : they both present a peak whose width is of the order of E_J/E_C (see Fig. 10). This clearly shows that the measurement of the critical current of the transistor constitutes an observation of the charge fluctuations in the island : the greater the charge fluctuations, the greater the supercurrent. A recent experiment also reported a similar observation in a device where the charge fluctuations were controlled by a flux [5].

In Fig. 10 we have also plotted the derivative $d\langle Q\rangle/dn_g$ of the average charge of the island

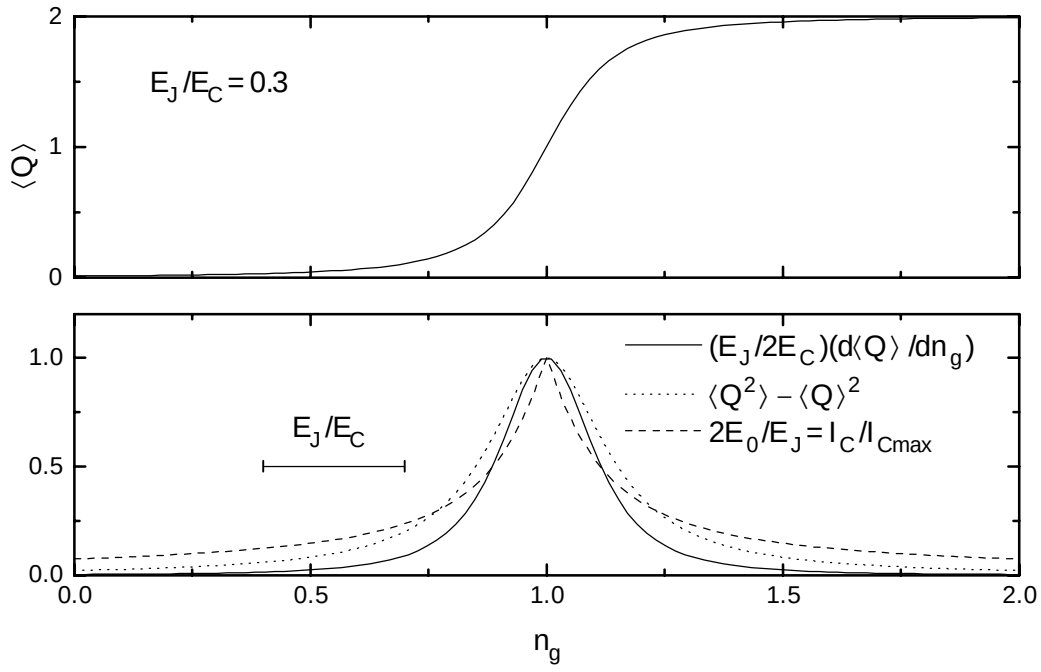

Fig. 10. *Top panel: charge of the island of a superconducting single electron box, for a ratio $E_J/E_C = 0.3$. Bottom panel : the derivative of the charge of the island of the box (full line), the fluctuations of the charge in the island of the box (dotted line) and the critical current of the transistor (dashes) all present a peak of width of the order of E_J/E_C. Both experiments observe, in a different manner, the coherent charge superposition inside the island.*

which would be obtained in a lock-in measurement of the charge of the island. This derivative is proportional to the power 3/2 of the charge fluctuations.
In conclusion, both the superconducting single electron box and the transistor demonstrate the same macroscopic quantum coherence in a different manner. Note however that the box experiment is in principle better suited to test the predictions of quantum mechanics [4] since its data can be interpreted directly [6], whereas in the transistor the critical current is not measured directly (see Chap. IV). At the time of this writing, experimental results on the superconducting box have not yet been published [7].

7. Duality with the dc squid

The transistor is in some sense the dual device of the DC SQUID. The correspondence is given in the following table :

SUPERCONDUCTING SINGLE ELECTRON TRANSISTOR	DC SQUID
junctions in series	junctions in parallel
island	loop
modulation of I_C by a charge	modulation of I_C by a flux
period $2e$	period $\Phi_0=h/2e$
sensitive detector for electrometry	sensitive detector for magnetometry
high input impedance (capacitor)	low input impedance (transformer)

Note however that the shape of the modulation of the critical current with respect to flux in a DC SQUID is different from the modulation of the critical current with the gate charge of the transistor. This is because both devices see a low impedance environment. The shape of the modulation of the critical current of the SQUID would be similar to that of the transistor if the SQUID was in a high impedance environment. Another difference between the SQUID and the transistor is that there is no equivalent of a flux transformer for charges (one can only make a capacitive divider, not a multiplier).

C. Poisoning of the supercurrent

The simple description of the transistor we have adopted here neglects the possibility to have unpaired electrons in the island and is essentially that which was first given by Likharev [8]. Matveev *et al*. [9] were the first to realise that quasiparticles could have a dramatic influence on the critical current of the transistor. We will here briefly go over their reasoning.

We assume the validity of the B.C.S. theory of superconductivity [10,11] in the small island of the transistor. Then, each odd-n (n = electron number in the island) state is degenerate with respect to the quasiparticle configuration. The minimum configuration energy of each odd-n state is Δ, the energy gap of the superconductor. If we plot the configuration + electrostatic energy of the lowest of the odd-n states with the energy of the ground even-n states, as a function of the gate voltage (see Fig. 11, top panel) we see that for $\Delta < E_C$, the state of lowest energy in the vicinity of odd integer values of n_g, is an odd-n state. At zero temperature, in these ranges of n_g it is favourable for a quasiparticle to enter the island in order for the system to be in its ground odd-n state. This odd-n state is Josephson-coupled to other odd-n states. Thus, odd-n states also form bands and can carry a supercurrent. The modulation of the critical current of the odd-n ground band with n_g is shifted by $\Delta n_g = 1$ with respect to that of the even-n ground band (see Fig. 11, bottom panel). If we assume that the system occupies the lowest available configuration + electrostatic energy state, we predict a modulation of the critical current with sharp "holes" in the vicinity of odd integer values of n_g (Fig. 11, bottom panel). These holes occur at places where we had predicted peaks of the supercurrent in absence of the quasiparticles, hence the name of "poisoning" of the supercurrent given to this effect. The depth and the width of the holes depend on the ratio Δ/E_C as shown in Fig. 12. When $\Delta > E_C$, odd-n states are unstable, no poisoning occurs, the modulation of the critical current is that predicted in Sec. B, with maxima at odd integer values of n_g. When the gap is zero, the modulation of the supercurrent is e-periodic, very weak, and the maxima of the critical current are displaced by $\pm 1/2$ with respect to the large Δ case.

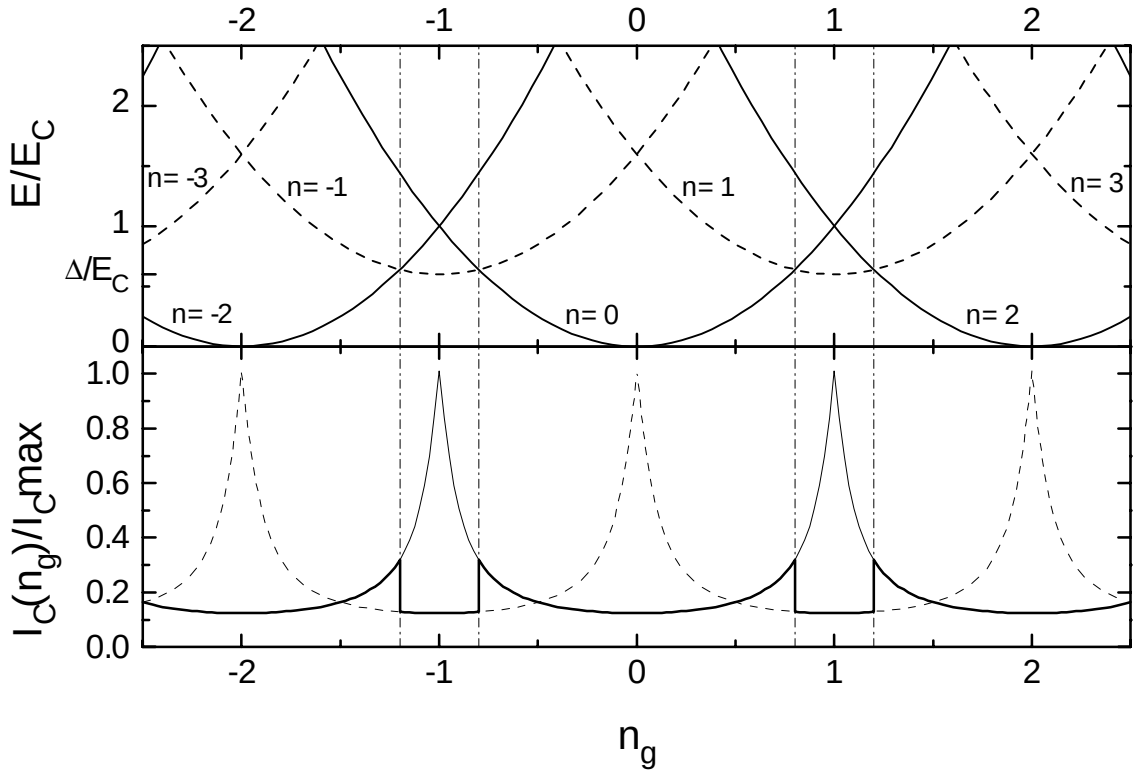

Fig. 11. *Top panel : Each parabola is the electrostatic + configuration energy of states of the transistor for a given number n of electrons in the island, plotted as a function of the gate charge. Parabolas of the lowest odd-n states (dashed lines) are higher by* Δ *than those of the even-n states (full lines). In the case where* $\Delta < E_C$ *depicted here, odd-n states are the lowest states of the system in the vicinity of odd integer values of* n_g*. Bottom panel : modulation of the critical current of the transistor with respect to the gate charge for the ground band formed by the even-n states (thin full line) and odd-n states (thin dashed line). A ratio* $E_J/E_C=0.3$ *was used for the calculation. If the transistor follows the state of lowest energy on the top panel, we predict a modulation of the critical current as indicated by the thick line. We see that the entrance of a quasiparticle in the island suppresses the supercurrent peak, hence the name of "poisoning" given to the effect.*

At finite temperatures, things are more complicated because of the entropic effect associated with the degeneracy of the odd-*n* states. In former experiments [12,6] we have demonstrated that the equilibrium occupation probability of odd-*n* states in a small superconducting island is governed by the odd-even free energy difference introduced by the Harvard group [13]. Predicting how this odd-even free energy difference will manifest itself experimentally in the transistor requires a precise description of how the measurements are performed. We will return to this problem in Chap. VI.

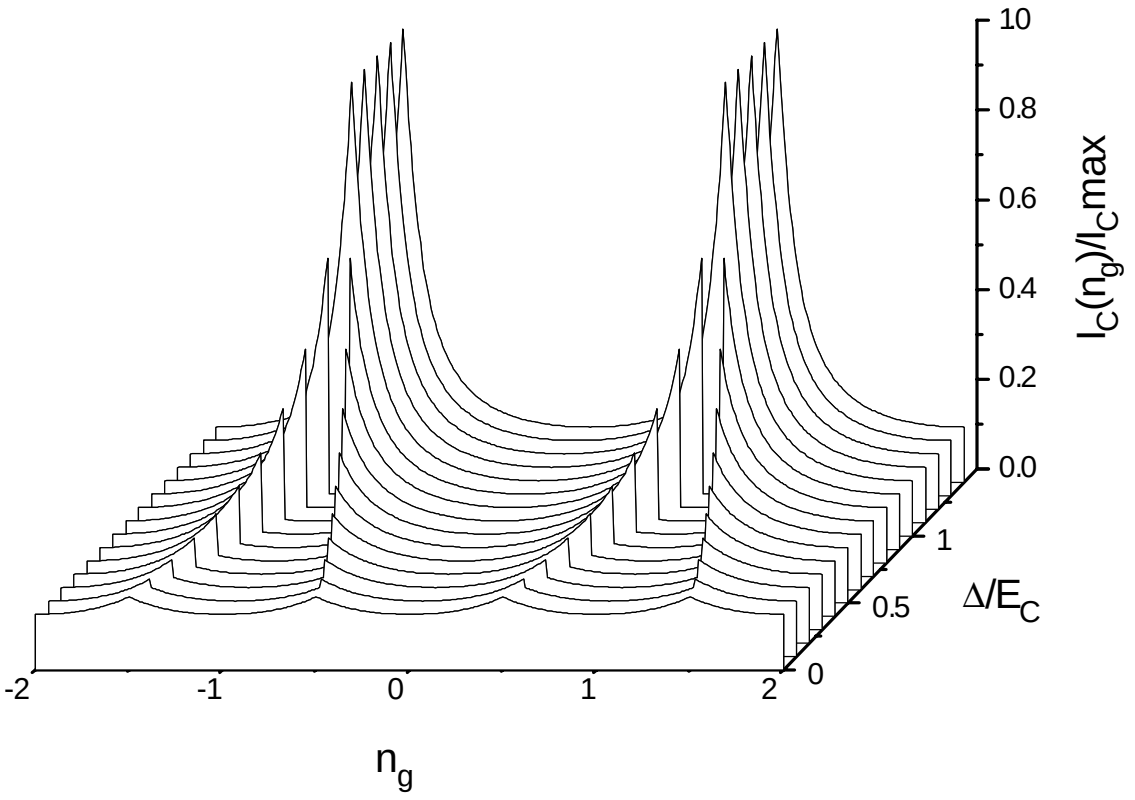

Fig. 12. *Modulation of the critical current of the transistor as a function of gate voltage for different values of the ratio Δ/E_C, showing the poisoning effect. A ratio $E_J/E_C=0.3$ was used for the calculation.*

D. The superconducting single electron transistor at finite voltage : resonant Cooper pair tunneling

When the transistor is biased at a finite voltage $V \ll 2\Delta/e$, the *I-V* characteristic is determined by both its internal structure and the electromagnetic environment : when a Cooper pair goes through the transistor, the energy $2eV$ provided by the source can either excite the oscillators of the environment or the levels of the internal structure of the transistor. These latter excitations manifest themselves as resonances whose positions in voltage depend on the gate voltage and the charging energy. The process responsible for these resonances is known in the literature as the “resonant tunneling of Cooper pairs” [14,15,16,17]. In the following we calculate analytically these resonances within a double perturbative approach with respect to the Josephson coupling and the environment.

1. Description of the system at finite voltage

The representation of the Hamiltonian of the transistor + environment system we will use here is based on the one we gave in Sec. II.B.3.c for a single junction. We can write the Hamiltonian as

$$H = H_{el} + H_J + H_{env}$$

where

$$\begin{aligned} H_{el} &= E_C\left(n^2 - 2nn_g\right) - 2ekV \\ H_J &= H_{J1} + H_{J2} = -2E_J \cos\frac{\delta}{2}\cos\theta \\ H_{env} &= \sum_{m=1}^{\infty} \frac{\left(2ek - Q_m\right)^2}{2C_m} + \frac{\left(\Phi_m\right)^2}{2L_m} \end{aligned} \qquad (1)$$

and where we use the notations n, θ, k, δ, E_C and n_g introduced in Sec. III.B.1 for the transistor, and Q_m, Φ_m, C_m, L_m ($m = 1,\ldots,\infty$) introduced in Sec. II.B for the oscillators of the environment. We assume that the junctions are identical. The state of the transistor (including here the voltage source) belongs to the space spanned by the kets $|n, k\rangle$ introduced in Sec. III.B.1 while the state of the environment oscillators belongs to the space spanned by the kets $|N_1,\ldots, N_\infty\rangle$ where the N_i are the occupation numbers of the harmonic oscillators. A state of the total system is then described as a tensorial product of the state of the transistor and that of the environment.

a) Unperturbed electrostatic states of the transistor at finite voltage

At finite voltage, the k-degeneracy of the $|n, k\rangle$ states with respect to the electrostatic energy is lifted because each pair gone through the transistor lowers the total energy of the circuit by $2eV$. As in the case of zero bias voltage, we can restrict our analysis to gate charges $n_g \in [0,1]$. The other values of n_g can be treated straightforwardly using the properties of symmetry and periodicity of the Hamiltonian with respect to n and n_g. We will first consider only the states having the two lowest island charges : $|n = 0, k\rangle$ and $|n = 2, k+1/2\rangle$ where k is an arbitrary integer. At zero voltage, these states have an electrostatic energy $E(n) = U(n/2 \bmod 2)$ independent of k, where $U = 4E_C(1-n_g)$ (Fig. 13a). At finite voltages the k degeneracy is lifted and the states have the energies $E(n,k) = E(n) - 2ekV$: the electrostatic energy levels form a double staircase as a function of k (Fig. 13b&c).

b) Role of the Josephson and environment perturbations ; qualitative description of the resonant Cooper pair tunneling

The effects of the Josephson and environment Hamiltonians on the unperturbed states we have just described will be very different from one another. The Josephson Hamiltonian alone preserves the discrete character of the states of the transistor while the coupling to the environment states confers a finite width and a finite lifetime to the states of the transistor. To take into account the difference in nature of these two perturbations, we will treat them on a different footing. We will first find the states of the transistor when only the Josephson coupling is considered. We then calculate the current which results from the transitions between these states induced by the coupling to the environmental degrees of freedom.

Without doing any calculation, it is possible to understand qualitatively the effect of the perturbations and the process of resonant Cooper pair tunneling. At voltages V higher than U/e (Fig. 13c), every state is unstable and decays towards the following. This decay is very similar to the process which gives rise to a current in a single junction at finite voltage (see Chap. IV).

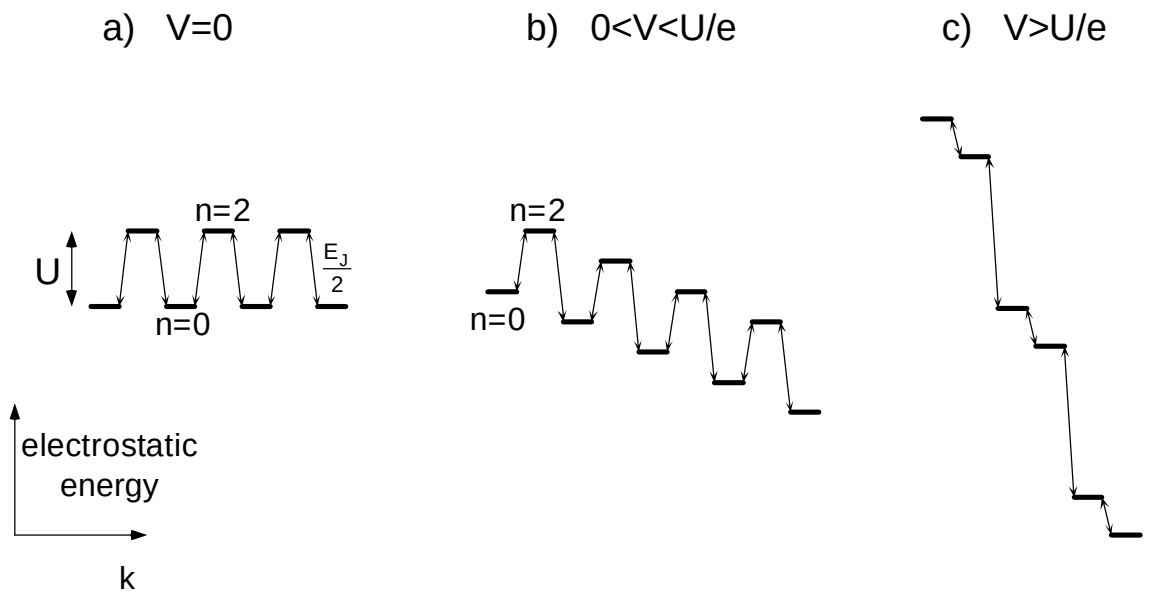

Fig. 13. *Electrostatic energy levels of the $|n,k\rangle$ states for three voltages. The thin arrows represent the Josephson coupling. a) V = 0, corresponding to the superconducting state of the transistor. States with one extra pair in the island (n = 2) are separated from the ground state by the gate voltage dependent energy $U = 4E_C(1-n_g)$. b) For voltages $0 < V < U/e$ the n = 0 states are metastable and each n = 2 states can decay toward two states. The relaxation is due to the coupling of the electromagnetic degrees of freedom with the electronic degrees of freedom. c) For $V > U/e$, every state is unstable and decays into the next one. The current through the transistor is the result of the sequential tunneling of Cooper pairs through each junction. This case is very similar to that of a single Josephson junction at finite voltage.*

At voltages V lower than U/e (Fig. 13b) the situation is more complicated and is very different from that of a single junction. At these voltages the states $|0,k\rangle$ are metastable, while the $|2,k+1/2\rangle$ states can now decay towards either $|0,k\rangle$ or $|0,k+1\rangle$. The metastable $|0,k\rangle$ states can still decay towards $|0,k'>k\rangle$ states via virtual states (co-tunneling process). These processes are particularly important when the states $|0,k\rangle$ and $|2,k+m+1/2\rangle$ are nearly degenerate (see Fig. 14a, in the case $m=1$), that is when $eV \approx U/(2m+1)$. At this point the two states we consider are coupled by high-order Josephson coupling : there can be a resonant transfer from $|0,k\rangle$ to $|2,k+m+1/2\rangle$. This latter state being unstable, the superposition will decay towards either $|0,k+m\rangle$ or $|0,k+m+1\rangle$ and the process can then start over again. This reasoning predicts resonances in the I-V characteristic at voltages $V = U/(2m+1)e$ (see Fig. 15a) which have been called “Cooper pair tunneling resonances”. The situation is reminiscent of the “radiative cascade” in atomic physics, where an atom placed in a resonant laser field can absorb and re-emit photons in a cyclic manner [18]. The treatment we perform in the following is inspired from that of the radiative cascade [18].

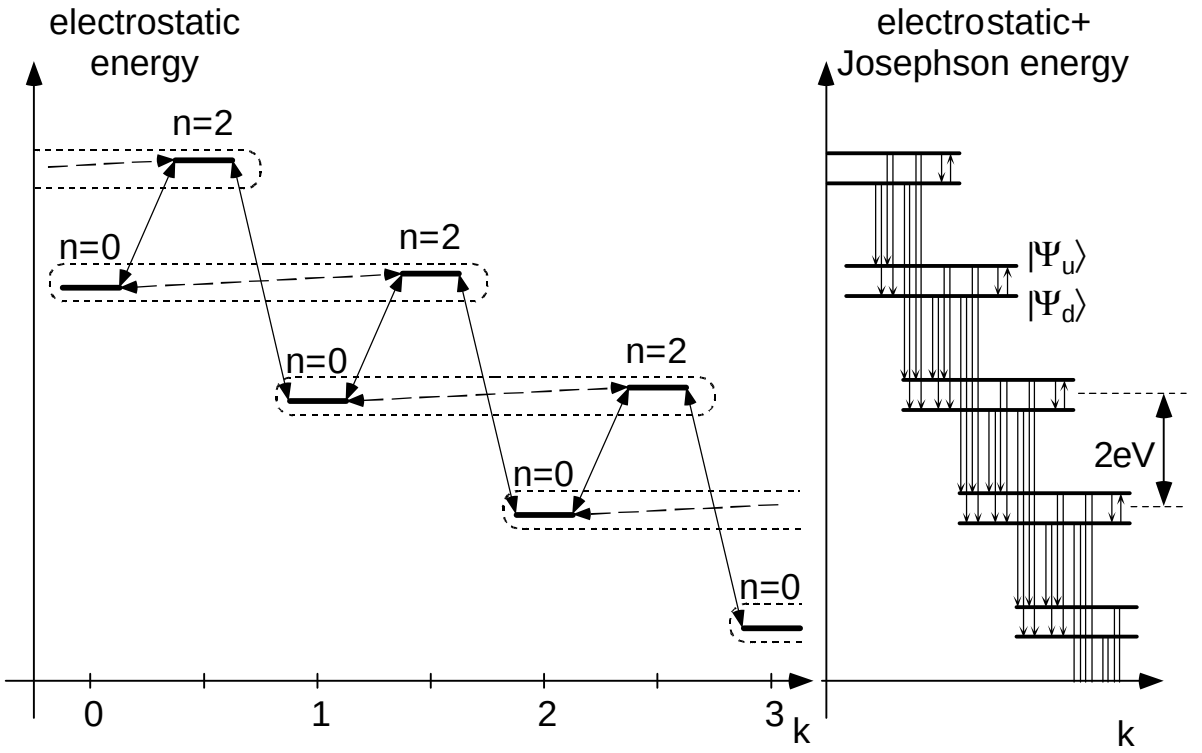

Fig. 14. *a) Electrostatic energy levels of the transistor at a voltage near U/3e. The thin full lines represent the Josephson coupling between the states. At this voltage, the states separated by 1 1/2 unit along the k axis are nearly degenerate. A higher-order Josephson coupling lifts this degeneracy. This high-order coupling can be handled perturbatively by the means of an effective Hamiltonian in the subspace spanned by two nearly degenerate states, as indicated by the dotted capsules. In these subspaces, the high order Josephson coupling can be replaced by an effective coupling as indicated by the thin dashed line joining the states. Each coupling arrow we have drawn has a corresponding decay channel due to the possibility of inelastic transition in the environment. b) After diagonalization of the effective Hamiltonians we are left with quasi-eigenstates among which photon-induced transitions (arrows) are possible. The current in the transistor corresponds to the cascade fromed by these transitions.*

Fig. 15. *(next page) a) Electrostatic energy levels as a function of V for the states indexed by n = 0 and n = 2 and k∈ [-10,10]. At zero voltage, the states with n = 2 have the energy $U = 4E_C(1-n_g)$. The dotted lines indicate the positions of the level crossings (which occur at eV/U = inverse of odd integer numbers). b) Numerical eigenenergies of the system when the Josephson coupling is taken into account. A value of $E_J = 0.3U$ was used in the calculation. Outer states and high order crossings are not well calculated because of the finite size of the matrix used in the calculation (21 levels). We see that the eigenenergies at zero voltage reconstruct the band structure already obtained (see Sec. III.B). At finite voltages the Josephson coupling turns level crossings into anticrossings. Moreover, these anticrossings are displaced toward higher voltages by the effect of the Josephson interaction. The dotted lines are the positions of the resonance given by a second-order perturbation theory calculation (see text). The figure shows that it is possible to treat each anticrossing locally as the anticrossing of a two level system. This is implemented by a 2×2 effective Hamiltonian for pairs of levels that come into resonance.*

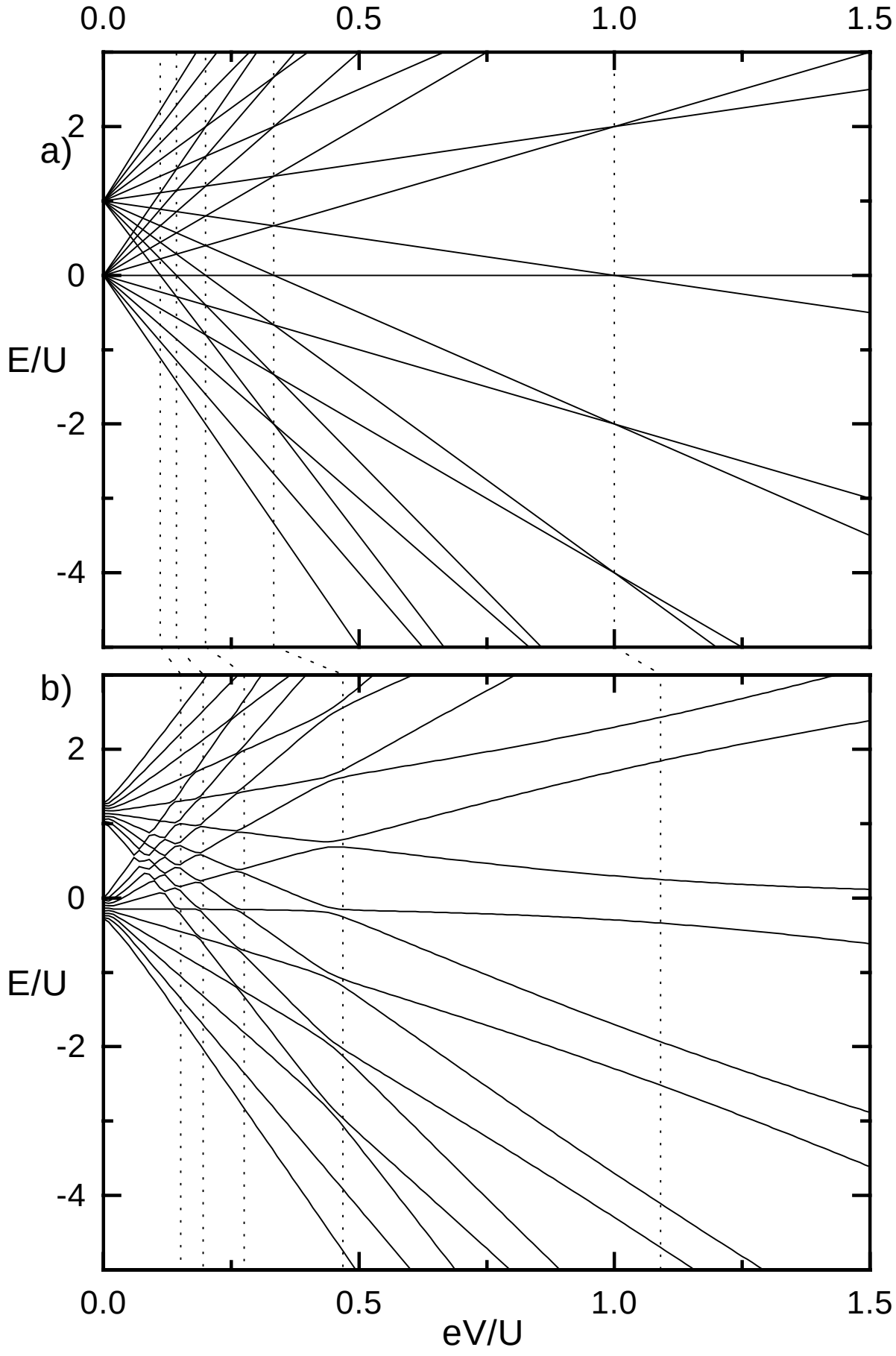
a)
b)
E/U
eV/U
0.0
0.5
1.0
1.5
2
0
-2
-4

2. Effect of the Josephson perturbation

We will now make an approximate diagonalization of the Josephson plus electrostatic Hamiltonian. The idea of our calculation is to treat the Josephson Hamiltonian as a perturbation to the lowest relevant order in the theory of perturbations. This amounts to keeping the minimal coherence in the system. The eigenbasis is obtained by block diagonalization of the perturbed Hamiltonian : we separate the total Hilbert space into 2-dimensional subspaces spanned by pairs of unperturbed states which come into resonance (level crossings in Fig. 14a). In each of these subspaces we write an effective Hamiltonian which is then easily diagonalized.

range of validity of the method and extensions

The 2×2 effective Hamiltonian for the two unperturbed states we want to block-diagonalize is meaningful only when the two eigenstates we obtain are well separated from the others. This excludes the cases where the electrostatic energy U becomes comparable or smaller than the Josephson coupling energy. This happens for a large Josephson coupling but also for any Josephson coupling near $n_g = 1$ since U vanishes for this gate voltage[2]. Also, when eV is comparable or smaller than the interlevel coupling energy E_J, there is no way to treat the Josephson Hamiltonian perturbatively and the situation is more complex.
When our simple 2×2 block diagonalization fails, it is still possible to find numerically an eigenbasis of the perturbed Hamiltonian. This eigenbasis must be periodic in k (period 1) and in energy (period $2eV$). It can be obtained by making a numerical diagonalization of the perturbed Hamiltonian with a sufficiently large number of unperturbed states for the side effects to be negligible. This is the approach used in Ref. 16.

a) EFFECTIVE HAMILTONIAN OF A PAIR OF NEARLY DEGENERATE STATES.

We consider the states $|a\rangle = |n = 0, k\rangle$ and $|b\rangle = |n = 2, k+q/2\rangle$, where q is an odd integer. We suppose the voltage V such that their electrostatic energies are nearly degenerate, *i.e.*

$$qeV \approx U .$$

We will use the notation $\mathcal{D}_k^q$ to designate the subspace of states spanned by $\{|0, k\rangle, |2, k+q/2\rangle\}$. We call P the projector on the subspace $\mathcal{D}_k^q$ and Q its complementary projector ($P+Q = \mathbb{1}$). If the states we consider are well separated from the others, we can use an effective Hamiltonian in $\mathcal{D}_k^q$ [18]:

---

[2] However, if one ignores the possibility of Zener tunneling between bands (see Sec. VI.C.4), the $n_g = 1$ case can be treated simply because the transistor then behaves similarly to a single junction

$$H^{eff} = \begin{bmatrix} E_a + R_{aa}(\bar{E}) & R_{ab}(\bar{E}) \\ R_{ba}(\bar{E}) & E_b + R_{bb}(\bar{E}) \end{bmatrix}$$

where the $R_{ij}(\bar{E})$ are the matrix elements of the restriction $PR(z)P$ of the displacement operator [18]

$$R(z) = H_J + H_J \frac{Q}{z - H_{el}} H_J + H_J \frac{Q}{z - H_{el}} H_J \frac{Q}{z - H_{el}} H_J + \ldots$$

to the subspace $\mathcal{D}_k^q$ calculated for the average energy $\bar{E} = (E_a + E_b)/2$, with $E_a = 0$ and $E_b = U - qeV$. Here, the Hamiltonian H_{el} is the unperturbed Hamiltonian and H_J is treated as a perturbation,

$$H_{el} = U(\frac{n}{2} \bmod 2) - 2eVk$$

$$H_J = -J \sum_k \left[|0,k\rangle\langle 2,k+\tfrac{1}{2}| + |0,k\rangle\langle 2,k-\tfrac{1}{2}| + h.c. \right]$$

where we have introduced the notation $J = E_J/2$, E_J being the Josephson coupling energy of the two supposedly identical junctions. We will calculate the matrix elements of the displacement operator at the leading order in the perturbation.

If $q > 1$, the displacement in energy $R_{aa}(\bar{E})$ and $R_{bb}(\bar{E})$ of the states is non zero only in second order in the perturbation while the effective coupling $R_{ab}(\bar{E})$ is non zero at order q in the perturbation.

We now introduce further approximations. Since we want to calculate resonances which will occur on a narrow voltage range, we will compute the matrix elements of the displacement operator at the expected voltage of the resonance and neglect their voltage dependence in the remaining part of the calculation. The voltage at which the resonance appears is determined by the equality

$$E_a + R_{aa}(\bar{E}) = E_b + R_{bb}(\bar{E}) \tag{2}$$

which should in principle be solved self-consistently, since $\bar{E}$ and E_b depend on the voltage of the resonance. The leading correction to the position of the resonance can be obtained by computing the matrix elements of the displacement operator using the unshifted position of the resonance $V = U/qe$, for which we have $\bar{E} = 0$.

Within these approximations the matrix elements of the displacement operator at the lowest order in the perturbation are then given by

$$R_{bb}(0) = -R_{aa}(0) = \frac{J^2}{U} \frac{2q^2}{q^2 - 1}$$

$$R_{ab}(0) = R_{ba}(0) = \frac{J^q}{U^{q-1}} \prod_{i=1}^{q-1} \left(\frac{i}{q} - i \bmod 2 \right)^{-1}.$$

Inserting these values in (2), we obtain the position of the resonance, at the leading order in the perturbation

$$V_q = \frac{U + 2R_{bb}(0)}{qe} = \frac{U}{qe} + \frac{J^2}{eU}\frac{4q}{q^2 - 1} + \mathcal{O}\left(\frac{J^4}{eU^3}\right) \tag{3}$$

instead of simply U/qe in absence of the perturbation.
In order to shorten the notations in the following we introduce

$$J_q = -R_{ab}(0)$$

$$D_q = \frac{\overline{E}}{2} + R_{bb}(0)$$

(note that D_q is voltage-dependent via $\overline{E}$) so that the effective Hamiltonian can be written

$$H^{eff} = \frac{\overline{E}}{2}\mathbb{1} - \begin{bmatrix} D_q & J_q \\ J_q & -D_q \end{bmatrix}$$

If $q = 1$, $|a\rangle$ and $|b\rangle$ are coupled at order one in the perturbation, but the displacement of the levels is still of the second order. We can use the same writing of the Hamiltonian as in the general case by letting $J_1 = J$ and $D_1 = \overline{E}/2 + J^2/U$.

b) Diagonalization of the effective Hamiltonian

We can now use the effective Hamiltonian for the states $|a\rangle$ and $|b\rangle$ to obtain the eigenstates of the system in this subspace. The effective Hamiltonian is rewritten as

$$H^{eff} = \frac{\overline{E}}{2}\mathbb{1} - \sqrt{D_q^2 + J_q^2}\begin{bmatrix} \cos 2\alpha & \sin 2\alpha \\ \sin 2\alpha & -\cos 2\alpha \end{bmatrix}$$

with

$$\begin{aligned} \cos 2\alpha &= D_q \Big/ \sqrt{D_q^2 + J_q^2} \\ \sin 2\alpha &= J_q \Big/ \sqrt{D_q^2 + J_q^2} \end{aligned} \tag{4}$$

The eigenstates of the system with their associated eigenenergy are given by

$$\begin{aligned} |\psi_d\rangle &= \cos\alpha\,|a\rangle + \sin\alpha\,|b\rangle \qquad & \mathcal{E}_d &= \frac{\overline{E}}{2} - \sqrt{D_q^2 + J_q^2} \\ |\psi_u\rangle &= \sin\alpha\,|a\rangle - \cos\alpha\,|b\rangle \qquad & \mathcal{E}_u &= \frac{\overline{E}}{2} + \sqrt{D_q^2 + J_q^2} \end{aligned} \tag{5}$$

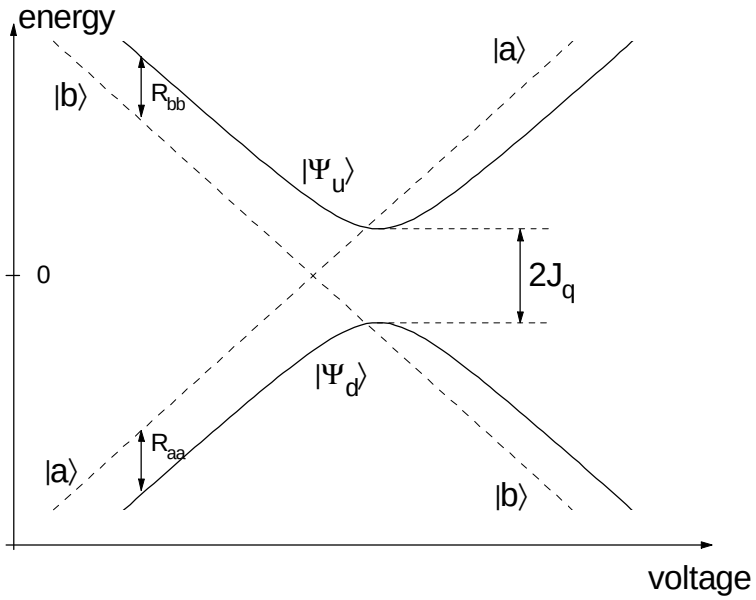

Fig. 16. *Eigenenergy levels of the effective 2×2 Hamiltonian near the resonance (The mean energy of the levels has been subtracted). The dotted lines are the energy levels without the perturbation.*

3. Effect of the environment ; transition rates

We now consider the effect of the coupling of the eigenstates of the electrostatic plus Josephson Hamiltonian with the oscillators of the electromagnetic environment. We will suppose that the environment is a weak perturbation of the system (*i.e.* it has an impedance much lower than h/e^2). The coupling to the continuum of states of the environment will give an imaginary part to the energies of the eigenstates of the electrostatic plus Josephson system. This imaginary part of the energy will generate transitions between the states that were calculated in the previous section (see Fig. 14b) and a current will result from these transitions. To obtain this current, we first need to calculate the rates of the numerous possible transitions between the pairs of states that we have obtained in the previous section. We suppose that the voltage is near V_q (Eq. (3)), so that the system is approximately diagonalized in the subspaces $\mathcal{D}_k^q$. We first consider the general case where $q > 1$ (the case $q = 1$ is easily obtained by simplifying the general treatment). Each quasi eigenstate of the subspace $\mathcal{D}_k^q$ can decay into each of the quasi eigenstates of the subspaces $\mathcal{D}_{k+(q-1)/2}^q$ and $\mathcal{D}_{k+(q+1)/2}^q$ (see Fig. 17). Due to the relatively high energy of these transitions (the voltage is not low by hypothesis), we neglect the reverse transitions for which the environment would have to provide the energy. There are also transitions of lower energies within the quasi eigenstates of the subspace $\mathcal{D}_k^q$ for which we take into account the possibility of “upward” transitions.

a) EXPRESSIONS FOR THE TRANSITION RATES.

We will now derive the expression of the transition rates. By expanding the squares in the Hamiltonian H_{env} (1) of the environment, the coupling of the environmental degrees of freedom to the transistor's degrees of freedom takes the form of a term $2ek\mathcal{V}$, where $\mathcal{V}$ is the total voltage across the oscillators of the environment, *i.e.* across the impedance $Z(\omega)$ seen by the transistor (see Sec. II.B.3.c). Thus, the transition rate Γ_{if} between any two states $|i\rangle$ and $|f\rangle$ of the system is given by Fermi's golden rule [19]

$$\Gamma_{if} = \frac{1}{\hbar^2}\left|\langle f|2ek|i\rangle\right|^2 S_{\mathcal{V}}(\omega_{if}), \tag{6}$$

where $\omega_{if} = (E_i - E_f)/\hbar$ and $S_{\mathcal{V}}(\omega)$ is the quantum spectral density of the fluctuations of the voltage $\mathcal{V}$ across the transistor at the frequency ω. This spectral density of noise is related to the impedance $Z(\omega)$ seen by the transistor via the fluctuation-dissipation theorem [19]:

$$S_{\mathcal{V}}(\omega) = 2\,\mathrm{Re}\,Z(\omega)\frac{\hbar\omega}{1-\exp(-\hbar\omega/k_B T)} \tag{7}$$

where T is the temperature of the electromagnetic environment. In the following we will suppose that the impedance of the environment at the frequencies that are considered here can be described by a resistance $R \ll R_K = h/e^2$ and we will note $\rho = R/R_K$.
We can derive an alternate expression for the transition rate (6) in the following way :

$$\Gamma_{if} = \frac{1}{\hbar^2}\left|\langle f|2ek|i\rangle\right|^2\left(\hbar\omega_{if}\right)^2\frac{S_{\mathcal{V}}(\omega_{if})}{\left(\hbar\omega_{if}\right)^2}$$

$$= \frac{1}{\hbar^2}\left|\langle f|[H_0,2ek]|i\rangle\right|^2\frac{S_{\mathcal{V}}(\omega_{if})}{\left(\hbar\omega_{if}\right)^2}$$

where $H_0 = H_{el} + H_J$. Then, we use the fact that

$$\left[2ek, H_0\right] = 2ei\frac{\partial H_0}{\partial\delta} = i\hbar I$$

where I is the current operator which can be expressed as

$$I = \frac{2e}{\hbar}E_J\sin\frac{\delta}{2}\cos\theta$$

$$= \frac{2e}{\hbar}\frac{E_J}{4}\sum_k\left\{|0,k\rangle\langle 2,k+\tfrac{1}{2}| + |2,k+\tfrac{1}{2}\rangle\langle 0,k+1| - h.c.\right\}$$

Thus, we obtain an alternate expression for the transition rate

$$\Gamma_{if} = \left|\langle f|I|i\rangle\right|^2\frac{S_{\mathcal{V}}(\omega_{if})}{\left(\hbar\omega_{if}\right)^2} \tag{8}$$

The two expressions (6) and (8) of the transition rates are rigorously equivalent. However, when applied to the calculation of a transition rate between the approximate eigenstates we have found in Sec. 2, one of them might give a zero rate while the other gives a non-zero rate. This discrepancy is due to the neglect of components of order E_J/eV or smaller in the approximate eigenstates. When higher order components are taken into account, expressions (6) and (8) give the same result. In the following we use the expression of the rate which gives a non-zero rate at the lowest order in the calculation of the eigenstates.

b) INTRA-DOUBLET TRANSITION RATES.

We now calculate the transition rates γ and γ' between the two quasi eigenstates $|\Psi_d\rangle$ and $|\Psi_u\rangle$ of a doublet (see Fig. 17). With the notations and the results (5) of Sec. 2b, expression (6) yields

$$\gamma = \frac{2\pi}{\hbar}\rho \frac{q^2 J_q^2}{\sqrt{J_q^2 + D_q^2}} \frac{1}{1-\exp\left(-2\sqrt{J_q^2 + D_q^2}\,\middle/\,k_B T\right)}$$

The second rate γ' is easily obtained from the detailed balance symmetry obeyed by the two rates :

$$\gamma' = \gamma \exp -\frac{\mathcal{E}_u - \mathcal{E}_d}{k_B T} = \gamma \exp -\frac{2\sqrt{J_q^2 + D_q^2}}{k_B T} \tag{9}$$

where T is the temperature of the environment.

c) INTER-DOUBLET TRANSITIONS

We use here the expression (8) to compute the transition rates between the quasi-eigenstates of different doublets. Using the expressions (5) of the quasi-eigenstates, we compute the squares of the matrix elements of the current figuring in (8) for the various transitions :

$$\Gamma_{dd}^{\pm}, \Gamma_{uu}^{\pm} : \left(\frac{eJ}{2\hbar}\right)^2 \cos^2\alpha \sin^2\alpha$$

$$\Gamma_{du}^{\pm} : \left(\frac{eJ}{2\hbar}\right)^2 \sin^4\alpha$$

$$\Gamma_{ud}^{\pm} : \left(\frac{eJ}{2\hbar}\right)^2 \cos^4\alpha$$

where α is defined by (4), and $J = E_J/2$, as previously. In the following we neglect the differences in the transition energy for the Γ^- rates and we take the average energy $(q\text{-}1)eV$ for all of them. Similarly, we take the energy $(q+1)eV$ for the Γ^+ rates. We further neglect the Boltzmann exponential in the denominator of (7), which is consistent with our neglect of the upward transitions between doublets. We thus obtain the final expression for the rates

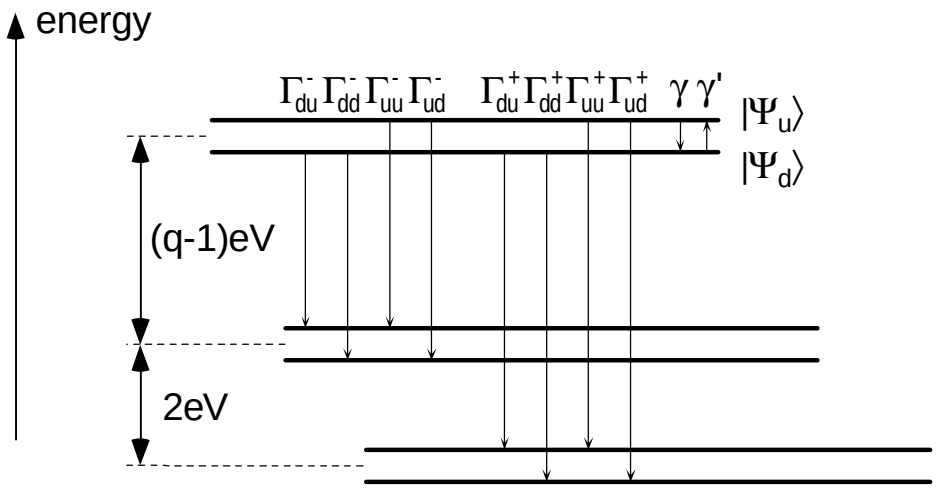

Fig. 17. *Different decay processes of the quasi-eigenstates of a doublet and labelling of the rates of the processes.*

$$\Gamma_{dd}^{\pm} = \Gamma_{uu}^{\pm} = \frac{2\pi}{\hbar}\rho\frac{2J^2}{(q\pm 1)eV}\cos^2\alpha\sin^2\alpha$$

$$\Gamma_{du}^{\pm} = \frac{2\pi}{\hbar}\rho\frac{2J^2}{(q\pm 1)eV}\sin^4\alpha$$

$$\Gamma_{ud}^{\pm} = \frac{2\pi}{\hbar}\rho\frac{2J^2}{(q\pm 1)eV}\cos^4\alpha$$

4. Calculation of the current

We now define the probability p_k^d (p_k^u) that the ground (excited) eigenstate $|\Psi_d\rangle$ ($|\Psi_u\rangle$) of the doublet $\mathcal{D}_k^q$ is occupied. We further define the total probability for the system to be in a ground or excited state of a doublet

$$P_d = \sum_{k=-\infty}^{+\infty} p_k^d$$

$$P_u = \sum_{k=-\infty}^{+\infty} p_k^u$$

which of course verify $P_d + P_u = 1$.

The equation of evolution of these probabilities is given by

$$\dot{P}_d = -\dot{P}_u = \left(\Gamma_{ud}^{+} + \Gamma_{ud}^{-} + \gamma\right)P_u - \left(\Gamma_{du}^{+} + \Gamma_{du}^{-} + \gamma'\right)P_d$$

Thus, the stationary value of the probabilities is given by

$$\overline{P}_d = 1 - \overline{P}_u = \frac{\Gamma_{ud}^{+} + \Gamma_{ud}^{-} + \gamma}{\Gamma_{ud}^{+} + \Gamma_{ud}^{-} + \Gamma_{du}^{+} + \Gamma_{du}^{-} + \gamma + \gamma'}.$$

From this point the current is easily obtained by summing the rates multiplied by the probability that their initial state is occupied and by the charge the process carries through the transistor. For each rate, the transferred charge through the transistor is given by :

$$\begin{aligned}
\Gamma^{\pm}_{dd}, \Gamma^{\pm}_{uu} &: \mathcal{Q}^{\pm}_{dd} = \mathcal{Q}^{\pm}_{uu} = (q \pm 1)e \\
\Gamma^{\pm}_{du} &: \mathcal{Q}^{\pm}_{du} = (2q\cos^2\alpha \pm 1)e \\
\Gamma^{\pm}_{ud} &: \mathcal{Q}^{\pm}_{ud} = (2q\sin^2\alpha \pm 1)e \\
\gamma &: \mathcal{Q} = -qe\cos 2\alpha \\
\gamma' &: \mathcal{Q}' = qe\cos 2\alpha
\end{aligned}$$

Finally, the steady-state cascade of transitions gives a current

$$\begin{aligned}
I_q = \overline{P}_d\left[\Gamma^-_{dd}\mathcal{Q}^-_{dd} + \Gamma^-_{du}\mathcal{Q}^-_{du} + \Gamma^+_{dd}\mathcal{Q}^+_{dd} + \Gamma^+_{du}\mathcal{Q}^+_{du} + \gamma'\mathcal{Q}'\right] + \\
\overline{P}_u\left[\Gamma^-_{uu}\mathcal{Q}^-_{uu} + \Gamma^-_{ud}\mathcal{Q}^-_{ud} + \Gamma^+_{uu}\mathcal{Q}^+_{uu} + \Gamma^+_{ud}\mathcal{Q}^+_{10} + \gamma\mathcal{Q}\right]
\end{aligned}$$

which can be slightly simplified using the fact that $\overline{P}_d + \overline{P}_u = 1$, $\Gamma^{\pm}_{uu} = \Gamma^{\pm}_{dd}$ and $\mathcal{Q}^{\pm}_{uu} = \mathcal{Q}^{\pm}_{dd}$:

$$I_q = \Gamma^-_{dd}\mathcal{Q}^-_{dd} + \Gamma^+_{dd}\mathcal{Q}^+_{dd} + \overline{P}_d\left[\Gamma^-_{du}\mathcal{Q}^-_{du} + \Gamma^+_{du}\mathcal{Q}^+_{du} + \gamma'\mathcal{Q}'\right] + \overline{P}_u\left[\Gamma^-_{ud}\mathcal{Q}^-_{ud} + \Gamma^+_{ud}\mathcal{Q}^+_{ud} + \gamma\mathcal{Q}\right] \qquad (10)$$

The case $q = 1$ can be treated in the same way by suppressing the processes corresponding to the Γ^- rates above.

a) *I-V* CHARACTERISTICS

To compute the I-V characteristics of the sample we simply add the currents I_q corresponding the various $q = 1, 3, 5\ldots$ This is of course not a good approximation as soon as the different resonances begin to overlap. This approximation is quite reasonable in most situations since the resonances are naturally well separated in voltage ; it does fail however near $n_g = 1$ and $V = 0$, but our diagonalization is not valid anyway in this range of parameters. In Fig. 18 we plot an *I-V* characteristic obtained in this manner for two values of the Josephson coupling. One immediately notices the qualitative difference between the $q = 1$ "resonance" and those of $q > 1$: the $q = 1$ resonance takes the shape of a rounded step. This step marks the onset of the sequential tunneling of Cooper pairs, as occurs in a single Josephson junction (see Fig. 13c). It is also clearly visible that the width of the resonance depends extremely rapidly on the value of the Josephson coupling for the high order resonances. This happens because this width is given by $J_q \propto (E_J/U)^q$.

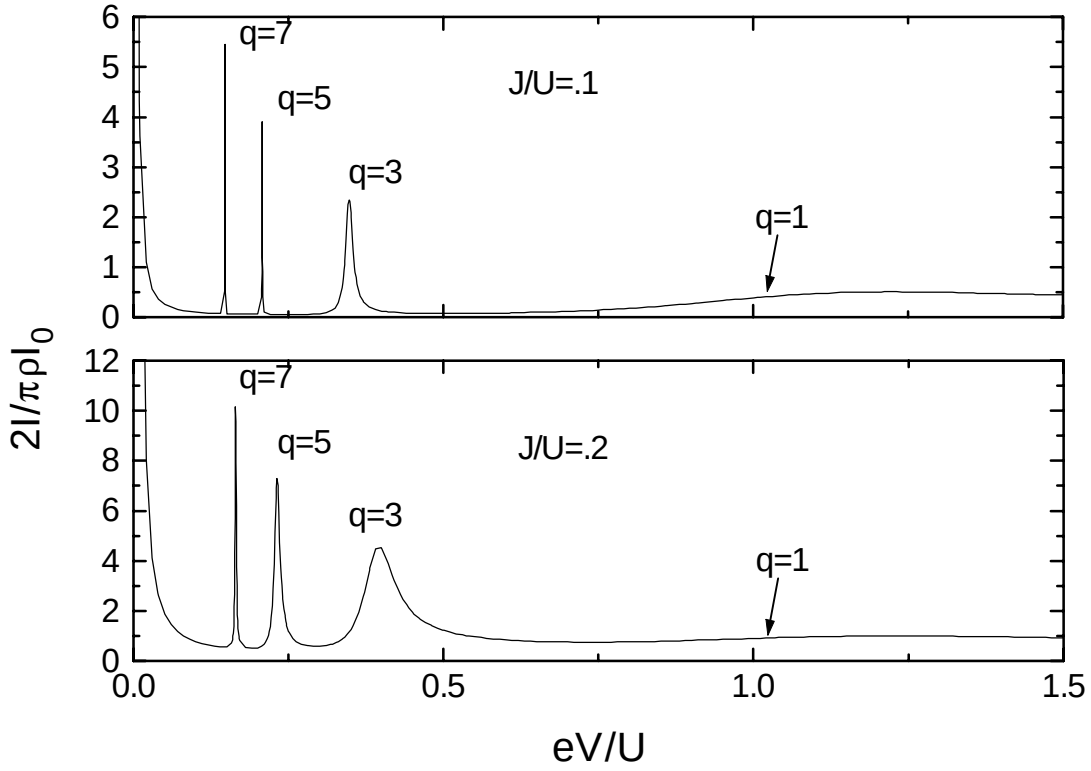

Fig. 18. *Theoretical I-V characteristic of a transistor. The curves were obtained using Eq. (10). Only the first excited charge state of the island is taken into account here, and the resonances of order higher than q = 7 have not been calculated. Two values of the Josephson coupling-charging energy ratio are considered. The q = 1 resonance is barely visible in both case : it is more a rounded step than a resonance. The other resonances are asymmetric in shape. Their width diminishes rapidly with increasing order of the resonance, and with decreasing strength of the Josephson coupling. The effect of energy-level displacement is clearly visible on the change in the q = 3 resonance when going from the top to the bottom panel.*

To further reproduce what is seen is the experiments we must also add the resonances due to the crossing of the $n = 0$ state with the $n = -2$ state which is the second charge state of the island in the domain $n_g \in [0,1]$. For this charge state we have $U = 4E_C(1+n_g)$ in the calculations of the resonances. The result of summing all these processes is shown in Fig. 19, for gate charges $n_g \in [-0.5,0.95]$.

The positions of the resonances in the V-n_g plane are shown in Fig. 20, in the case were $E_J \ll E_C$. The resonances fall on lines diverging from the $V = 0$, n_g = (odd integer) points, where the switching current of the transistor is maximum. One can think of the peaks in the supercurrent modulation with the gate voltage as resulting of the build-up of all the resonances due to the resonant Cooper pair tunneling.

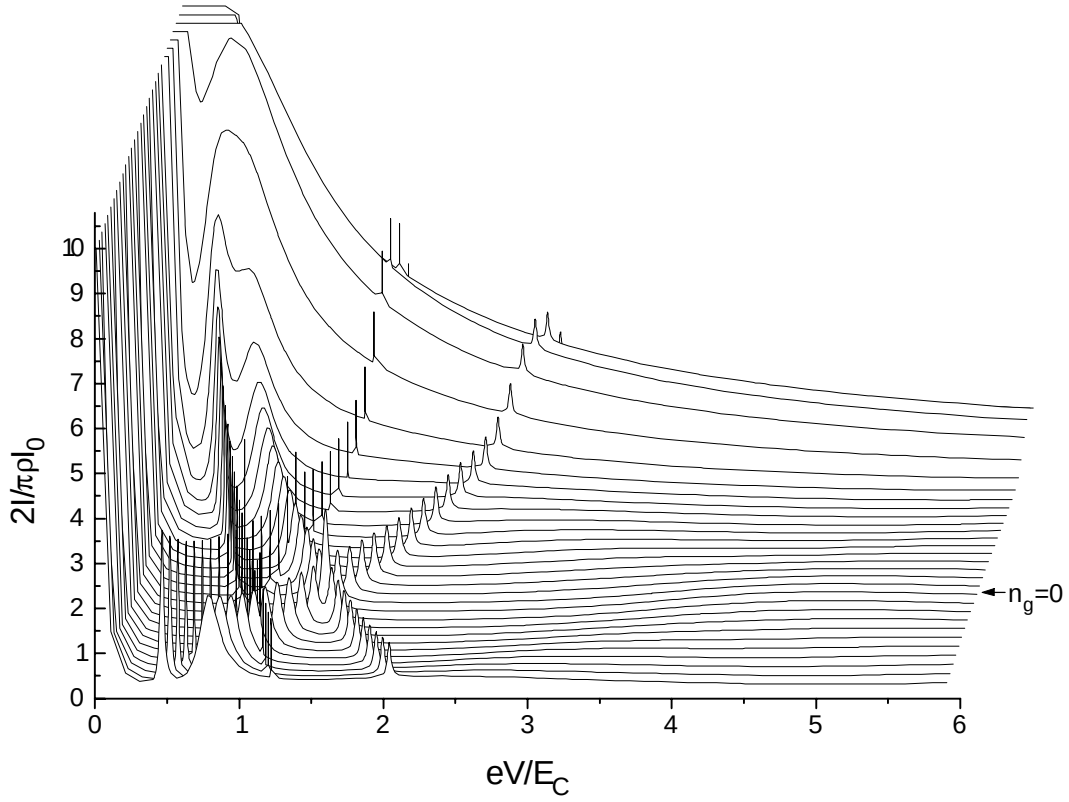

Fig. 19. *Simulated I-V characteristics for different gate charges. The gate charge ranges from n_g = -0.5 (bottom trace) to n_g = .95 (top trace), the n_g = 0 trace is indicated by an arrow on the right hand side. We have used the model described in the text but using this time the first two excited charge states of the island and a ratio E_J/E_C = 4/5. Also, for each of these charge states we have calculated the resonance only up to the q = 5 level crossing*

5. Application : determination of the charging energy of the transistor

The crossing of the resonances visible in Fig. 19 at $n_g = 0$ is of great practical importance : it allows a precise determination of the charging energy of the transistor. These resonance crossings corresponds to the degeneracy of the $n = \pm 2$ levels at $n_g = 0$. In particular, the crossing of the resonances of order $q = 3$ is particularly well suited for this purpose because it is clearly seen in the experiments (see Sec. V.C.) and much more precise than the smooth shoulder made by the $q = 1$ resonance. According to Eq. (2), this particular crossing of resonances at $n_g = 0$ occurs at the voltage V such that

$$eV \approx \frac{4E_C}{3} + \frac{3E_J^2}{32E_C}$$

which is easily inverted to yield

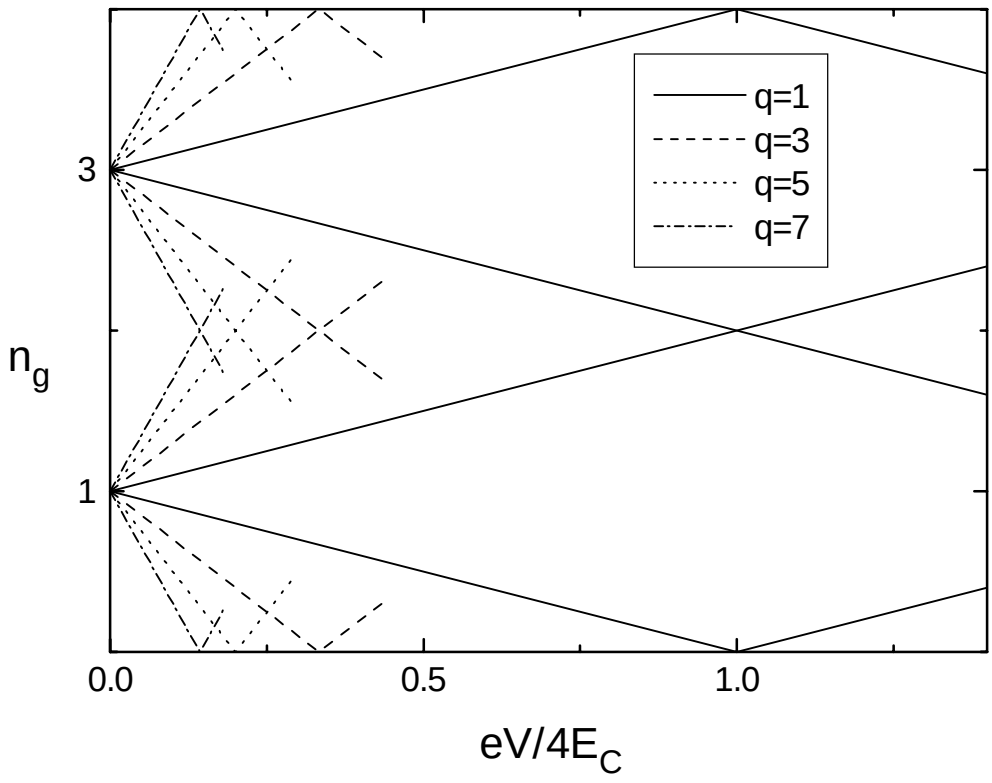

Fig. 20. *Positions of the current peaks due to resonant Cooper pair tunneling of order q = 1,3,5,7 in the V-n_g plane, for a $E_J << E_C$. The supercurrent peak of the transistor can be thought to result of the accumulation of these resonances near V=0.*

$$E_C = \frac{3}{4}\left(eV + \sqrt{(eV)^2 - E_J^2/2}\right)$$

$$E_C = \frac{3eV}{4} - \frac{3E_J^2}{32eV} + \mathcal{O}\left(\frac{E_J^4}{(eV)^3}\right)$$

The correction brought by the Josephson coupling can be evaluated with the independently determined value of E_J given by the Ambegaokar-Baratoff formula. In our experiments it never exceeded 1% of the dominant term. This was also of the order of precision we had on the position of the crossing of the resonances. The correction could thus be ignored. Let us stress the practical importance of this determination of the charging energy : the charging energy is usually obtained by fitting the temperature dependence of the *I-V* characteristic of the transistor in the normal state. This method is tedious (it takes hours) and gives a typical accuracy on the value of the charging energy of the order of 10%. With the method described in this section we could obtain rapidly (no changing of the temperature was required) an accuracy of a few percent on the charging energy (see Chap. VI.).

References for Chap. III

[1] P. Lafarge, Ph.D. Thesis, Université Paris 6 (1993).

[2] J. M. Martinis, M. H. Devoret, and J. Clarke, Phys Rev. **B 35**, 4682 (1987).

[3] W. C. Stewart, Appl. Phys. Lett. **12**, 277 (1968); D. E. McCumber, J. Appl. Phys. **39**, 3113 (1968).

[4] F. Neumann, G.-L. Ingold, and H. Grabert, Phys. Rev. **B 50**, 12811 (1994)

[5] W. J. Elion, M. Matters, U. Geigenmüller, and J. E. Mooij, Nature **373**, 594 (1994).

[6] P. Lafarge, P. Joyez, D. Esteve, C. Urbina, and M. H. Devoret, Nature **365**, 422 (1993).

[7] V. Bouchiat, M. H. Devoret, D. Esteve, P. Joyez, C. Urbina and D. Vion, in preparation.

[8] D. V. Averin and K. K. Likharev, in *Mesoscopic Phenomena in Solids*, ed. by B. Al'tshuler, P. Lee, and R. Webb (Elsevier, Amsterdam, 1991), Chap. 6.

[9] K. A. Matveev, M. Gisselfält, L. I. Glazman, M. Jonson and R. I. Shekhter, Phys. Rev. Lett. **70**, 2940, 1993.

[10] J. Bardeen, L. N. Cooper and J. R. Schrieffer, Phys. Rev. **108**, 1175 (1957).

[11] M. Tinkham, *Introduction to Superconductivity* (McGraw-Hill, New York, 1975).

[12] P. Lafarge, P. Joyez, D. Esteve, C. Urbina and M. H. Devoret, Phys. Rev. Lett. **70**, 994 (1993).

[13] M. T. Tuominen, J. M. Hergenrother, T. S. Tighe and M. Tinkham, Phys. Rev. Lett. **69**, 1997 (1992).

[14] A. Maassen van den Brink, L. J. Geerligs, and G. Schön, Phys. Rev. Lett. **67**, 3030 (1991).

[15] A. Maassen van den Brink, A. A. Odintsov, P. A. Bobbert, and G. Schön, Z. Phys. **B 85**, 459 (1991).

[16] P. A. Bobbert and A. A. Odintsov, unpublished (1991).

[17] D. B. Haviland, Y. Harada, P. Delsing, C. D. Chen, and T. Claeson, Phys. Rev. Lett. **73**, 1541 (1994)

[18] C. Cohen-Tannoudji, J. Dupont-Roc and G. Grynberg, *Atom-photon interactions. Basic processes and applications*, (Wiley, New York, 1992).

[19] G.-L. Ingold and Yu. V. Nazarov, in *Single Charge Tunneling*, edited by H. Grabert and M. H. Devoret (Plenum, New York, 1992), Chap. 2.

IV. SWITCHING CURRENT OF SMALL JOSEPHSON DEVICES

At $T = 0$ the Josephson coupling energy in the superconducting single electron transistor (SSET) should manifest itself as a zero-voltage supercurrent branch in the *I-V* characteristic of the device. However, small Josephson junctions have Josephson coupling energies so low (typically a fraction of a Kelvin) that it is not possible experimentally to reach a regime where thermal fluctuations can be neglected. Under these conditions supercurrent flow in these experiments tends to be suppressed. In the past, this question has been well studied both experimentally and theoretically for resistively shunted junctions [1,2]. However, in our experiments, like in most experiments seeking to observe quantum fluctuations of the phase, the transistor was "unshunted" : the two junctions were biased at dc by a nearly ideal current source. We have observed a well defined "superconducting branch" (*i.e.* at nearly zero voltage) and a hysteretic behaviour. A parameter of great practical importance in this case is the maximum supercurrent one can drive through the transistor which we call the switching current.

In the following, we present a comprehensive approach of the problem of a Josephson junction imbedded in a classical arbitrary electromagnetic environment and we elucidate the question of the relationship between the switching current of an unshunted junction and its critical current. Most of the analysis readily applies to the more general problem of Josephson devices like SQUIDs and SSETs.

A. Theoretical aspect of the measurement of a Josephson junction

1. Description of a typical experimental set-up

In typical experiments, a Josephson junction is biased using a dc current source $\mathcal{I}$ and one measures the dc voltage $\mathcal{V} = \langle \mathcal{V}(t) \rangle$ across the junction. A schematic of the experimental set-up is shown in Fig. 1a. We use linear quadrupoles $\mathcal{Q}_1$ and $\mathcal{Q}_2$ to describe the electromagnetic properties of the leads (possibly containing filtering elements) connecting the junction to the current source and to the voltage measuring apparatus. The junction itself is described as a capacitance c_j in parallel with a pure tunnel element. Using Norton's theorem, the dipole seen by the pure tunnel element can be replaced by a dc current source I_b in parallel with an

admittance[1] $Y(\omega)$ (Fig. 1b). In this description the properties of the electromagnetic environment of the tunnel element are entirely contained in the admittance $Y(\omega)$.

After solving the dynamics of the system in this representation, going back to the dc currents and voltages in the original $\{\mathcal{I}, \mathcal{V}\}$ representation is simply a matter of applying a linear

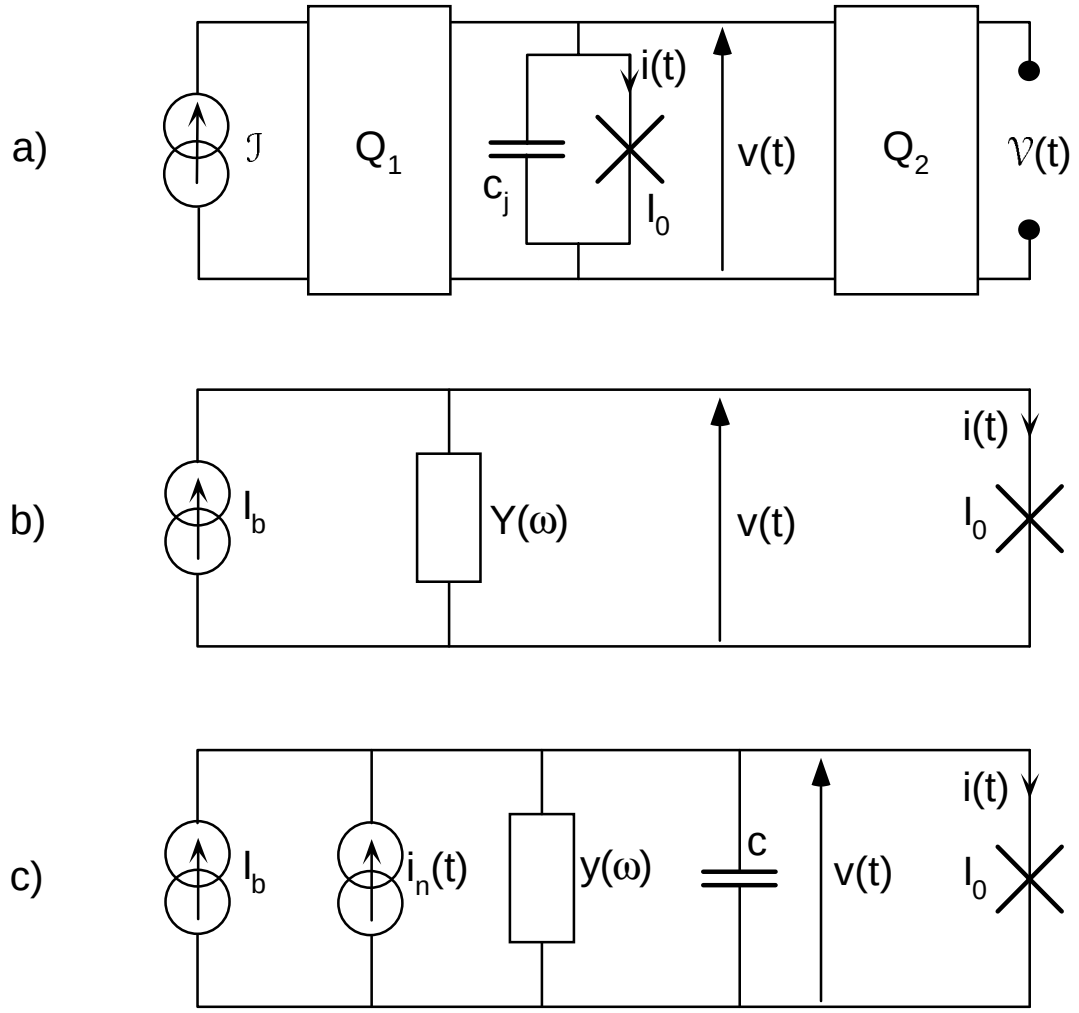

Fig. 1. ***a)*** *Typical set-up used to measure the current-voltage characteristic of Josephson junctions. The leads containing filtering elements which connects the junction to the bias source* $\mathcal{I}$ *and to the voltage measuring apparatus (voltage* $\mathcal{V}(t)$*) are described by the quadrupoles* $\mathcal{Q}_1$ *and* $\mathcal{Q}_2$*. The electrical behaviour of the junction itself is modelled by a capacitance* c_j *in parallel with a pure tunnel element whose critical current is* I_0*. By use of Norton's theorem, the set-up is equivalent to* ***b)****, where the electromagnetic environment of the pure tunnel element is entirely contained in the admittance* $Y(\omega)$*. The admittance* $Y(\omega)$ *can be formally separated into the parallel combination of a capacitor c and another admittance* $y(\omega)$ *as indicated in* ***c)****. The thermal noise generated by the admittance is modelled by the noise current source* $i_n(t)$*.*

---

[1] Since we describe here a current bias of the junction with a parallel connection of electrical elements (see Fig. 1b & c), it is more convenient to use admittances rather than impedances. The admittance $Y(\omega)$ we introduce

transformation on $I_J = \langle i(t)\rangle$ and $V = \langle v(t)\rangle$, the average values of the current flowing through the junction and the voltage across the junction, respectively.

The admittance $Y(\omega)$ can further be decomposed as the parallel combination of a capacitance c and an admittance $y(\omega)$ given by

$$c = \lim_{\omega\to\infty} \frac{Y(\omega)}{j\omega}$$

$$y(\omega) = Y(\omega) - jc\omega$$

The capacitance c is the junction's own capacitance c_j increased by some extra capacitance brought by the leads. The thermal noise generated by the dissipative part of the admittance $y(\omega)$ is described by a noise current source $i_n(t)$ in parallel with the admittance. The spectral density of this noise source is

$$S_{i_n}(\omega) = 4k_B T \,\mathrm{Re}\, y(\omega).$$

2. Equations of dynamics for the system

We now want to analyse the dynamics of the circuit represented in Fig. 1c. The impedance seen by the junction at high frequency is in practice always of the order of the vacuum impedance $Z_0 \approx 377\ \Omega$ which is much below $R_K \approx 25.8\ \mathrm{k}\Omega$. This permits us to treat the phase δ of the junction as a classical variable [3]. Kirchhoff's law applied to the circuit of Fig. 1c gives

$$I_b + i_n(t) = i(t) + \int_0^{+\infty} v(t-\tau)\tilde{y}(\tau)\mathrm{d}\tau + c\dot{v}(t) \qquad (1)$$

where $\tilde{y}(t) = \frac{1}{2\pi}\int_{-\infty}^{+\infty} y(\omega)\mathrm{e}^{j\omega t}\mathrm{d}\omega$ is the inverse Fourier transform of $y(\omega)$, $i(t)$ is the current flowing through the tunnel junction and $v(t)$ is the voltage across the junction. The current $i(t)$ flowing through the junction is given by the Hamilton equation

$$i(t) = \frac{1}{\varphi_0}\frac{\partial E(\delta)}{\partial \delta} = \frac{E_J}{\varphi_0} f'(\delta)$$

where $\varphi_0 = \Phi_0/2\pi = \hbar/2e$ and δ itself is a dynamic quantity. In the latter equation $E(\delta) = E_J f(\delta)$ is the equation of the lowest energy band of the effective junction, E_J is the Josephson coupling energy and $f(\delta)$ and $f'(\delta)$ are periodic even and odd functions of amplitude 2 ($f(\delta) = -\cos\delta$ for a single junction, see Chap. III for the case of the transistor). It is useful to introduce the critical current $I_0 = E_J/\varphi_0$ of the junction. The voltage $v(t)$ across the junction is related to the phase by the equation

$$v(t) = \varphi_0 \dot{\delta}(t).$$

Written in terms of δ, Eq. (1) gives

---

here is simply connected to the impedance $Z(\omega)$ we have used in Chap. II by $Y(\omega) = 1/Z(\omega)$.

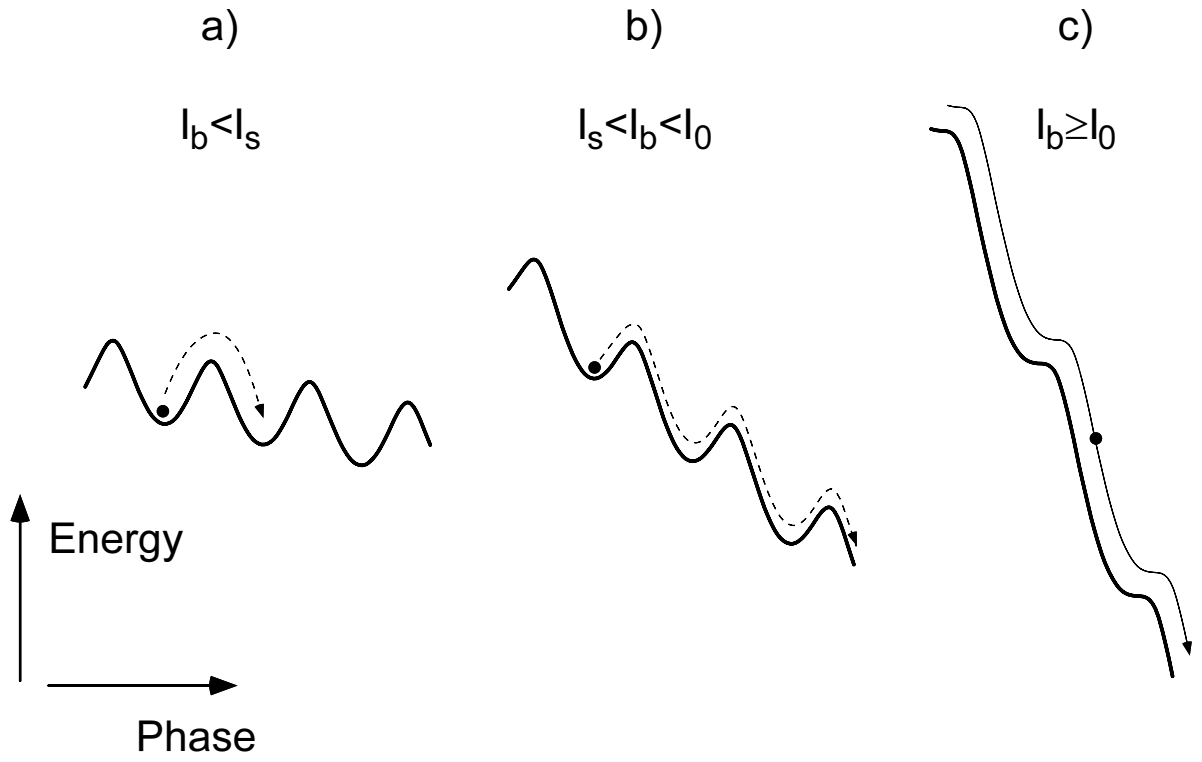

Fig. 2. *The dynamics of the phase difference of a Josephson device in presence of a driving current is that of a particle in a tilted washboard potential. The tilt of the potential is proportional to the driving current and the friction the particle experiences is provided by the admittance of the environment.* ***a)*** *If the current is too weak, the particle can only diffuse from well to well under the influence of thermal fluctuations.* ***b)*** *When the potential is tilted over a critical value I_s called the switching current, the energy gained going down the potential is on average greater than the energy lost by friction and the particle runs away, leading to a finite voltage state. The value of the switching current depends greatly on the damping of the particle : the lesser the damping, the lower I_s.* ***c)*** *For a current greater than the critical current I_0 the tilted potential no longer has any local minima : there cannot be a static solution for the phase.*

$$I_b + i_n(t) = I_0 f'(\delta) + \varphi_0 \int_0^{+\infty} \dot{\delta}(t-\tau)\tilde{y}(\tau)\mathrm{d}\tau + \varphi_0 c\ddot{\delta}. \qquad (2)$$

The evolution of δ is identical to that of a particle of mass $c\varphi_0^2$ in the tilted potential $\varphi_0(I_0 f(\delta) - I_b\delta)$ (see Fig. 2), with a random force $\varphi_0 i_n(t)$ and a friction force described by the kernel $\varphi_0^2\tilde{y}(t)$.

3. Discussion of the solutions

A supercurrent in the junction corresponds strictly speaking to a static solution for the phase ($\dot{\delta} = 0$). For bias currents I_b greater than I_0, the tilted potential has no local minima, and there are only dynamic solutions for the phase, associated with a finite dc voltage across the junction. At currents lower than I_0, Eq. (2) admits static solutions corresponding to the particle sitting at local minima of the potential. These static solutions are unstable against thermal

fluctuations and the particle will diffuse from well to well giving rise to a departure of the supercurrent branch from the zero voltage axis. The difficult part of the problem is the discussion of the stability of this diffusive motion. This problem can be treated numerically [4]. A weak point of this numerical approach is that it does not provide much intuition on the behaviour of the system when the parameters vary. In the following we use an approach based on the current-voltage characteristic of the junction in its electromagnetic environment. This approach, which does not rely on a particular calculational technique, gives a more general albeit only qualitative understanding of the behaviour of the system.

a) CURRENT-VOLTAGE CHARACTERISTIC OF THE JUNCTION IN ITS ELECTROMAGNETIC ENVIRONMENT.

A general discussion of the stability of the dynamics can be done using the notion of current-voltage characteristic of the junction in its electromagnetic environment. The I_J-V characteristic is plotted in the $\{V, I_J\}$ plane where $V = \langle v(t) \rangle$ is the average voltage across the junction and $I_J = \langle i(t) \rangle$ is the average current flowing through the junction. The I_J-V characteristic is defined as the set of points of the $\{V, I_J\}$ plane where the average power delivered by the current source I_b is equal to the average power dissipated in the admittance $y(\omega)$. In this definition, "average" means an average over the pseudo-period $\mathcal{T}$ or a relevant time for the evolution of the system followed by a thermodynamic ensemble average.
In the absence of thermal fluctuations, the motion of the phase is deterministic, and the average power balance is obtained for solutions of the differential equation (2) for which $\dot{\delta}$ is periodic.
The low-voltage shape of the characteristic is obtained from the standard phase diffusion picture [3] which predicts a low differential resistance branch which meets the $V = 0$ axis at $T = 0$. The asymptotic high-voltage behaviour of the characteristic is quite universal : at voltages high enough, the Josephson frequency $\Omega = V/\varphi_0$ becomes larger than any other characteristic frequency of the system, and the velocity of the phase becomes essentially constant ($\dot{\delta} \approx \Omega$, the phase almost does not feel the rugosity of the potential), with a slight sinusoidal modulation at the Josephson frequency Ω. This slight modulation is responsible for the dc current I_J flowing through the junction which can be evaluated as follows. The constant velocity of the phase is associated with an ac Josephson current $i(t) = I_0 \sin \Omega t$. Since the junction is a non-dissipative element, the power dissipated in the environment by the ac Josephson current $P_{ac} = I_0^2/2 \mathrm{Re} Y(\Omega)$ is equal to the apparent dc power $P = I_J V = I_b V - V^2 Y(0)$ delivered by the source to the junction [5]. This power conversion can be seen as a partial rectification of the ac Josephson current by the junction itself combined with the admittance $Y(\omega)$. Therefore, asymptotically we predict the shape of the characteristic to be

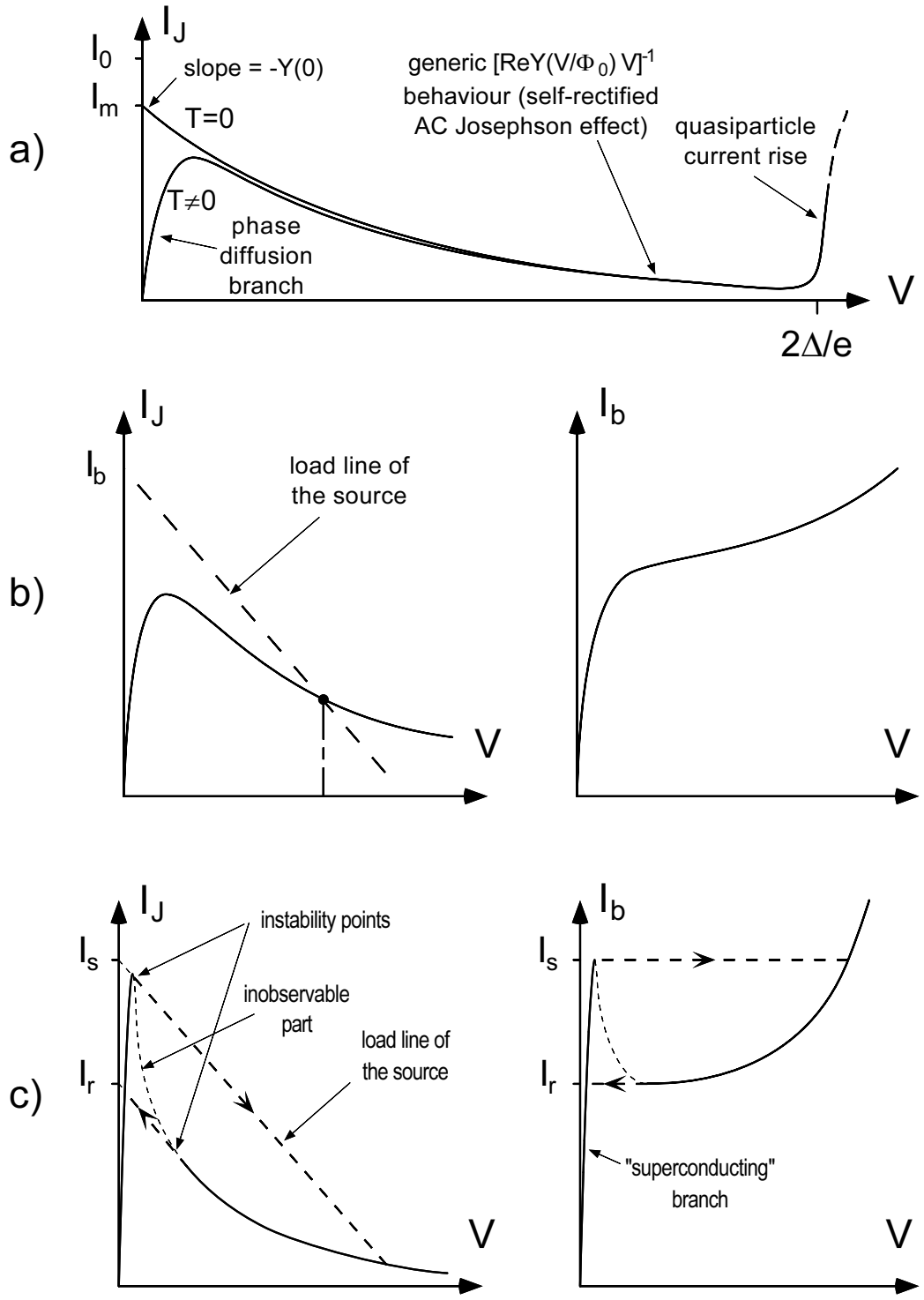

Fig. 3. ***a)*** *General shape of the current voltage characteristic of a Josephson junction, plotted in the {V, I_J} plane, where V is the average voltage across the junction and I_J is the average current flowing through it.* ***b)*** *&* ***c)*** *Two types of behaviour of a Josephson junction in an electromagnetic environment depending on the relative value of the differential conductance of the characteristic and the dc conductance of the source. Each case is plotted in the {V, I_J} plane on the left panel and in the usual {V, I_b} coordinates on the right panel b) Non-hysteretic behaviour. c) Hysteretic behaviour.*

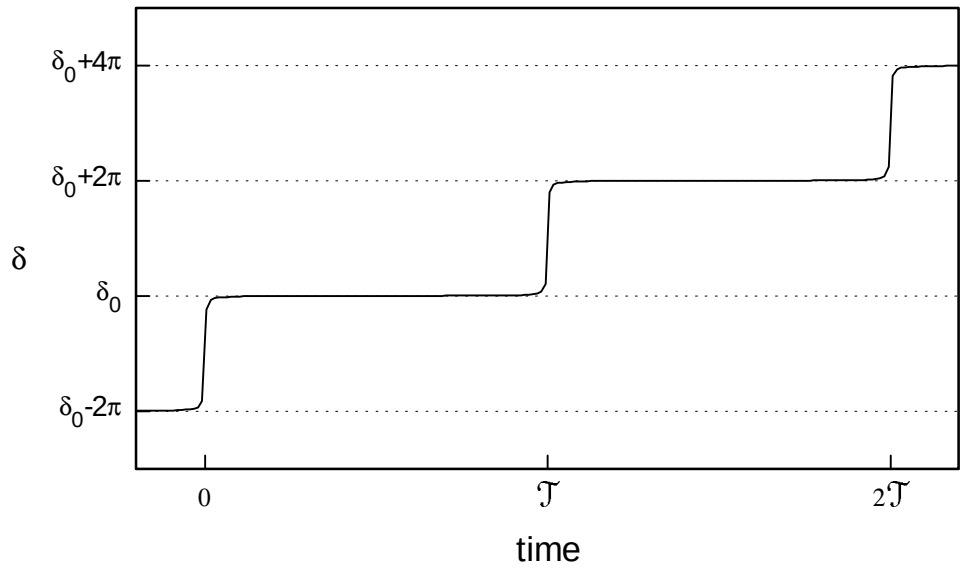

Fig. 4. *The periodic evolution of the phase corresponding to a point on the characteristic of the junction, at zero temperature and for a vanishing average voltage consists of a succession of 2π phase jumps well separated in time. The system spends most of the time crossing the local maxima of the tilted potential (located at* $\delta = \delta_0$ *modulo* 2π*) at very small velocity.*

$$I_J = \frac{I_0^2}{2V\,\mathrm{Re}\,Y\left(V/\varphi_0\right)}$$

Frequently, the admittance depends weakly on the frequency in this frequency range and this gives a $1/V$ dependence of the current at large voltages. This of course ceases to be true as soon as the voltage is high enough to break Cooper pairs. At this voltage the characteristic of the junction presents a steep increase of the current, due to quasiparticles. Assuming a very smooth shape of the characteristic, these remarks bring us to draw a qualitative I_J-V characteristic (see Fig. 3a). Of course, if the admittance $Y(\omega)$ has particular features like resonances, we expect to see them somehow in the characteristic [6,3].

At $T = 0$, the point at which the characteristic leaves the $V = 0$ axis is denoted by I_m. The bias current I_m is the minimum current for which, in absence of thermal fluctuations, the particle launched at a local maximum of the potential with infinitesimal initial velocity reaches the next maximum. We will now establish that the characteristic reaches this point with a slope given by $-Y(0)$ (note that $Y(0)$ is real since $\mathrm{Im}Y(\omega)$ is a continuous odd function). For a vanishing average voltage V across the junction, the motion of the phase consists of independent 2π jumps separated in time by an arbitrarily long interval $\mathcal{T} = \Phi_0/V$ (see Fig. 4). The average voltage across the junction is

$$V = \frac{\varphi_0}{\mathcal{T}} \int_{-\mathcal{T}/2}^{\mathcal{T}/2} \mathrm{d}t\dot{\delta}$$

and the average current I_Y flowing though the admittance is

$$I_Y = \frac{1}{\mathcal{T}} \int_{-\mathcal{T}/2}^{\mathcal{T}/2} \mathrm{d}t \; i_Y(t) = \frac{\varphi_0}{\mathcal{T}} \int_{-\mathcal{T}/2}^{\mathcal{T}/2} \mathrm{d}t \left(\dot{\delta} * \tilde{Y} \right)(t)$$

where * is the convolution product and $\tilde{Y}(t)$ the inverse Fourier transform of the admittance $Y(\omega)$. As $V \to 0$ the ratio I_Y/V is given by

$$\lim_{V \to 0} \frac{I_Y}{V} = \lim_{\mathcal{T} \to \infty} \frac{\int_{-\mathcal{T}/2}^{\mathcal{T}/2} \mathrm{d}t \left(\dot{\delta} * \tilde{Y} \right)(t)}{\int_{-\mathcal{T}/2}^{\mathcal{T}/2} \mathrm{d}t \dot{\delta}(t)} = \frac{\int_{-\infty}^{+\infty} \mathrm{d}t \left(\dot{\delta} * \tilde{Y} \right)(t)}{\int_{-\infty}^{+\infty} \mathrm{d}t' \, \dot{\delta}(t)}$$

$$= \frac{\int_{-\infty}^{+\infty} \mathrm{d}t \;\; \mathrm{FT}^{-1} \left\{ \tilde{\dot{\delta}}(\omega) Y(\omega) \right\}}{\int_{-\infty}^{+\infty} \mathrm{d}t' \, \dot{\delta}(t)}$$

$$= \frac{Y(\omega = 0) \tilde{\dot{\delta}}(\omega = 0)}{\tilde{\dot{\delta}}(\omega = 0)} = Y(0)$$

Here $\tilde{\dot{\delta}}(\omega)$ is the Fourier transform of $\dot{\delta}(t)$. Since $I_J + I_Y = I_b$, we finally obtain that

$$\lim_{V \to 0} \frac{\mathrm{d}I_J}{\mathrm{d}V} = -Y(0).$$

Similarly, the sign of the curvature of the characteristic at zero voltage is given by the sign of the derivative of the average power lost by friction with respect to the average voltage across the junction. This can be justified by the following reasoning : if the average power lost by friction decreases with increasing voltage, it induces an avalanche on the voltage which is the sign of a hysteretic behaviour of the system. As we will show below, the hysteretic behaviour can only exist if the differential conductance of the characteristic of the junction becomes smaller than $-Y(0)$ which can only happen if the curvature of the characteristic is negative at $V = 0$.

The voltage scale associated with the temperature and the admittance is $V_T = k_B T/\varphi_0 \mathrm{Re}Y$. One expects finite temperature characteristics to be given by a sort of convolution of the zero-temperature characteristic with a function of width V_T.

b) Dynamic stability of the current-voltage characteristic : hysteretic and non-hysteretic behaviour.

Once this I_J-V characteristic is obtained, the discussion of the stability of a bias point is very simple : a bias point is stable only if the dc conductance $Y(0)$ of the bias source and the differential conductance of the junction $\mathrm{d}I_J/\mathrm{d}V$ verify

$$\frac{\mathrm{d}I_J}{\mathrm{d}V} + Y(0) > 0.$$

This criterion distinguishes the points of the I_J-V characteristic which represent stable and unstable power equilibrium.

One can then separate the experimental behaviour of Josephson junctions in an electromagnetic environment in two categories : (i) non hysteretic behaviour if the differential conductance of the junction remains greater than the opposite of the dc conductance of the environment at all voltages (Fig. 3b). This is the case for dc shunted junctions. (ii) hysteretic behaviour if the differential conductance of the junction is smaller than the opposite of the dc conductance of the environment on part of the voltage domain (Fig. 3c). In this latter case, starting from the zero bias, when the bias current is increased, the system first follows a low differential resistance branch (called the "supercurrent branch") and then switches to a high voltage state at the instability point. The bias current I_b at this instability point defines the switching current I_s in a hysteretic set-up. The measured value of the switching current can fluctuate around this value due to the effect of the random noise current $i_n(t)$; our simple approach does not predict the amplitude of these fluctuations. When the bias current is reduced from over I_s the bias point follows the high voltage branch down to a second instability point at $I_b = I_r$ which is called the retrapping current.

c) STATIC HYSTERESIS

The hysteretic behaviour we have just defined is a dynamic hysteresis : it is the dynamics of the particle already escaped from a well which is stable or unstable. This dynamic hysteresis must not be confused with the static hysteresis of Josephson junctions often discussed in the literature. This static hysteresis is associated with the escape of the particle out of the first well. This escape can either happen by thermal activation over the potential barrier or by macroscopic quantum tunneling [7]. The escape times for both of these phenomena vary roughly exponentially with the size of the barrier. At low temperature ($E_J \gg k_B T$) and low tilt of the potential, the escape time out of this first well can be much larger than the relevant experimental time scale. Escape out of the first well can only occur within the experimental time scale when the potential is tilted to a point where the height of the barrier is sufficiently reduced. Thus, at low enough temperature, the bias current corresponding to this tilt of the potential can become larger than the current I_m, provided that $I_m < I_0$. Under these conditions, when the particle escapes, it produces a switching of the system to a stable finite voltage state given by the intersection of the load line of the source (drawn from the point of the $V = 0$ axis at which the particle escaped) with the characteristic. This implies that at sufficiently low temperatures the experimental behaviour of a junction can be hysteretic even though its I_J-V characteristic is not hysteretic in the sense given in b) (case of resistively shunted junctions with high enough quality factor), and the hysteresis cycle can be widened if the set-up is already intrinsically hysteretic. In the case of experiments on small junctions ($E_J \not\gg k_B T$),

activation of the particle out of the well usually happens on a time scale much shorter than the characteristic experimental time scale and such a static hysteresis is not observed.

B. Application to non-resistively-shunted junctions

In the following we will develop our analysis of the dynamics of the system in the case where the junction is not shunted at DC, that is where $Y(\omega = 0) = 0$ (The case of the shunted junction has been thoroughly studied in the past [1,2]). As we will see, for this biasing scheme the behaviour of a Josephson junction is essentially hysteretic. For the purpose of definiteness and simplicity, we will suppose that the admittance $y(\omega)$ can be described by the series combination of a capacitor C and a resistor R as indicated in Fig. 5. This specific model of the electromagnetic environment is easy to implement experimentally. In this configuration thermal fluctuations can be modelled by a noise current source $i'_n(t)$ in parallel with the resistance. The noise current $i'_n(t)$ verifies :

$$\langle i'_n(t) i'_n(0) \rangle = 2k_B T R \delta(t)$$

($\delta(t)$ is here the Dirac delta function, not the phase).

The equations of dynamics (equivalent to Eq. (2)) of the system shown in Fig. 5 are given by the coupled first order differential equations :

$$c\dot{v} = I_b + i'_n(t) + \frac{u - v}{R} - I_0 f'(\delta) \tag{3a}$$

$$C\dot{u} = \frac{v - u}{R} - i'_n(t) \tag{3b}$$

$$\varphi_0 \dot{\delta} = v \tag{3c}$$

where we have three time-dependent variables, $\delta(t)$ the phase of the junction, $v(t)$ the voltage across the junction and $u(t)$, the voltage across the capacitance C (see Fig. 5). One can eliminate u and v between the equations to obtain a third-order differential equation in δ which is still equivalent to (2) :

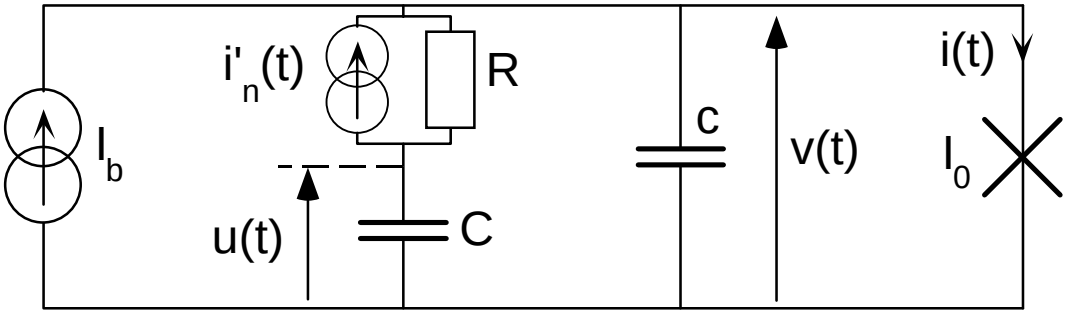

Fig. 5. *Simple model of the environment of an unshunted Josephson junction.*

$$RCc\varphi_0\dddot{\delta} + (C+c)\varphi_0\ddot{\delta} + RCI_0 f''(\delta)\dot{\delta} + I_0 f'(\delta) = I_b + RC\dot{i}'_n(t). \quad (4)$$

In contrast with (2), this latter equation is local in time but the price we have paid is that it is now non-linear. In absence of the friction terms in $\dot{\delta}$ and $\dddot{\delta}$, the "plasma frequency" of the small oscillations of the phase at a local minima of the potential is

$$\omega_p = \sqrt{\frac{I_0}{\varphi_0(C+c)}} \quad (5)$$

Using this characteristic frequency we can define a quality factor Q for the motion of the phase in the potential

$$Q = \frac{1}{RC\omega_p}. \quad (6)$$

In the following, we further restrict our analysis to two extreme cases : a "large" friction case ($Q \ll 1$) and a "weak" friction case ($Q \gg 1$).

1. Large friction limit

In this section we further suppose that $c \ll C$ (this is easily achieved for small-area junctions), and that the dynamics of the phase is overdamped ($Q \ll 1$) which is equivalent to having

$$RC \gg \frac{\varphi_0}{RI_0}.$$

Under these assumptions, we can neglect the small capacitance c in the second term of Eq. (4). Furthermore, at the characteristic frequency ω_p, the friction term in $\dddot{\delta}$ in (4) is smaller by c/C than the friction term in $\dot{\delta}$ and it can be neglected. Thus, the small capacitance c does not affect the results.

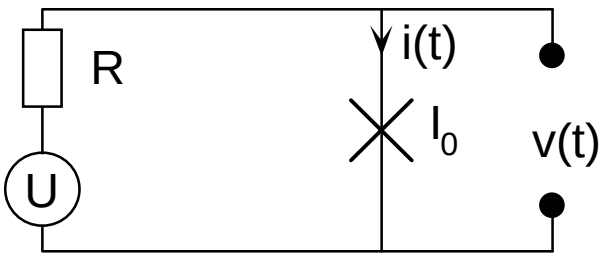

Fig. 6. *Pure Josephson element biased by an ideal voltage source trough a resistor.*

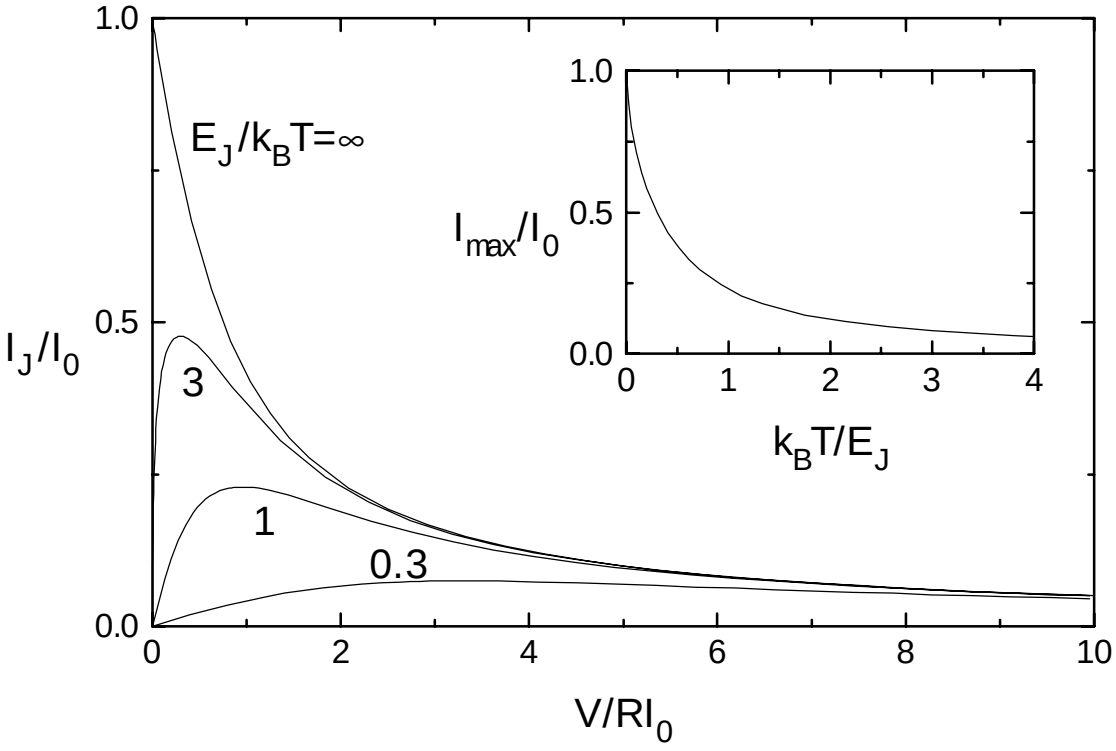

Fig. 7. *I_J-V characteristic of a highly damped Josephson junction, for different temperatures. Inset: temperature dependence of the maximum of the I_J-V characteristic. For an ideal current bias, this corresponds to the switching current I_s.*

Going back to the system of first order differential equations (3) these considerations show that *v* is not a real degree of freedom of the system. The system (3) can be simplified as

$$\frac{\varphi_0}{RI_0}\dot{\delta} = \frac{RI_b + u + Ri_n'(t)}{RI_0} - f'(\delta) \tag{7a}$$

$$RC\dot{u} = v - u \tag{7b}$$

These latter equation clearly show that the characteristic evolution time of *u* is much larger than that of δ. It is therefore possible to treat *u* as a quasistatic quantity in (7a). Equation (7b) can subsequently be integrated using the average value of $v = \varphi_0\dot{\delta}$ provided by the integration of (7a). It is important to point out here that the differential equation (7a) is equivalent to that of a Josephson junction of negligible capacitance connected in series with a resistor *R* and a voltage source $U = RI_b + u$. (see Fig. 6). This problem is solved in the literature for the single Josephson junction ($f(\delta) = -\cos\delta$) [8]. The current flowing through the junction is given by

$$I_J(U,T) = I_0\,\mathrm{Im}\left[\frac{I_{1-i\eta}(E_J/k_BT)}{I_{-i\eta}(E_J/k_BT)}\right] \tag{8}$$

where I_n is the modified Bessel function of complex order and

$$\eta = \frac{U\varphi_0}{k_B T R} = \frac{U}{RI_0}\frac{E_J}{k_B T}.$$

In this formula, U and T denote the bias voltage and the temperature, respectively. The $I_J(V)$ characteristic of the junction can be obtained from the relation $U = V + RI_J$ and Eq. (8). Such $I_J(V)$ characteristics are plotted for several temperatures in Fig. 7. Going back to our current-biased junction, the load line of the source is horizontal, thus the switching current is obtained by finding the maximum of the current as a function of V

$$I_s(T) = \underset{U}{\mathrm{Max}}\, I_J(U,T) = \underset{V}{\mathrm{Max}}\, I_J(V).$$

Note that this switching current depends only on the temperature, and not on the value of the resistance R (provided damping remains large, of course).

2. Weak friction limit

We now turn to the case where the response time RC of the admittance $y(\omega)$ is much shorter than the inverse plasma frequency (5) of the system, which corresponds to a weak damping ($RC\omega_p \ll 1$). In this limit we can go back to Eq. (2) and make a short-time expansion of the convolution product :

$$\int_{-\infty}^{+\infty} v(t-\tau)\tilde{y}(\tau)\mathrm{d}\tau = \sum_{k=0}^{\infty} \frac{v^{(k)}(t)}{k!}\int_{-\infty}^{+\infty}(-\tau)^k \tilde{y}(\tau)\mathrm{d}\tau = \sum_{k=0}^{\infty}\frac{(-j)^k}{k!}v^{(k)}(t)y^{(k)}(\omega=0). \qquad (9)$$

Replacing in (2) and using $v = \dot{\delta}\varphi_0$, one obtains a differential equation for δ

$$\varphi_0\left[(c+C)\ddot{\delta} + RC^2\dddot{\delta} + \ldots\right] + I_0 f'(\delta) = I_b + i_n(t)$$

where the term in $\dot{\delta}$ has vanished since $y(0) = 0$. The evolution of δ is still that of a particle of mass $(c+C)\varphi_0^2$ in the tilted potential $E_J f(\delta) - \varphi_0\delta I_b$ but this time with a leading friction term of the form $\varphi_0^2 RC^2\ddot{\delta}$. The expansion (9) used here can also be used for other admittances, in particular for a resistive shunt in which case the friction also has a viscous component.

We will now determine the value of the bias current I_m previously introduced in Sec. A.3.a. We recall that it is defined as the minimum current for which, in absence of thermal fluctuations, the particle launched at a local maximum of the potential with infinitesimal initial velocity reaches the next maximum. For currents greater than I_m, the energy gained going from one local maximum of the potential to the next is greater than the energy lost by friction in this movement : the particle accelerates. As the particle gains kinetic energy, the variations of the velocity are reduced and, as a consequence, the friction experienced by the particle decreases (the dc component of the velocity does not dissipate since $y(0) = 0$): there is an avalanche effect which gives the hysteretic behaviour of the system.

Let us now give an estimate of the current I_m based on the energy balance argument : at the tilt $I_b = I_m$, the work W of the friction force on an interval $[\delta_0, \delta_0 + 2\pi]$ going from one local

maximum of the potential to the next balances the energy gain $2\pi I_m\varphi_0$ due to the tilt of the potential. The work W is given by

$$W = \varphi_0^2 RC^2 \int_{\delta_0}^{\delta_0+2\pi} \mathrm{d}\delta\, \dddot{\delta}.$$

Since friction is weak, we use the free dynamics of the particle to make the approximate replacement

$$\dddot{\delta} = -\frac{I_0}{\varphi_0(C+c)} f''(\delta)\dot{\delta}$$

and the kinetic energy theorem gives

$$\dot{\delta} = \sqrt{\frac{2I_0\left(f(\delta_0) - f(\delta) - (\delta_0 - \delta)s_m\right)}{\varphi_0(C+c)}}$$

where $s_m = I_m/I_0$. This gives

$$W = -\sqrt{2}\varphi_0^2 RC^2 \left(\frac{I_0}{\varphi_0(C+c)}\right)^{3/2} \int_{\delta_0}^{\delta_0+2\pi} \mathrm{d}\delta f''(\delta)\sqrt{f(\delta_0) - f(\delta) - (\delta_0 - \delta)s_m}$$

The energy balance states that $W = -2\pi I_m\varphi_0$; this yields an estimate of I_m :

$$I_m = \alpha\varphi_0 RC^2 \left(\frac{I_0}{\varphi_0(C+c)}\right)^{3/2}, \tag{10}$$

where

$$\alpha = \frac{\sqrt{2}}{2\pi} \int_{\delta_0}^{\delta_0+2\pi} \mathrm{d}\delta f''(\delta)\sqrt{f(\delta_0) - f(\delta) - (\delta_0 - \delta)s_m}$$

is a dimensionless coefficient of order unity which depends on I_m through s_m. Thus, Eq. (10) must in principle be solved self-consistently for $s_m = I_m/I_0$. However, one can show that the current I_m is much smaller than the critical current I_0 :

$$\frac{I_m}{I_0} = \frac{\alpha}{Q}\frac{C}{C+c} \ll 1.$$

This allows us to take $s_m = 0$ to evaluate α, which yields for the single Josephson junction ($f(\delta) = -\cos\delta$) :

$$\alpha = \frac{\sqrt{2}}{2\pi} \int_{\pi}^{3\pi} \mathrm{d}\delta \cos\delta\sqrt{1+\cos\delta} = \frac{4}{3\pi}$$

and thus,

$$\frac{I_m}{I_0} = \frac{4}{3\pi Q}\frac{C}{C+c}.$$

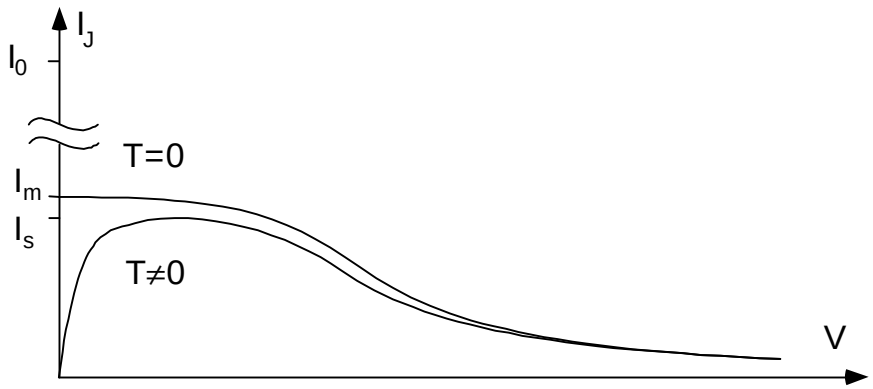

Fig. 8. *Approximate form of the zero-temperature and finite-temperature I_J-V characteristic of a weakly damped unshunted junction.*

From this value of I_m, the asymptotic behaviour at large voltage and the hysteretic behaviour of the system, we can draw a tentative zero-temperature characteristic of the junction (see Fig. 8).

More work is needed to analyse precisely the temperature dependence of this switching current, but we can try to sketch it here. The voltage scale associated to the thermal fluctuations is $V_T = k_B T R/\varphi_0$. We expect thermal fluctuations to round the I_J-V characteristic on a voltage scale of the order of V_T. The switching current I_s of the junction is given by the maximum of the rounded I_J-V curve. Given the flat aspect of the characteristic at low voltage for weakly damped junctions (see next section), we expect a weak effect of the temperature on I_s up to a temperature of the order of QE_J/k_B. If our reasoning is correct we predict that at low temperatures I_s is essentially equal to I_m. If true, our reasoning also has important consequences on the interpretation of experimental results : an apparent saturation of the switching current at low temperature (before a maybe inaccessible ultra-low temperature regime where a situation of static hysteresis is reached) is not necessarily the sign of quantum tunneling.

3. *I-V* characteristics of unshunted junctions for arbitrary damping at zero temperature

We now consider a junction in a circuit corresponding to that of Fig. 5 in the case where the capacitance c is negligible but for arbitrary quality factor $Q = 1/RC\omega_p = \sqrt{\varphi_0/R^2 C I_0}$. In this case, one can obtain the I_J-V characteristic at zero temperature by numerical calculation. The characteristics are obtained by finding the stationary solutions for the motion of the phase. The characteristics plotted for various Q form a family of curves admitting the $Q = 0$ curve as high voltage asymptote in the V/RI_0 reduced voltage (Fig. 9). The current I_m at which the characteristic reaches the zero voltage axis decreases when the Q is increased (Fig. 10). The

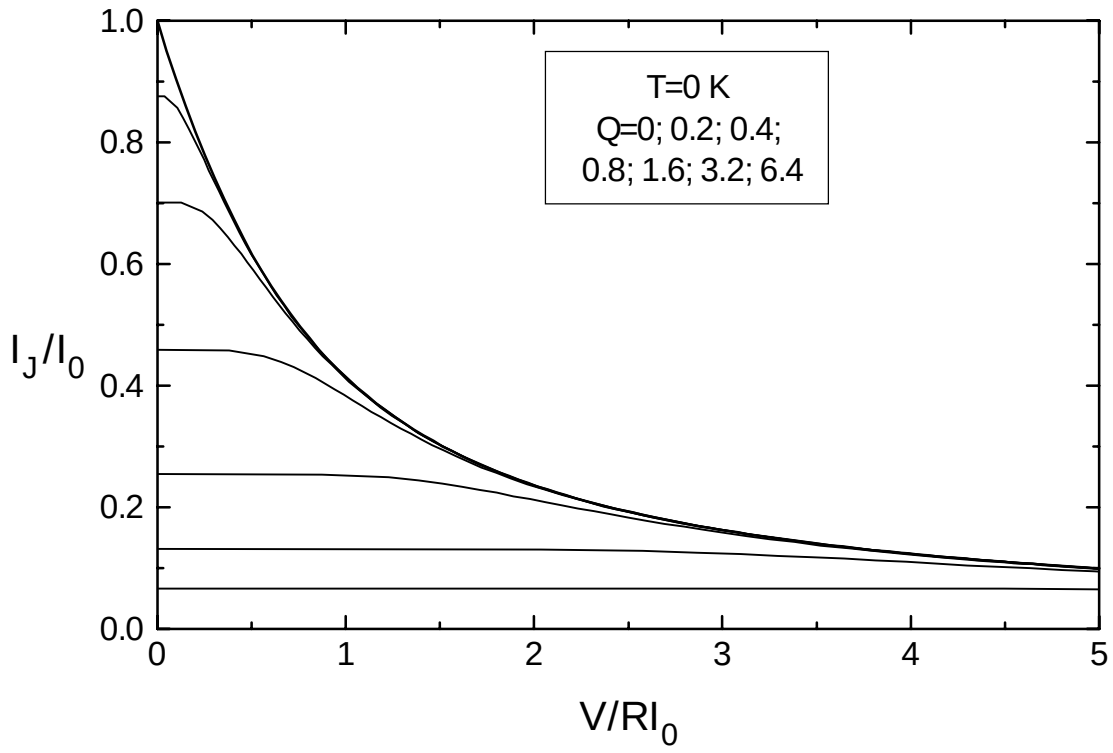

Fig. 9. *I_J-V characteristics of unshunted junctions at zero temperature, for several values of the damping. The quality factor of the small oscillations of the system are (top curve to bottom curve) Q = 0; 0.2, 0.4; 0.8; 1.6; 3.2; 6.4. In these coordinates, the curves all admit the Q = 0 characteristic as high voltage asymptote.*

dependence of I_m with Q interpolates between the low-Q limit $I_m/I_0 = 1–2\pi Q^2$ and the high-Q limit $I_m/I_0 = 4/3\pi Q$, as shown by the inset of Fig. 10.

Conclusion

We have discussed here the stability of the dynamics of the phase of a Josephson junction using the notion of *I-V* characteristic of the junction. Finding the *I-V* characteristic of a Josephson junction in its environment is generally a difficult problem, but some features of the characteristics can be found from general arguments for simple models of environments. Our main result consists in finding the zero-temperature switching current of unshunted junctions. We establish that it depends crucially on the damping provided by the environment of the junction, by a purely classical effect.

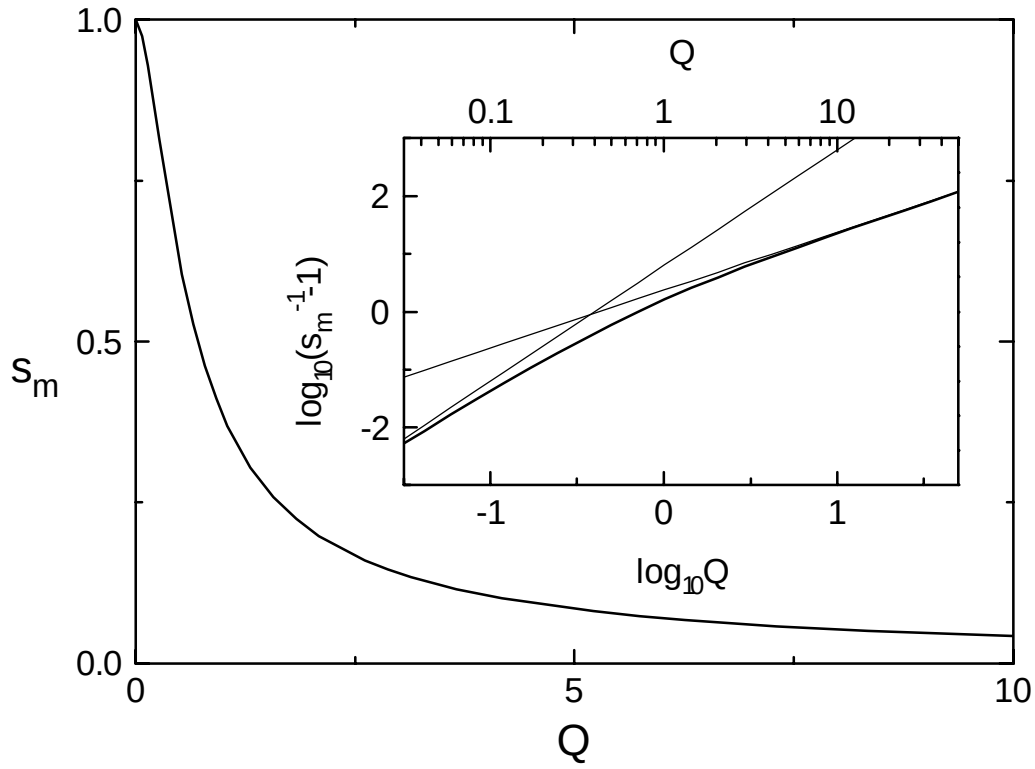

Fig. 10. *Dependence of the ratio $I_m/I_0 = s_m$ with quality factor Q where I_m is the current at which the zero-temperature characteristic reaches the zero voltage axis. Inset: log-log plot showing the asymptotic behaviour of s_m at low and high Q. The straight lines correspond to the limits $s_m = 4/3\pi Q$ and $s_m = 1–2\pi Q^2$ at high and low Q, respectively.*

References for Chap. IV

[1] W. C. Stewart, Appl. Phys. Lett. **12**, 277 (1968); D. E. McCumber, J. Appl. Phys. **39**, 3113 (1968).

[2] A. Barone and G. Paternò, *Physics and Applications of the Josephson Effect* (Wiley-Interscience, New York, 1982).

[3] G. L. Ingold, H. Grabert, and U. Eberhardt, Phys. Rev. **B 50**, 395 (1994)

[4] R. L. Kautz, and J. M. Martinis, Phys. Rev. **B 42**, 9903 (1990).

[5] see for instance K. K. Likharev in *Dynamics of Josephson Junctions and circuits* (Gordon and Breach, New York, 1986), Chap. 12.

[6] T. Holst, D. Esteve, C. Urbina, and M. H. Devoret, Phys. Rev. Lett. **73**, 3455 (1994).

[7] M. H. Devoret, D. Esteve, C. Urbina, J. Martinis, A. Cleland and J. Clarke in *Quantum Tunneling in Condensed Media* edited by Yu. Kagan and A. J. Leggett (Elsevier, Amsterdam, 1992), Chap. 6.

[8] Yu. M. Ivanchenko and L. A. Zil'berman, Zh. Eksp. Teor. Fiz. **55**, 2395, (1968) [Sov. Phys. JETP **28**, 1272 (1969)]

V. EXPERIMENTAL TECHNIQUES

A. Sample fabrication

All the samples were prepared using the shadow mask technique [1,2], with triple-angle evaporation [3] to produce in sequence : 1) the Al island of the transistor, 2) the Al counter-electrode of the junctions and finally 3) the Cu normal-metal leads of the transistor which acted as quasiparticle filters (See Fig. 1 & 2 and Sec. V.B.3). We started with either a bare oxidised silicon substrate or a custom-made substrate with an insulated ground plane (Fig. 4) which was used to microfabricate directly on-chip capacitors. These substrates then received two layers of polymer from which the suspended mask was made [4]. The polymers where sequentially spun to the desired thickness and baked. The top layer consisted of PMMA (MW : 950k), and the bottom layer was a PMMA-MAA copolymer. This bilayer was patterned in a scanning electron microscope, at 35 keV, at a magnification of 5000 for the smallest details and using a dose of about 2 pC/μm^2. The mask was then developed in a solution of MIBK–Propanol-2 (1:3 vol.). The undercut in the copolymer is adjusted so that the bottom layer can suspend the smallest details of the mask formed by the remaining top layer. The sample was then placed in an electron-gun evaporation machine and pumped down to a pressure $<10^{-6}$ mb. We first evaporated a 20 nm-thick film of pure Al at normal incidence. The insulating layer of the tunnel junctions was then grown by a controlled oxidisation of the Al at an O_2 pressure of the order of 10^{-1} mb for three minutes. Next, the counter-electrodes of the junctions were formed by evaporating 20 nm of Al at an incidence angle of about 20°. Immediately after, we evaporated 30 nm of Cu at an angle of -20° to form the normal-metal leads of the transistor. The deposition rate of all the evaporations was regulated at 1.0 nm/s. The sample was then immersed a few minutes in warm (≈ 35°C) acetone to dissolve the polymers and to lift-off the metal layers deposited onto the mask. The sample was tested by measuring its tunnel resistance at room temperature, with an ohmmeter and a 2 MΩ resistance in series to limit the current to less than ≈100 nA.

A plot of the computer-generated pattern used for the fabrication of the on-chip capacitively shunted transistor is shown in Fig. 3a. The transistor itself is at the centre of the figure. An enlargement of this area is shown in Fig. 3b. Each shade in these figures corresponds to one of the five magnification and e-beam current steps which were used to expose the whole transistor. A SEM picture of an actual sample is shown in Fig. 2, showing the three images of the mask. The capacitors defined by the large house-shaped surfaces in Fig. 3a and the underlying ground plane are 2.5 mm^2 in area, they are in the leads of the transistor. The

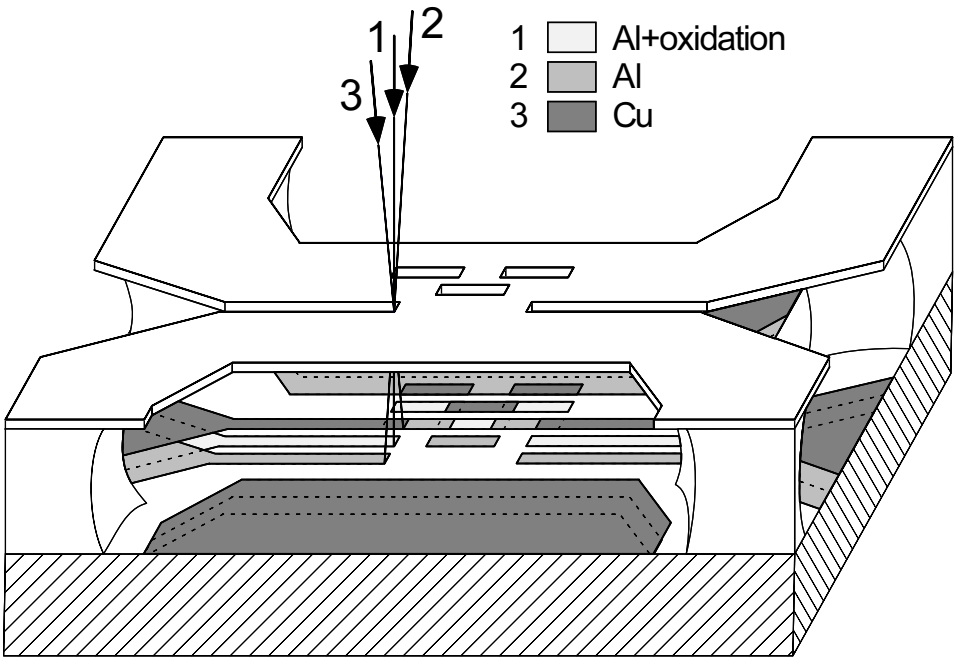

Fig. 1. *Schematic 3D view of the triple evaporation process trough a suspended mask.*

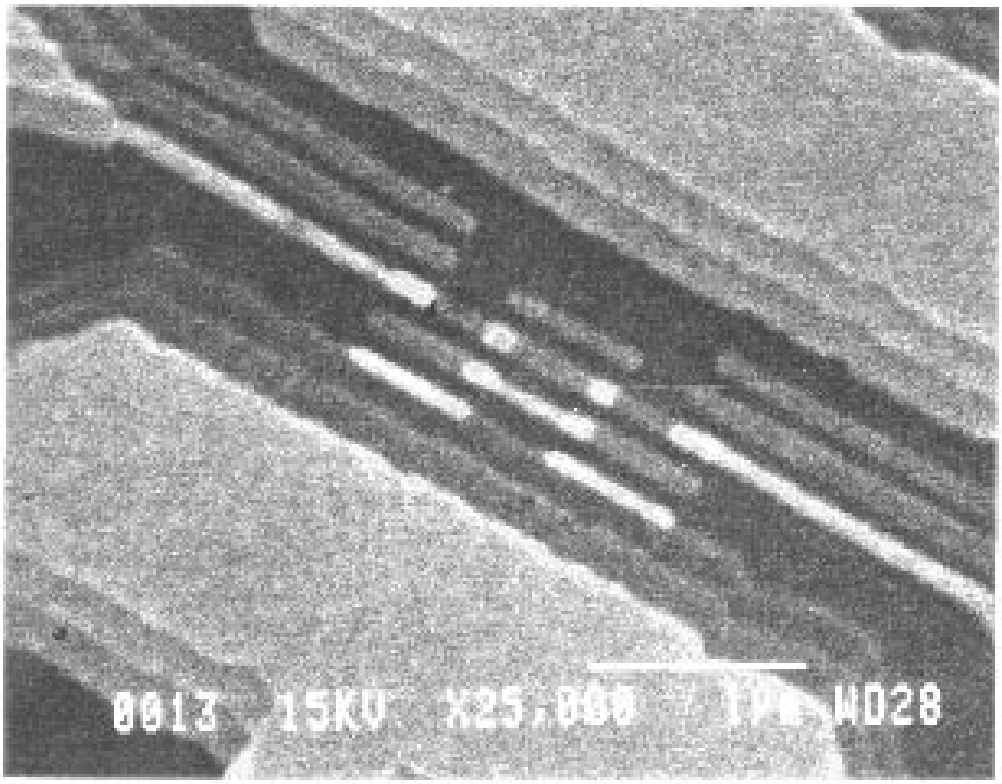

Fig. 2. *Scanning electron microscope picture of an actual sample, showing the three images of the mask at a magnification of 25000. The lighter strips correspond to the copper layer. The junctions are visible as white dots at the overlap of the strips in the centre of the picture. The supernumerary isolated islands which result from the triple evaporation process have no influence on the behaviour of the device.*

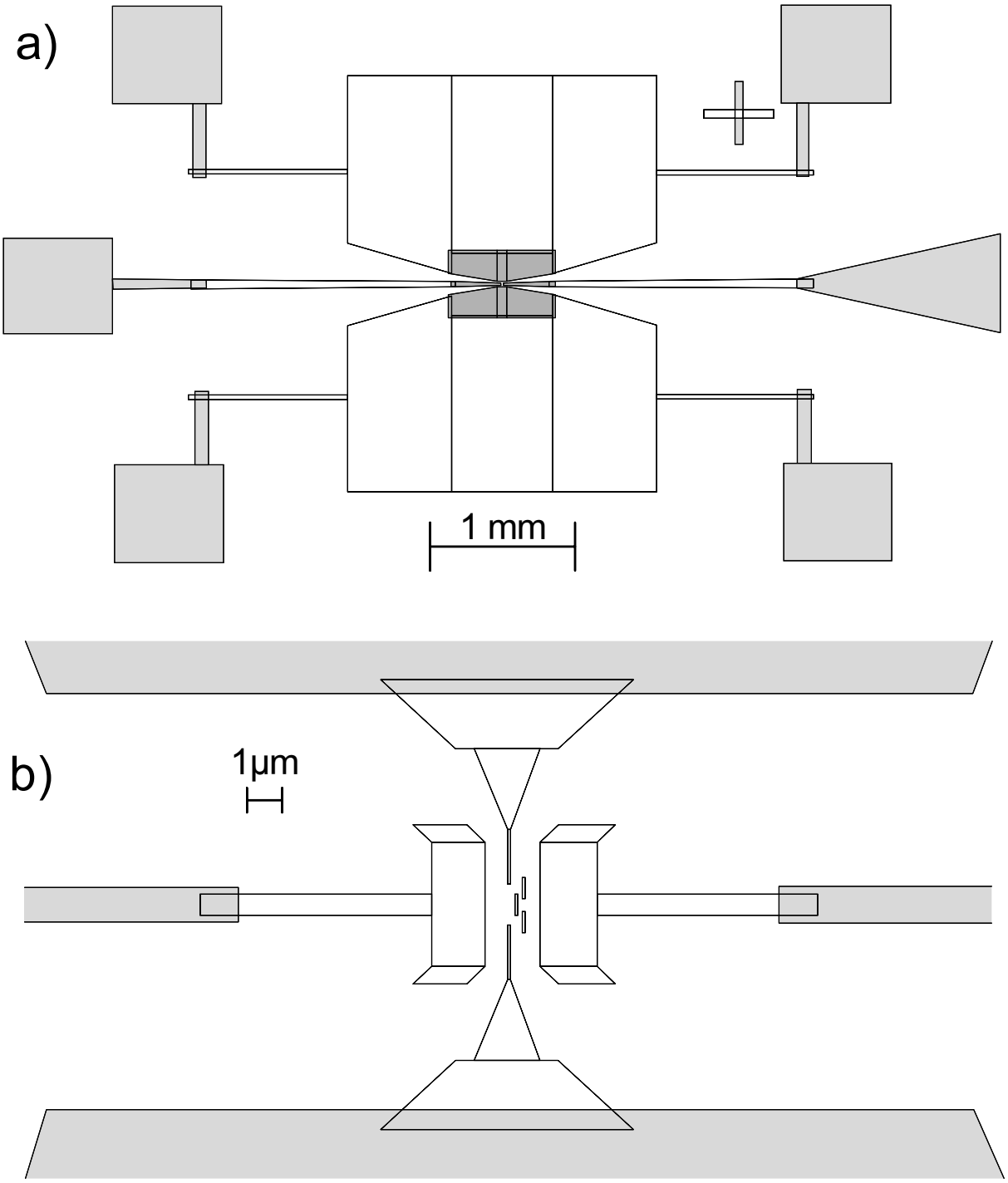

Fig. 3. *a) Computer-generated pattern sent to the scanning electron microscope to expose the mask. The various shades correspond to different magnifications steps and current doses. b) enlargement by a factor of 250 of the centre of a), showing the smallest details of the mask.*

capacitances of the capacitors are calculated using the parameters of the Si_3N_4 insulating layer ($\varepsilon_r \approx 7$, thickness = 1.5 µm); this yields ≈100 pF per capacitor. The narrow horizontal strips constitute two gates which could be used indifferently. Note the high degree of symmetry of the pattern. This symmetry cancels any mutual inductance between the gates and the leads of the transistor which were suspected to cause resonances in the electromagnetic environment in

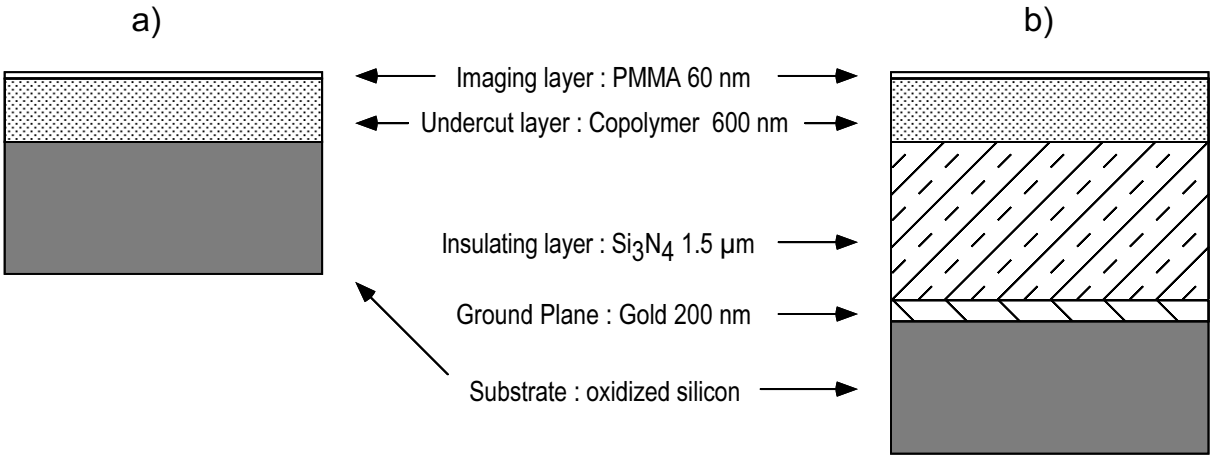

Fig. 4. *The two types of substrates used for the fabrication of the transistor. a) standard oxidised silicon substrate (500 nm thermal oxide) with the two polymer layers used to make the suspended mask. b) Improved substrate which incorporates a ground plane entering in the fabrication of the on-chip capacitors.*

a previous design of the mask. In one sample (#13), the copper layer was replaced by a spin-glass alloy (Cu-Mn, 2%wt Mn) to increase dissipation in the environment and to prevent proximity effect in the normal-metal (see Sec. V.B.1).

B. Experimental setup

Once fabricated, the sample was glued onto a small copper plate using silver paint. The plate itself was mounted on an integrated circuit socket. The pads of the circuit were connected to the pins of the socket using silver paint and copper wires. One of the sockets we have used also was fitted with a coaxial line connected directly on-chip for the AC Josephson effect measurements. The socket was then plugged into a connector in the dilution refrigerator. The copper plate supporting the sample was thermally anchored to the mixing chamber using a copper braid. Two concentric copper shields anchored to the mixing chamber of the refrigerator surrounded the sample. All the leads running from room temperature to the sample were made through carefully filtered coaxial lines (see Fig. 5). On each of the bias line, measurement line and gate line, a typical attenuation of 120 dB of the microwave noise was achieved by using microfabricated dissipative meander-line filters which were developed in our lab and which are described elsewhere [5]. The bias line incorporated a mechanical switch in a shielded box at 4K with which we could change the source impedance from 12 MΩ to 30 kΩ, depending on what type of measurement was desired. The voltage across the sample was amplified using a battery-powered low-noise pre-amplifier (Ithaco model 1201), from which it was sent to the data acquisition apparatus. The current was not measured directly in this setup, it was rather calculated using the input voltage at the top of the cryostat, the measured voltage on the sample and the predetermined values of the resistors used in the bias line (see Fig. 6a).

We did the measurements of the switching current of the transistor in the high source impedance configuration (see Fig. 6c). Starting from the superconducting state of the transistor, we applied a current ramp to the transistor. We determined the switching current by measuring the time it took for the voltage across the transistor to reach a threshold value, corresponding to the switching of the transistor to a non-superconducting state. Both the synchronisation signal of the ramp and the signal coming from the pre-amplifier were used to trigger a high-speed timer (Philips model PM6654C) which measured the elapsed time between the two trigger signals. The value of the switching current was then calculated from the parameters of the ramp and the bias line. The whole measurement of a modulation curve of the transistor was automated : a computer program controlled the gate voltage (Keithley source model 230) and acquired the time measurement via an IEEE link.

The other biasing mode was used to record the *I-V* characteristics of the sample (see Fig. 6b). It was especially useful to observe resonances at finite voltages in regions where the current bias scheme is unstable. This imperfect voltage bias had also the advantage of being intrinsically stable (barring hysteresis of the sample, of course) as compared to the usual "perfect" voltage bias. Such a bias set-up can in principle be achieved with a current amplifier using the virtual ground technique. This virtual ground is usually implemented by a feed-back system at ambient temperature. This type of feed-back system always realises a trade-off between filtering of the noise in the feed-back loop and the time constant of the feed-back which both limit the stability of the voltage on the sample. In our setup however, the more filtering you apply, the less noise you have. The counterpart is that in our setup you are restricted to using rather high source impedances. This is because if you use a small source impedance the current is calculated by subtracting numbers of the same magnitude : the absolute accuracy of all the measurements limits your precision, and, more important, the signal-to-noise ratio decreases.

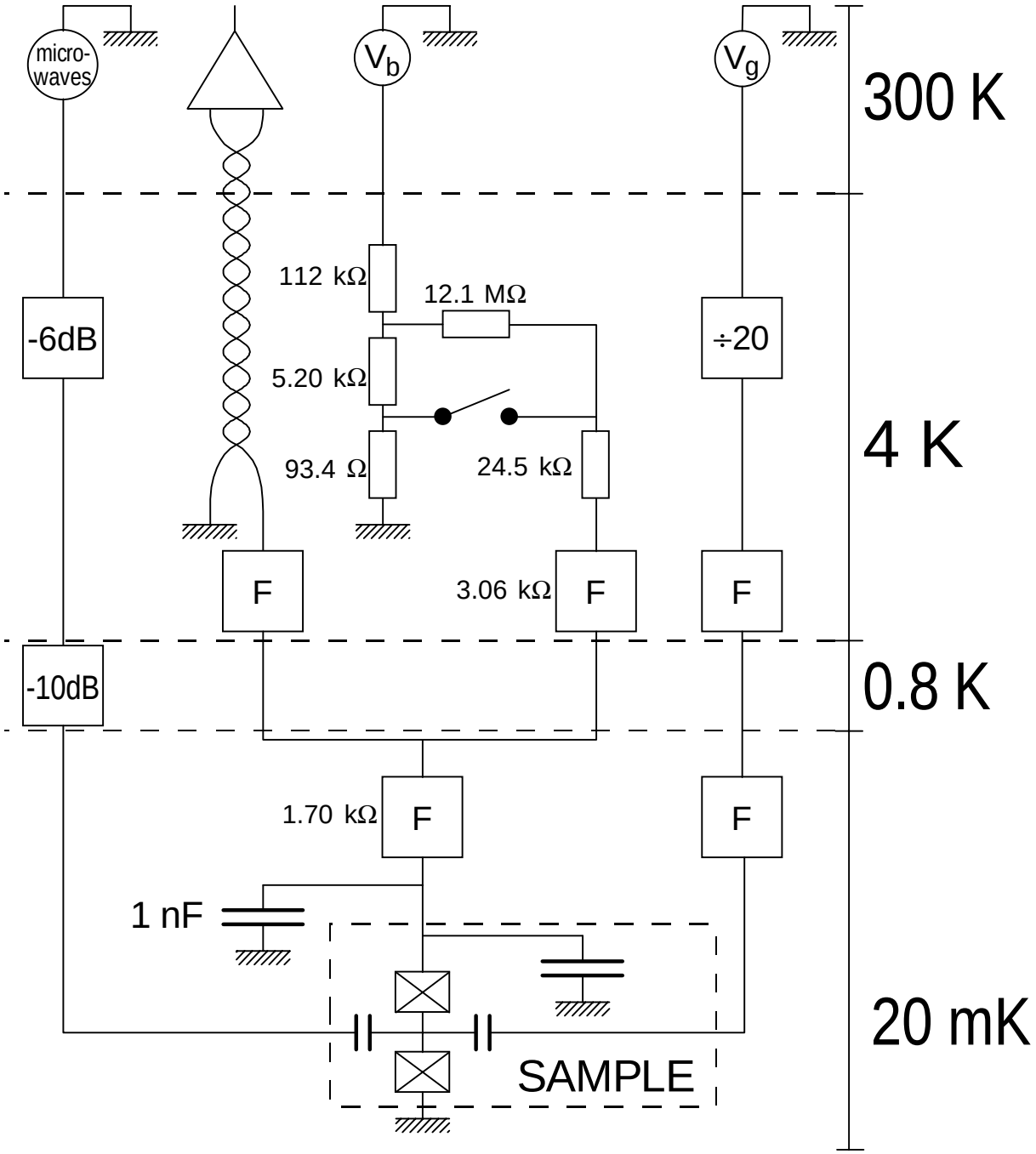

Fig. 5. *Schematic of the electrical wiring of the experiment inside of the dilution refrigerator. All the lines consists of coaxial cables, except the twisted-pair cable going to the preamplifier which itself is inside a screening tube. The square elements marked F are custom-made dissipative microwave filters (see text). The bias line (driven by the voltage source V_b) could either be used as an almost ideal DC current source (switch open) with an impedance of 12 MΩ or as a source with an impedance of ≈30 kΩ (switch closed). The configuration of the microwave line shown here corresponds to the latest experiments (samples 9-13) where we tried to produce fractional Shapiro steps by modulating the gate voltage (see Sec. V.C.2.b). The low attenuation on the microwave line (left) was needed to compensate for the small value of the coupling capacitor on-chip, but did not add any significant noise.*

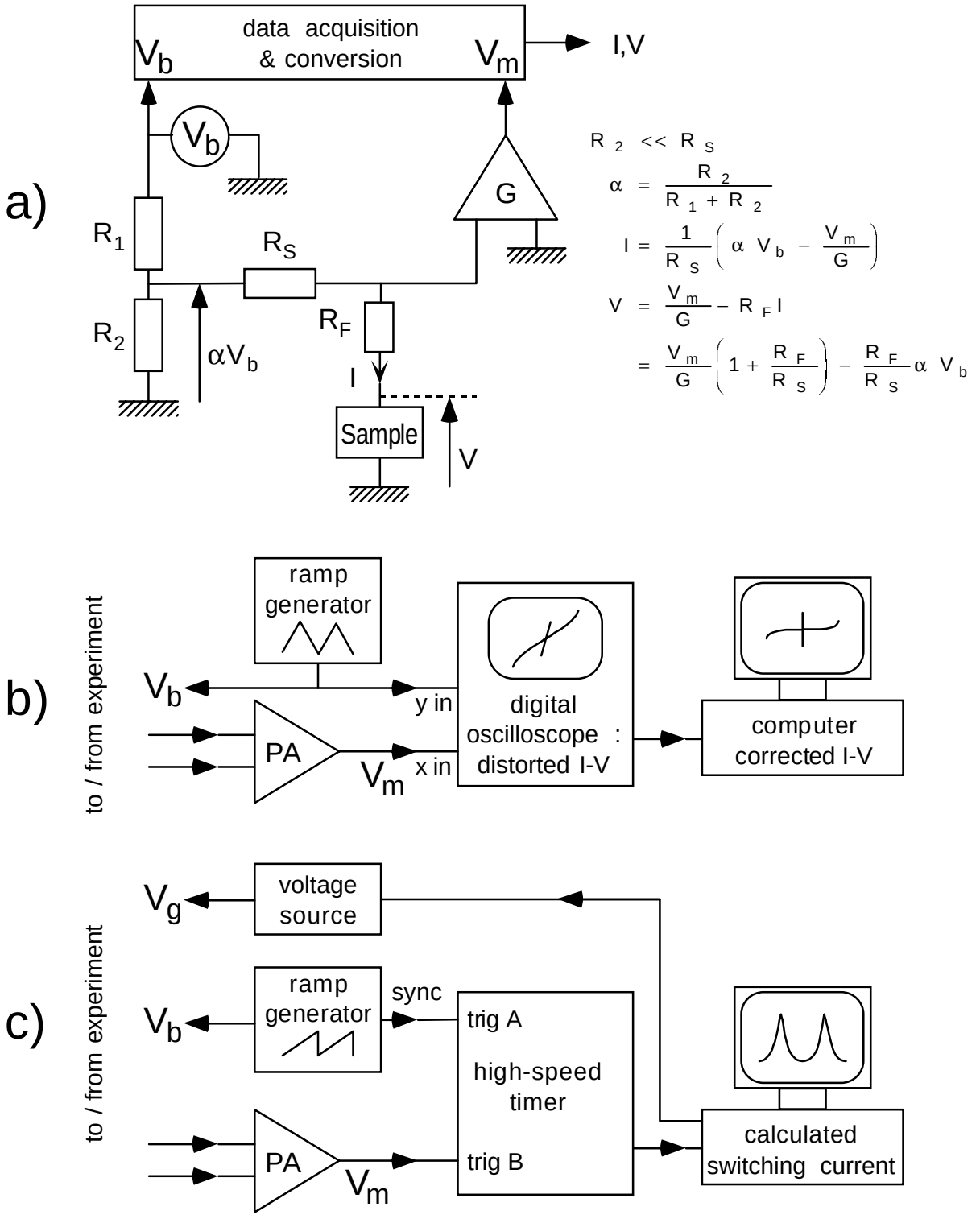

Fig. 6. *a) Principle of the electrical measurements performed on the samples. The voltage V_m measured by the pre-amplifier of gain G corresponds to the voltage V across the sample plus the voltage drop across the resistance R_F of a filter. The current flowing through the sample is obtained from the voltage drop across the resistance R_S. b) The recording of an IV characteristic was done by the acquisition of the raw voltages delivered by the ramp generator and the pre-amplifier followed by a post-treatment on a computer. c) The recording of the switching current data was entirely automated (see text).*

References for Chap. V

[1] G. J. Dolan, Appl. Phys. Lett. **31**, 337 (1977).

[2] G. J. Dolan and J. H. Dunsmuir, Physica **B 152**, 7 (1988).

[3] D. B. Haviland, L. S. Kuzmin, P. Delsing, K. K. Likharev, and T. Claeson, Z. Phys. **B 85**, 339 (1991).

[4] P. Lafarge, Ph.D. Thesis, Université Paris 6 (1993).

[5] D. Vion, P. F. Orfila, P. Joyez, D. Esteve and M. H. Devoret, J. Appl. Phys. **77**, (1995).

VI. EXPERIMENTAL RESULTS

A. Overview of the *I-V* characteristic

Before going into the details of the experiments, let us first give an overview of the general features present in the *I-V* characteristic of the transistor. The typical *I-V* characteristic of a transistor is presented in Fig. 1. It resembles strongly that of two large (*i.e.* large capacitance, small charging energy) Josephson junctions connected in series in that it shows a pronounced gap for $|V| < 4\Delta/e$ and a nearly vertical "supercurrent" branch at $V = 0$.

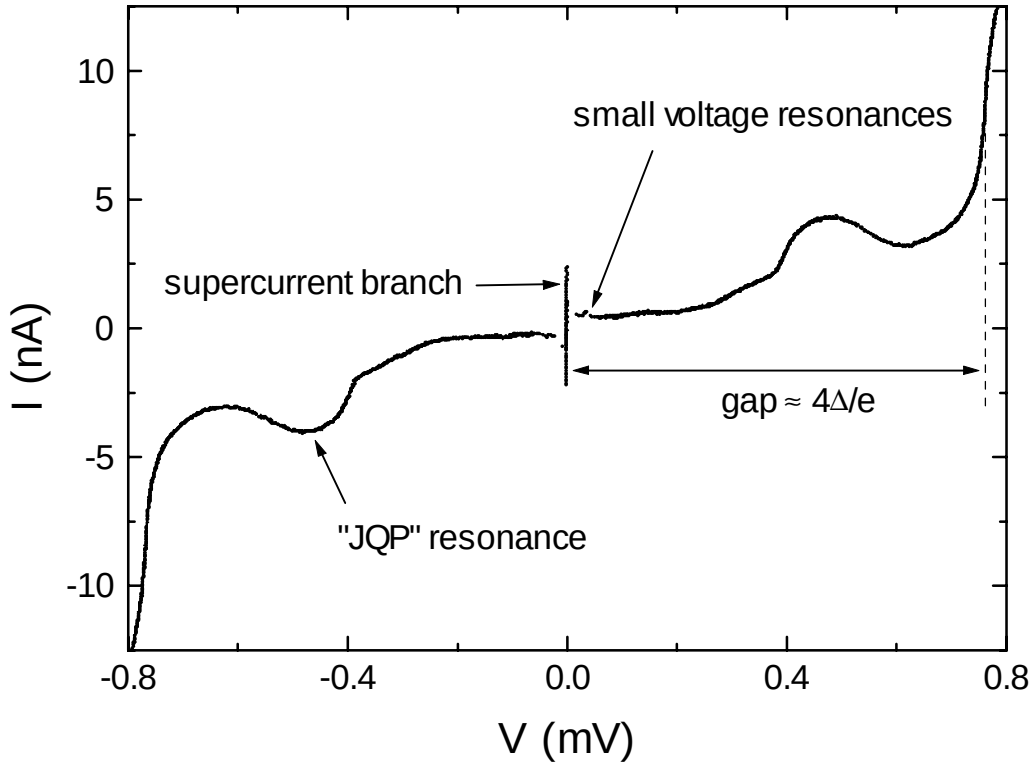

Fig. 1. *Main features of a typical I-V characteristic of a superconducting single electron transistor with the main features outlined. The acronym JQP stands for "Josephson plus Quasi-Particle". This conduction process is described in the text. (Data from sample 13, taken in the low-impedance bias mode).*

One notices however the presence of a broad resonance in the characteristic at $V \approx 2\Delta/e$ which corresponds in large junctions arrays to the switching of the Josephson junction with the second smallest critical current. This resonance was first observed and analysed by Fulton and Dolan who called its mechanism the "Josephson plus quasiparticle cyclic process" [1]. It results from a conduction process involving the presence of quasiparticles in the island, these quasiparticles acting as "catalyst" for electronic transfer.

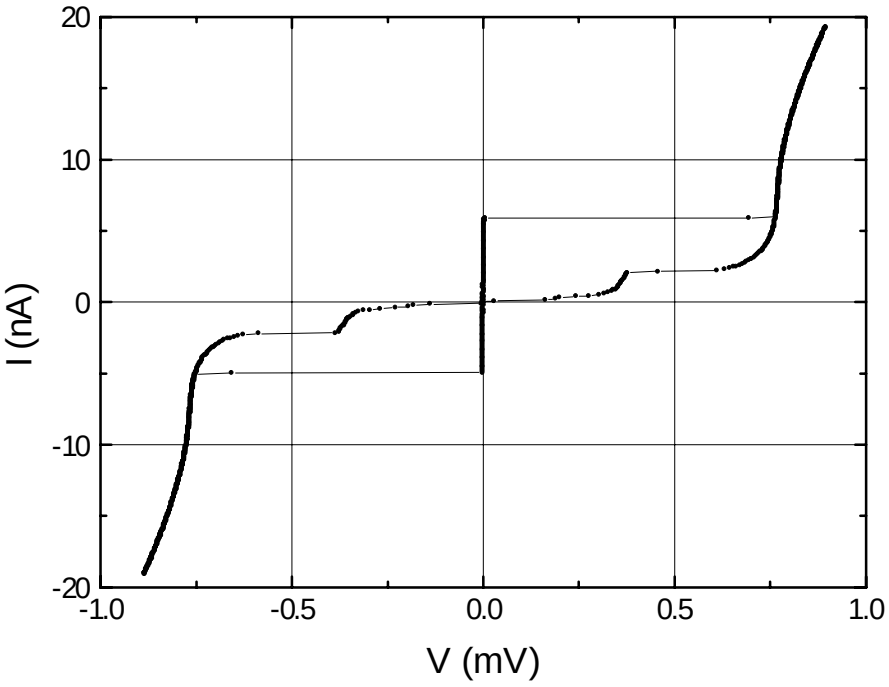

Fig. 2. *Current-Voltage characteristic of a transistor with a nearly ideal current bias. One notices the large hysteresis loop. The similarity of the JQP resonance with the $2\Delta/e$ plateau present in the I-V characteristic of two large Josephson junctions (see Fig. 3) is much more pronounced in this measurement of the characteristic. (Data from sample 13)*

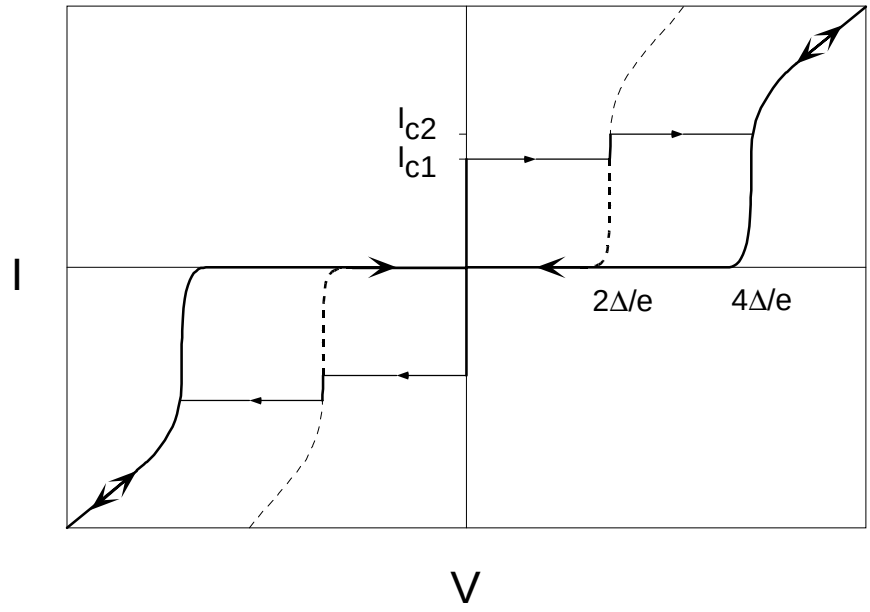

Fig. 3. *Schematic of the I-V characteristic of two large Josephson junctions connected in series and biased by an ideal current source. When the critical current I_{C1} of the weakest junction is reached, the system switches to a voltage plateau at $2\Delta/e$ corresponding to the gap of a single junction. When the bias current is increased further, one reaches the critical current I_{C2} of the second junction and the voltage switches to $4\Delta/e$, the sum of the gaps of the two junctions.*

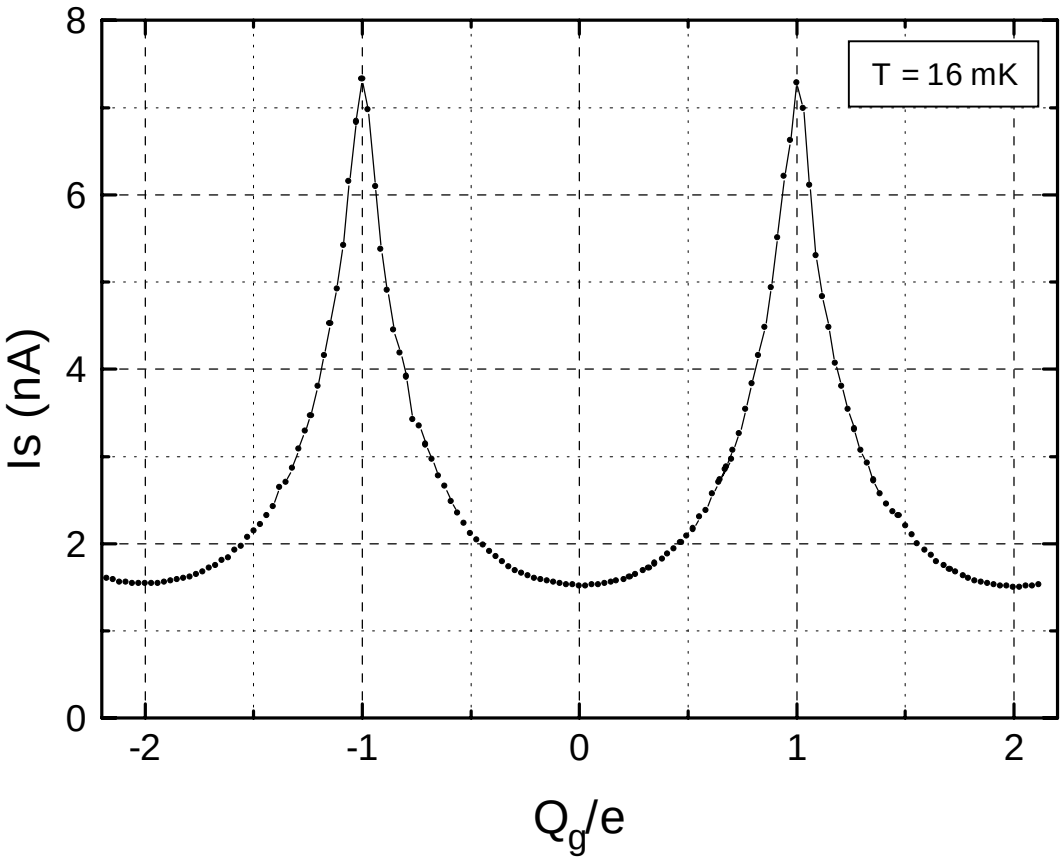

Fig. 4. *An example of modulation of the switching current with the gate charge. (Data from sample 13).*

The essential difference with a system of large junctions however, is the fact that the whole characteristic is modulated by the gate voltage. The most spectacular modulation is that of the supercurrent branch which was not observed in early experiments on the transistor [1,2,3,4]. We call the maximum supercurrent that can flow through the transistor, the switching current of the transistor. For a bias current exceeding the switching current, the transistor switches rapidly to a finite voltage state, owing to its hysteretic behaviour (see Fig. 2 and Chap. IV). The variations of the switching current as a function of gate voltage is shown in Fig. 4.

This gate-voltage modulation is 2*e*-periodic with respect to the charge present on the electrode of the gate capacitor. The 2*e*-periodicity is a manifestation of the odd-even asymmetry of the island of the transistor. It corresponds exactly to the 2*e*-periodicity of the staircase of the superconducting single electron box experiment [5]. As we shall see, our experiments have proven that the existence of a sizeable supercurrent branch is tightly connected to perfect 2*e*-periodicity. In previous experiments on the transistor [1,2,3,4], perfect 2*e*-periodicity had never been achieved and the supercurrent remained orders of magnitude smaller than theoretical predictions, as illustrated by Fig. 5. Our experiments provide a coherent explanation for these features and reconcile the former experiments with the theory. Our results further

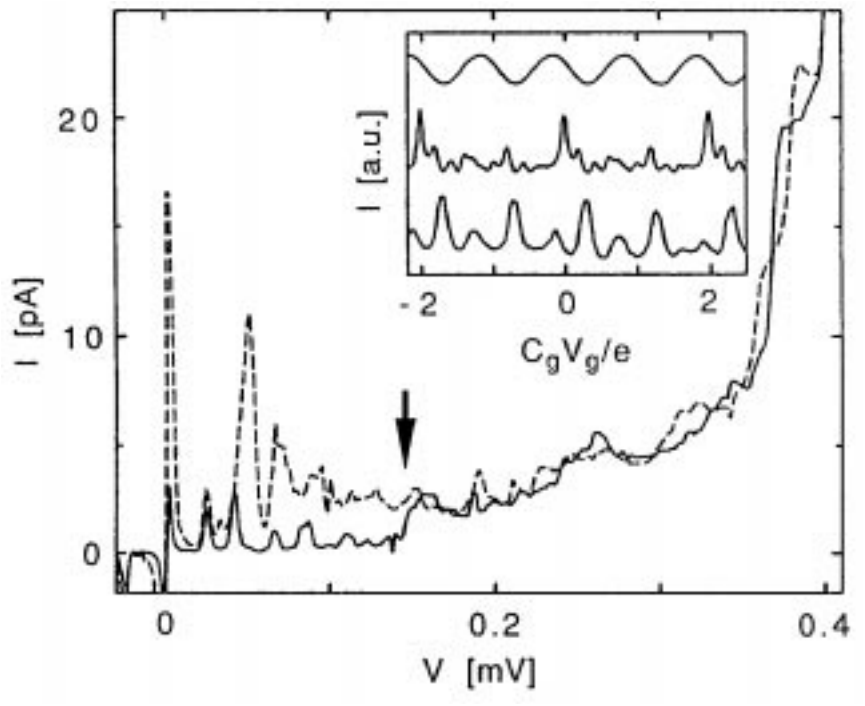

Fig. 5. *Current-voltage characteristic of a superconducting single electron transistor of the Delft group (reproduced from Ref. 3, with permission) for two values of the gate charge at 10 mK. The modulation of the amplitude of the supercurrent peak (leftmost resonance) is plotted in the inset (lower curve). The modulation is e-periodic in the gate charge and the maximum amplitude of the supercurrent (indicated by the scale of the main figure) is much lower than the theoretical prediction (≈5 nA for this sample whose total tunnel resistance was 58 kΩ). The arrow indicates the position of the "Coulomb gap for Cooper pairs" which is what we call the first order resonant Cooper pair tunneling process (see Sec. C.1).*

demonstrate the role played by the dissipation in the electromagnetic environment of the transistor on the experimental critical current of the device. These points are explained in detail in the following section.

We have also analysed the features of the transistor at finite but low voltages. First of all, far enough from $V = 0$, the modulation with the gate charge becomes *e*-periodic. The cross-over to *e*-periodicity occurs when the transport voltage can provide the odd-even free energy difference, that is when $V \gtrsim D(T,H)/e$. In the voltage region comprised between the supercurrent branch and the “JQP” peak, we have analysed the mechanisms of the resonances that appeared in the *I-V* characteristic. Such resonances have always been observed previously in the characteristics of the transistors (see *e.g.* Fig. 5), but their variations with the gate voltage remained unexplained. Some resonances were moving with the gate voltage while others were only changing in amplitude but none could unambiguously be associated to a given phenomenon. By controlling the electromagnetic environment of the transistor we have established that fixed resonances are “parasitic” resonance in the impedance of the environment. In one instance we have used these fixed resonances as frequency “markers” : we

interpreted the doubling of the voltage at which these frequencies appeared as a signature of a Zener effect (see Sec. C.4). We will also present measurements of AC Josephson effect.
In samples with a clean electromagnetic environment we could observe the gate voltage dependent resonances with unprecedented accuracy. These resonances are caused by what is known as “resonant Cooper pair tunneling”. These resonances form a hierarchy of which the first three orders have been observed. These resonances are also a way to measure the charging energy of the island. This will be explained in Sec. C.1

B. Modulation of the supercurrent

In a current-bias set-up, the transistor displays a hysteretic behaviour when the current is cycled (see Fig. 2). When the current of the source is ramped from zero, the *I-V* characteristic first follows the superconducting branch, and then at a given value of the source current, it suddenly “switches” to a large voltage. This defines the switching current of the transistor. The *I-V* characteristic forms a large hysteresis loop : the current must be reduced to nearly zero to bring the transistor back in its superconducting state. The repetitive measurement of the switching current in the same conditions usually yields a peaked distribution (see Sec. B.2) which in a first approximation can be characterised by a single number.

1. Switching current vs. critical current

For all the samples except one[1], the modulation of the measured switching current was 2*e*-periodic and in qualitative agreement with the theoretical prediction : its shape was qualitatively correct and the aspect ratio of the peaks varied in agreement with the parameters. However, in the first samples, the switching current was quantitatively well below the theoretical critical current. By microfabricating a specific on-chip electromagnetic environment for our latter samples (see Chap. V), we were able to prove that the ratio between the switching current and the critical current is fixed by the dissipation in the electromagnetic environment of the transistor.

a) Experimental evidence of the role of dissipation on the switching current

To test the role of the environment on the switching current, we made samples where the electromagnetic environment of the transistor was well controlled by construction. It incorporated a large capacitor in the leads of the device and parasitic resonances in the

[1] One sample out of 13 was completely *e*-periodic (see appendix B). We explain this by a finite number of excited states inside the BCS gap, down to very low energy. What surprises us is that this problem does not occur more frequently.

environment were suppressed by geometrically cancelling most mutual inductances. The electromagnetic environment of the transistor in these samples is well described by a simple lumped element model (see Fig. 6).

With this arrangement we were able to prove that the dissipation in the environment plays a crucial role in fixing the switching current. In our arrangement, dissipation was exclusively due to the resistance of the normal-metal quasiparticle filters. This resistance was of a few ohms when the normal metal was pure copper. When we cooled these samples to the lowest temperatures however, superconductivity could contaminate the copper by “proximity effect”, the effect of which was to reduce this resistance. When we measured the switching current of these transistors, we saw it decreasing with temperature, as expected from a reduction of the dissipation (see Sec. IV.B.3 and Fig. 7). We could check that this was indeed proximity effect by applying a small magnetic field. This magnetic field destroyed the proximity effect in the copper and spectacularly increased the switching current.

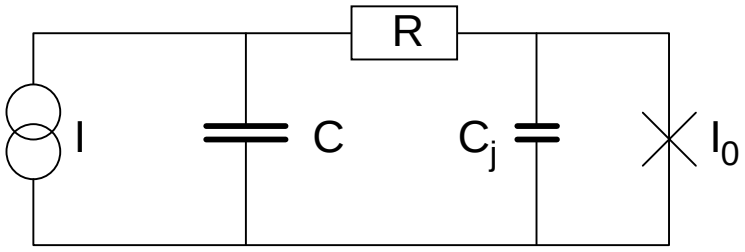

Fig. 6. *Realistic lumped element model of the electromagnetic environment of the transistor for the samples with microfabricated capacitors on chip. The cross represents the pure effective Josephson element equivalent to the transistor and C_j the capacitance of the effective junction. The large capacitance was C = 1.8 nF (which consisted of 50 pF on-chip plus the rest on the sample mount in the refrigerator) and R was the resistance of the normal-metal leads of the transistor. The typical series capacitance C_j of the transistor is of the order of 10^{-15}* F *and can be completely neglected.*

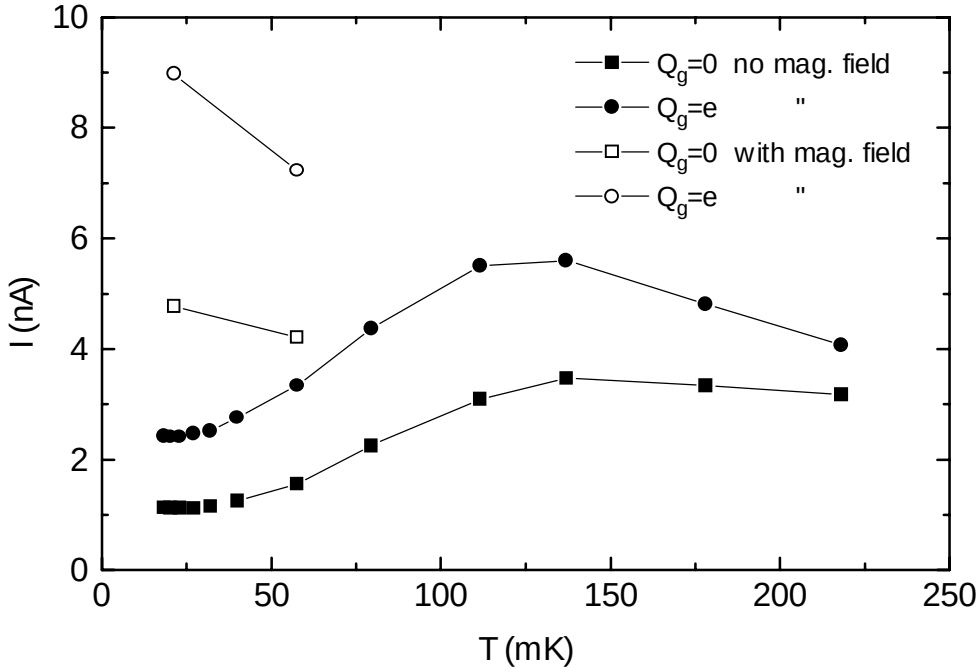

Fig. 7. *Influence of the dissipation in the environmental impedance on the switching current of the transistor. In a sample where the normal-metal leads were made of pure copper, superconductivity penetrated the normal metal. This phenomenon known as "proximity effect" reduced the resistance of the metal and, as a consequence, reduced the switching current of the transistor. This effect is clearly visible below 120 mK. When a moderate magnetic field was applied to the sample to prevent development of the proximity effect, the switching current spectacularly increased (open symbols). (Data from sample 11. The effect was also observed with sample 8).*

b) SWITCHING CURRENT FOR STRONG DAMPING

In sample 13 we replaced the pure copper of the normal-metal leads by a spin glass alloy (Cu-Mn, 2% wt Mn). The presence of the Mn spins forbade the development of any proximity effect, thus the resistance of the normal metal remained constant with temperature. Moreover the resistance being that of an alloy, it was then much higher than for the pure copper previously used : 400 ohms instead of a couple of ohms.

A plot of the low-temperature modulation of the switching current is shown in Fig. 8. and the experimental dependence of the switching current versus the temperature is shown in Fig. 9. One clearly sees that the low temperature reduction of the switching current observed in Fig. 7 has been suppressed by using the spin-glass alloy, as expected.

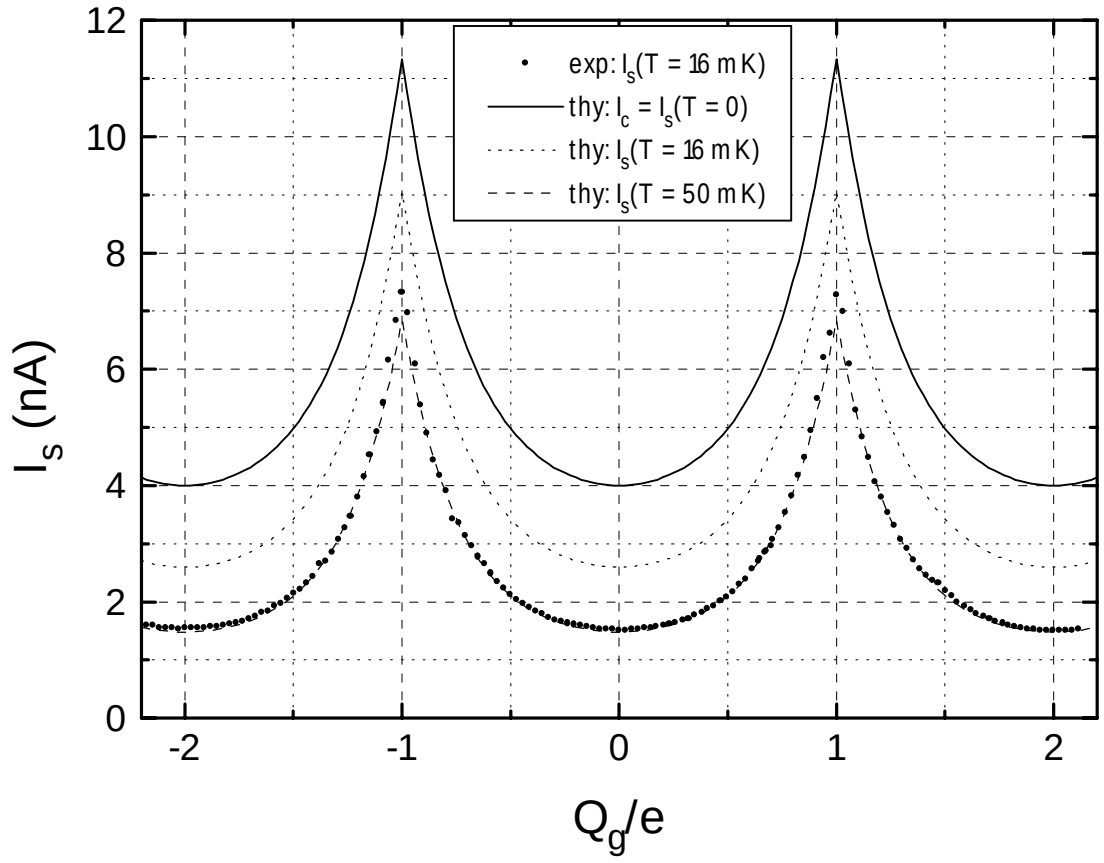

Fig. 8. *Low temperature switching current (dots) and the critical current of a transistor (top curve, no fitting parameters), as a function of the gate charge $Q_g = C_g V_g$ for sample #13. The critical current which is the theoretical maximal supercurrent would correspond to the switching current at T=0. Our theory of the switching current for overdamped Josephson junctions permits the calculation of the switching current at finite temperature (dots T = 16 mK; dashes T = 50 mK). The T=16 mK data can only be fitted if one supposes the temperature of the electromagnetic environment to be 50 mK (dashes). This hot-electron effect was to be expected because of Joule effect in the normal-metal filters.*

In this sample we had $C = 1.8$ nF, $C_j \approx 0.5$ fF, $R = 400\Omega$ and $4.0 < I_C(n_g) < 11.4$ nA. The values of $I_C(n_g)$ were calculated using the three-band model of the transistor described in Sec. III.B.4. This model was applied using the experimentally determined value of $E_C/k_B = 660$ mK (see Sec. III.D.5) and the value $E_J/k_B = 520$ mK of the Josephson coupling for a single junction of the transistor calculated from the Ambegaokar-Barratoff formula corrected of charging effects (see Sec. II.C). Writing the electrical equations of the circuit, one sees that C_j is unimportant and that the characteristic frequency of the small oscillations of the phase in its potential is

$$\frac{\omega_0}{2\pi} = \sqrt{\frac{I_C}{2\pi\Phi_0 C}} \sim 12.5 - 21.5 \text{ MHz}.$$

The quality factor for these oscillations is

$$Q = \frac{1}{RC\omega_0} \sim 0.01 - 0.02$$

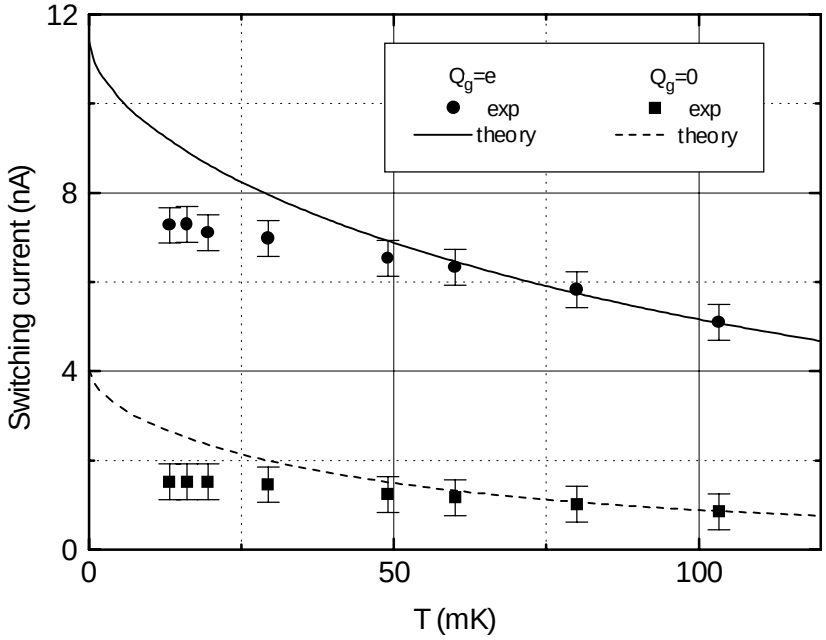

Fig. 9. *Comparison of experimental value of the switching current with the theory of strongly damped Josephson junctions plotted as a function of the thermometer's temperature. At high temperature, a very good agreement is obtained without any adjustable parameter. The deviation appearing below ~60 mK can be explained by heating effects in the sample (see text). Data from sample 13.*

Thus, the dynamics of the phase in this sample was strongly overdamped. If we suppose that the shape of the ground band of the transistor is not important, we can calculate the switching current as explained in Sec. IV.B.1 for an overdamped single junction. The full line in Fig. 9 and the theoretical $I_s(n_g)$ curves in Fig. 8 where obtained using this theory. Agreement between the theory and the experiment is very good at temperatures above ~60 mK. Below this temperature the discrepancy can be explained by a hot electron effect in the sample. One could estimate the electronic temperature in the sample using the formula [6]

$$P = \Sigma V\left(T_e^5 - T_{ph}^5\right). \tag{1}$$

In this formula, $P = RI^2$ is the power given to the electrons, V is the volume of the metal, $\Sigma \approx 2$ nWµm^{-3}K^{-5} is a material dependent parameter which measures the coupling of electrons with phonons, T_e is the (unknown) electronic temperature and T_{ph} is the phonon temperature which is equal to the thermometer's temperature. The volume of metal to take into account is here an ill-defined quantity which is certainly much larger than the volume of the resistors. A rigorous treatment would require solving the differential equations of heat in the geometry of the sample. However, putting some realistic figures in Eq. (1), one sees that it is actually very likely that electrons are hot enough to explain the deviation of the data at low temperature.

Note that by going to this overdamped situation we have reached the maximum switching current which can be achieved in a non-shunted system : no modification of the environment can further increase the switching current at any temperature (apart from reducing the heating effect, of course).

c) SWITCHING CURRENT FOR LOW DAMPING

In our first samples the impedance of the electromagnetic environment of the transistor was not controlled, but one can reasonably assume that the friction was very weak at the plasma frequency of the phase. Due to our lack of knowledge of the admittance in parallel with the transistor, we can simply predict along the lines of reasoning exposed in Sec. IV.B.2 a scaling of the switching current with the effective Josephson energy of the transistor :

$$I_s \propto E_0^{3/2}$$

This scaling agreed well with experiments (see Sec. 3a below and paper in appendix A).

2. Fluctuations of the switching current and noise measurements

The fluctuations of the switching current on repeated measurements have several origins : (i) In the parameter domain where we were working, the switching of the transistor was normally thermally activated, thus thermal fluctuations could widen the distribution. (ii) The switching current being very sensitive to the charge the island "sees", any movement of charge in the vicinity of the island (*e.g.* noise in the gate voltage) yields fluctuations of the switching current. In one occasion we observed that such a charge noise was the dominant contribution to the width of the distribution of I_s : At a given value of n_g the width of the nearly Gaussian distribution of I_s was proportional to $\mathrm{d}\langle I_s\rangle/\mathrm{d}n_g$ (see Fig. 10). From the proportionality constant one can express the noise as a standard deviation of the gate charge of the order of $4\ 10^{-3}\ e$. From the absence of correlations in successive measurements at a repetition rate of 45 Hz, we conclude to a faster dynamic of the noise mechanism. This noise was slowly decreasing with time, on the scale of days, indicating that some relaxation was going on and proving that the noise was not simply due to poor filtering. We interpret this charge noise as rapid movements of charges, probably located in the substrate of the sample.

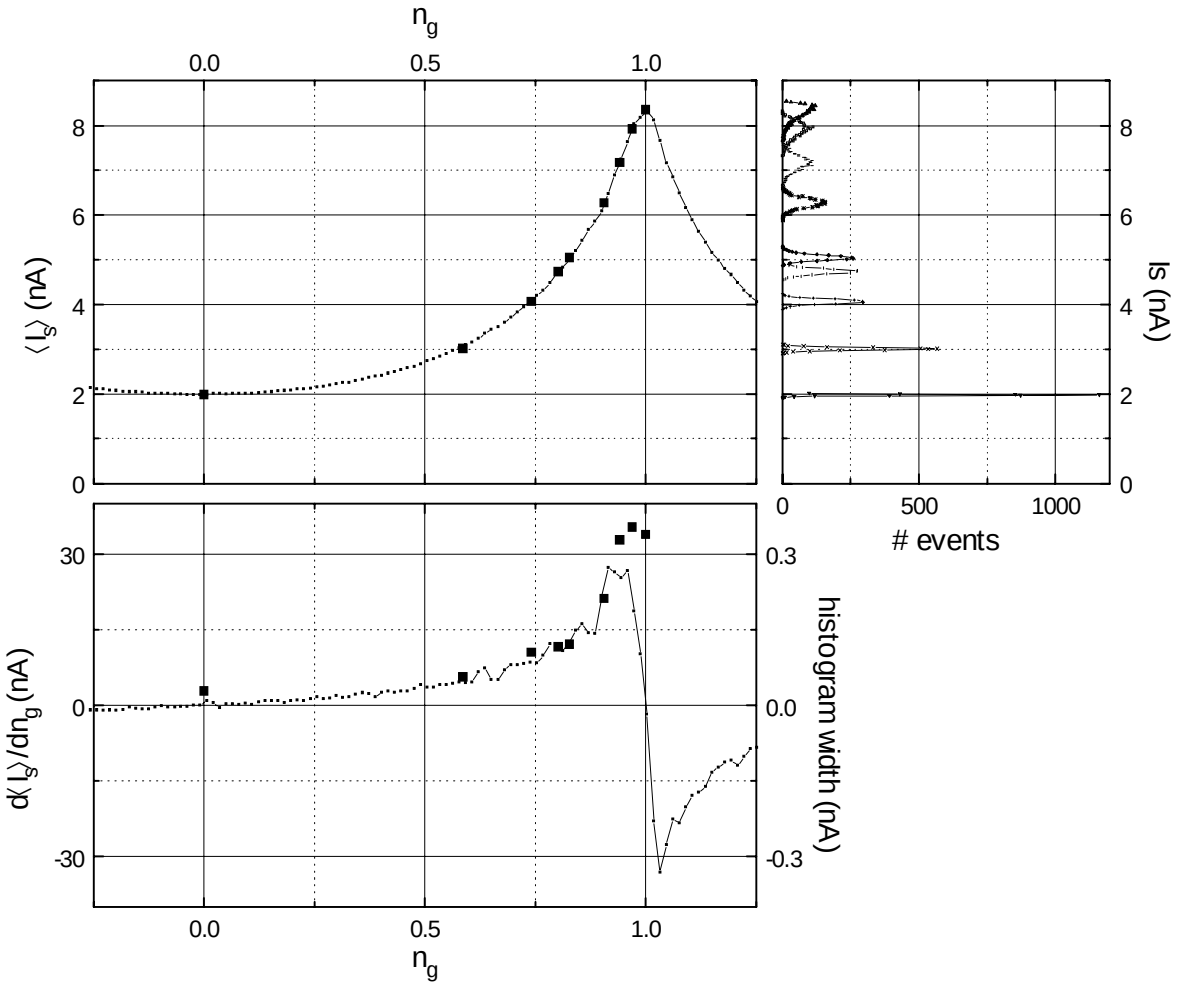

Fig. 10. *Top right panel : Histograms of switching current for sample 13, taken at gate voltages indicated by the black squares on the top left panel. On the top left panel we have also plotted the average switching current as a function of the gate charge. Bottom panel : Plot of the derivative of the average switching current with respect to the gate charge (dots + line; left axis) and width of the histograms (black squares; right axis) vs. gate voltage. The width of the histograms is nearly proportional to the derivative of the average switching current with respect to the gate charge. This is consistent with a width of the histograms originating in rapid motion of random charges near the transistor.*

Another conclusion of these measurements is that the intrinsic histogram width mentioned in (i) is very narrow (not larger than the histogram at $n_g = 0$). This narrow distribution is an essential piece of information on the finite temperature switching process (see Chap. IV.). Here, we will rather translate this width in terms of limit performance of the transistor used as an electrometer. By analogy with optics, we can define the charge resolving power of the transistor as the charge noise figure given above. Note that this resolving power only gives an indication on the performance of the device and that the actual limit is only imposed by the number of measurements and therefore by the amount of time available to measure a given charge. If we suppose that the narrowest histogram we observe (at $n_g = 0$) is fixed by the actual intrinsic fluctuations of the switching current of the transistor, and if a fabrication technique

could suppress the charge noise we observe (perhaps by fabricating a suspended island), we can estimate the limit resolving power of such a transistor to be $\approx 3\ 10^{-4}\ e$.
If the transistor was actually going to be used as an electrometer, it would certainly be interesting to make it non-hysteretic. This can be done by placing a resistive shunt between the source and drain electrodes. This non hysteretic superconducting single electron transistor should offer better performance than its normal-metal counterpart ($10^{-4}\ e/\sqrt{\text{Hz}}$ proven sensitivity [7]), owing to the higher current and lower output impedance it presents.

3. Poisoning of the supercurrent

We have presented the zero-temperature picture of the poisoning of the supercurrent introduced by Matveev *et al.* [8] in Sec. III.C. We will here discuss how this phenomenon may appear in experiments due to dynamic effects. We will present experimental results in one of these cases.
In the Matveev *et al.* description of the phenomenon, the parameter which controls the parity effects in the island of the transistor is Δ/E_C. However, at finite temperature we know that the equilibrium probability of odd or even occupation of the island is governed by the odd-even free energy difference $D(T,H)$ in the island [4,5], not the gap[2]. Moreover, what is measured experimentally is a switching current, not exactly the critical current. As already explained in Chap. IV, the process during which the effective junction switches results from the dynamics of the system. To give a detailed prediction of the effect of quasiparticle poisoning on an experiment, it is necessary to know the timescales on which the various phenomena occur. Thus, we introduce the characteristic timescales τ_s of the switching of the transistor to finite voltage, τ_{oe} of the odd-even equilibration time in the island, and τ_r the ramp time of the current during a measurement of the switching current. We can envision several simple limit cases, as indicated below :

i. $\tau_{oe} \gg \tau_r \gg \tau_s$

The parity changes in the island occur on time scales greater than the time it takes to measure the switching current. A given measurement will give the switching current corresponding to the parity at the moment the measurement is performed. If the measurements are repeated on a time scale greater than τ_{oe} we will obtain two values of the switching current corresponding to the odd or even occupancy of the island. The ratio of the frequency of these measurements will be given by the Boltzmann factor $\exp(-D(T,H)/k_BT)$.

ii. $\tau_r \gg \tau_{oe} \gg \tau_s$

At any value of the current, the island samples both the odd and even state. If at one given time

---

[2] At zero magnetic field, the odd-even free energy difference $D(T,H)$ is approximately given by

$$D(T,0) = \Delta - k_B T \ln N$$

where Δ is the gap of the superconductor and $N=\Delta\rho$, ρ being the density of states in the island.

it is possible for the transistor to switch, it will switch because this is the fastest phenomenon. Thus, the switching current will correspond to the minimal critical current of the odd or even state of the island. This predicts a weak *e*-periodic modulation of the switching current exactly as if the gap did not exist. The effect of poisoning is extreme.

iii. $\tau_r \gg \tau_s \gg \tau_{oe}$

In this case, during the process of switching the phase can be thought to evolve in an average potential corresponding to the odd and even occupation of the island in a ratio given by the Boltzmann factor $\exp(-D(T,H)/k_BT)$. The switching current is then a sort of average between the switching which would occur for pure even or odd occupation of the island. The shape of the gate charge modulation of the switching current at low temperature and low magnetic field is a rounded version of that predicted by Matveev *et al.* At higher temperatures and magnetic fields, the poisoning leads to a complex modulation pattern of the switching current with respect to the gate charge, with a non monotonous dependence in temperature. This is the case encountered in the paper reprinted in appendix A. In the following section we present a complete set of data showing the manifestation of this effect.

a) EXPERIMENTAL OBSERVATION OF THE POISONING

We present here data of switching current modulation from sample #5 which demonstrate the effect of quasiparticle poisoning of the supercurrent as a function of temperature and magnetic field. The figures presented here constitute a superset of those presented in the article given in appendix A. The theoretical curves accompanying the data were obtained using the argument of average potential for the phase presented in point iii) above and using a scaling $I_m \propto I_C^{3/2}$ for the zero-temperature switching current I_m of the sample. This scaling corresponds to a weak damping of the phase which is relevant for this sample (see Sec. IV.B.2). In this weak friction limit the switching current is supposed to depend weakly on temperature, hence we compare directly the experimental switching current at finite temperature to I_m. For a complete description of how the experimental curves were obtained, the reader is referred to the article. It is important to mention that the whole set of theoretical curves presented here are obtained using a unique set of parameters for the model.

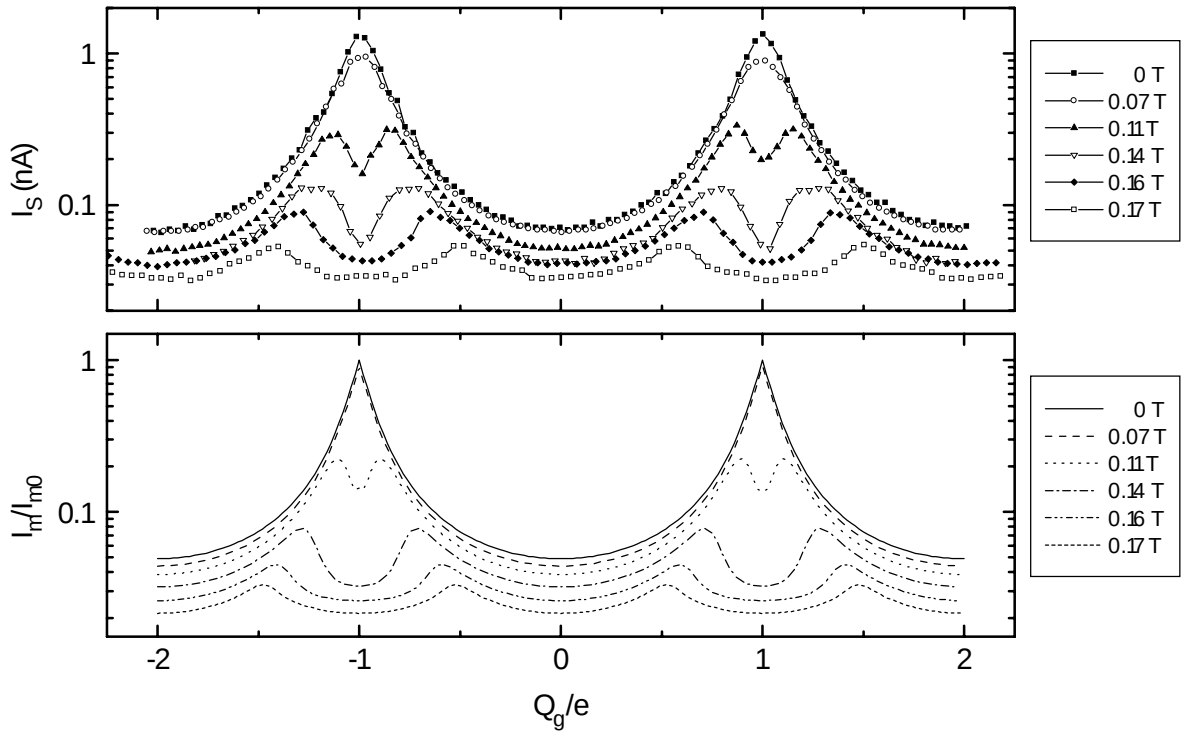

Fig. 11 A. *Modulation of the switching current at T = 65 mK for an increasing magnetic field. Note the logarithmic scale. The dip appearing at odd integer values of Q_g/e corresponds to the poisoning. These low-temperature data correspond to a rounded version of the theory of Matveev et al. [8] (see for comparison Fig. 12 of Chap. III.). I_{m0} is the maximum switching current (see article).*

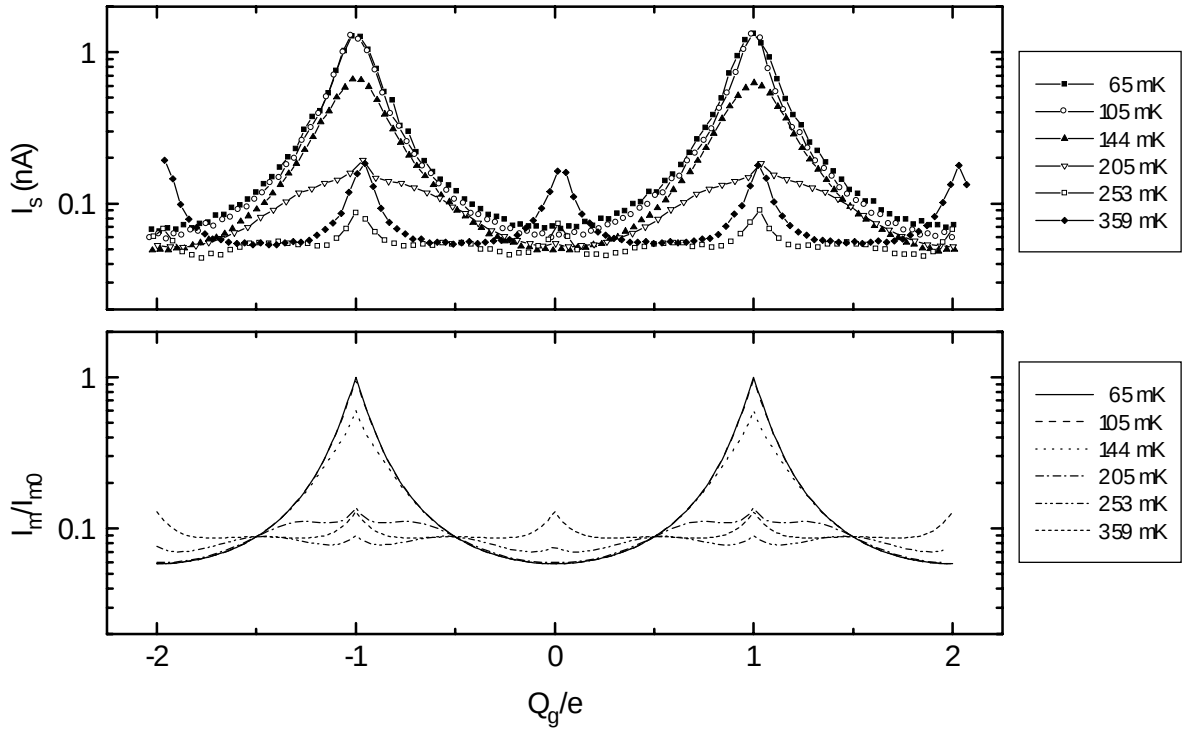

Fig. 11 B. *Temperature dependence of the modulation of the switching current at zero magnetic field. Note the complex cross-over from 2e-periodicity to e-periodicity with*

temperature. It corresponds to the vanishing of the odd-even free energy difference in the island.

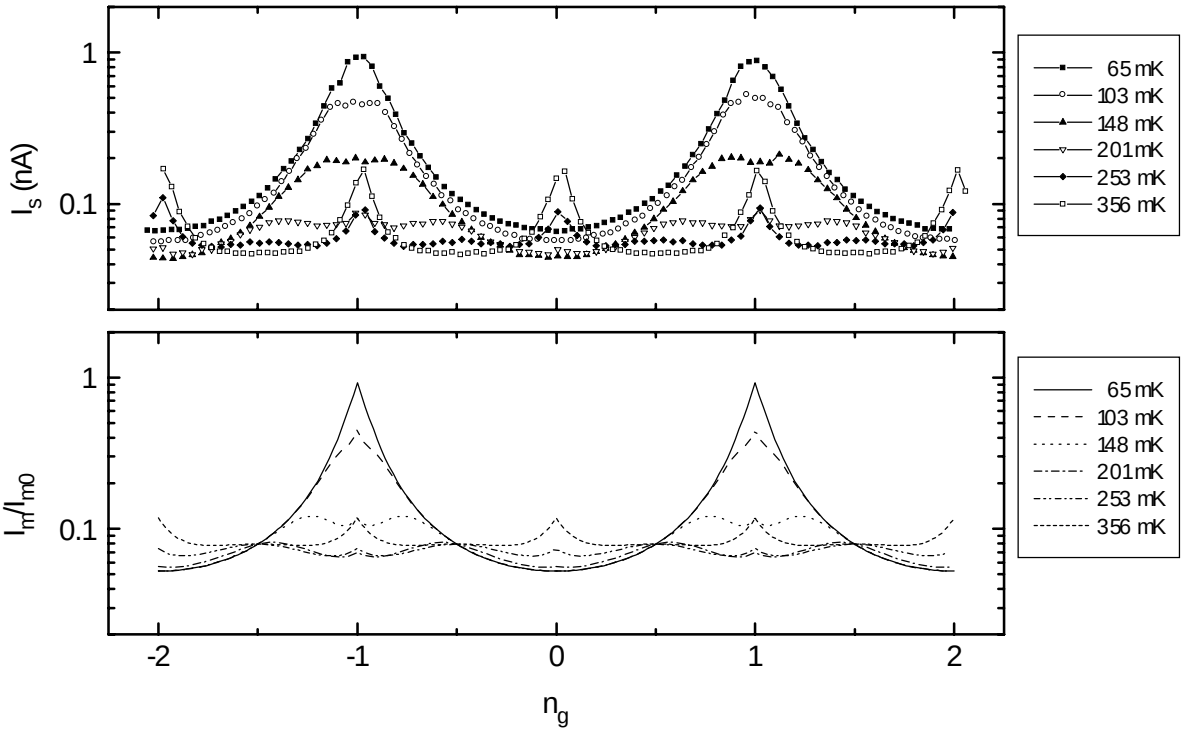

Fig. 11 C. *Temperature dependence of the modulation of the switching current at H = 0.07 T.*

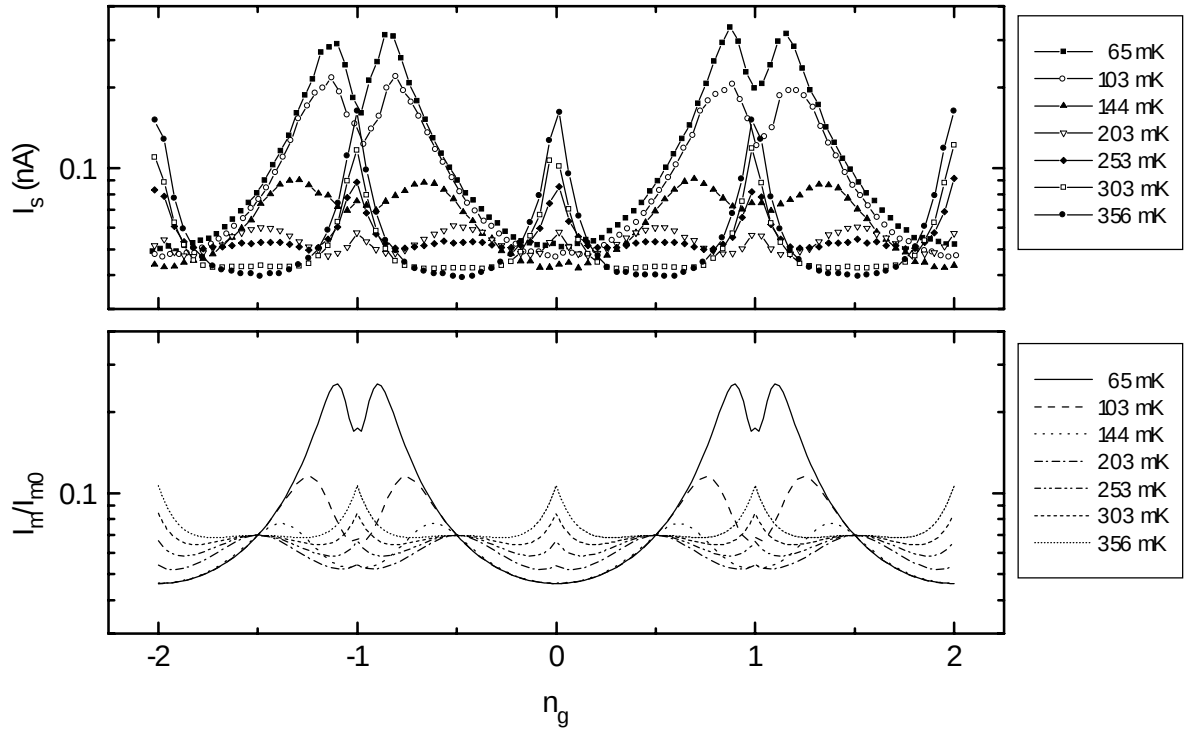

Fig. 11 D. *Temperature dependence of the modulation of the switching current at H = 0.11 T.*

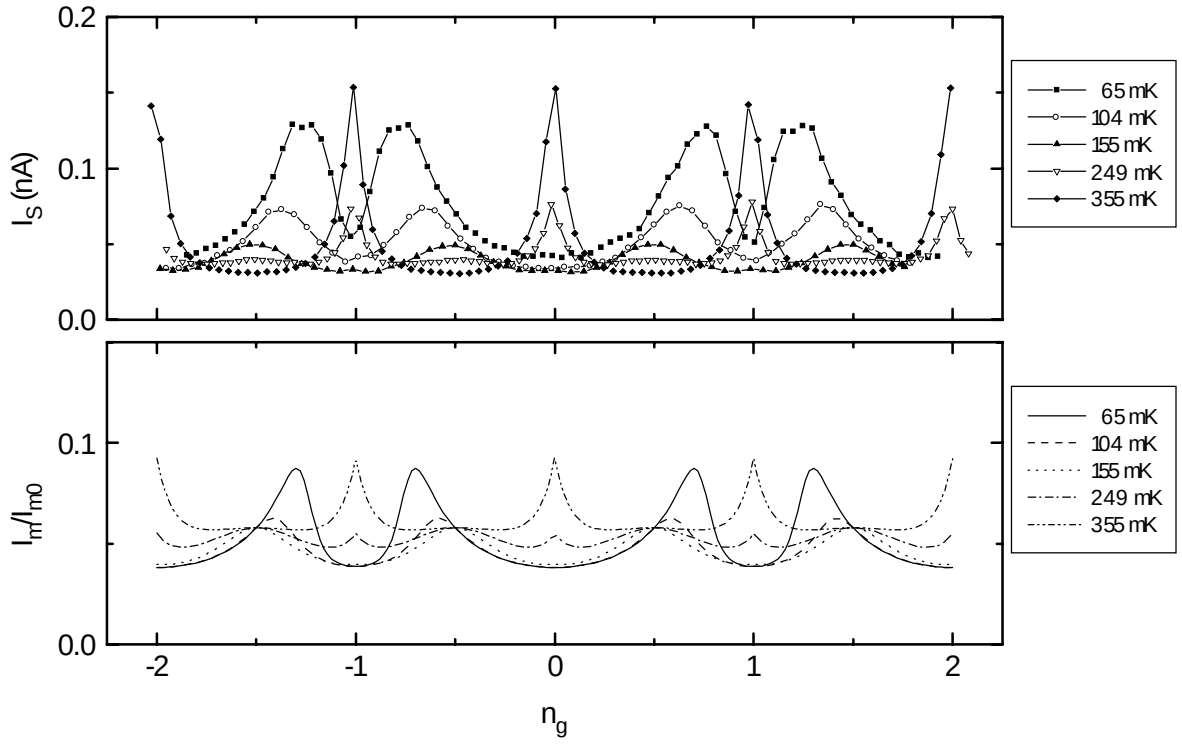

Fig. 11 E. *Temperature dependence of the modulation of the switching current at H = 0.14 T. Note that at this field the peaks in the modulation move a lot with temperature. Note also that for this field and the following, the high-temperature modulation is greater in amplitude than the low-temperature modulation.*

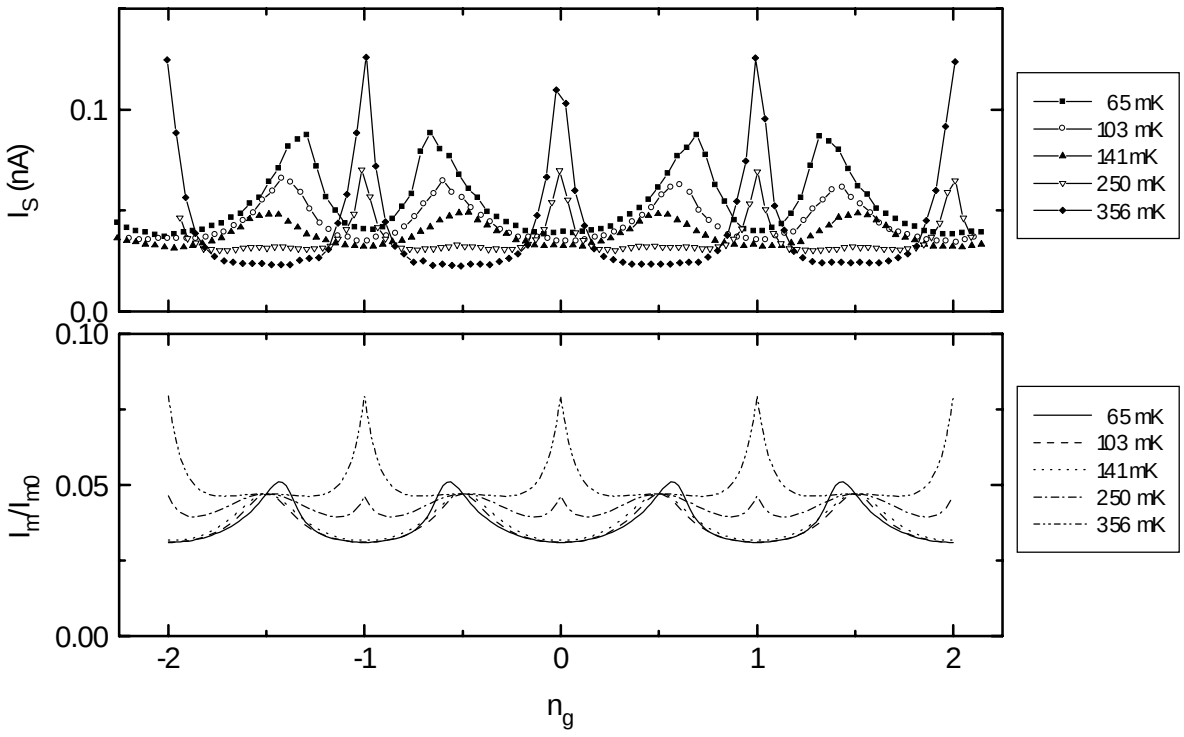

Fig. 11 F. *Temperature dependence of the modulation of the switching current at H = 0.16 T.*

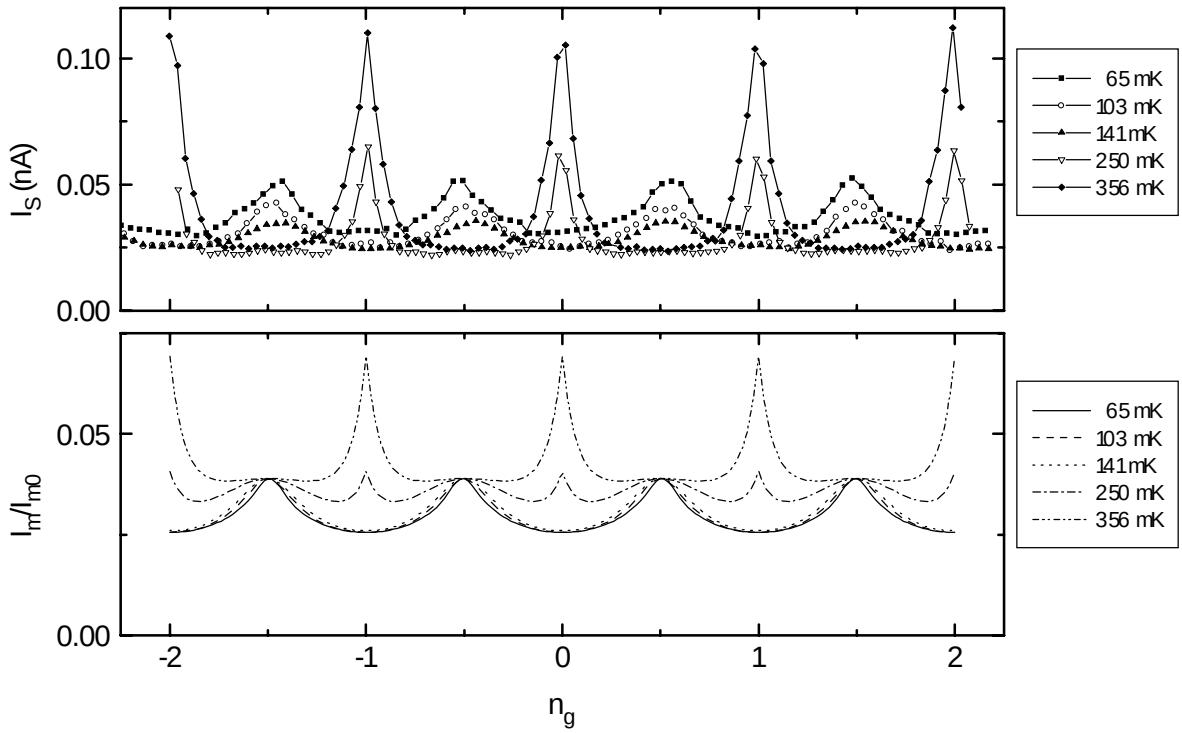

Fig. 11 G. *Temperature dependence of the modulation of the switching current at H = 0.17 T. At this field, the low-temperature switching current is already nearly e-periodic. In this situation, as the temperature increases, the position of the peaks in the switching current change from half-integer values of Q_g/e to integer values of Q_g/e.*

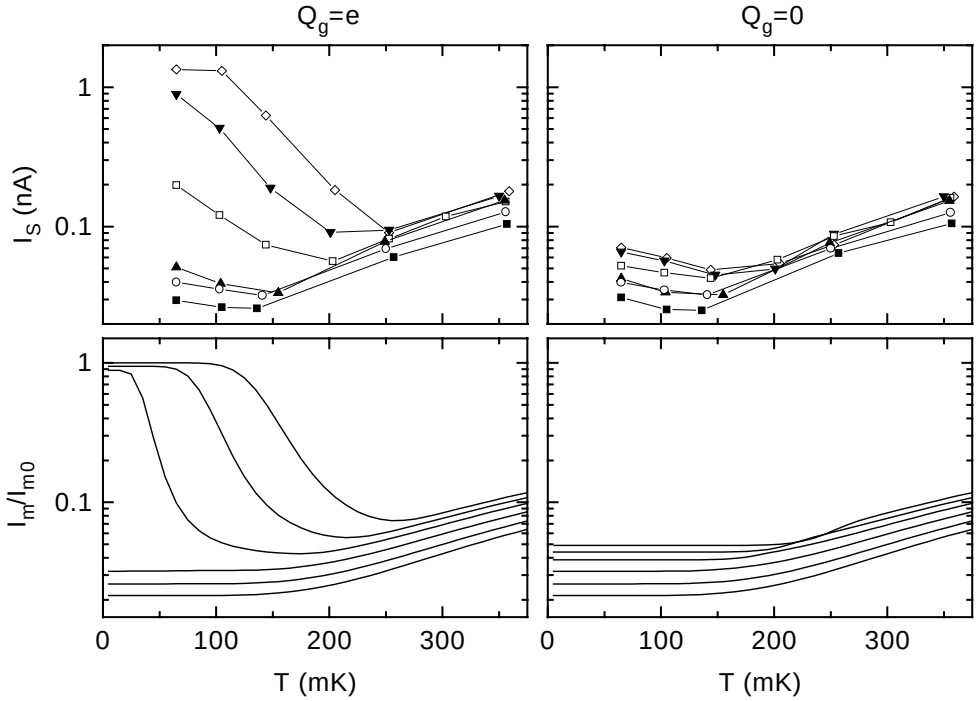

Fig. 11 H. *Top panels: experimental switching current as a function of temperature for $Q_g = 0$ and $Q_g = e$. Top to bottom, same field values as in Fig. 11 A. Bottom panels: theoretical predictions for the same conditions as in top panels. The theory curves reproduce the strongly non-monotonic temperature dependence found in the experiment at $Q_g = e$ for low fields.*

b) THE PROBLEM OF OUT-OF-EQUILIBRIUM QUASIPARTICLES

The description we have made so far of the experimental consequence of poisoning always supposed that quasiparticles were at thermal equilibrium. This is not necessarily the case in experiments. For example, out-of-equilibrium quasiparticles can be created by the absorption of infrared photons by the superconducting electrodes of the transistor, and the relaxation mechanism of these quasiparticle may be quite slow. If there are many such out-of-equilibrium quasiparticles, it is like having no gap for the excitations and then the poisoning is extreme : one measures a weak *e*-periodic modulation of the supercurrent.

As we understand it now, all the previous experiments on the superconducting transistor where more or less plagued with this problem of poisoning by uncontrolled quasiparticles. This was recently checked by Hergenrother *et al.* : by improving the screening of the sample in their dilution refrigerator they observed a better ratio of odd to even peaks [9].

In our experiments on the transistor we avoided this problem of out-of-equilibrium quasiparticles by fabricating our samples with normal-metal leads very close to the island (see Chap. V). This normal metal acted as a trap (or a filter) for out-of-equilibrium quasiparticles : such a quasiparticle entering the normal metal decays in energy and cannot subsequently re-enter the superconductor. Very recently the same quasiparticle filter technique was applied successfully in Delft : the modulation of a transistor became 2*e*-periodic.

With our samples, when we reduced the odd-even free energy by applying a magnetic field and/or raising the temperature we could recover an *e*-periodic modulation pattern of the switching current corresponding to a complete poising (see previous section). For some parameters we could obtain a modulation pattern of the switching current very similar in shape and amplitude to the modulation of the supercurrent peak observed in previous experiments [3,4] (see Fig. 12). This observation also seems to confirm the hypothesis of poisoning in former experiments.

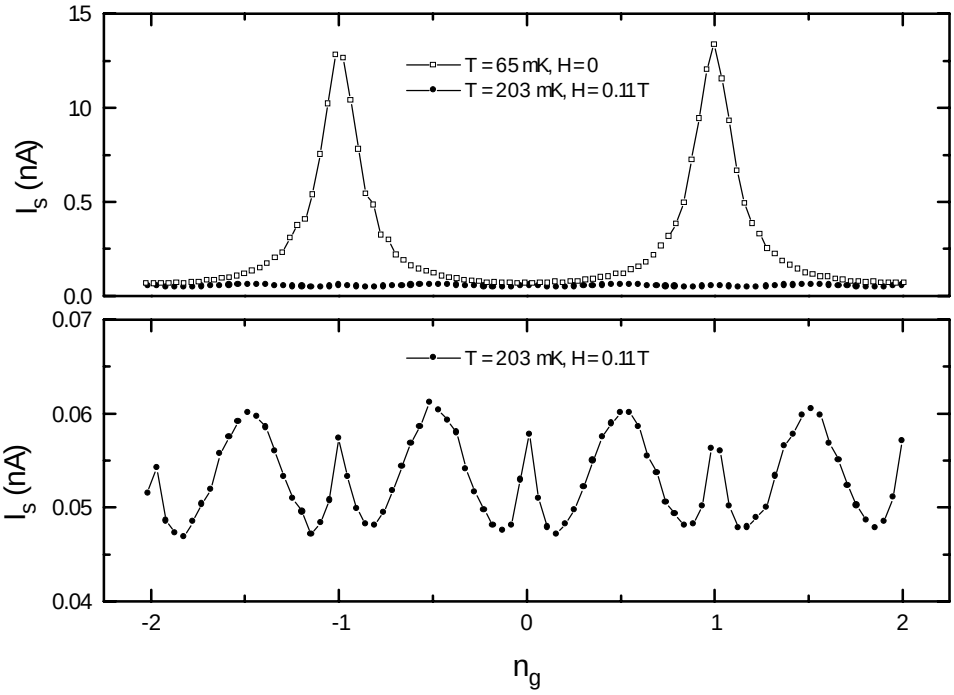

Fig. 12. *Top panel : modulation of the switching current of sample #5 at T=65 mK and H=0 (open squares) and T=203 mK and H=0.11 Tesla (black dots). Bottom panel : magnification of the T=203 mK and H=0.11 Tesla curve. The magnetic field and the temperature suppressed the odd-even free energy difference : the modulation pattern became e-periodic with a very weak amplitude, corresponding to a complete poisoning. This modulation pattern is strikingly similar to that observed in previous experiments (see bottom curve of inset of Fig. 5 and top curve of Fig. 2 of Ref. 4)*

c) POSSIBLE APPLICATIONS

As already mentioned, out-of-equilibrium quasiparticles can be created by infrared photons incident on the superconductor. It is thus possible to envision the fabrication of a very sensitive (ideally single-photon) IR detector based on this effect : the leads of the transistor serve as antennas and the transistor is biased just below its switching current at $Q_g = e$. When a photon strikes the superconductor, it creates two quasiparticles. If one of them reaches the island before recombination the transistor switches to a large voltage (see Fig. 2) : the system is its own amplifier! One can then rearm the detector by cycling the current to zero. For a correct operation, the detector must be cooled well below the odd-even symmetry breaking temperature (~250 mK for Al islands), its environment must be cold enough not to dazzle it, and the photon flux to measure must be weaker than the relaxation rate of quasiparticles in the device.

C. Finite Voltage

1. Resonant Cooper pair tunneling

Our understanding of the gate voltage dependent resonances of the transistor is based on the resonant tunneling of Cooper pairs described in Sec. III.D. In order to compare our experimental results with our model of the process, we must first describe precisely how we made the measurement of these resonances because it has an important consequence on the analysis of the data. We measured these resonances with a bias source of intermediate impedance (≈30 kΩ bias impedance, see Chap. V). The bias source was ramped down to zero, to get as close as possible to the supercurrent branch. Ramping the source up would have masked the lowest voltages because of the hysteresis of the characteristic. This method together with the source impedance prevented the correct observation of the narrow resonances predicted by our model, because of the intrinsic instability of the bias scheme in parts of the *I*-*V* characteristic where the differential conductance d*I*/d*V* is negative and greater in absolute value than the source conductance (see Fig. 13).

Thus, if our model is correct, we can at best observe *I*-*V* characteristics with truncated resonances. We have simulated such a truncation in Fig. 15 & 14, using the parameters of the samples which gave the measures plotted in the same figures. The results are semi-quantitatively correct, except near n_g = odd integer where our model is known to be incorrect. In Fig. 15 one clearly sees the current peaks due to the various orders of resonant tunneling of Cooper pairs (up to the fifth order), with a position in agreement with the theory. High order resonances had never been observed so clearly in previous experiments (see *e.g.* Fig. 16 and Ref. 10).

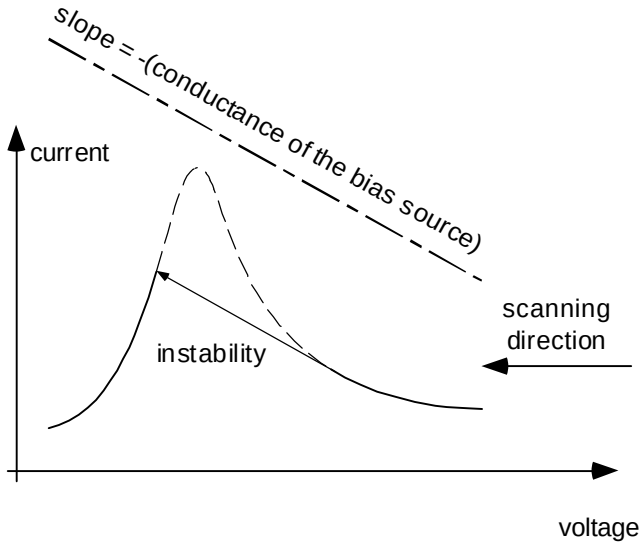

Fig. 13. *The imperfect bias source we used could not reveal the sharp resonances predicted by the theory because of an intrinsic instability.*

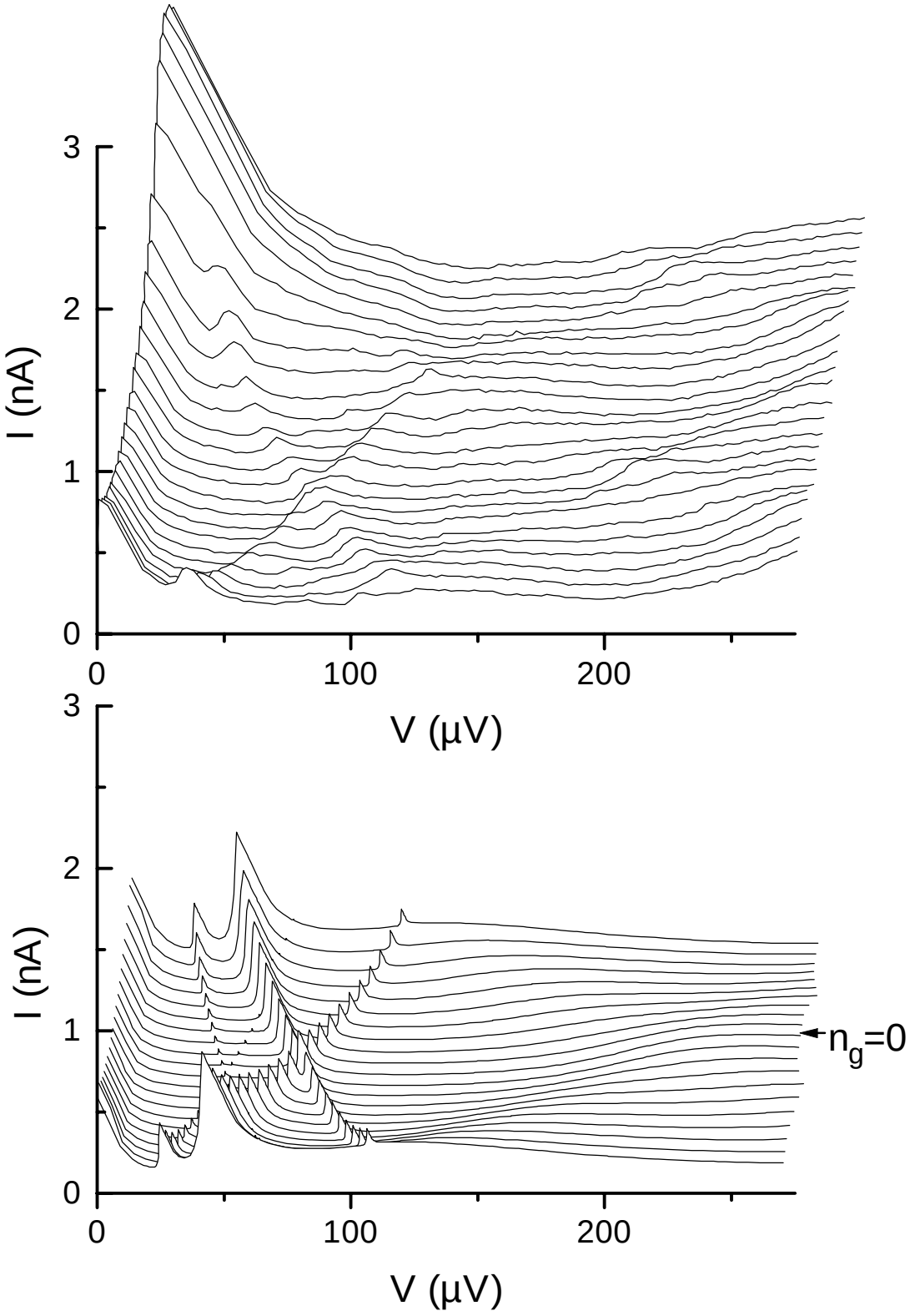

Fig. 14. *Comparison of experimental results of sample 13 (top, -0.5 < n_g < 1.0) with our model (bottom, -0.5 < n_g < 0.5, the Josephson energy is rather large so that the model is only valid in a limited range around n_g = 0), with no other adjustable parameter than the charging energy. Experimental results are less marked than what is predicted.*

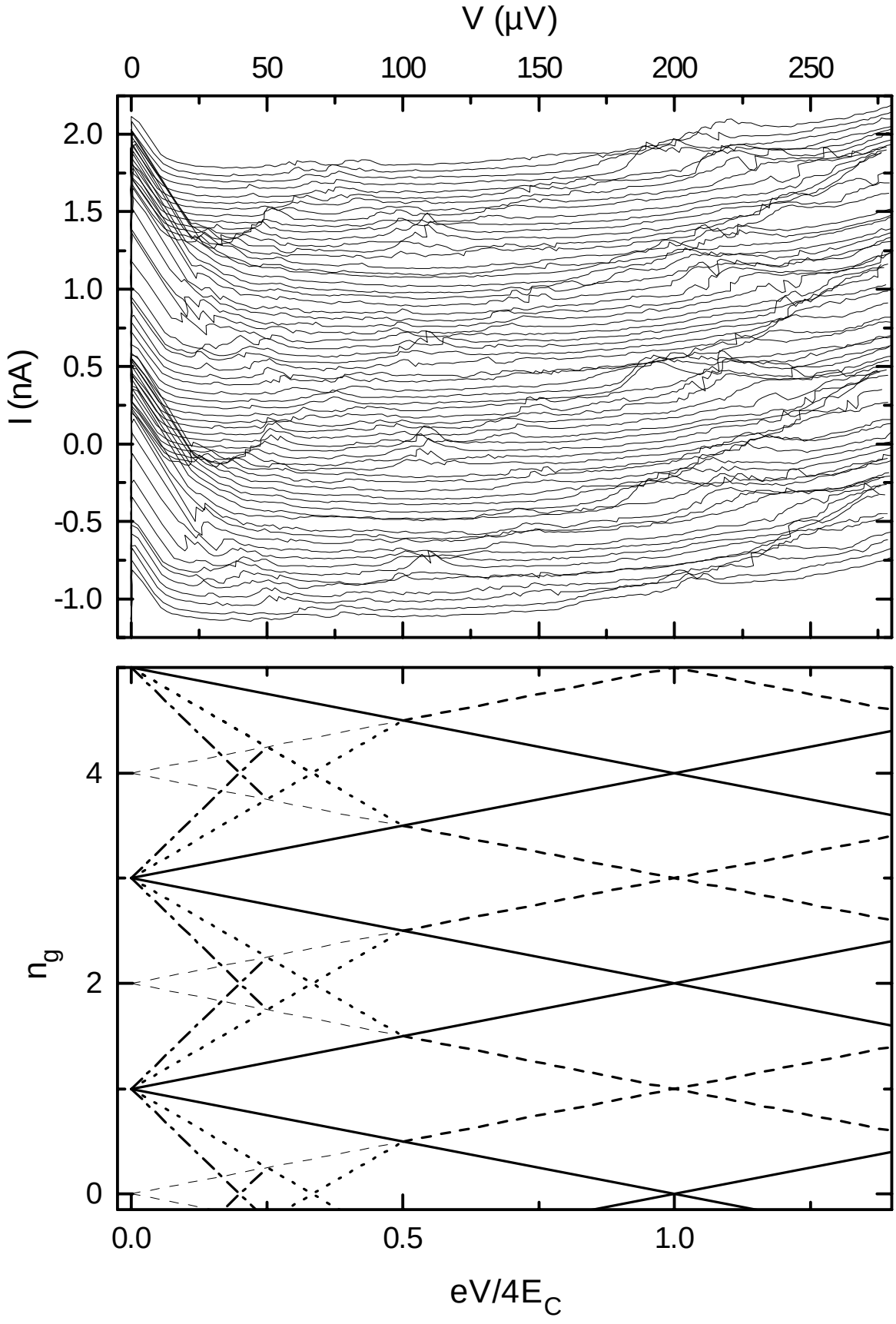
V (μV)
0
50
100
150
200
250
2.0
1.5
1.0
0.5
0.0
-0.5
-1.0
I (nA)
4
2
0
n_g
0.0
0.5
1.0
$eV/4E_C$

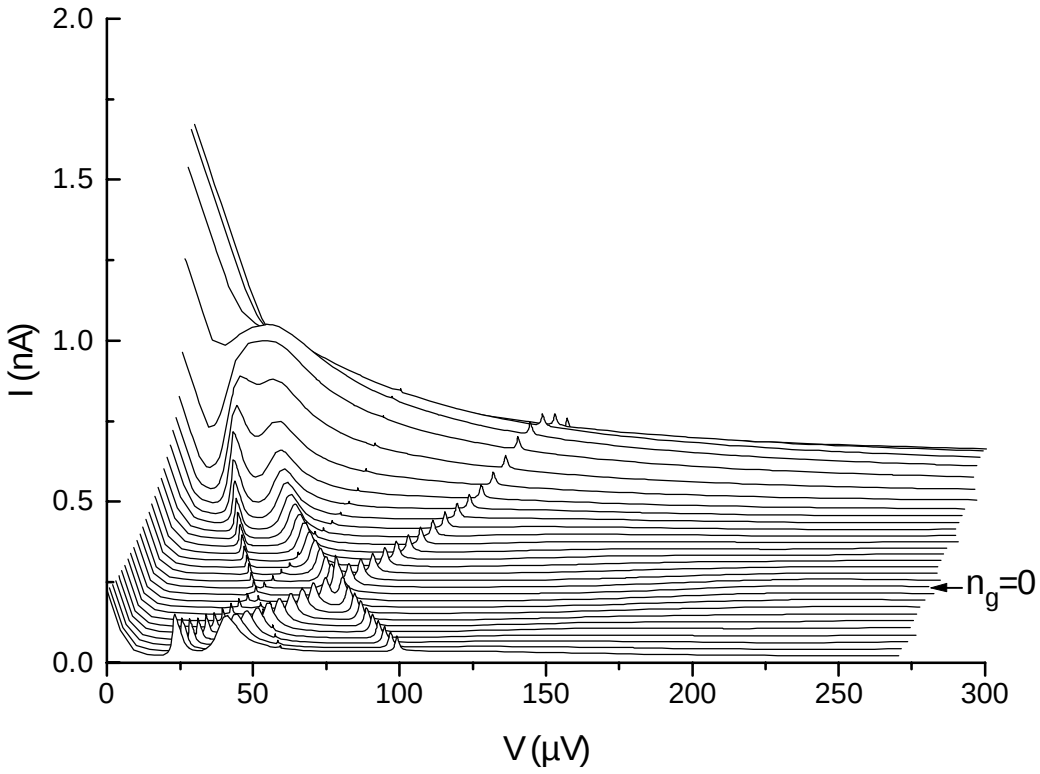

Fig. 15. *Left page, top figure : experimental I-V characteristics for several gate charges. A span of about 2 periods in the gate voltage is covered. One clearly sees the resonances corresponding to the resonant Cooper pair tunneling of order q = 1, 3, 5. (Data from sample 7).*
Bottom figure : theoretical positions of the resonances in the n_g-V plane, at a scale compatible with the top figure. Heavy lines correspond to the observed resonances in the top figure for the orders q = 1 (full lines), q = 3 (dotted lines), q = 5 (dash-dot). The dashed lines indicate the position of the q = 1 resonance corresponding to a loss of the 2e-periodicity (odd-n states). These resonances are observed experimentally over 100 μV (heavy section of the dashed lines in the bottom figure).
This page : calculated I-V characteristics with the parameters of the sample of the top left figure. We have used the model described in Sec. III.D with a truncation of the unstable parts of the characteristics. A detailed comparison is difficult because of the poor signal-to-noise ratio for the peaks in the experimental data.

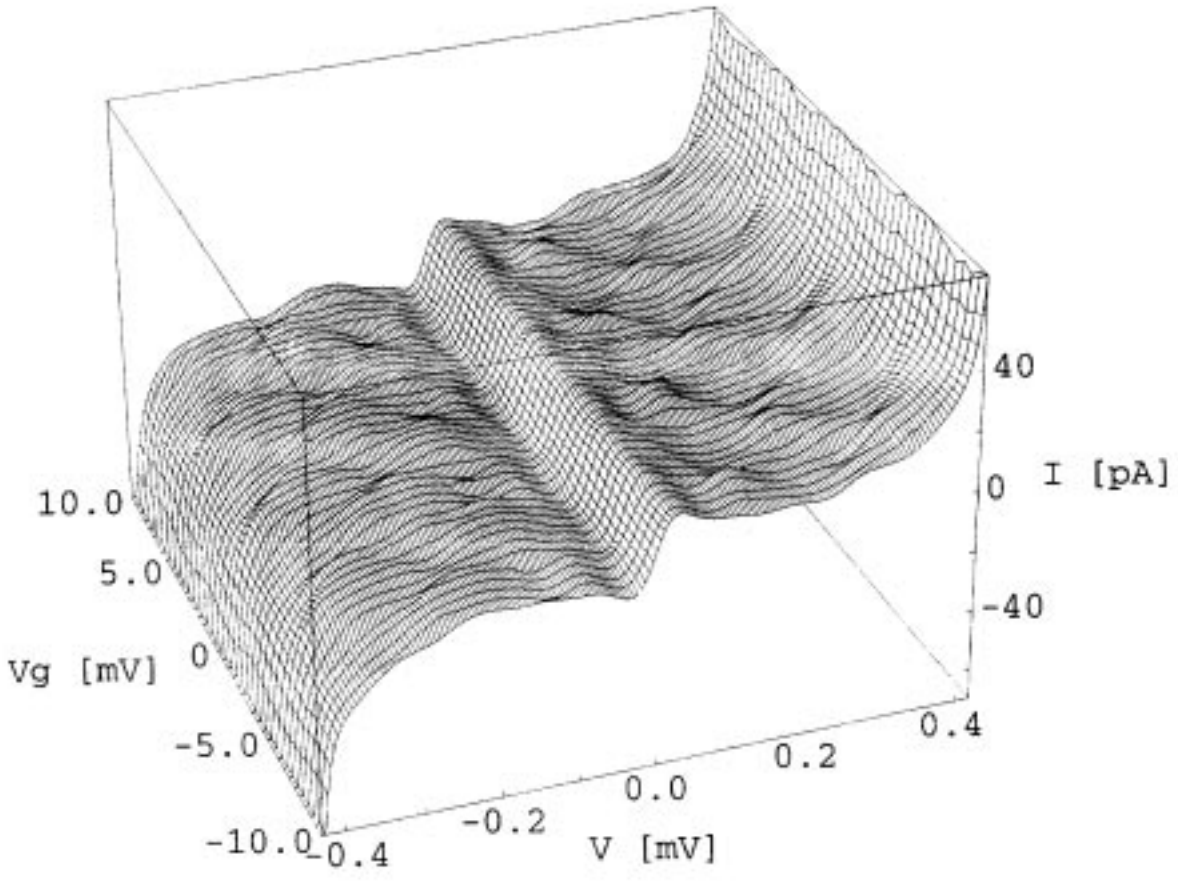

Fig. 16. *Data from the Göteborg group (reproduced from Ref. 11, with permission) showing resonant Cooper pair tunneling of first order.*

2. AC Josephson effect

a) "NORMAL" SHAPIRO STEPS

When the transistor is biased at a finite voltage, if the impedance in the environment of the transistor is negligible, the phase difference across the transistor evolves linearly in time according to the Josephson relation $d\delta/dt = 2\pi V/\Phi_0$. We suppose that the transistor stays in its lowest energy band. In this case, the current flowing through the transistor averages to zero. If a sinusoidal modulation is superimposed on the DC voltage, the velocity of the phase is modulated and an average current can possibly flow in the device. In particular, when the Josephson frequency $\nu = V/\Phi_0$ is a multiple of the irradiation frequency *f*, the *I-V* characteristics develops voltage plateaux which are like the supercurrent branch, but transposed at finite voltage. These voltage plateaux are called "Shapiro steps". They correspond to a locking of the dynamics of the phase on the external frequency. That these are a replica of the supercurrent branch can be understood by a rewriting of the Hamiltonian at

finite voltage. We make the hypothesis that the lowest band of the transistor can be replaced by a sinusoidal band (which is a good approximation near $n_g = 0$) :

$$H(V_{DC}, A) = -E_J^{eff} \cos\delta$$

with

$$\frac{\Phi_0}{2\pi}\dot{\delta} = V_{DC} + A\cos\Omega t$$

where A is the amplitude of the microwave modulation and $\Omega = 2\pi f$ its circular frequency. Integrating this last equation and replacing in the former one yields

$$H(V_{DC}, A) = -E_J^{eff} \cos\left[\frac{2\pi V_{DC} t}{\Phi_0} + \frac{2\pi A}{\Phi_0 \Omega}\sin\Omega t\right].$$

The cosine can be expanded using Bessel functions :

$$H(V_{DC}, A) = -E_J^{eff} \sum_n J_n\left(\frac{A}{\Phi_0 f}\right)\cos\left[\left(\frac{2\pi}{\Phi_0}V_{DC} - n\Omega\right)t\right]$$

$$= \sum_n J_n\left(\frac{A}{\Phi_0 f}\right)H(V_{DC} - n\Phi_0 f,\, A = 0)$$

When the voltage is equal to a particular multiple of $\Phi_0 f$ the corresponding term in the sum above will give a replica of the supercurrent branch with a coupling energy reduced by a factor $J_n(A/\Phi_0 f)$. The other terms contribute by an oscillatory current which averages to zero.

For the data shown in Fig. 17 & 18, we provoked the appearance of Shapiro steps using a microwave generator and an antenna inside the cryostat. The coupling of the microwaves to the DC bias line of the transistor was not controlled in this experiment, it depended strongly on the frequency. A recording of Shapiro steps obtained this way is shown in Fig. 17. We observed well developed voltage plateaux at voltages multiple of $\Phi_0 f$. The data were taken at $Q_g = 0$ where the ground band of the transistor is nearly sinusoidal and where the transistor behaved essentially as a single Josephson junction.

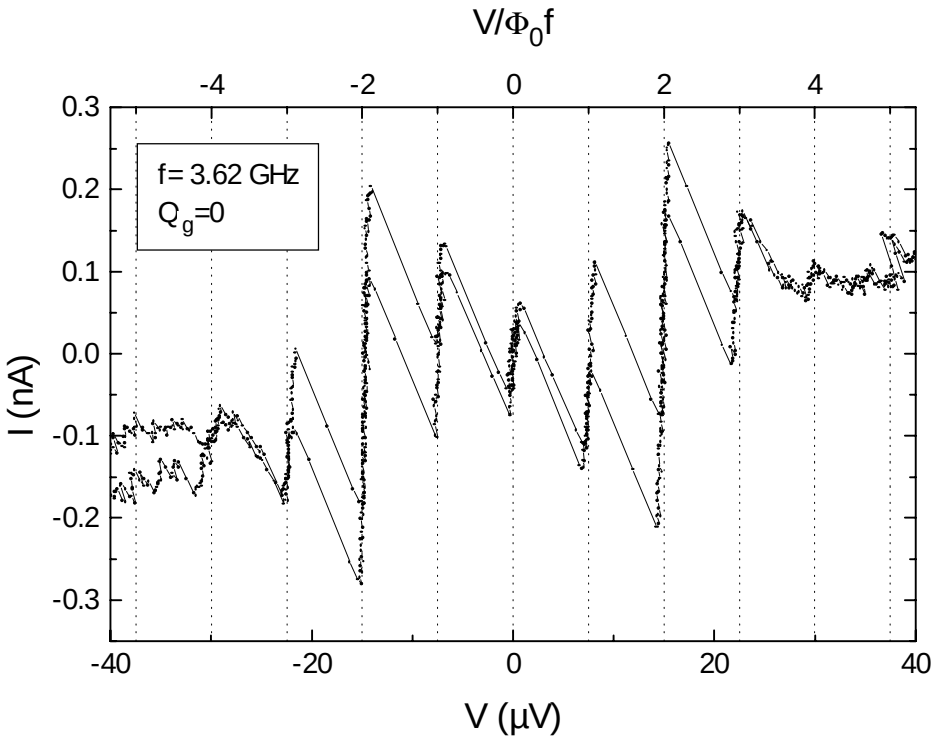

Fig. 17. *Shapiro steps observed under microwave irradiation of a transistor at f = 3.62 GHz. The gate charge was $Q_g = 0$. The top axis is graduated in units of $\Phi_0 f$, the theoretical interval between the steps. Data from sample 7.*

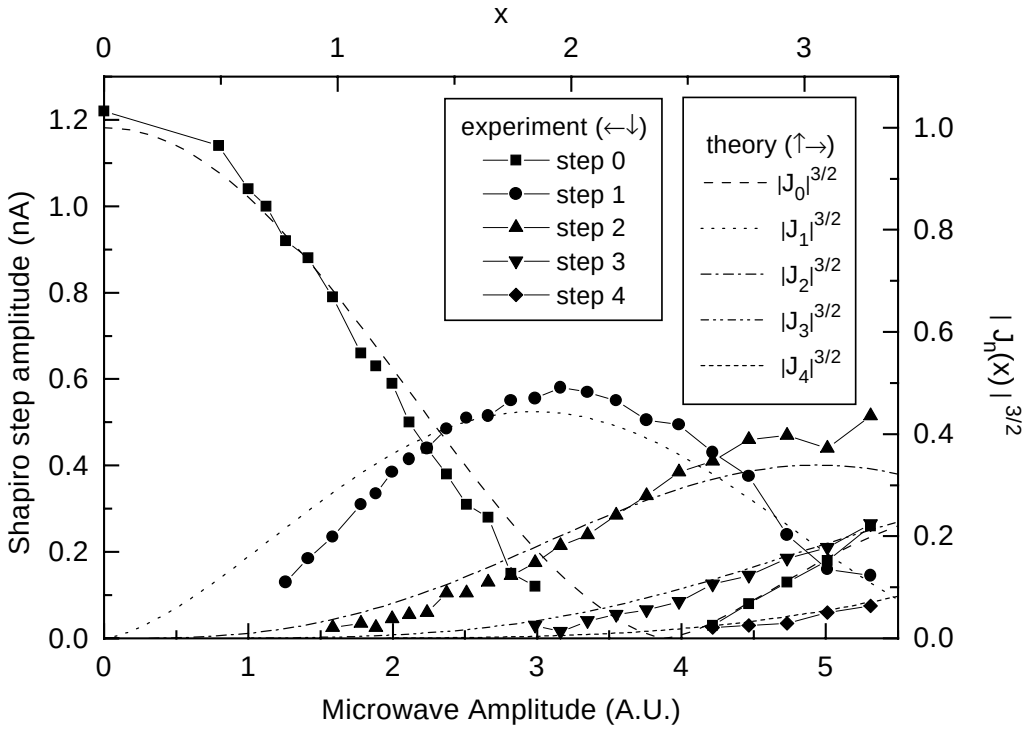

Fig. 18. *Measured amplitude of the Shapiro steps as a function of the microwave amplitude (left and bottom axis). Some points could not be measured because of the hysteresis of the I-V characteristic. The data is compared with the power 3/2 of the Bessel functions J_n (top and right axis). Data from sample 7.*

The data shown here correspond to a sample with a tailored electromagnetic environment (see Chap. V), but with a rather low damping. For this type of damping we have established that the amplitude of the supercurrent branch scaled as a power $3/2$ of the Josephson coupling energy (see Chap. IV). Therefore, we expect that the amplitude of the n^{th} Shapiro steps should vary with the microwave amplitude as $|J_n(A/\Phi_0 f)|^{3/2}$. The measured amplitude of the various Shapiro steps as a function of the microwave amplitude is plotted in Fig. 18, along with the power $3/2$ of the Bessel functions, for comparison. The agreement is quite good in spite of the crudeness of the description used here.

In samples 5 and 13, the odd Shapiro steps disappeared near $Q_g = e$. This is understood as Zener effect between the two lowest bands of the transistor. This effect is explained in Sec. 4.

b) FRACTIONAL SHAPIRO STEPS

By connecting the microwave line carefully to one of the gates of the transistor, we tried to generate fractional Shapiro steps. The idea is to produce a microwave modulation of the gate charge so that the system follows a trajectory in the $\{n_g,\delta\}$ plane which picks mostly positive contributions to the current. Trace a) of Fig. 19 gives an example of such a trajectory which would yield the $1/2$ harmonic of the normal Shapiro step (the frequency of the microwave excitation of the gate charge is twice that of the motion of δ in the band).

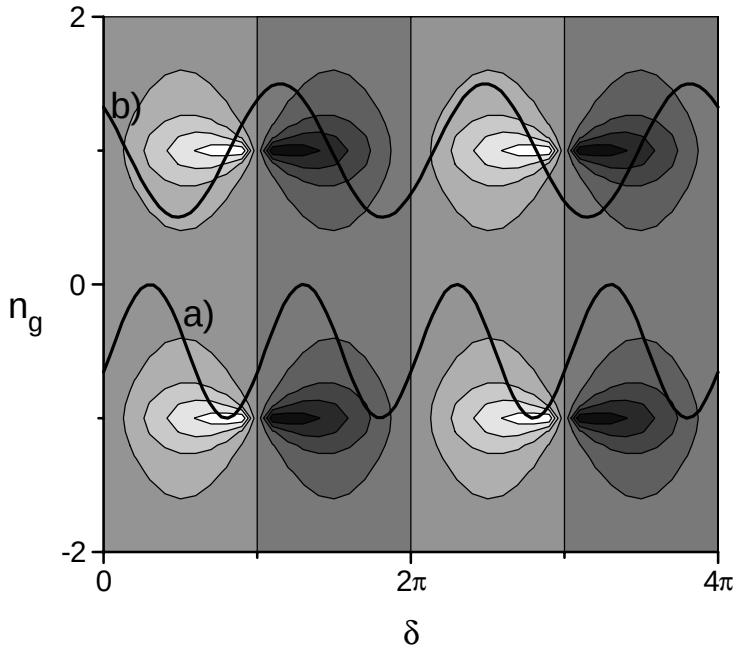

Fig. 19. *Trajectories in the $\{n_g,\delta\}$ plane which should produce sub-harmonic Shapiro steps. The lighter-tinted areas correspond to positive instantaneous current, and the darker to negative current (the instantaneous current is obtained by taking the derivative of the ground band energy with respect to δ). The plotted trajectories a) and b) pick more positive than negative current, thus they should give a Shapiro step. a) would give the $\Phi_0 f/2$ step and b) the $2\Phi_0 f/3$.*

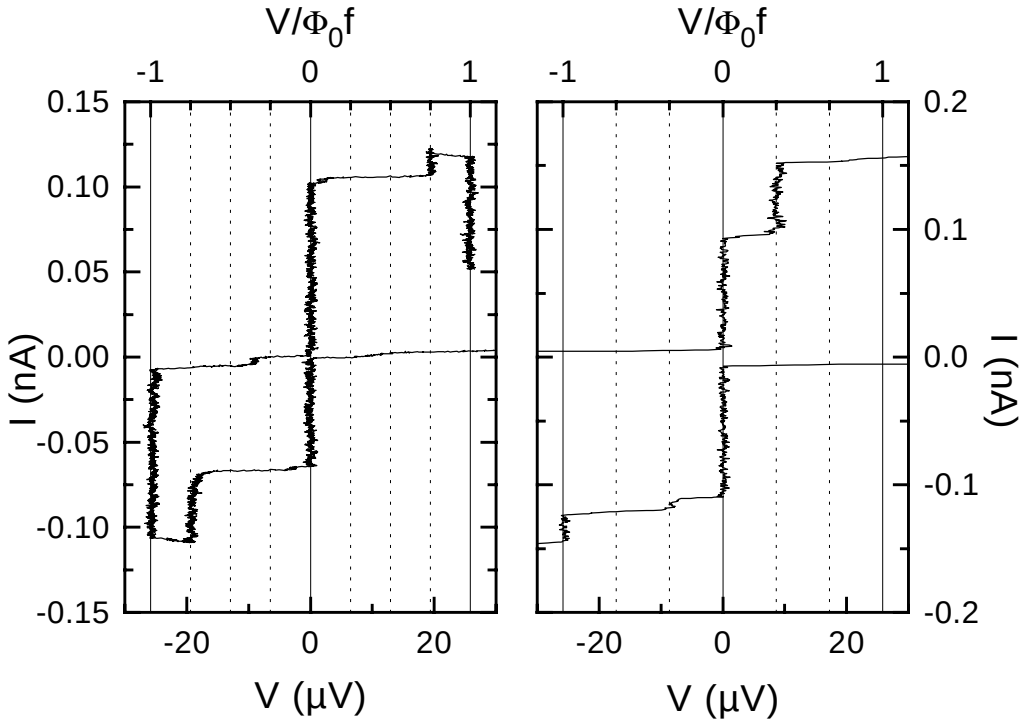

Fig. 20. *Possible fractional Shapiro steps observed in sample 5. The microwave frequency was $f = 12.471$ GHz. Left panel shows two steps at a 3/4 of the voltage $V = \Phi_0 f$ of the first standard Shapiro steps, and right panel shows a step at 1/3 of the first Shapiro step.*

We did not succeed to do this in a well controlled manner. In particular, our samples with a clean electromagnetic environment never displayed these resonances. We observed sometimes resonances that looked like these fractional harmonics (see Fig. 20) but we could not draw any conclusions because of several problems :

(i) In these experiments, the coupling of the microwaves was not controlled : we simply used an antenna to radiate the microwaves inside of the cryostat. In this set-up the microwaves certainly did not couple exclusively to the gate voltage. Moreover, transmission of the microwaves was extremely dependent on the frequency and we could only observe this phenomenon in narrow frequency windows.

(ii) These samples had many low-frequency resonances which could always be interpreted as an arbitrary fraction of the first ordinary Shapiro step.

(iii) On the contrary, maybe these resonances of the environment participated in stabilising the phenomenon which otherwise would have been too unstable to be observed.

3. Fixed resonances

Our first samples had an essentially uncontrolled electromagnetic environment. They displayed resonances in the *I-V* characteristic whose center voltage was independent of the gate voltage, but whose amplitude could depend on gate voltage. An example of such resonances is shown in Fig. 21 where two resonances stand out at $V = 40$ µV and $V = 80$ µV. Other resonances are obviously present in the voltage range 20-60 µV, but none seems to have a constant position with gate voltage, they are caused by the resonant Cooper pair tunneling. We interpret the two fixed resonances as self-induced Shapiro steps caused by resonance in the electromagnetic environment of the transistor : At finite voltage the transistor emits an AC current at the Josephson frequency in the leads. If the impedance of the environment presents a resonance at this frequency, it produces a current peak in the *I-V* characteristic [12,13]. Several facts support this hypothesis:

(i) The resonances shown in Fig. 21 appear at voltages multiple of 40 µV, as expected for Shapiro steps at a frequency and its multiples.

(ii) The resonances were highly enhanced by very little microwave irradiation at the corresponding frequency.

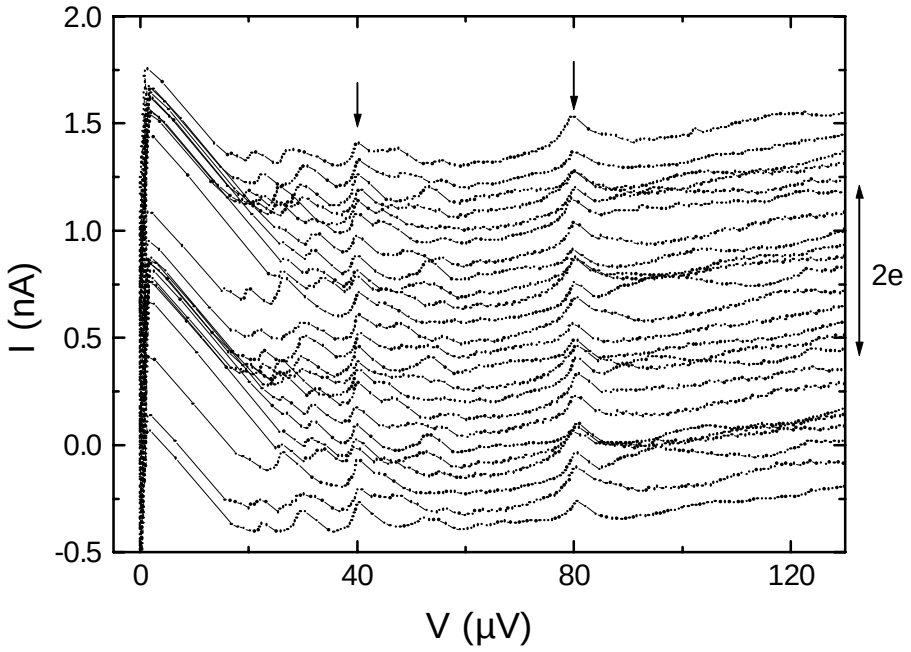

Fig. 21. *Low voltage I-V characteristics of a sample for several values of the gate charge Q_g (each trace has been offset for clarity; about 2 periods of Q_g are covered). Resonances clearly appear at fixed voltages (arrows). Here the resonance at 80 μV corresponds to the first harmonic of the other one. We interpret these resonances as self-induced Shapiro steps at $f \approx 20$ GHz and 2f. Data from sample 8.*

(iii) In samples with carefully designed electromagnetic environments, these resonances did not appear.

4. Zener effect

Samples 5 and 13 had a peculiar behaviour for gate voltages close to $Q_g = e \mod 2e$: It seemed that the relation between the frequency and the voltage for the AC Josephson effect was changing.

This was particularly visible on the displacement of fixed resonances of sample 5 of the environment, as illustrated by Fig. 22a. It was also visible on the AC Josephson effect, for which the odd harmonics of the Shapiro steps disappeared close to $Q_g = e$ (see Fig. 23). This doubling of the voltage is interpreted as the doubling of the period of the $E(\delta)$ relation corresponding to a Zener effect between the two lowest bands of the transistor (Fig. 24).

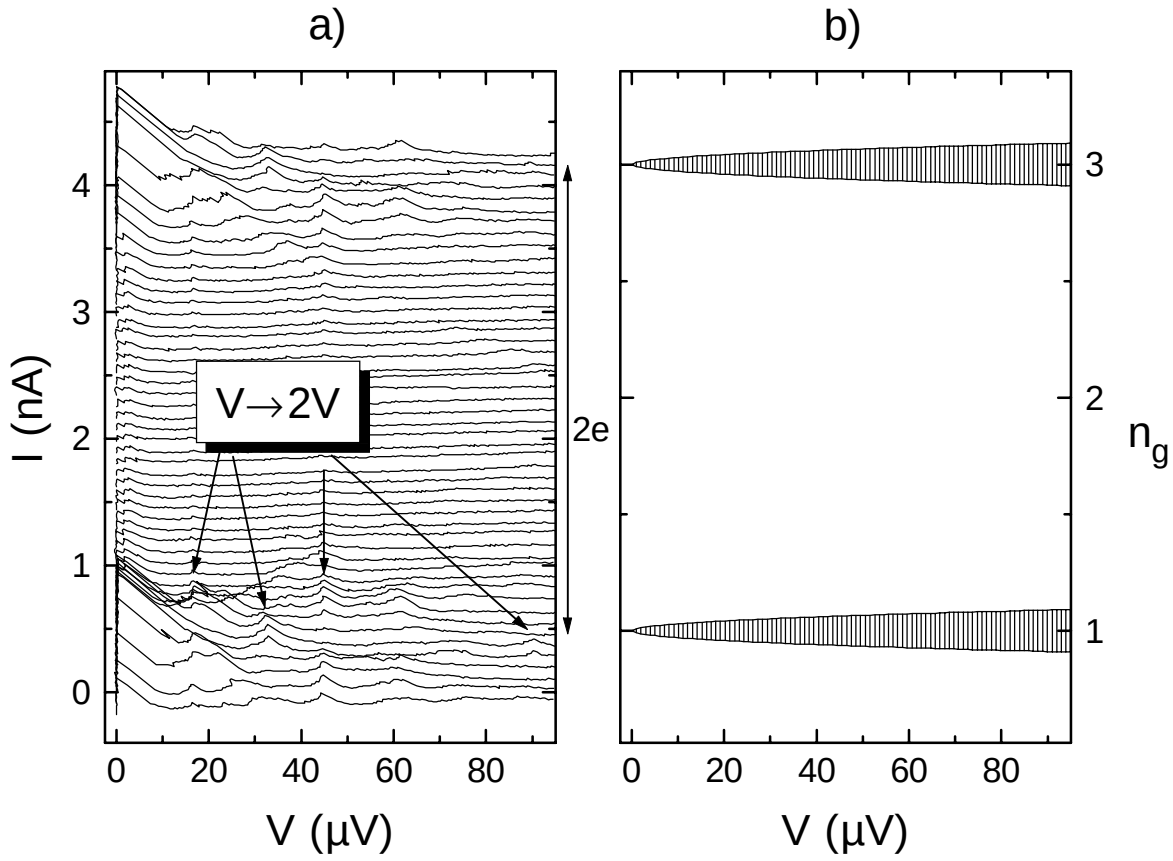

Fig. 22. ***a)*** *I-V characteristics of a sample, for different gate voltages. A span of a little more than one period in the gate voltage is covered and traces are offset by 0.09 nA for clarity. The doubling of the voltage of self-induced Shapiro steps around $Q_g = e$ mod 2e is interpreted as Zener effect between the two lowest bands of the transistor (Data from sample 5).* ***b)*** *At the same scale, the hatched areas are domains of the V-n_g plane where the Zener probability is greater than 1/2, assuming perfect symmetry of the junctions.*

When the gate charge Q_g becomes close to e, these bands tend to pinch at $\delta = \pi$ mod 2π. The pinching is perfect only if $E_{J1} = E_{J2}$ and $Q_g = e$, in the other cases the gap between the bands only reduces to

$$\varepsilon = 2\sqrt{\left(\frac{E_{J1} - E_{J2}}{2}\right)^2 + \left(2E_C(1-n_g)\right)^2} \ .$$

A finite voltage V across the transistor corresponds to a given velocity of the phase $\dot{\delta} = 2\pi V/\Phi_0$. Zener effect occurs when the phase cannot "take the turn" at the anticrossing of levels and changes band : if the system does not spend enough time in the vicinity of the anticrossing, it cannot follow adiabatically the lowest level. The characteristic evolution time of the state of the system at $\delta = \pi$ is $\tau = \hbar/\varepsilon$ and the time it spends in the vicinity of the anticrossing is of the order of $\tau' = \varepsilon / E_J \dot{\delta} = \varepsilon\Phi_0/2\pi E_J V$, where $E_J = (E_{J1}+E_{J2})/2$ is the average Josephson coupling energy of the two junctions. One thus expects a crossover from

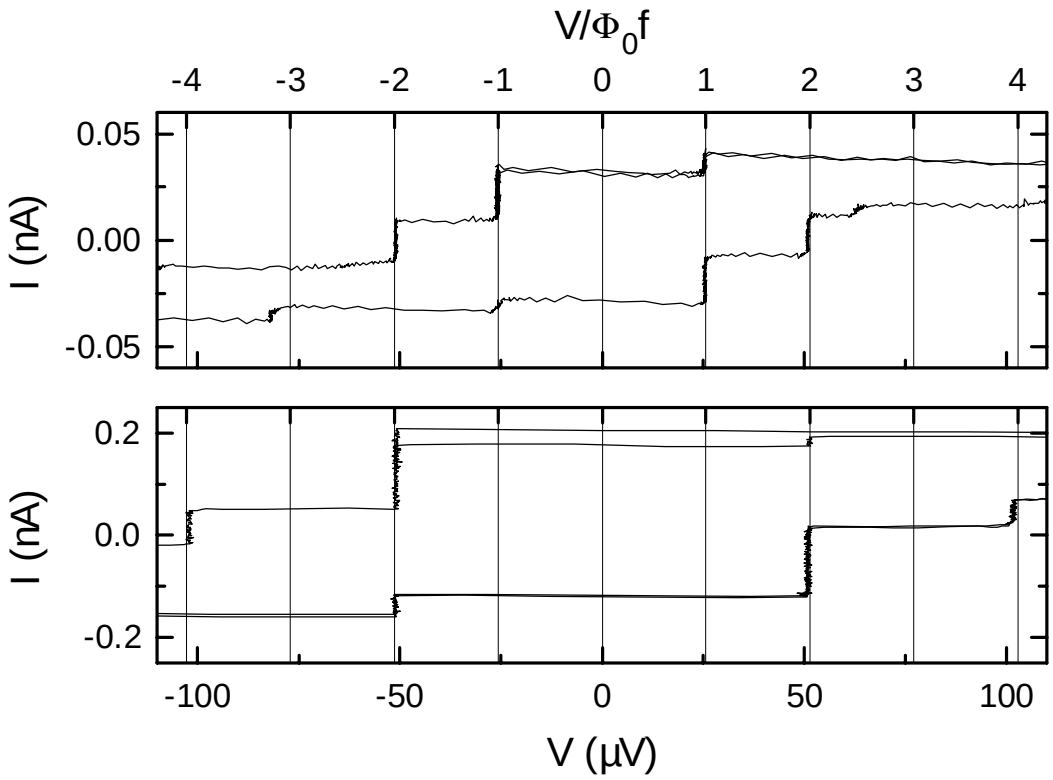

Fig. 23. *Shapiro steps taken with sample 5 under microwave irradiation at f = 12.465 GHz. Top panel : Shapiro steps taken near Q_g = 0. Steps 1 and 2 are clearly seen. Bottom panel : near Q_g = e steps 2 and 4 are the only one visible. The odd Shapiro could not be observed near this gate voltage, except at high microwave power where the modulation became e-periodic. The doubling of the voltage of the steps is interpreted as a signature of Zener tunneling between the two lowest bands of the transistor (see text).*

adiabatic behaviour when $\tau \ll \tau'$ to Zener tunneling for $\tau \gg \tau'$. An exact treatment [14] gives the probability of Zener tunneling at one anticrossing of the bands :

$$P_Z = \exp\left(\frac{-\pi\tau'}{\tau}\right) = \exp\left(\frac{-\pi\varepsilon^2}{2E_J eV}\right)$$

For a given voltage, the Zener transitions can occur only if ε is small enough. This means it will only occur in the vicinity of $Q_g = e$ and only if $|E_{J1}\text{-}E_{J2}|$ is small enough. This explains why the effect was not visible in all the samples : it requires very symmetrical junctions. When the Zener probability is close to one, the transistor behaves as if the period of the energy band as a function of the phase had doubled. In particular, the AC current the transistor emits in the environment has a frequency divided by two ; it requires a voltage twice as high to emit at the previous frequency. This qualitatively explains the observations. We will now try to make a quantitative comparison. Assuming perfectly symmetrical junctions, we can calculate P_Z as a function of the gate charge and of the voltage for the sample of Fig. 22a. For this purpose we use the independently measured parameters of the sample $E_J/k_B = 275$ mK and $E_C/k_B = 1.0$ K.

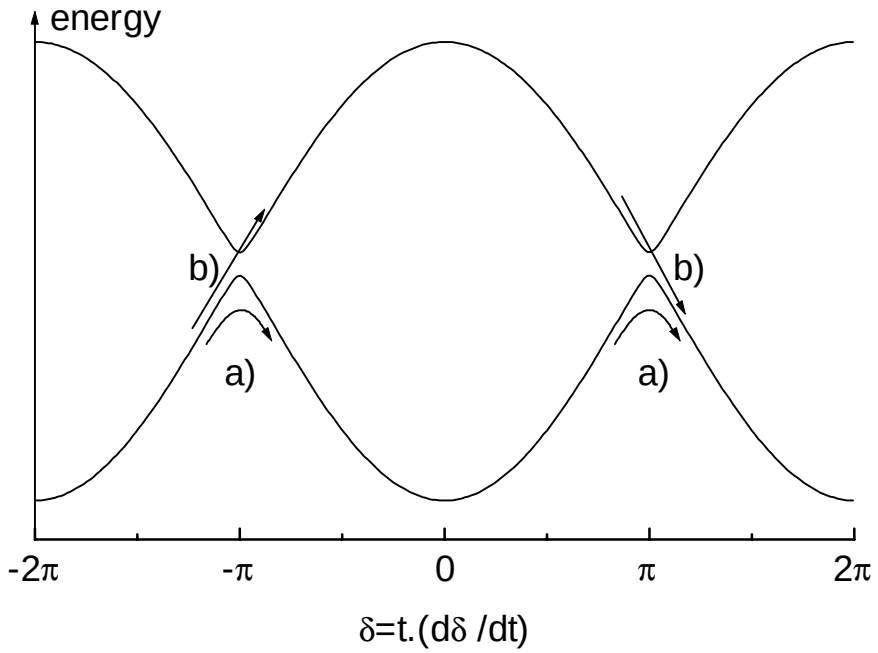

Fig. 24. *Plot of the two lowest bands of the transistor near $Q_g = e$. If the gap between the bands remains too large or if the velocity of the phase is low, the motion of the phase is "adiabatic", following the ground energy band (a). On the opposite, if the gap is small enough, and the voltage high enough, the velocity of the phase can provoke Zener transitions (b), doubling the period of the E(δ) relation.*

The result of the calculation is shown in Fig. 22b, where the shaded areas correspond to ranges of gate charge and voltage for which $P_Z > 1/2$. These areas correspond quite well to the domains where the doubling of voltage is visible in Fig. 22a, with no fitting parameters.

We must point out though, that the observation of Shapiro steps necessitates a non strictly uniform motion of the phase, contrarily to what we have supposed here. Thus, the preceding analysis needs to be refined somehow to take this effect into account.

References for Chap. VI

[1] T. A. Fulton, P. L. Gammel, D. J. Bishop and L. N. Dunkleberger, Phys. Rev. Lett. **63**, 1307 (1989).

[2] T. A. Fulton and G. J. Dolan, Phys. Rev. Lett. **59**, 109 (1987).

[3] L. J. Geerligs, V. F. Anderegg, J. Romijn, and J. E. Mooij, Phys. Rev. Lett. **65**, 377 (1990).

[4] M. T. Tuominen, J. M. Hergenrother, T. S. Tighe and M. Tinkham, Phys. Rev. Lett. **69**, 1997 (1992).

[5] P. Lafarge, P. Joyez, D. Esteve, C. Urbina, and M. H. Devoret, Nature **365**, 422 (1993).

[6] M. L. Roukes, M. R. Freeman, R. S. Germain, R. C. Richardson, and M. B. Ketchen, Phys. Rev. Lett. **55**, 422 (1985).

[7] L. J. Geerligs, V. F. Anderegg, and J. E. Mooij, Physica **B 165-166**, 973 (1990).

[8] K. A. Matveev, M. Gisselfält, L. I. Glazman, M. Jonson and R. I. Shekhter, Phys. Rev. Lett. **70**, 2940, 1993.

[9] J. M. Hergenrother, J. G. Lu, M. T. Tuominen, D. C. Ralph, and M. Tinkham, preprint (1994).

[10] A. Maassen van den Brink, L. J. Geerligs, and G. Schön, Phys. Rev. Lett. **67**, 3030 (1991).

[11] D. B. Haviland, Y. Harada, P. Delsing, C. D. Chen, and T. Claeson, Phys. Rev. Lett. **73**, 1541 (1994)

[12] J. Zimmerman, J. Appl. Phys. **42**, 30 (1971)

[13] T. Holst, D. Esteve, C. Urbina, and M. H. Devoret, Phys. Rev. Lett. **73**, 3455 (1994).

[14] K. Mullen, Y. Gefen, and E. Ben Jacob, Physica **B 152**, 172 (1988)

VII. CONCLUSION

When we started this work the behaviour of the superconducting single electron transistor was not clearly understood in comparison with its normal-state version. The cause of these difficulties are now identified : the initial description of the transistor considered only the role of the charging energy E_C and of the Josephson energy E_J whereas two other quantities play a least as large a role, (i) the distribution of quasiparticles in the superconducting electrodes described by an effective temperature T^* and the related odd-even free-energy difference $D(T^*, H)$ and (ii) the impedance $Z(\omega)$ seen by the transistor. By conducting a series of experiment we could progressively disentangle the effects associated with these quantities.

Undoubtedly, the most decisive step in this direction was the fabrication of the normal-metal quasiparticle filters in our samples. This innovation allowed the observation of the long-sought-after "perfect 2*e*-periodicity" of the transistor : the shape of the supercurrent modulation with the gate voltage was qualitatively in agreement with the theoretical predictions. In itself the observation of this modulation constituted the first observation of macroscopic quantum coherence.

The role of these quasiparticle filters is to achieve an effective thermalization of long-lived out-of-equilibrium quasiparticles in the superconductors that otherwise prevent the observation of macroscopic quantum coherence. This effect of destruction of the coherence is nicknamed the "poisoning" of the supercurrent by quasiparticles; it was probably the main cause of *e*-periodicity in early experiments on the transistor. By applying a magnetic field and/or raising the temperature we have been able to decrease the odd-even free-energy in the island of the transistor and we then observed in details the effects of the quasiparticle poisoning of the supercurrent. These observations were found to be in good agreement with theory, which proves that quasiparticles are indeed at thermal equilibrium when filters are used. The poisoning effect may be used as principle for an ultra-sensitive infra-red detector.

By microfabricating a well-characterized electromagnetic environment for the transistor, we could further clarify the observations in the low-voltage part of the current-voltage characteristics of the samples : we discriminated the resonances due to the electromagnetic environment of the transistor and those due to "resonant Cooper pair tunneling". With a purely RC electromagnetic environment, the "parasitic" resonances due to the environment are eliminated whereas those due to "resonant Cooper pair tunneling" remain. These latter resonances depend on the gate voltage of the transistor and form a hierarchy. We observed for the first time the first three orders of this hierarchy. These resonances allow a precise

determination of the charging energy of the device. Previously, the determination of this essential parameter had always been approximate.
In two samples we could observe an other type of macroscopic quantum phenomenon : Zener tunneling between the two lowest bands of the transistor. Unfortunately, the effect does not yield itself to an easy investigation in this system and our results are still preliminary.
Last but not least, our experiments also yielded results whose scope extends farther than just the superconducting single electron transistor : we have shown how the electromagnetic environment plays a capital role in small Josephson junction systems. First of all, we have calculated the renormalization of the Josephson coupling energy in presence of a perturbative environment. For Josephson junctions fabricated by usual techniques, this renormalization is dominated by charging effects, if any. The second important result concerns the magnitude of the experimental supercurrent in these systems. We have presented a new analysis of the behaviour of these systems based on the notion of current-voltage characteristic of a junction in its environment. We distinguish between two types of hysteretic behaviour for the system : (i) a static hysteresis at very low temperature and, (ii) depending on the environment, a dynamic hysteresis at higher temperatures. Many experiment concerning Josephson junctions (including our experiments on the transistor) are done in the current bias mode : the device is not shunted at dc. In this setup, we have found that the system has a dynamic hysteretic behavior and we explained how the observed switching current is related to the critical current of the device and to the damping provided by the electromagnetic environment. We predict in particular that the switching current of underdamped systems is inversely proportional to the quality factor of the circuit at the plasma frequency of the system and we conjecture that it should depend very weakly on temperature. Our data in two extreme situations (over- and under-damped system) agree with this description.

We have now reached a point where we can explain the experimental observations at low voltage on the transistor in a quite wide range of parameters for the system.
The knowledge gained in these experiments should apply to a wide variety of circuits where Coulomb and/or Josephson effects are present. In particular, it is now clear that one should pay great attention to the design of the electromagnetic environment of such circuits. The control of the quasiparticle population is also an imperious goal if quantum superposition of charge states is sought.

During this work however, we have not answered all the initial questions : we do not understand what controls the quality of the superconducting order in the island. At the point we are, having defects in the density of states seems to be a matter of chance : only one out of thirteen samples was *e*-periodic at low temperature, indicating the presence of low-lying

excited states in the island. Nevertheless, if one considers making multiple-island circuits, this apparent low probability of defect can soon become a serious problem.

A possible extension of the experiments described in this work is the precise investigation of the phenomenon of macroscopic quantum tunneling. It would be interesting to observe the influence of the strength of dissipation on coherence. A superconducting single electron box experiment should be well suited for this purpose. Another extension of this work would be the realisation of a superconducting device for metrological application such as the superconducting Cooper pair pump.

APPENDIX A

We reprint here a paper originally published in Physical Review Letters, volume 72, number 15, pp. 2458-2461, 1994.

Observation of Parity-Induced Suppression of Josephson Tunneling in the Superconducting Single Electron Transistor

P. Joyez, P. Lafarge, A. Filipe, D. Esteve and M.H. Devoret

Service de Physique de l'Etat Condensé, CEA-Saclay

F-91191 Gif-sur-Yvette, France

Abstract: We have measured the supercurrent branch of a superconducting single electron transistor as a function of gate charge, temperature and magnetic field. At low temperature and magnetic field, the switching current goes from a minimum to a maximum when the gate charge is varied from 0 to *e*, as expected for an island in the ground state with an even electron number. When the odd electron number ground state becomes populated by an increase of temperature or field, the Josephson tunneling is strongly suppressed, in agreement with theoretical predictions.

PACS 73.40.Gk, 73.40.Rw, 74.50.+r

The consequences of the duality of phase and number-of-particle variables are particularly well illustrated by the competition between Josephson tunneling and single electron charging phenomena in ultrasmall superconducting junction systems [1,2]. One of the simplest devices consists of two Josephson junctions in series [3,4,5,6]: the number of Cooper pairs on the middle "island" tends to be fixed by the charging energy $E_C = e^2/2C_\Sigma$ of the island while the associated phase tends to be fixed by the Josephson coupling energy E_J of the two junctions which we suppose identical for simplicity. Here C_Σ refers to the total capacitance of the island. This model system has been investigated theoretically in detail [1,7,8,9]. For large area junctions ($E_J \gg E_C$) the charging effects are overcome by Josephson tunneling and the maximum supercurrent that can flow through the two junction system is just $I_0 = 2eE_J/\hbar$, the maximum supercurrent of each junction. However, for small area junctions ($E_J \ll E_C$), the maximum supercurrent should strongly depend on the polarisation charge Q_g applied to the island by means of a gate electrode, hence the name of "superconducting single electron transistor" given to such device. When $Q_g = e \bmod 2e$, i.e. when states differing by one Cooper pair in the island are degenerate, the maximum current should attain $I_0/2$ while for $Q_g = 0 \bmod 2e$ it should fall to a value of order I_0E_J/E_C [1] (here and in the following, we assume for convenience that the neutral island has an even number of electrons). Recently Matveev *et al.* [9] have shown theoretically that this simple electrostatic modulation of Josephson tunneling will be observed only if the parity of the number n of excess electrons on the island can be kept even for all Q_g. This requires that the odd-even free energy difference D [5,10] of the island is greater than E_C. When $D < E_C$, the island is unstable, in the vicinity of $Q_g = e$, with respect to the entrance of a quasiparticle. This quasiparticle prevents the formation of the coherent superposition of charge states at $Q_g = e$, and therefore "poisons" Josephson tunneling. A complex Q_g-dependence of the supercurrent should then be observed. In this Letter we present an experiment on the superconducting single electron transistor in which, for the first time, we observe the characteristic features resulting from poisoning of Josephson tunneling.

The sample was prepared using standard e-beam lithography and shadow mask evaporation techniques [11]. The main difference with previous experiments is the use of the 3-angle evaporation technique of Haviland *et al.* [12] in order to fabricate in a single pump-down the alumina-covered Al island electrode, the two Al drain and source electrodes and the Cu (3% wt. Al) buffer electrodes (see device layout in the inset of Fig. 1). We believe that these last electrodes allow the quasiparticle population in the transistor to reach the thermal equilibrium value and prevent uncontrolled poisoning of Josephson tunneling by out-of-equilibrium quasiparticles from the rest of the circuit. The contact between the Cu and Al electrodes is sufficiently good to have a negligible influence on the behavior of the transistor at low voltages. The electrical wiring between the sample and the measuring apparatus at room

temperature was made through a series of cryogenic filters as in previous experiments [10]. From the measurement of the device with the Al electrodes brought in the normal state by a magnetic field, we obtained the relation between the gate charge Q_g and gate voltage U, and we could estimate $E_C/k_B = 1.0$ K. The normal resistance of the two junctions in series was $R_N = 49.2$ kΩ. The value $\Delta = 180$ μeV of the gap of the superconducting aluminum was extracted from the large scale I-V characteristic of the sample in zero magnetic field. Using the Ambegaokar-Baratoff relation [13] we deduced from R_N and Δ the Josephson energy $E_J/k_B = 275$ mK and critical current $I_0 = 2eE_J/\hbar = 11.4$ nA of each junction, supposing they are identical. In Fig. 1 we show the sub-gap current-voltage (I-V) characteristic of the junction at $T = 20$ mK and for $Q_g \simeq e$. A supercurrent branch is clearly seen with nearly zero voltage like in the recent experiment by Eiles and Martinis [6]. Its residual slope was measured to be less than 100 Ω, our resistance resolution given the wiring of the sample to the external apparatus. This branch defines a switching current I_s at which the device switches to a voltage set by the resistance of the current bias source, which was 12.1 MΩ for the data we present in the remainder of this paper.

In Fig. 2a we show the variations of I_s as a function of the gate charge Q_g for several values of the magnetic field and at $T = 65$ mK. At lower temperatures the data did not change except for Q_g/e in the vicinity of ±0.75 modulo 2 where we observed what we interpret as a low voltage self-induced Shapiro step [14] and which slightly biased the measurement of the switching current. At low magnetic fields, the switching current varied monotonically when the gate charge was varied from 0 to e. As the field increased, the peak at $Q_g = e$ became a dip, a behavior corresponding to the poisoning of Josephson tunneling by a single quasiparticle. This dip widened as the field was increased further, in agreement with Ref. 9.

In order to compare our experimental results to theory, we now make a minimal extension of Ref. 9 to take into account finite temperature and environmental impedance. The states of the transistor are conveniently characterized by two quantum numbers, the number $n = (N\text{-}N')$ of excess electrons on the island and by the charge flow index $k = (N+N')/2$, where N and N' denote the number of electrons having crossed the junctions (see Fig. 3a). The Josephson Hamiltonian couples states with different k but with the same parity of n and we can thus separate the manifold of states into odd-n and even-n manifolds. In the following, the superscript p will designate a given parity, even or odd. Inside a manifold of parity p, we now perform a change of representation, in which the new states are indexed by n and δ, the total phase difference of the transistor, which is the variable canonically conjugate to k. If we now restrict the span of n to the three lowest electrostatic energy states, we can exactly diagonalize the sum of the Josephson and electrostatic Hamiltonians. In contrast with the treatment of Ref. 9, this procedure takes into account the degeneracy of the first excited charge states that occurs at $Q_g = 0$ ($= e$) when p is even (odd). We obtain a ground state energy band $E_0^p f_0^p(\delta)$,

where the function f_0^p is such that Max{ f_0^p }-Min{ f_0^p } = 2, for arbitrary values of the parameters E_J, E_C and Q_g (see Fig. 3b). In this calculation we assume a gate voltage invariant Josephson coupling E_J for each of the junction (this is valid since the energy gap Δ of the superconductor is such that $E_C \ll 2\Delta$). The 2π-periodic $E_0^p f_0^p(\delta)$ function is equivalent for the transistor to the energy-phase relation $-E_J\cos(\delta)$ for a single Josephson junction; in particular it goes from a minimum to a maximum when δ goes from 0 to π. The transistor can thus be seen as an effective junction with a gate charge-dependent effective Josephson coupling energy E_0^p.

The relation between the *I-V* characteristic observed experimentally and the energy-phase relation depends on both the temperature T and the admittance $Y(\omega)$ which, in the lumped element model of the electromagnetic environment of the junction, is in parallel with the bias current source I. This admittance will govern the dynamics of δ which is analogous to that of a particle in the tilted potential $E_0^p f_0^p(\delta) - (\Phi_0/2\pi)\delta I$, where $\Phi_0 = h/2e$. In the case of interest here, where the response time of the admittance is short compared to the characteristic time of the evolution of δ, we can write the differential equation obeyed by δ as:

$$\frac{\Phi_0}{2\pi}\left[Y(0)\dot{\delta} - jY'(0)\ddot{\delta} - \frac{1}{2}Y''(0)\dddot{\delta} + \ldots\right] + \frac{2\pi E_0^p}{\Phi_0}\frac{\mathrm{d}f_0^p}{\mathrm{d}\delta} = I.$$

This equation generalizes the equation of motion of the resistively and capacitively shunted junction (RCSJ) model [15] to an effective Josephson element shunted by a general admittance.

For $I \le I_{c0} = \left(2\pi E_0^p/\Phi_0\right)\mathrm{Max}\left\{\mathrm{d}f_0^p/\mathrm{d}\delta\right\}$, this equation admits a zero-voltage solution ($\dot{\delta} = 0$) corresponding to the particle sitting in a minimum of the tilted potential. This solution is unstable against thermal fluctuations and therefore the particle will diffuse from well to well in the potential, giving rise to a departure of the supercurrent branch from the zero-voltage axis. However, for $I_m \le I < I_{c0}$ this diffusive motion is itself unstable against the runaway down the potential [16], where I_m is the current for which, on the average, the energy gain due to the tilt of the potential becomes greater than energy loss due to friction. In the weak friction limit appropriate to our experiment, the runaway current I_m is given by:

$$I_m = \Phi_0\left[\alpha Y(0)\left(\frac{E_0^p}{\Phi_0^2|Y'(0)|}\right)^{1/2} + \beta Y''(0)\left(\frac{E_0^p}{\Phi_0^2|Y'(0)|}\right)^{3/2} + \ldots\right],$$

where α, β, ... are dimensionless coefficients which are weakly dependent on f_0^p. The first term in the expansion corresponds to the well known $4I_0/\pi RC\omega_p$ result of the RCSJ model [17]. Here, since we have an unshunted junction, this term vanishes and the Q_g-dependence of I_m is dominated by the second term. In view of the importance of thermal fluctuations in our experiment $\left(E_0^p \le E_J/2\right)$, we will compare the Q_g-dependence of the measured switching

current with the theoretical Q_g-dependence of I_m rather than of the critical current I_{c0} considered by Matveev *et al.* [9].

We now make a crucial assumption. We assume that the inverse of the transition rate between the odd-*n* and even-*n* states is much smaller than the characteristic time of the runaway process. This assumption of rapid odd-even transition is justified since the normal electrodes, which provide the quasiparticle involved in the transition, are very close to the island [18]. In the calculation of the switching current, we thus replace E_0^p by the Boltzmann average $E_0^{av} = E_0^{odd} p_{odd} + E_0^{even} p_{even}$ where p_{odd} and p_{even} are the probabilities of being in an odd- or even-*n* state, respectively, and which verify:

$$p_{odd/even} \propto \sum_{n\ odd/even} \exp\left\{-\left[E_C\left(Q_g/e-n\right)^2 + (n \bmod 2) D(T,H)\right]\Big/ k_B T\right\}.$$

Here $D(T,H)$ is calculated as in Ref. 19.

Using this analysis we can calculate the function $I_m(Q_g,H,T)$ in which enters the unknown scale parameter $Y''(0)/Y'(0)^{3/2}$ and two adjustable parameters: i) the parameter ρ of the reduction of I_0 due to penetration of magnetic field in the junctions [14] defined by $I_0(H) = I_0(1-\rho H^2)$ in the low field limit of relevance here and ii) the critical field H_c such that $D(0,H > H_c) = 0$, which corresponds to the field at which $I_m(Q_g)$ becomes *e*-periodic at $T = 0$. In Fig. 2b, we plot $I_m\left(Q_g, H, T = 65\,\mathrm{mK}\right)/I_{m0}$ where $I_{m0} = I_m\left(Q_g = e, H = 0, T = 65\ \mathrm{mK}\right)$ using the best fit values $\rho = 18.5\ \mathrm{T}^{-2}$ and $H_c = 0.20$ T which are consistent with the junction geometry and with a previous measurement of D [19], respectively. These values are also used in the other comparisons described below. A close agreement with the experimental results is obtained. The validity of our model can be checked further on the temperature dependence of the I_m versus Q_g data shown in Fig. 4 taken for the intermediate field $H = 0.11$ T. Experiments at higher temperatures agree less closely with theory, the relative amplitude of the peaks being greater in experiment than in theory. We believe this is due to the neglect of the departure of I_s from I_m induced by thermal fluctuations in the phase diffusion state. However, the non-monotonous behavior of the $Q_g = e$ switching current as a function of temperature is well captured by our model, as shown in Fig. 5 where we also plot the $Q_g = 0$ switching current for comparison. Note that the recovery above 250 mK of *e*-periodicity, due to the vanishing of the odd-even free energy difference, was also found in other experiments [5,10]. Our model predicts the detailed features of this recovery: the odd manifold contributes dominantly to the current at $Q_g = 0$ and the even manifold contributes dominantly to the current at $Q_g = e$ but, at intermediate temperatures, the switching current is maximum at $Q_g \simeq e/2$ as in the high field limit of Ref. 9.

In conclusion, we have shown that in a Josephson system where the number of quasiparticles was controlled, experimental measurements of charging effects can be explained

by a minimal model, in contrast with preceding experiments. As Fig. 4 exemplifies, the competition between the charging energy, the Josephson energy and the odd-even free energy difference produces a complex behavior of the supercurrent as a function of gate charge, magnetic field and temperature. This intrinsic complexity, together with the difficulties associated with the control of out-of-equilibrium quasiparticles, probably explains why the data in the superconducting state has always been found harder to interpret than in the normal state.

ACKNOWLEDGEMENTS

We are grateful to John Martinis for sending us results prior to publication, and for helpful discussions. We also acknowledge P. F. Orfila for technical help. This work is supported in part by the Bureau National de la Métrologie under contract No. 93-2-46-0018 and by the Commission of the European Community under contract No. ERBSC1*CT000631.

References

[1] D. V. Averin and K. K. Likharev, in *Mesoscopic Phenomena in Solids*, ed. by B. Al'tshuler, P. Lee, and R. Webb (Elsevier, Amsterdam, 1991), Chap. 6.

[2] *Single Charge Tunneling*, ed. by H. Grabert and M. H. Devoret, (Plenum, New York, 1992).

[3] T. A. Fulton, P. L. Gammel, D. J. Bishop and L. N. Dunkleberger, Phys. Rev. Lett. **63**, 1307 (1989).

[4] L. J. Geerligs, V. F. Anderegg, J. Romijn, and J. E. Mooij, Phys. Rev. Lett. **65**, 377 (1990).

[5] M. T. Tuominen, J. M. Hergenrother, T. S. Tighe and M. Tinkham, Phys. Rev. Lett. **69**, 1997 (1992).

[6] T. M. Eiles, and J. M. Martinis submited to Phys. Rev. Lett. (1993).

[7] A. Maassen van den Brink, L. J. Geerligs, and G. Schön, Phys. Rev. Lett. **67**, 3030 (1991).

[8] A. Maassen van den Brink, A. A. Odintsov, P. A. Bobbert, and G. Schön, Z. Phys. B **85**, 459 (1991).

[9] K. A. Matveev, M. Gisselfält, L. I. Glazman, M. Jonson and R. I. Shekhter, Phys. Rev. Lett. **70**, 2940, 1993.

[10] P. Lafarge, P. Joyez, D. Esteve, C. Urbina and M. H. Devoret, Phys. Rev. Lett. **70**, 994 (1993).

[11] G. J. Dolan and J. H. Dunsmuir, Physica **B 152**, 7 (1988).

[12] D. B. Haviland, L. S. Kuzmin, P. Delsing, K. K. Likharev, and T. Claeson, Z. Phys. **B 85**, 339 (1991).

[13] V. Ambegaokar and A. Baratoff, Phys. Rev. Lett. **10**, 486 (1963).

[14] A. Barone and G. Paternò, *Physics and Applications of the Josephson Effect* (Wiley-Interscience, New York, 1982)

[15] W. C. Stewart, Appl. Phys. Lett. **12**, 277 (1968); D. E. McCumber, J. Appl. Phys. **39**, 3113 (1968).

[16] R. L. Kautz, and J. M. Martinis, Phys. Rev. **B 42**, 9903 (1990).

[17] M. Büttiker, E. Harris, and R. Landauer, Phys. Rev. **B 28**, 1268 (1983).

[18] D. V. Averin and Yu. V. Nazarov, Phys. Rev. Lett. **69**, 1993 (1992).

[19] P. Lafarge, P. Joyez, D. Esteve, C. Urbina, and M. H. Devoret, Nature **365**, 422 (1993).

Figures

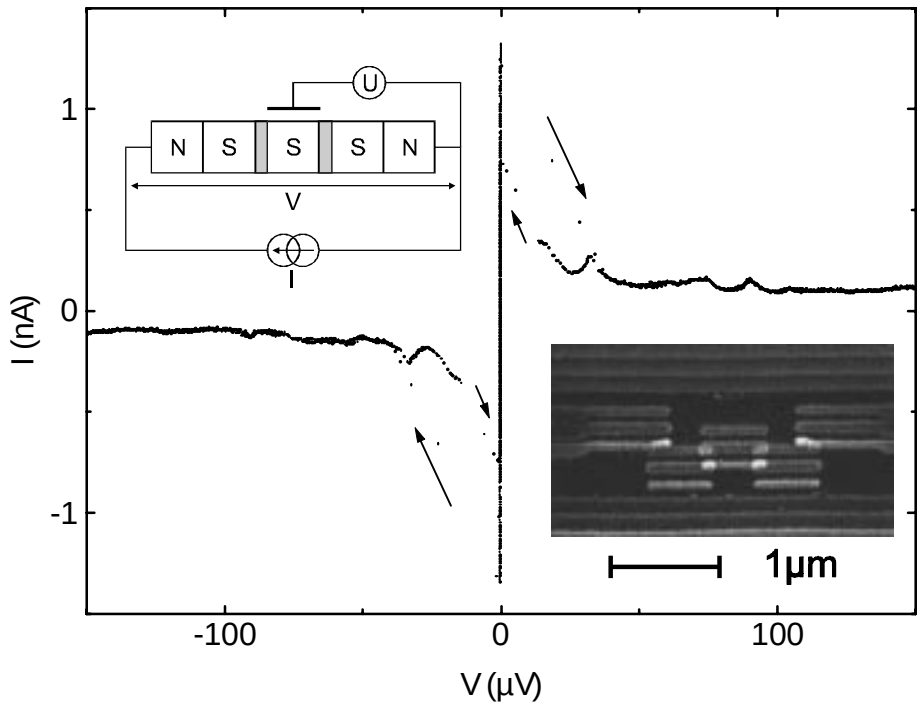

Fig. 1 Current-voltage characteristic of superconducting single electron transistor whose lay-out is shown in upper left inset. The letters N and S refer to normal (Cu) and superconducting (Al) electrodes. The tunnel barriers are indicated by grey rectangles. The gate voltage U induces on the middle island a gate charge Q_g whose value is e for the data shown. The temperature was 20 mK. The maximum current defines the switching current I_s. Lower right inset is an electron micrograph of the device. The current flows through the middle strip only. The top electrode is the gate.

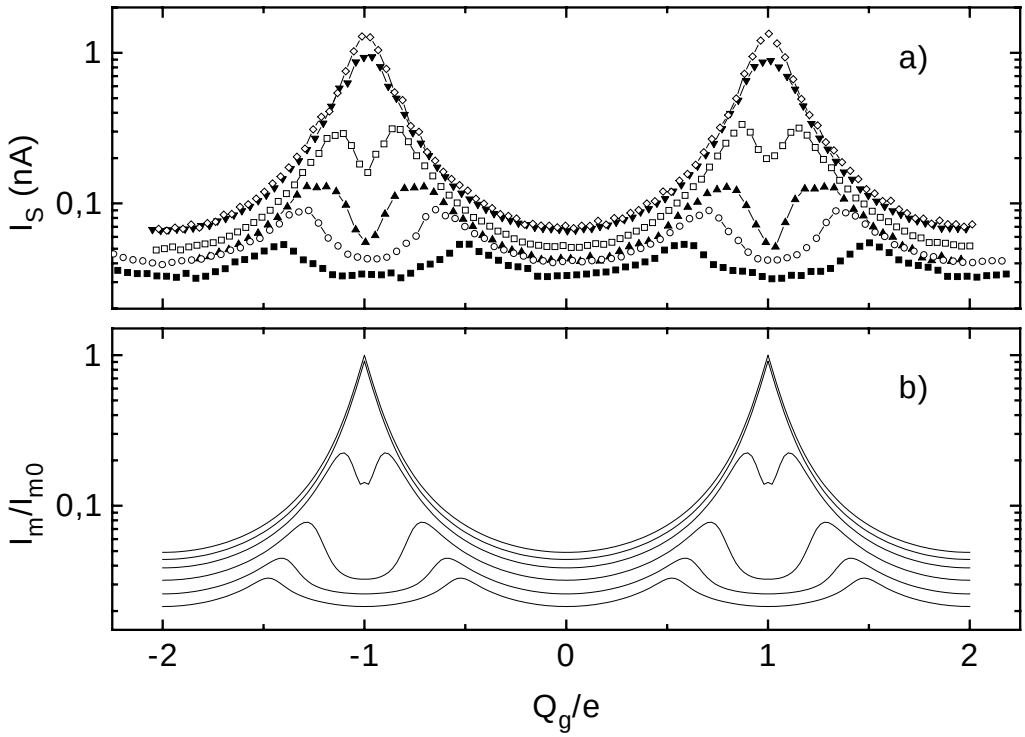

Fig. 2 a) Switching current as a function of gate charge, for several values of the magnetic field H, at $T = 65$mK. Top to bottom: $H = 0$, 0.07, 0.11, 0.14, 0.16, 0.17 T. The dip at odd integer values of Q_g/e corresponds to the poisoning of Josephson tunneling by the entrance of one quasiparticle in the island. b) Theoretical runaway current as a function of gate charge, for the same field values as in a).

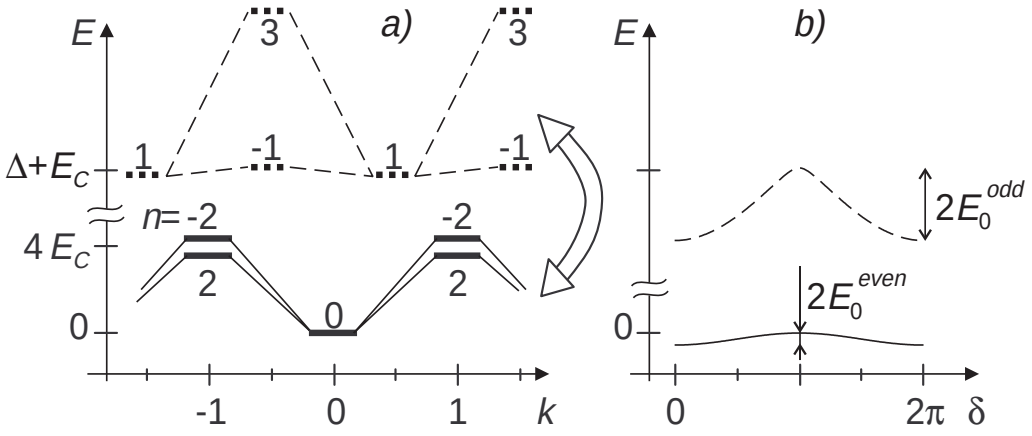

Fig. 3a) Energy levels of the transistor at $Q_g = 0.02e$. The number n labelling the levels refer to the number of electrons in the middle island. The number k is the charge transfer index. The lines joining the levels represent the Josephson coupling. Only levels with the same parity of n are coupled. The even-n manifold (levels in solid line) and the odd-n manifold (levels in dashed line) are weakly coupled by the cotunneling of one electron from a normal lead to the middle island (double arrow). b) Lowest energy bands corresponding to the even and odd manifolds. The variable δ is canonically conjugate to k.

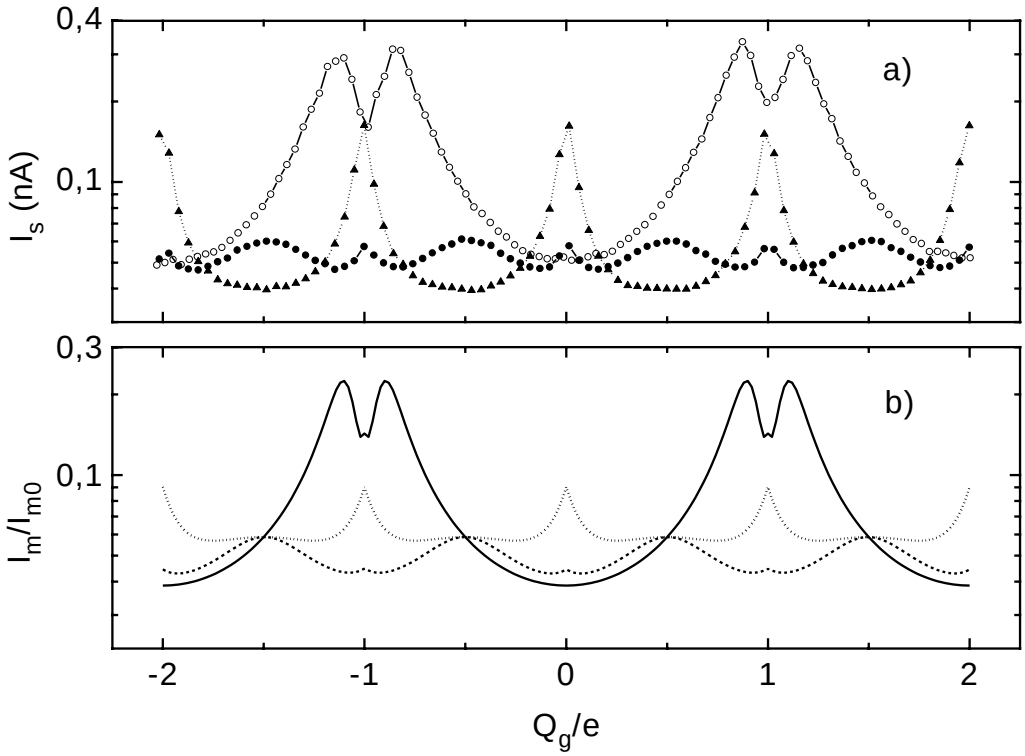

Fig. 4 a) Switching current as a function of gate charge, at $H = 0.11$ T and for several values of the temperature T, showing the complex transition from 2e-periodicity to e-periodicity with the increase of T. Open dots: $T = 65$ mK; solid dots: $T = 203$ mK; triangles: $T = 356$ mK. b) Theoretical runaway current as a function of gate charge, for the same temperature values as in a) (the full and dotted line correspond to the lowest and highest temperatures, respectively).

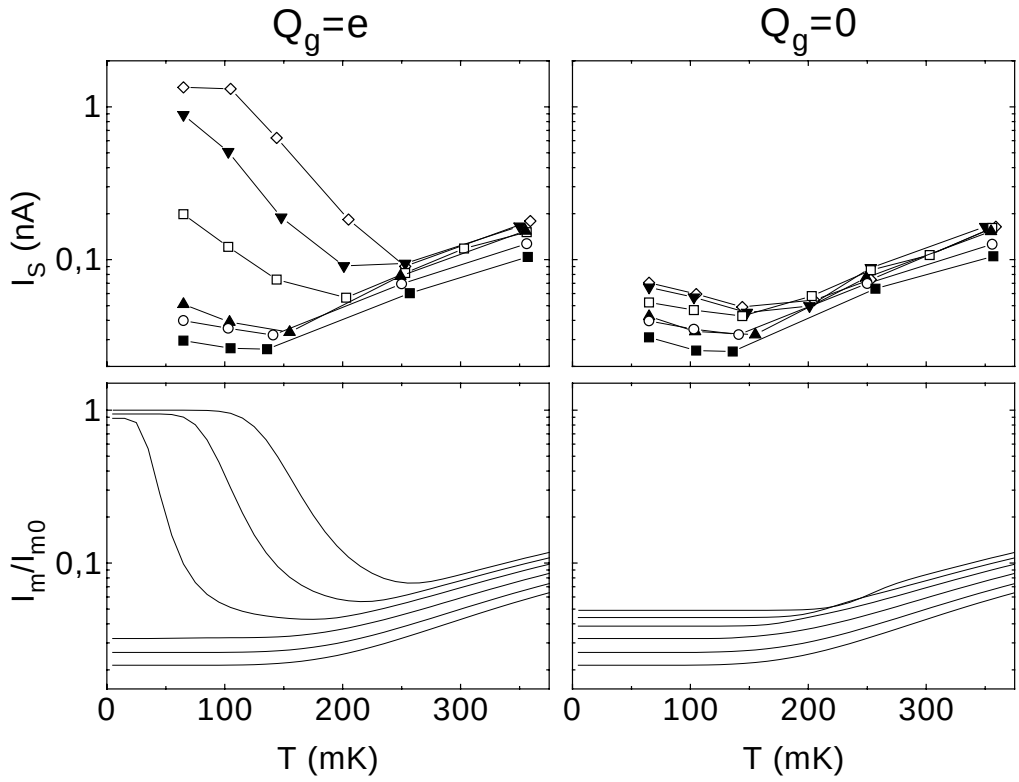

Fig. 5 Top panels: experimental switching current as a function of temperature for $Q_g = 0$ and $Q_g = e$. Top to bottom, same field values as in Fig. 2. Bottom panels: theoretical runaway current for the same conditions as in top panels. The theory curves reproduce the strongly non-monotonic temperature dependence found in the experiment at $Q_g = e$ for low fields.

APPENDIX B

Characteristics of the samples

sample #	date	e or $2e$ period.	R_t (kΩ)	E_J/k_B (mK)	I_0 (nA)	$I_s max$ (nA)	$\frac{I_s max}{I_C max}$	E_c/k_B (K)	on-chip capacitors?	fixed resonances
1	02/04/93	$2e+e$	120	125	5.2	0.002	0.08%	*1**	no	
2	20/04/93	$2e$	59.0	254	10.6	0.3	5.6%	*0.3**	no	
3	24/05/93	$2e$	41.0	366	15.3	1.1	14%	*0.3**	no	
4	09/06/93	$2e$	53.0	283	11.9	1.3	22%	*1**	no	
5	22/07/93	$2e$	49.2	305	12.8	1.3	20%	1.0	no	yes
6	08/11/93	$2e$	44.7	336	14.1	0.9	13%	1.1	no	yes
7	01/12/93	$2e$	24.8	605	25.3	3.0	24%	0.64	yes	no
8	04/01/94	$2e$	17.0	882	37.0	6.0	32%	0.46	yes	yes
9	12/01/94	$2e$	56.8	264	11.1	0.6	11%	$\approx .65^{\dagger}$	yes	$no^{\dagger}$
10	07/02/94	$\boldsymbol{e}$	30.0	500	20.9	0.1	1.1%	0.41	yes	no
11	09/02/94	$2e$	21.8	688	28.8	9.0	62%	0.69	yes	yes
12	13/04/94	$2e$	≈25						yes	
13	19/04/94	$2e$	30.0	500	20.9	7.3	70%	0.66	yes	no

Table 1. Main characteristics of the samples we have measured. All these samples had normal-metal leads to prevent quasiparticle poisoning. In column four, we give the period of the modulation of the supercurrent with respect to the gate charge. Column 5 : total tunnel resistance of the sample at low temperature. Column 6 and 7, calculated Josephson Coupling energy E_J of each junction (assumed identical) and critical current I_0 of each junction obtained using Ambegaokar-Baratoff equation. Column 8 : ratio of maximum measured switching current to maximal critical current of the transistor $I_C max = I_0/2$. Column 9 : Charging energy of the sample determined using the gate voltage dependent resonances (see Sec. V.C.1), except (*) for samples 1-4 (rough estimates based on temperature dependence of charging effects or normal-state *I-V* characteristics.). Column 10 indicates if the sample incorporated on-chip microfabricated capacitors (see Chap. VI). Column 11 reports observation of gate voltage independent resonances (these were not looked after in samples 1-4).

Miscellaneous information : Samples 1 and 2 were voltage biased. Sample 1 was not perfectly $2e$-periodic because its normal-metal filters were too short (they were made longer in subsequent experiments). A cryogenic problem prevented cooling of sample 2 below 50 mK.

Samples 3 and 12 were destroyed accidentally by an electrostatic shock. Sample 4 could not be measured in the normal state (superconducting coil disabled). Sample 5 was used for the paper given in appendix A. Sample 7 and 8 had two samples on the same chip and showed finite-voltage fixed resonances in spite of a microfabricated environment, possibly because of the poor symmetry of the mask. Temperature measurements made on sample 8 were unreliable because of a thermalisation problem. Measurements at finite voltage on sample 9 had a poor signal to noise ratio due to the smallness of the current which prevented a precise determination of some parameters (†). Samples 9 to 13 had a coaxial microwave cable connected directly on chip for AC Josephson effect measurement, but the coaxial cable used with sample 9 was too resistive and heated up the sample when microwaves were applied. Sample 10 was completely *e*-periodic. Samples 8 and 11 showed a decrease of the switching current with the temperature below 100 mK (see Sec. V.B.1). In sample 13, normal-metal leads of the transistor were made of a spin glass alloy Cu-Mn (2% wt. Mn).